Anisotropy of Mudrocks: Quantifying Controls and Fabric Implications in the Horn River Basin

by

Vivian Tariere Ebufegha

A thesis submitted in partial fulfillment of the requirements for the degree of

Doctor of Philosophy

In
Geophysics

Department of Physics
University of Alberta

ABSTRACT

Shales are widely occurring and highly heterogeneous sedimentary rocks. They exhibit significant variation in composition and distribution of matrix constituents and pores/fracture networks, which can affect their petrophysical and geomechanical properties. These variations are important for determining the integrity of shales as caprocks, and for optimizing hydrocarbon recovery techniques (such as hydraulic fracturing) where shales form unconventional reservoirs. In this thesis, a detailed laboratory study on the application of magnetic and electrical anisotropy in understanding these variations in composition and matrix spatial distribution (petrofabric) in shales and mudstones of the Muskwa, Otter Park and Evie members of the Horn River Basin is presented. Despite increased interest in unconventional shale reservoirs, studies on quantitative anisotropy controls in shales are limited, especially studies comparing results from different quantitative techniques.

Three techniques were investigated: (1) Bulk magnetic susceptibility and the anisotropy of magnetic susceptibility (AMS), (2) Electrical resistivity and the anisotropy of electrical conductivity (AEC), and (3) The anisotropy of magnetic remanence (AMR). To test the reliability of these anisotropy techniques as tools for quantitative fabric analysis, their results were compared with one another and with observations from core analysis, thin section analysis, SEM imaging, and geochemical analysis.

Bulk susceptibilities of slabbed core for a well penetrating all three members of the Horn River Group showed that the concentration of clay minerals was primarily responsible for the higher magnetic susceptibilities in the Lower Muskwa and Otter Park, while low bulk susceptibilities in the Upper Muskwa and Evie were due to higher total organic carbon (TOC) and quartz concentrations. Whilst the correlations with clay and quartz content was expected, this, to our

knowledge, is the first time a correlation between TOC and magnetic susceptibility has been shown.

Room temperature anisotropy of magnetic susceptibility (AMS) values determined from 18 directional magnetic susceptibility measurements made on sodium silicate impregnated samples showed good correlation with TOC and gamma ray readings, and little to no correlation with clay concentration. Results indicated that organic matter concentration dictates mineral grain alignment in the Horn River Group. No previous studies have reported a relationship between TOC and AMS.

Room temperature AMS principal axes primarily defined normal and inverse fabrics. Inverse AMS fabrics due to uniaxial stable single domain grains were identified for the first time to our knowledge in shales. A comparison with anisotropy of isothermal remanent magnetization (AIRM) principal orientations confirmed the presence of inverse fabrics due to uniaxial stable single domain grains. Previously such inverse fabrics had only been reported in igneous and metamorphic rocks.

Low temperature directional magnetic susceptibilities were also measured between -100°C and room temperature and used to determine (i) the illite clay content and (ii) variations in %AMS and principal orientations with temperature. Illite is the main paramagnetic mineral in the Horn River Group, and a series of template curves were developed that allowed the determination of illite concentrations from susceptibility-temperature curves by utilizing the enhancement of paramagnetic susceptibility with decreasing temperature. The illite contents obtained strongly correlated with relevant independent geochemical data from mass spectrometry. Based on the variation of AMS and principal AMS orientations with low temperature, the paramagnetic subfabric was also isolated. When principal orientations remained approximately consistent with temperature paramagnetic minerals had the same orientation as other matrix components.

Comparison with anisotropy of magnetic remanence orientations allowed one to distinguish whether inverse AMS fabrics observed at room temperature were due to the presence of stable single domain grains, or ferroan calcite/siderite or a combination of both. Moreover, the low temperature AMS measurements revealed clear and enhanced anisotropy in samples that appeared to be weakly anisotropic at room temperature. This provides a novel method for identifying subtle features like lineations (in shales and other geological samples containing paramagnetic minerals) that may not be recognized from conventional room temperature AMS measurements.

The spatial arrangement of pores was quantified in terms of the anisotropy of electrical conductivity (AEC). Principal conductivity orientations suggested that pore spaces are strongly aligned in a bedding parallel direction similar to the mineral components from the AMS principal orientations. The Horn River Group samples were not found to be transversely isotropic with respect to electrical conductivity, and 3D AEC measurements provided a better description of their electrical conductivity anisotropic properties.

DEDICATION

This thesis is dedicated to my parents, Akposeiyifa and Edith Ebufegha, and to my siblings, Kate, Akpos, Doubra, Tammy, Tonbra and Ebi.

ACKNOWLEDGEMENTS

Firstly, I would like to thank my supervisor Dr. David K. Potter for giving me the opportunity to pursue this degree. I am grateful that he allowed me the freedom to explore various interests. For his invaluable insights throughout the course of my research, I am very grateful. I am also grateful to members of my defense committee, Dr. Douglas Schmitt, Dr. Tony Morris, Dr. Vadim Kravchinsky and Dr. Hassan Dehghanpour, for carefully reviewing my thesis and providing constructive feedback.

Special thanks to the British Columbia Oil and Gas Commission, Dr. Nicholas Harris, and Dr. Hassan Dehghanpour for providing the core samples used for this work. Dr. Nicholas Harris is also appreciated for providing geochemical data for the Horn River Group samples studied.

Many thanks to Dr. Vadim Kravchinsky for allowing me access to his laboratory, and to Mark Labbe and Martin Von Dollen for their assistance with sample preparation. I am also grateful to Paul Davis and Leonard Wampler for their invaluable help in the electronics shop.

I could not have come this far without the support of my family and friends. I thank my parents for the many sacrifices they made for me to get to this point, and my siblings for their limitless encouragement. I am especially grateful to Iwasam Agube for his unwavering support and encouragement, and for the many MATLAB tutorials.

Table of Contents

List of Tables

Chapter 3: Room temperature magnetic susceptibility and Anisotropy of Magnetic Susceptibility (AMS)

Chapter 4: **Quantifying shale mineralogy and anisotropy from low temperature magnetic susceptibility measurements**

Chapter 5: Electrical Resistivity and Anisotropy of Electrical Conductivity (AEC)

List of Figures

Chapter 2: Study area and sample characterization

Chapter 3: Room temperature magnetic susceptibility and Anisotropy of Magnetic Susceptibility (AMS)

Chapter 5: Electrical Resistivity and Anisotropy of Electrical Conductivity (AEC)

Chapter 6: Anisotropy of magnetic remanence (AMR)

Chapter 7: Comparison of results from different techniques

List of symbols and abbreviations

B	Magnetic induction (magnetic flux density)
H	Magnetic field strength
M	Induced magnetization
χ_v	Volume susceptibility
χ_m	Mass susceptibility
d	density
A/m	Amperes per meter
k	Boltzmann constant = 1.38×10^{-16} erg/K
T	Temperature
T_c	Curie temperature
C	Curie constant
T_N	Néel temperature
K_{ij}	Magnetic susceptibility tensor
k_1	Maximum susceptibility axis
k_{max}	Maximum susceptibility axis
k_2	Intermediate susceptibility axis
k_{int}	Intermediate susceptibility axis
k_3	Minimum susceptibility axis
k_{min}	Minimum susceptibility axis
AMS	Anisotropy of Magnetic Susceptibility
AMR	Anisotropy of Magnetic Remanence
AEC	Anisotropy of Electrical Conductivity
HRG	Horn River Group
SD	Stable single domain
MD	Multidomain
μ	Permeability of free space ($4\pi \times$ 10-7 V.s/A.m)
M_s	Saturation magnetization
TOC	Total Organic Carbon

List of symbols and abbreviations

mT	Millitesla
T	Tesla
IRM	Isothermal Remanent Magnetization
χ_{para}	Paramagnetic susceptibility
k(T)	Magnetic susceptibility as a function of temperature
LTAMS	Low Temperature Anisotropy of Magnetic Susceptibility
ICP-MS	Inductively Coupled Plasma Mass Spectrometry
RT	Room temperature
EDX	Energy Dispersive X-ray
ρ	Electrical resistivity
R	Electrical resistance
A	Cross sectional area
L	Length across which current flows
Ωm	Ohm meter
S/m	Siemens per meter
ρ_w	Resistivity of saturating electrolyte
ρ_{bulk}	Bulk resistivity
ø	Porosity
m	Cementation factor
k	Saturation exponent
F	Formation factor
EDL	Electrical double layer
σ	Electrical conductivity
J	Current density
E	Electric field
VTI	Vertical Transverse Isotropy
ρ_v	Transverse resistivity
ρ_h	Longitudinal resistivity

List of symbols and abbreviations

V Potential difference (voltage) between two points

I Current

AC Alternating current

σ_{max} maximum conductivity axis

σ_{int} Intermediate conductivity axis

σ_{min} minimum conductivity axis

AARM Anisotropy of anhysteretic remanent magnetization

AIRM Anisotropy of Isothermal Remanant Magnetization

Chapter 1

Introduction

1.1 Terminology

The terms ‘shale’, ‘mudstone’, ‘claystone’ and ‘mudrock’ are commonly interchangeably used to refer to fine grained sedimentary rocks consisting primarily of clay and silt size particles. Several authors, including Lundegard and Samuels (1980), Spears (1980), Stow and Piper (1984) and Zee Ma and Holditch (2015) however propose the use of the term ‘mudrock’ as a general group name for all fine grained siliciclastic sedimentary rocks (claystones, shales, mudstones, and siltstones). In this scheme, the term ‘shale’ is used to describe laminated, fissile, and typically clay rich fine grained rocks (Boggs, 2009), and mudstones are blocky, non- fissile fine grained sedimentary rocks (Tucker, 1981). Claystones and siltstones are defined based on the dominant grainsize fraction they contain. Claystones are made up of more than 50 percent clay sized grains (grains <4μm), and siltstones consist of more than 50 percent silt sized grains (grains between 4μm and 62μm) (Folk, 1974). In this thesis, the term ‘mudrock’ is used as a group name. Shales are defined as laminated, fissile, typically argillaceous mudrocks, while mudstones are more brittle, non-fissile, sometimes argillaceous varieties.

1.2 Research motivation and objectives

Mudrocks are complex, highly heterogeneous and widely occurring sedimentary rocks. They make up about 60% to 70% of sedimentary basins (Broichhausen et al 2005). They are good source rocks

because of their organic matter richness, and, due to their low permeability, are capable of being both hydrocarbon traps (reservoirs) and seals (Ingram and Urai, 1999; Spencer, 1989). Due to their low permeability, however, hydrocarbon production from mudrock reservoirs only became economically viable with advancements in hydraulic fracturing and horizontal drilling. Although these technologies have in the last decade significantly improved production, many challenges still limit optimum recovery of hydrocarbons from these unconventional reservoirs. One such challenge is the inability to predict how fracture networks, induced by hydraulic fracturing, will propagate through a given rock mass. The mechanical response of a rock to stress is dependent on rock fabric, that is, it is dependent on a rock sample's composition, the shape, distribution and spatial arrangement of its grains, pores and fractures. Rocks with similar composition but different spatial arrangement of grains and or fracture networks will have different mechanical properties. A thorough understanding of rock fabric is therefore crucial for successful exploitation of shale and mudstone reservoirs.

This thesis investigates the application of anisotropy as a quantitative means of describing shale and mudstone fabric. Its main objectives are to quantify anisotropy, and determine the factors controlling anisotropy, in the Horn River Group mudrocks, using thin sections, magnetic anisotropy, and electrical anisotropy. Since anisotropy may be a key factor controlling the performance of mudrocks as seals/caprocks, findings can potentially help determine the effectiveness of a given mudrock as a hydrocarbon seal. Results can also potentially improve methods of exploiting unconventional shale and mudstones reservoirs (i.e., improve hydraulic fracturing procedures).

1.3 Organization of Thesis

This thesis is divided into eight chapters. **Chapter 1** introduces the research objectives and **Chapter 2** introduces the study area and samples used. Each anisotropy technique investigated is discussed in a separate chapter. For each technique, the methods used to determine the anisotropy tensor and degree are detailed, and the implications for shale and mudrock fabric are discussed.

In addition to describing the mineralogical and sedimentological characteristics observed in thin section images of Muskwa, Otter Park and Evie samples, **Chapter 2** also includes a

characterization of anisotropy degree based on textural features observed in thin section photomicrographs (both plane polarized light images and reflected light images).

Chapter 3 focuses on room temperature bulk volume magnetic susceptibility and anisotropy of magnetic susceptibility (AMS) of core samples from the Muskwa, Otter Park and Evie formations. No sample preparation was required for the bulk volume magnetic susceptibility measurements since probe measurements were directly taken on core samples. A method of keeping fissile shales intact for directional AMS measurements is described, and the magnetic fabrics observed are interpreted in terms of petrofabric.

In **Chapter 4**, the variation of mudrock bulk magnetic susceptibility and AMS with temperature is investigated. The application of the Curie law in quantifying mineralogy and isolating paramagnetic subfabrics is examined. The enhancement of paramagnetic susceptibility with decreasing temperature, make the novel methods described in this chapter ideal for studying the fabric of low susceptibility mudrocks such as siliceous and calcareous sections of the Muskwa and Evie.

Chapter 5 is centered on resistivity and the anisotropy of electrical conductivity. A novel method of determining the electrical conductivity tensor is detailed, and the validity of assuming vertical transverse isotropy with respect to electrical resistivity is tested.

In **Chapter 6**, the anisotropy of isothermal remanent magnetization is used to quantify the fabric of ferrimagnetic minerals in the Horn River Group. This allows one to separate out the fabric of the ferrimagnetic minerals from the matrix diamagnetic and paramagnetic minerals. A comparison of AMS and AMR also allows one to check for the presence of stable single domain (SD) grains.

Results from the different techniques are compared in **Chapter 7**, and in **Chapter 8** all conclusions are summarized and recommendations for further studies are presented.

1.4 List of publications

Peer reviewed conference proceedings

Ebufegha, V., and Potter, D.K., 2014. A comparison of quantitative techniques for determining the 3D anisotropy of shale samples: Application to Horn River Shales, British Columbia, Canada. Proceedings of the 2014 International Symposium of the Society of Core Analysts, 8-11 September 2014, Avignon, France. Paper SCA2014-011 (12 pages).

Ebufegha, V.T., and Potter, D.K., 2016. Quantifying shale mineralogy and anisotropy from low temperature magnetic susceptibility measurements. Proceedings of the 2016 International Symposium of the Society of Core Analysts, 21-26 August 2016, Snowmass, Colorado, USA. Paper SCA2016-033 (12 pages).

Peer reviewed journal papers

Ebufegha, V.T., and Potter, D.K., 2016. A comparison of quantitative techniques for determining the 3D anisotropy of shale samples: Application to Horn River Shales, British Columbia, Canada (In preparation)

Ebufegha, V.T., and Potter, D.K., 2016. Quantifying shale mineralogy and anisotropy from low temperature magnetic susceptibility measurements (In preparation).

Ebufegha, V.T., and Potter, D.K., 2016. Combined anisotropy of magnetic susceptibility and anisotropy of electrical conductivity in mudrock fabric analysis (In preparation).

Ebufegha, V.T., and Potter, D.K., 2016. Correlations between total organic content (TOC), geochemistry and magnetic susceptibility (In preparation).

Conference presentations and abstracts

Ebufegha, V.T., and Potter, D.K. (2014, September). A comparison of quantitative techniques for determining the 3D anisotropy of shale samples: Application to Horn River Shales, British

Columbia, Canada. International Symposium of the Society of Core Analysts, Avignon, France.

Ebufegha, V.T., and Potter, D.K. (2015, May). Low- temperature magnetic anisotropy in shales and mudstones: Application in modelling mineralogy and fabric in the Horn River Basin, British Columbia. GeoConvention 2015, Calgary, Alberta.

Ebufegha, V. T., and Potter, D.K. (2015, June). A method for determining 3D Anisotropy of Electrical Resistivity in multifaceted shale and mudstone samples: Application to the Horn River Basin, British Columbia. AAPG 2015 Annual Convention and Exhibition (ACE), Denver, Colorado.

Ebufegha, V.T., and Potter, D.K. (2016, August). Quantifying shale mineralogy and anisotropy from low temperature magnetic susceptibility measurements. International Symposium of the Society of Core Analysts, Snowmass, Colorado, USA.

1.5 References

Broichhausen, H., Littke, R., and Hantschel, T., 2005. Mudstone compaction and its influence on overpressure generation, elucidated by a 3D case study in the North Sea: International Journal of Earth Sciences, 94, 956-978.

Boggs, S., 2009. Petrology of sedimentary rocks. Cambridge University Press, p.194.

Folk, R.L., 1974. Petrology of sedimentary rocks. 3rd Edition Hemphill Publishing Company, pp. 182.

Ingram, G.M., and Urai, J. L., 1999. Top-seal leakage through faults and fractures: the role of mudrock properties. In Aplin, A.C., Fleet, A.J., and Macquaker, J.H.S., 1999. Mudstones: Physical and fluid flow properties. The Geological Society of London, 125-135.

Lundegard, P.D., and Samuels, N.D., 1980. Field classification of fine-grained sedimentary rocks. J. Sed. Petrol. 50, 781-786.

Spears, D.A., 1980. Towards a classification of shales. J. Geol Soc. London, 137, 125-129.

Spencer, C.W., 1989. Review of characteristics of low-permeability gas reservoirs in Western United States. AAPG Bulletin, 73, 613-629.

Stow, D.A.V., and Piper, D.J.W., 1984. Deep-water fine-grained sediments; history, methodology and terminology. Geol. Soc. London, Special Publications 15, 3-14.

Zee Ma, Y., and Holditch, S., 2015. Unconventional oil and gas resources handbook: evaluation and development. Gulf professional publishing, p.73.

Tucker, M.E., 2009. Sedimentary petrology: An introduction to the origin of sedimentary rocks. John Wiley and Sons, p.92.

Chapter 2

Study area and sample characterization

2.1 Study area

2.1.1 The Horn River Basin

The Horn River Basin is located in northeastern British Columbia and extends into the southern Northwest and Yukon Territories (**Figure 2.1**). It occupies an area of about 12,000km^2 and is surrounded by the Slave point carbonate platform to the east, the Presqu'ile Barrier to the south, and the Bovie Fault Zone to the west. The Bovie Fault Zone separates it from the Liard Basin (Williams, 1983; Oldale and Munday, 1994; Morrow et al., 2002; Ross and Bustin, 2008).

The Devonian (Givetian-Frasnian) basinal mudrocks of the Horn River Group are the subject of this study. The group consists of the Evie, Otter Park and Muskwa Formations. **Figure 2.2** shows the stratigraphic relationships between these three formations. The Evie is overlain by the Otter Park, which is in turn overlain by the Muskwa. On the western side of the basin, the group is underlain by carbonates of the Nahanni Formation, and on the eastern side it is underlain by dolostones and limestones of the Keg River formation. The Fort Simpson Formation conformably overlies the Muskwa (Ferri et al., 2012).

The Horn River Group was deposited over the platforms of the lower Keg River and Nahanni formations following a major marine transgression (Reynolds and Munn, 2010). The Evie member is the most electrically resistive and radioactive member, consisting generally of black to dark grey, organic rich, pyritic and calcareous mudstones and laminated shales. It is thickest close to the

Presqu'ile Barrier (over 75m), thinning westward to less than 40m toward the Bovie Fault (**Figure 2.2**) (B.C. Ministry of Energy and Miners, 2011; B.C. Oil and Gas Commission, 2012; Chen and Hannigan, 2015).

The Otter Park Member consists generally of grey to black laminated, argillaceous shales and siliceous and calcareous mudstones. It reaches a maximum thickness of over 270m in the southeast part of the basin where more argillaceous and calcareous shales occur, thinning to the north and west where gamma ray readings are higher (B.C. Ministry of Energy and Miners, 2011; B.C. Oil and Gas Commission, 2012).

The Muskwa Member consists of dark grey to black organic rich, pyritic, siliceous shales and mudstones. It is also characterized by high electrical resistivities and gamma ray readings. It is 30m thick close to the Presqu'ile barrier and thickens westward to over 60m close to the Bovie Fault. It extends further east than the Otter Park and Evie Members, past the Horn River Basin, over the barrier complex, into Alberta (**Figure 2.2**). It is stratigraphically equivalent to the Duvernay Shale (B.C. Ministry of Energy and Mines, 2011; B.C. Oil and Gas Commission, 2012).

2.1.2 Study well

Slabbed core from the Imperial Oil KOMIE D-069-K/094-O-02 well, whose location is shown in **Figure 2.1**, was used in this study. The interval consists of an approximately 182m thick section that penetrates all of the Muskwa, Otter Park and Evie Formations. At this location, the Muskwa is about 60m thick, the Otter Park is 85m thick and the Evie is 37m thick.

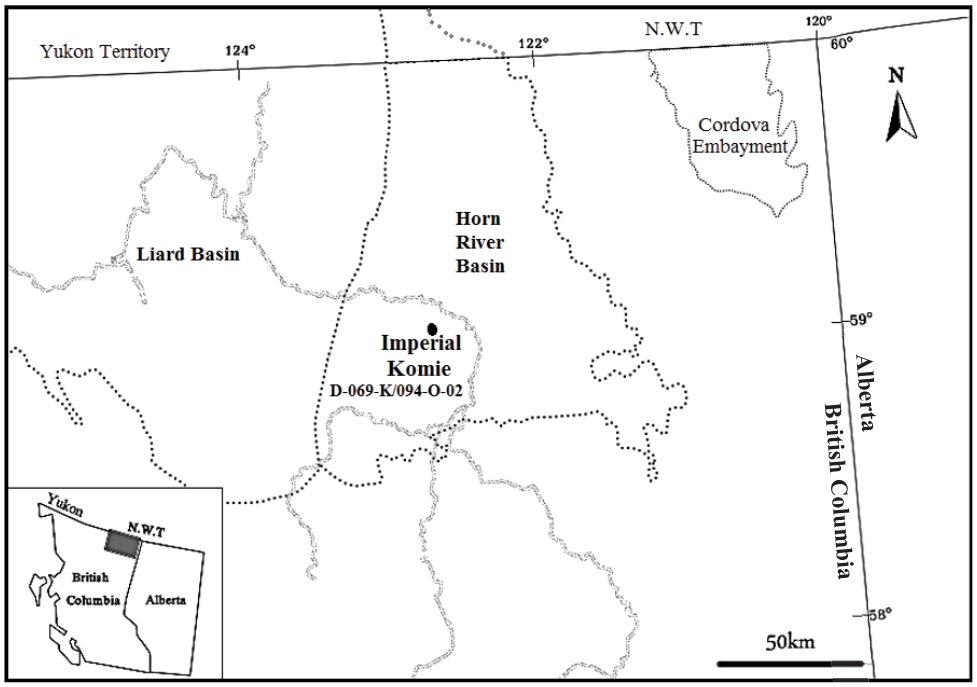

Figure 2.1: Map showing the location of the Horn River Basin (modified from Perez et al., 2012).

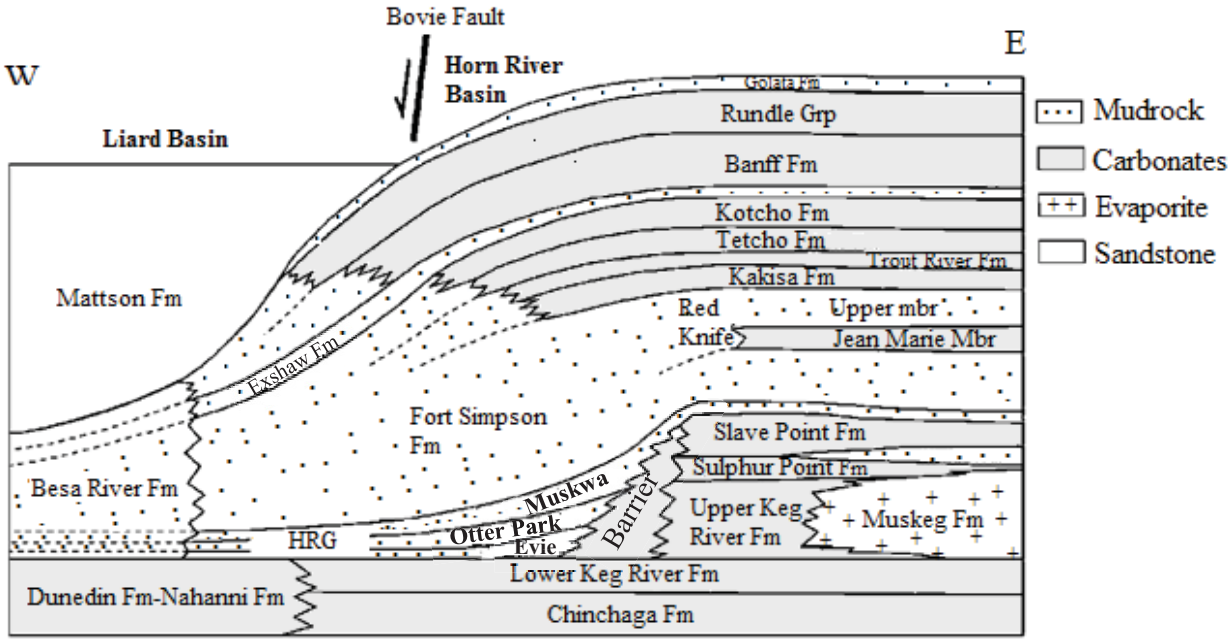

Figure 2.2: Cross section showing stratigraphic relationships between Upper Palaeozoic shelf and basinal sequences. The Horn River Group (HRG) formations are the formations of interest (modified from Ferri et al. 2012).

2.2 Sample characterization: Thin section petrography

2.2.1 Introduction

In this section, the compositional and textural characteristics, as observed in thin section photomicrographs, of each Member of the Horn River Group in the studied well are described. Based on these textural observations, the degree of anisotropy is defined. Chalmers et al (2012) attempts a similar anisotropy characterization, classifying samples that show preferred orientation of grain long axes or laminations as highly anisotropic, and samples rich in quartz or carbonates and lacking matrix preferred orientation as moderately or poorly anisotropic. In several sections of all three Horn River Group formations from the Imperial Komie well, the opacity of organic matter obscures many textural properties, limiting the reliability of this method as a means of determining the degree of anisotropy.

2.2.2 Methodology

Thin sections (approximately 30μm thick) were cut parallel to the bedding plane, normal to the bedding plane and at 45° to the bedding plane. They were examined under plane polarized, cross polarized and reflected UV light. For reflected light microscopy, thin sections were polished. In plane and crossed polarized light, major matrix minerals and any textural properties such as mineral defined layering and laminations were identified, and under reflected light ore minerals, like pyrite, and the fabrics they define were identified. Strongly laminated/well bedded intervals and intervals with strongly aligned grains were classified as strongly anisotropic, while those with no obvious preferred orientation in plane polarized or reflected light were classified as poorly anisotropic.

2.2.3 Results

The following are the five main lithofacies identified in the studied well:

1. Massive pyritic mudstones

2. Laminated, argillaceous and pyritic shales

3. Laminated argillaceous shales with sparse pyrite framboids

4. Lenticular bedded mudstones

5. Calcareous mudstones

Lithofacies 1: Massive to poorly laminated pyritic mudstones

This lithofacies dominates the top 30m of the Muskwa and intervals of the lower 35m of the Otter Park. In hand sample, it is characterized by dark grey to black mudstones. In thin section, it consists of massive and poorly laminated, quartz rich mudstones with pyritic intervals. Thin section photomicrographs shown in **Figures 2.3** and **2.5D** show pyrite occurring either as clusters of angular to sub-angular crystals (framboids) or as individual crystals randomly dispersed in the matrix. Thin clay and organic rich laminae define the laminated texture of poorly laminated intervals (**Figures 2.3C**). This lithofacies is also characterized by high organic matter concentrations. Total Organic Matter (TOC) ranges from 0.5% to 6.85%.

On the basis of thin section characteristics, samples in this lithofacies are moderately to poorly anisotropic. Reflected light images show some preferred orientation of the long axes of pyrite replaced bioclasts (**Figure 2.3B**). Pyrite crystals that make up framboids also show some alignment of long axes (**Figure 2.3E** and **2.3F**). Plane polarized light images are only useful in organic matter poor sections. Quartz richness and poorly defined laminations further suggest moderate to poor anisotropy.

Lithofacies 2: Laminated, argillaceous and pyritic shales

In the Imperial Komie well, this lithofacies occurs in the lower 20m of the Muskwa and in sections of the top 48m of the Otter Park. In thin section, it is characterized by alternations of organic rich clay intervals and siltstone intervals (**Figure 2.4**). Thin section images taken under plane polarized light show that the organic rich clay intervals consist of opaque, bedding parallel, lens shaped features (**Figure 2.4B**) that under reflected UV light, are observed to be made up of pyrite clusters (framboids) (**Figure 2.4C**). Since these pyrite framboids are elongate and strongly aligned parallel to the bedding plane, pyrite may be a contributor to anisotropy in the Otter Park and Lower

Muskwa. The presence of clay rich laminations and bedding parallel, strongly aligned pyrite framboids suggest that samples in this lithofacies are strongly anisotropic.

Lithofacies 3: Laminated argillaceous shales with sparse pyrite framboids

These have the lowest organic matter concentration. TOC ranges from 0.46 % to 2.57 %. They dominate the upper 48m of the Otter Park. Like lithofacies 2, in thin section this lithofacies consists of alternations of clay rich layers and silty layers (**Figure 2.5A**, **2.5B** and **2.5D**). Thin section images also show that clay rich intervals contain numerous bedding parallel, elongate and strongly aligned organic matter stringers (**Figure 2.5C**). This lithofacies differs from lithofacies 2 in that pyrite is not restricted to the clay-organic rich layers, but rather, occurs as sparse clusters of randomly oriented crystals or individual crystals randomly distributed in both silty and clay rich layers (**Figure 2.5E, 2.5F**). Elongate lens shaped pyrite framboids are rare. On the basis of thin section observations, samples in this lithofacies are highly anisotropic.

Lithofacies 4: Lenticular bedded mudstones

The mudrocks of lithofacies 4 occur primarily in the lower 35m of the Otter Park. In thin section it consists of discontinuous, wavy to straight, parallel laminae as shown in **Figure 2.6B** and **2.6 C**. The discontinuous, elongate lenticular laminae are made of fine grained quartz, and they sit in a clay-organic matter matrix whose concentration varies. In more clay rich intervals, as shown in **Figure 2.6C**, quartz lenses are thinner and more discontinuous than in clay-poor intervals (**Figure 2.6B**). Reflected light images show some pyrite grains randomly distributed in the rock matrix (**Figure 2.6D**). Mudstones in this lithofacies are also highly anisotropic on the basis on thin section observations because their lenticular laminae are strongly aligned.

Lithofacies 5: Calcareous mudstones

This lithofacies is only found in the Evie member. It is rich in carbonate minerals and consists of gray, massive to thinly bedded calcareous mudstones and limestones. Thin section images shown in **Figures 2.7A** and **2.7D** show elongate, bedding parallel bioclasts sitting in an organic rich

matrix. Images taken under reflected light show some pyrite grains, but also emphasize the bedding parallel texture defined by matrix components (**Figures 2.7B** and **2.7C**). The strongly aligned bioclasts indicate that these mudstones are highly anisotropic.

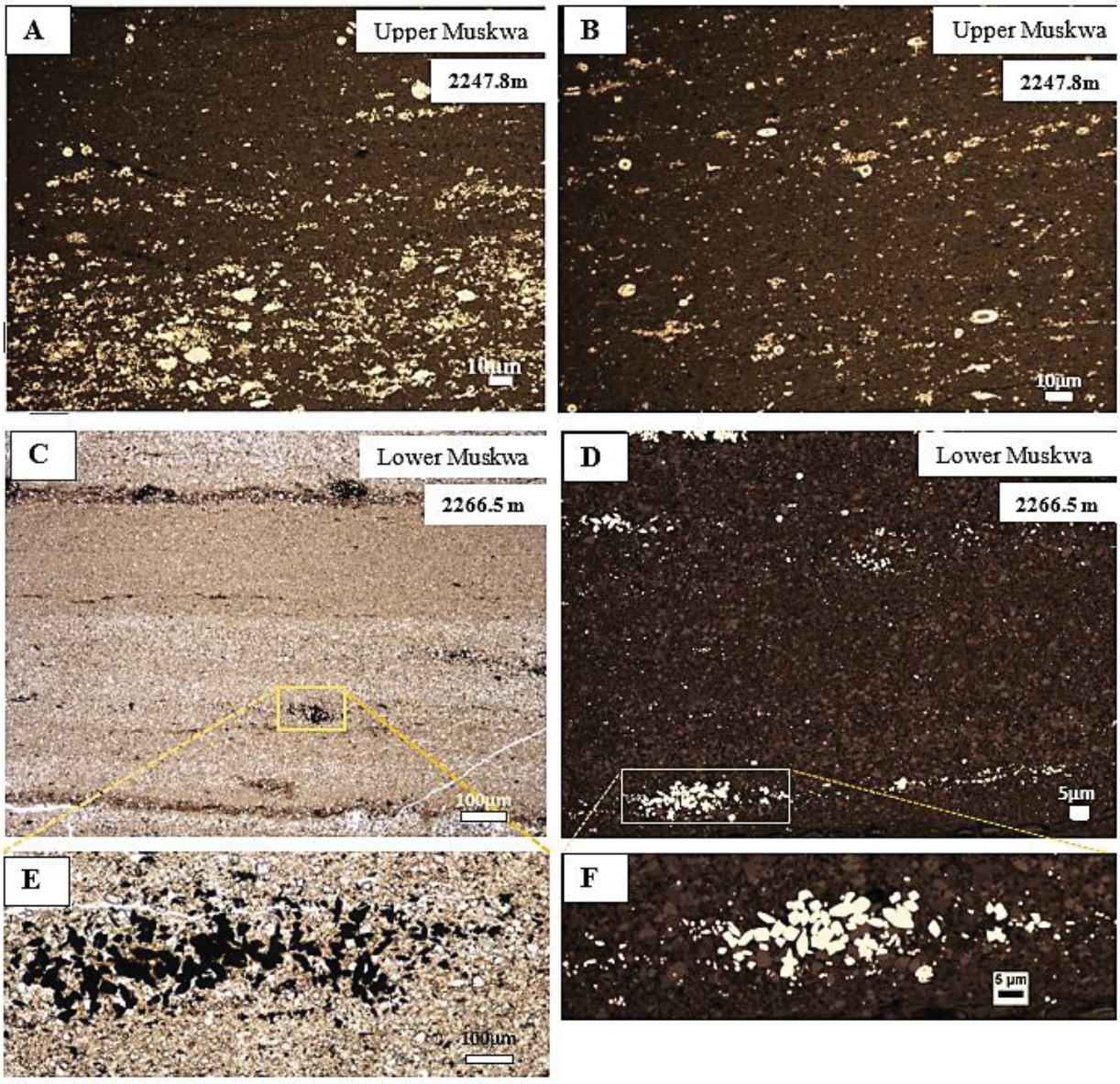

Figure 2.3: Thin section images of Muskwa samples cut perpendicular to the bedding plane. Images C and E were taken under plane polarized light and images A, B, D and F were taken under reflected light on polished thin sections. Textural properties and mineralogy at 2247.8m (A and B) were challenging to determine under plane polarized light because of organic richness. Under reflected light, however, randomly dispersed pyrite-replaced shell fragments were observed. Under reflected light (C) shows sub-angular to angular opaque clusters sparsely distributed in a quartz rich matrix. Images (D) and (E) confirm that opaque clusters in (C) are pyrite clusters (framboids).

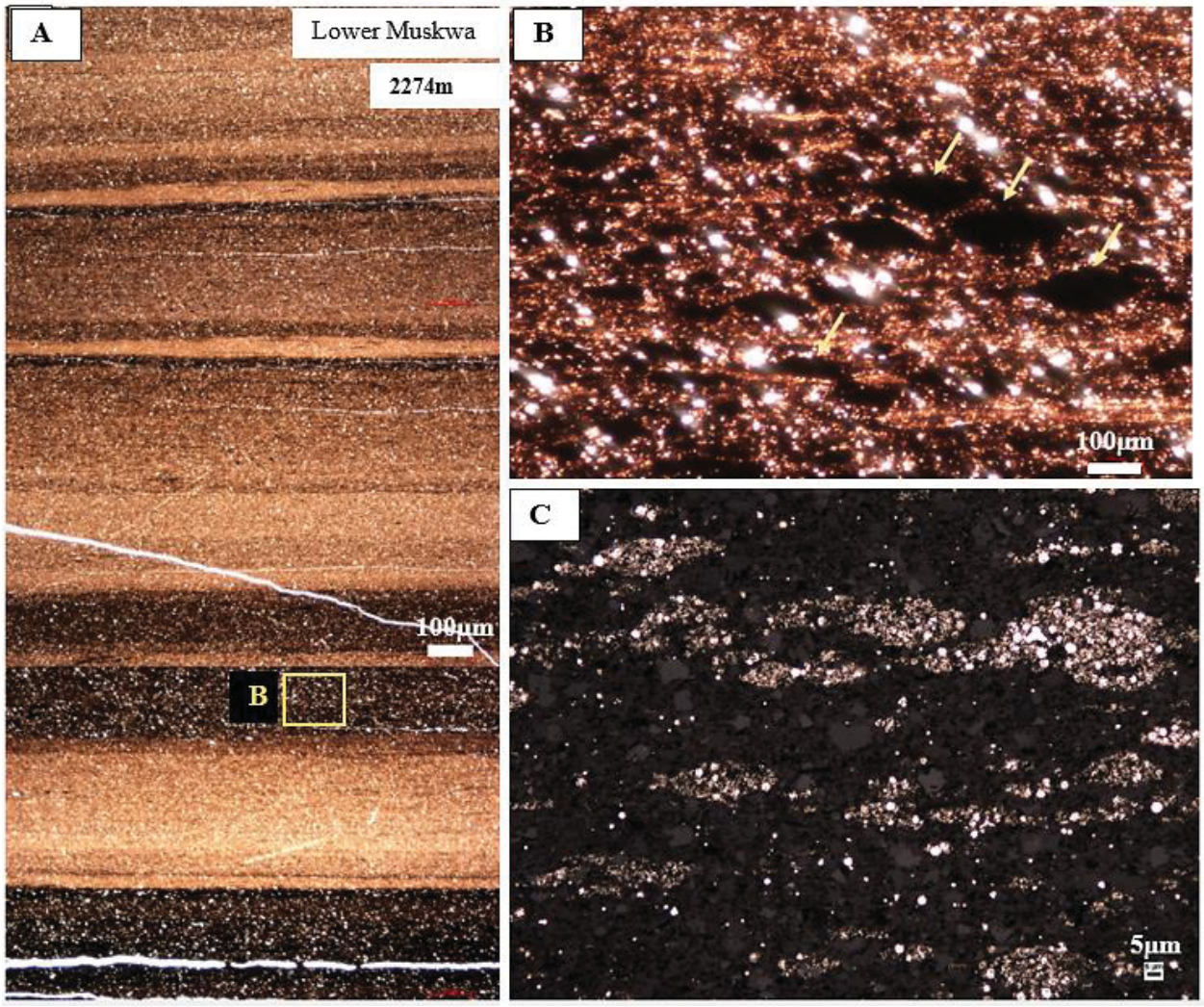

Figure 2.4: Thin section images of a Lower Muskwa sample cut perpendicular to the bedding plane. Images A and B were taken under plane polarized light, while C was taken under reflected light on a polished thin section. (B) is a magnification of the area marked 'B' in **Figure (A)** and **(C)** confirms that elongate, bedding parallel, lens shaped components in the clay and organic rich layers are pyrite clusters (framboids).

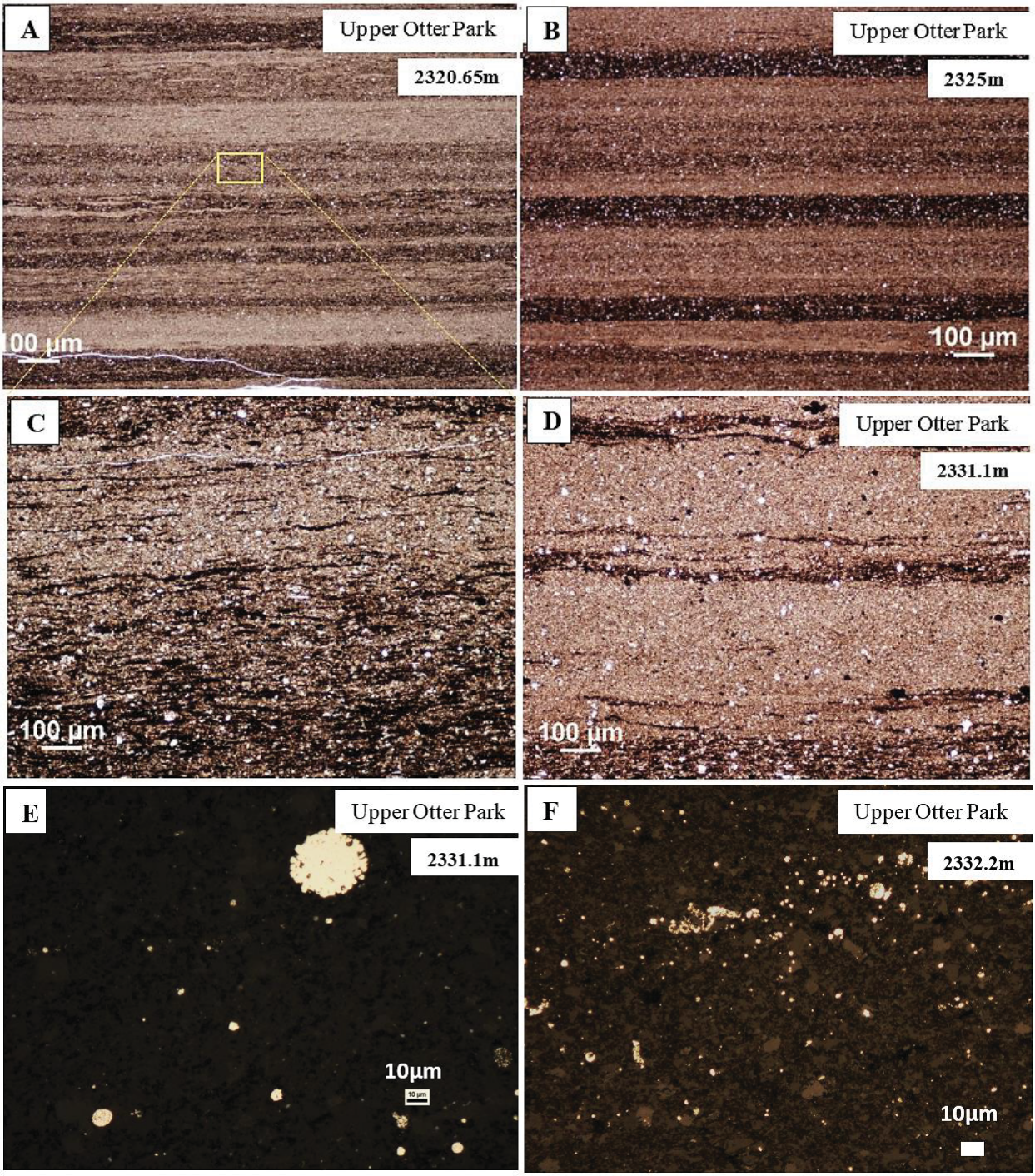

Figure 2.5: Thin section images of Upper Otter Park samples. Images A, B, C and D were taken under plane polarized light while E and F were taken under reflected light on polished thin sections. Image (C) is a magnification of the rectangle enclosed area in (A). It shows bedding parallel organic matter stringers. Images (E) and (F) show pyrite framboids and crystals occurring randomly in the rock matrix.

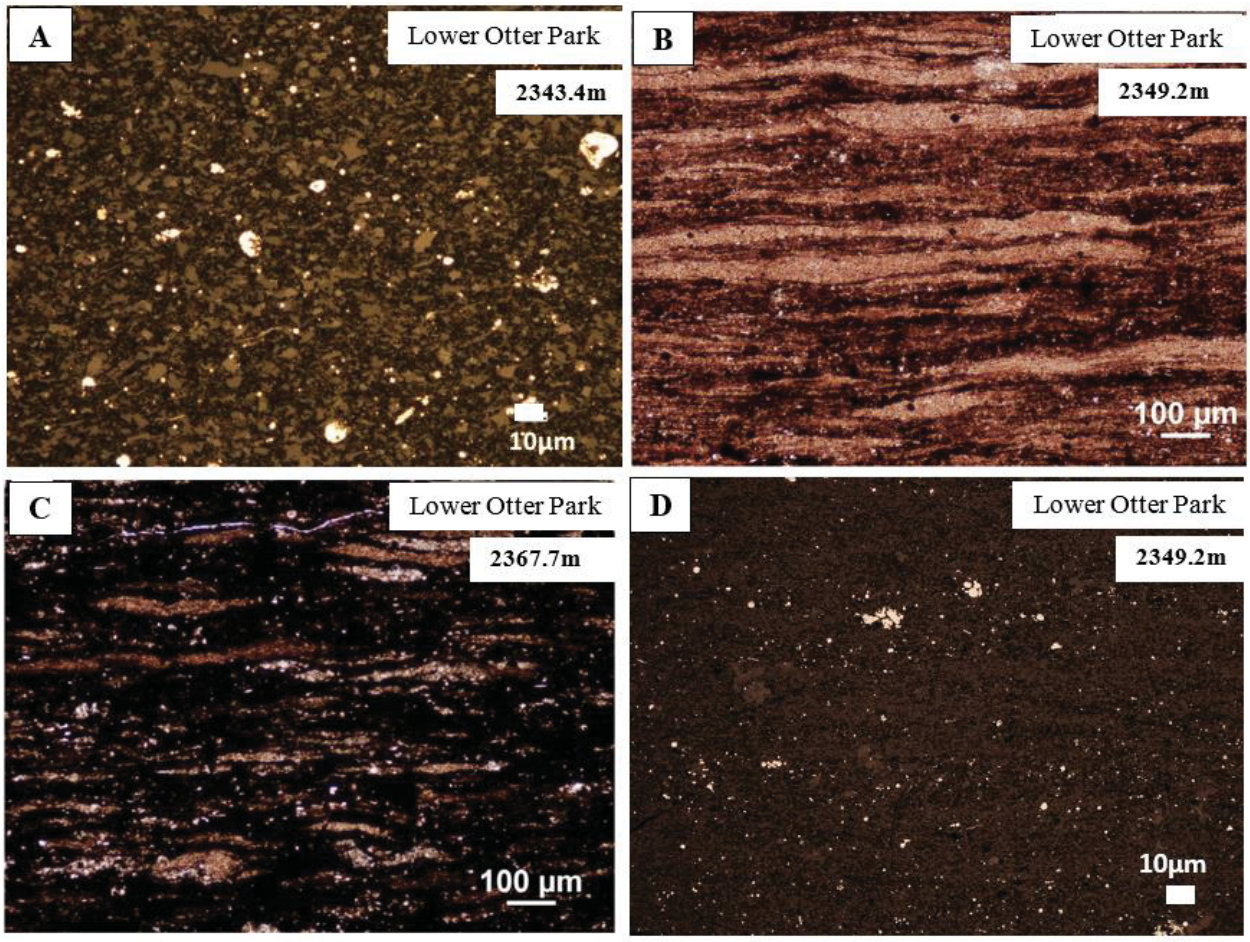

Figure 2.6: Thin section images of Lower Otter Park samples. Images B and C were taken under plane polarized light, and images A and D were taken under reflected light on polished thin sections. Reflected light images show randomly dispersed pyrite crystals.

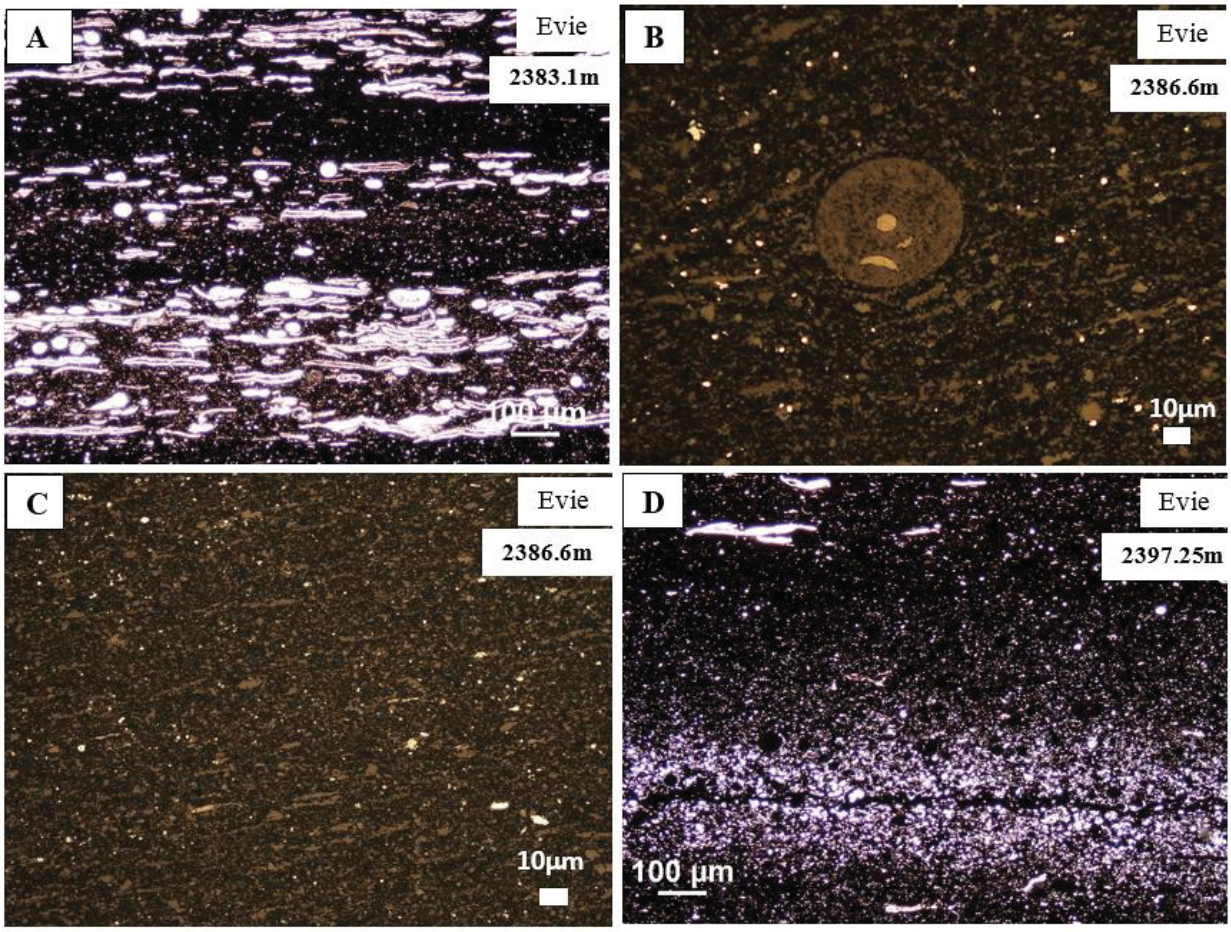

Figure 2.7: Thin section images of Evie samples. Images A and D were taken under plane polarized light, and images B and C were taken under reflected light on polished thin sections. Strongly aligned shell fragments indicate that the Evie is strongly anisotropic.

2.3 References

British Columbia Ministry of Energy and Mines., 2011. Ultimate Potential for unconventional natural gas in northeastern British Columbia's Horn River Basin, pp. 39.

British Columbia Oil and Gas Commission., 2012. Investigation of observed seismicity in the Horn River Basin, pp. 29.

Chalmers, G.R.L., Ross, D.J.K., and Bustin, R. M., 2012. Geological controls on matrix permeability of Devonian Gas shales in the Horn River and Liard basins, northern British Columbia, Canada. International Journal of Coal Geology. 103, 120-131.

Chen, Z., and Hannigan, P., 2015. A shale gas resource potential assessment of Devonian Horn River Strata using a well-performance method. Canadian Journal of Earth Science, 53, 156-167.

Ferri, F., Hickin, A.S., and Reyes, J., 2012. Horn River basin–equivalent strata in Besa River Formation shale, northeastern British Columbia (NTS 094K/15). In: Geoscience Reports 2012, British Columbia Ministry of Energy and Mines, 1-15.

Morrow, D.W., Zhao, M., and Stasiuk, L.D., 2002. The gas-bearing Devonian Presqu'ile dolomite of the Cordova embayment region of British Columbia, Canada: dolomitization and the stratigraphic template. AAPG Bulletin, 86 (9), 1609-1638.

Perez, M., Goodway, B., and Purdue, G., 2012. Integrated workflows for shale gas and case study results for the Horn River Basin, British Columbia, Canada. The Leading Edge, Special section: Seismic inversion for reservoir properties.

Reynolds, M.M., and Munn, D.L., Development update for an emerging shale gas giant field-Horn River Basin, British Columbia, Canada. SPE 130103.

Ross, D.J.K., and Bustin, R.M., 2008. Characterizing the shale gas resource potential of Devonian Mississippian strata in the Western Canada sedimentary basin: Application of an integrated formation evaluation. American Association of Petroleum Geologists Bulletin, 92(1), 87-125. doi:10.1306/09040707048.

Williams, G. K., 1983. What does the term Horn River Formation mean? Bulletin of Canadian Petroleum Geology, 31, 117-122.

Chapter 3

Room temperature magnetic susceptibility and Anisotropy of Magnetic Susceptibility (AMS)

3.1 Magnetic susceptibility

3.1.1 Introduction

All materials consist of charged particles (electrons) in motion. The motion of electrons about their axis and about their nucleus generates currents which in turn produce magnetic fields. In an external magnetic field of magnitude H, the motion of electrons is modified, and a magnetization M is induced in the material. The ratio of induced magnetization (magnetic moment per unit volume) to magnetic field intensity is the material's magnetic susceptibility χ.

$$\chi_v = \frac{M}{H} \tag{3.1}$$

where χ_v, called the volume susceptibility, is the magnetic susceptibility per unit volume. M and H are in units of A/m so volume magnetic susceptibility is dimensionless. It can be converted to magnetic susceptibility per unit mass χ_m (mass susceptibility) as follows:

$$\chi_m = \frac{\chi_v}{d} \tag{3.2}$$

where d is the density of the material and mass magnetic susceptibility is in $m^3\,kg^{-1}$.

The application of magnetic susceptibility to rock studies relies on the fact that each mineral or rock constituent has a characteristic response in an external magnetic field, and thus a characteristic magnetic susceptibility or range of magnetic susceptibilities. The magnetic susceptibility of a rock sample can therefore provide useful information not only about its composition, but also its mineral concentrations.

3.1.2 Classes of magnetic materials

Based on the response of electron spins or atomic moments to an external magnetic field, materials are classified as diamagnetic, paramagnetic, ferromagnetic, ferrimagnetic or antiferromagnetic. The following is a description of each class of material.

Diamagnetism

Induced magnetization, M, and applied field strength, H, are directly proportional, so magnetic flux density, B, and H are also directly proportional. As the magnetic susceptibility, χ, relates M and H, the magnetic permeability, μ, relates B and H.

$$B = \mu H \tag{3.3}$$

where

$$\mu = \mu_0 (1 + \chi) \tag{3.4}$$

where μ_0 is the permeability of free space ($4\pi \times 10^{-7}$ V.s/A.m).

Combining equations (3.1), (3.3) and (3.4) yields

$$B = H + 4\pi M \tag{3.5}$$

Dividing equation (3.5) by H yields

$$B/H - 1 = 4\pi M/H$$

$$B/H - 1 = 4\pi \chi_v \tag{3.6}$$

where B/H is the magnetic permeability of the material. If (B/H -1) < 0, B < H and χv (magnetic susceptibility) is negative, a material is said to be diamagnetic (Jain et al 2007).

Diamagnetic materials have filled atomic shells (all electrons are paired). As such, magnetic moments produced due to the orbital motion of electrons cancel out, resulting in zero net magnetization in the absence of an external magnetic field. In an applied magnetic field, changes in the orbital motion of electrons produces a weak magnetic dipole moment that in accordance with Lenz's law, opposes the external applied field (Aruldhas, 2010; Jain et al, 2007). The magnitude of the induced magnetization is very small, typically on the order of -10^{-5} CGS units or -0.8×10^{-7} SI, and it decreases as the external magnetic field is increased (**Figure 3.1**). When the external field is removed, net magnetization returns to zero.

Diamagnetism is a property of all materials, but because it is so weak, it is overshadowed where stronger forms of magnetism (paramagnetism or ferromagnetism) are also present. Water, oil, quartz, calcite and dolomite are examples of diamagnetic substances and minerals (Thompson and Oldfield, 1986).

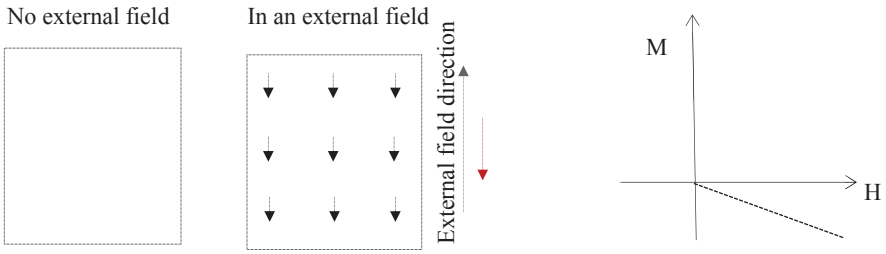

Figure 3.1: Arrangement of magnetic moments in a diamagnetic material and the associated magnetization (M) versus applied field (H) plot.

Paramagnetism

If $(B/H - 1) > 0$, $B > H$ and χ_v (magnetic susceptibility) is positive, a material is said to be paramagnetic (Jain et al., 2007). Individual atoms that make up paramagnetic materials possess permanent magnetic moments due to the spin of unpaired electrons in partially filled orbitals. As long as atomic moments do not interact with one another and because of thermal agitation, permanent moments are randomly oriented, cancelling out to produce a net magnetization of zero in the absence of an external magnetic field. When a magnetic field is applied, the torque produced acts on the atomic moments, causing them to tend towards alignment in the direction of the applied

field. The result is a partial alignment of moments in the direction of the applied field and a small positive net magnetization that increases with increased alignment of moments as applied field increases (**Figure 3.2**). As the field is removed, atomic moments become increasingly randomized by their thermal agitation. When the field is completely removed, the moments completely randomize, cancelling out to produce zero net magnetization.

Paramagnetic magnetic susceptibility is typically on the order of 10^{-3} SI to 10^{-5} SI. Since paramagnetic susceptibility is small compared to ferromagnetic and ferrimagnetic susceptibility, its contribution to the bulk susceptibility of a sample will only be significant if there is very little to no ferromagnetic and ferrimagnetic contribution. Clays like illite, chlorite, and smectite, as well as pyrite are examples of common paramagnetic minerals in mudrocks (Parés, 2015).

There is an inverse relationship between paramagnetic susceptibility and temperature. This increase in paramagnetic susceptibility with decreasing temperature is described by the Curie-Weiss law. It is explained by the decrease in thermal agitation or excitement of atomic or ionic sub-lattices, and hence increase in ordering of atomic moments with decreasing temperature. At increasingly lower temperatures, thermal energy kT (k= Boltzmann constant= 1.38×10^{-16} erg/K) is increasingly less than the energy required to align atomic moments in the direction of applied field.

Paramagnetism is also observed in ferromagnetic materials that are above their Curie temperature and in antiferromagnetic materials that are above their Néel temperature. Above these temperatures, thermal energy overcomes the interaction energy between the adjacent spins. Curie's law is only valid for temperatures below the saturation magnetization of a material's components since above the saturation magnetization, all atomic moments are already aligned parallel to the applied field and no additional increase in magnetization is possible with further increase in applied field.

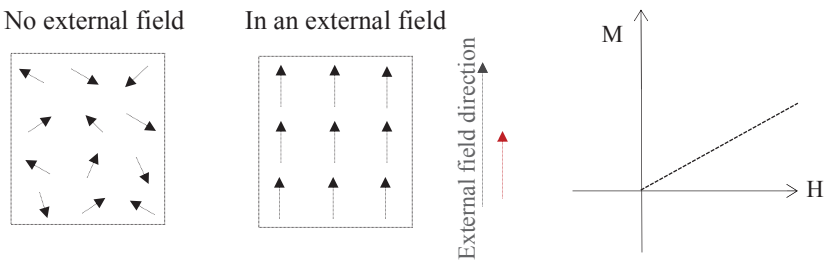

Figure 3.2: Arrangement of magnetic moments in a paramagnetic material and the associated magnetization (M) versus applied field (H) plot.

Ferromagnetism

In ferromagnetic materials, a strong coupling or interaction of neighbouring magnetic moments causes parallel alignment of moments within magnetic domains. In an applied field, all moments align parallel to themselves and to the applied field resulting in a net magnetization several orders of magnitude larger than that of paramagnetic materials. When the field is removed, net magnetization does not return to zero as with paramagnetism, rather the material retains some of the magnetization. This magnetization that remains after removal of the applied field is called remanent magnetization and has found applications in paleomagnetism and rock fabric studies.

With increasing field strength, induced magnetization increases to a maximum $\boldsymbol{M}_s$ called the saturation magnetization (**Figure 3.3**), above which any further increase in applied field strength results in no increase in induced magnetization. At and above the saturation magnetization, all atomic and ionic moments in the material are aligned in the direction of the applied field.

Ferromagnetism does not occur at all temperatures. Above a critical temperature, $T_{c,,}$ called the Curie temperature, thermal energy overcomes the interaction induced order of moments, causing the material to behave like a paramagnet. Above the Curie temperature, ferromagnets will therefore obey the Curie-Weiss law. Ferromagnetism is common in transition metals, especially oxides of nickel, cobalt and iron.

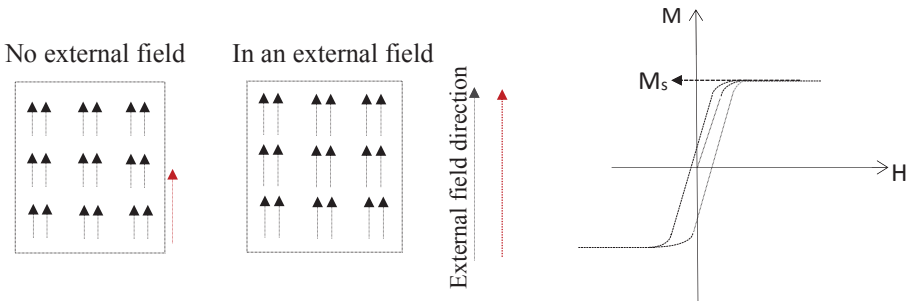

Figure 3.3: Arrangement of magnetic moments in a ferromagnetic material and the associated magnetization (M) versus applied field (H) plot.

Ferrimagnetism

In ferrimagnetic materials, a strong coupling also exists between the moments of neighbouring electrons or ions. Unlike ferromagnetism where the moments of coupled sub-lattices are equal and parallel, coupled moments of sub-lattices in ferrimagnetic materials are unequal and antiparallel (**Figure 3.4**). Since the magnetic moment of one sub-lattice is stronger, ferrimagnets have a resultant net magnetization. Like ferromagnets, they also retain a remanent magnetization when an applied field is removed, and they become paramagnets above the Curie temperature. Magnetite is an example of a ferrimagnetic mineral with a Curie temperature of about 580°C (Smith, 1956).

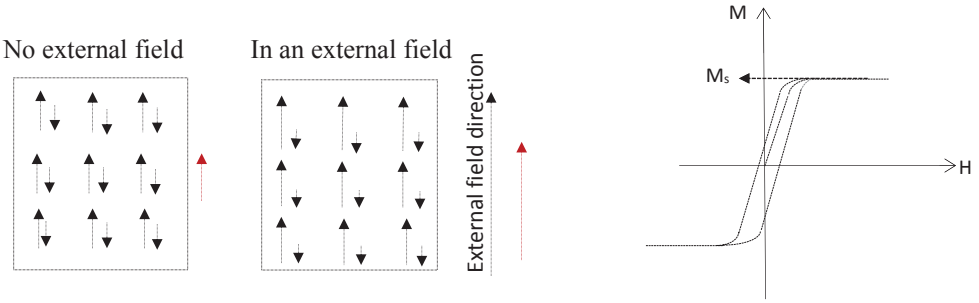

Figure 3.4: Arrangement of magnetic moments in a ferrimagnetic material and the associated magnetization (M) versus applied field (H) plot.

Antiferromagnetism

In antiferromagnetism, two coupled sub-lattices have equal but antiparallel magnetic moments (**Figure 3.5**). When the two sub-lattices are perfectly equal and anti-parallel, there will be no net magnetization. However, if sub-lattices have slightly canted moments, a weak net magnetization is observed. Antiferromagnetic materials have a small positive susceptibility, and upon removal of an external field, do no retain a remanent magnetization.

Above a critical temperature known as the Néel or ordering temperature (T_N), thermal energy becomes large enough to disrupt the magnetic ordering of moments and antiferromagnetic materials become paramagnetic. Ilmenite is an example of an antiferromagnetic mineral (Merrill, 2010) and hematite is an example of a canted antiferromagnetic mineral (Dunlop and Ozdemir, 1997; Bødker et al. 2000).

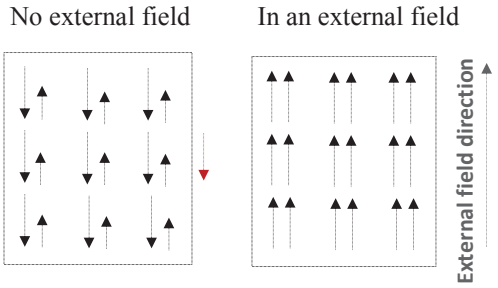

Figure 3.5: Arrangement of magnetic moments in an antiferromagnetic material.

3.1.3 Magnetic minerals in mudrocks

Shales and mudstones are a heterogeneous mix of diamagnetic, paramagnetic and small amounts of ferrimagnetic minerals. Clay minerals are the primary paramagnetic minerals and along with the primary diamagnetic minerals (quartz and calcite), make up more than half of the total composition of an average mudrock. Other paramagnetic minerals like pyrite and feldspar are usually present in secondary amounts (Grim et al 1937; Yaalon, 1962).

Illite and chlorite are the most common clay minerals in mudrocks, but smectite and kaolinite may also be present. They are all sheet silicates consisting of two fundamental units: SiO_4 tetrahedra

and Mg^{2+}, Al^{3+} or Fe^{2+} octahedra. SiO_4 tetrahedra consist of silicon or aluminium atoms bonded to four oxygen atoms, while octahedra consist of aluminium, magnesium or iron cations bonded to either six hydroxyl (OH^-) ions or two hydroxyl ions and four oxygen atoms (**Figure 3.6**). Clay minerals differ in the type of cations they contain and in the stacking pattern of tetrahedral and octahedral sheets (Bjorlykke, 2010).

Illite is a 2:1 sheet silicate, that is, each unit consists of two silica tetrahedra with an octahedral layer whose central cation is Al^{3+}. The octahedral layer is sandwiched between the two tetrahedral layers (TOT structure). Two TOT units are joined by K^+ ions of the interlayer (**Figure 3.8**). Smectite, another 2:1 sheet silicate, has an interlayer that expands when water replaces potassium in the interlayer (Bjorykke, 2010). Chlorite is a 2:1:1 sheet silicate consisting of two tetrahedral layers and two magnesium (Mg^{2+}) or iron (Fe^{2+}, Fe^{3+}) dominated octahedral layers (TOTO structure) (**Figure 3.7**). There can be substantial substitution of ions in the octahedral and tetrahedral sites, so although two different illite samples, for example, have the same basic structure, their specific chemical compositions will vary.

The response of a given clay mineral to an applied magnetic field (magnetic susceptibility) is dependent on the concentration of iron (Fe^{2+}, Fe^{3+}) and sometimes manganese (Mn^{2+}) in the octahedral layers. **Table 3.1** lists the important clay minerals, their general chemical formulas and typical mass magnetic susceptibilities. Chlorites are usually richer in iron than other paramagnetic clays so typically have significantly higher magnetic susceptibilities.

Quartz (SiO_2), calcite ($CaCO_3$), and sometimes dolomite ($CaMg(CO_3)_2$) are the main diamagnetic minerals in mudrocks. Their diamagnetism is due to an adjustment in the orbital motion of electrons such that a weak field that opposes an applied field is produced according to Lenz's law. **Table 3.1** also lists the range of magnetic susceptibilities for these minerals.

Small amounts of the ferrimagnetic mineral magnetite (Fe_3O_4) may also be present in mudrocks. Magnetite has an inverse spinel structure (Hill et al., 1979). It consists of oxygen ions that are packed in a cubic arrangement and are in tetrahedral and octahedral coordination with divalent and trivalent iron (Fe^{2+} and Fe^{3+}). Fe^{3+} ions occupy both tetrahedral and octahedral sites while Fe^{2+} ions only occupy tetrahedral sites (Cornell and Schwertmann, 2006). The tetrahedral and octahedral sites comprise the two magnetic sublattices, A and B, with antiparallel spins (Butler, 1992). Like paramagnetic minerals, its response in an applied field is related to its iron content,

but because of strong interactive forces between moments, its magnetic susceptibilities are orders of magnitude greater than those of paramagnetic minerals (**Table 3.1**).

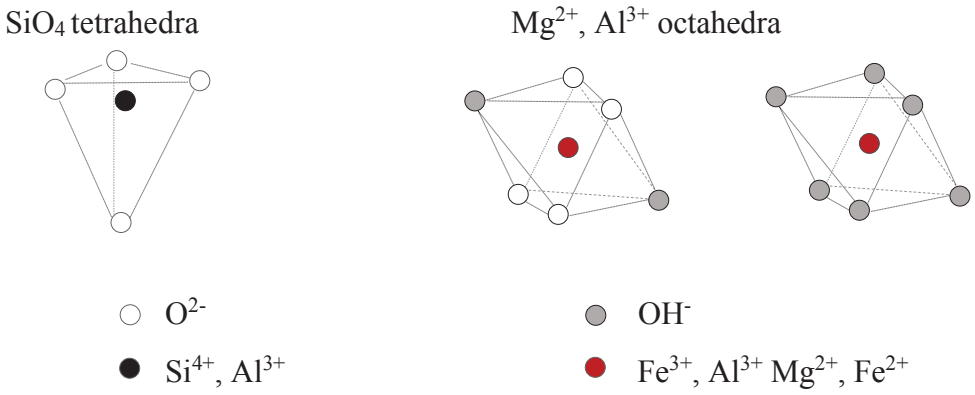

Figure 3.6: Schematic of the fundamental units that make up sheet silicates (modified from Bjorlykke, 2010).

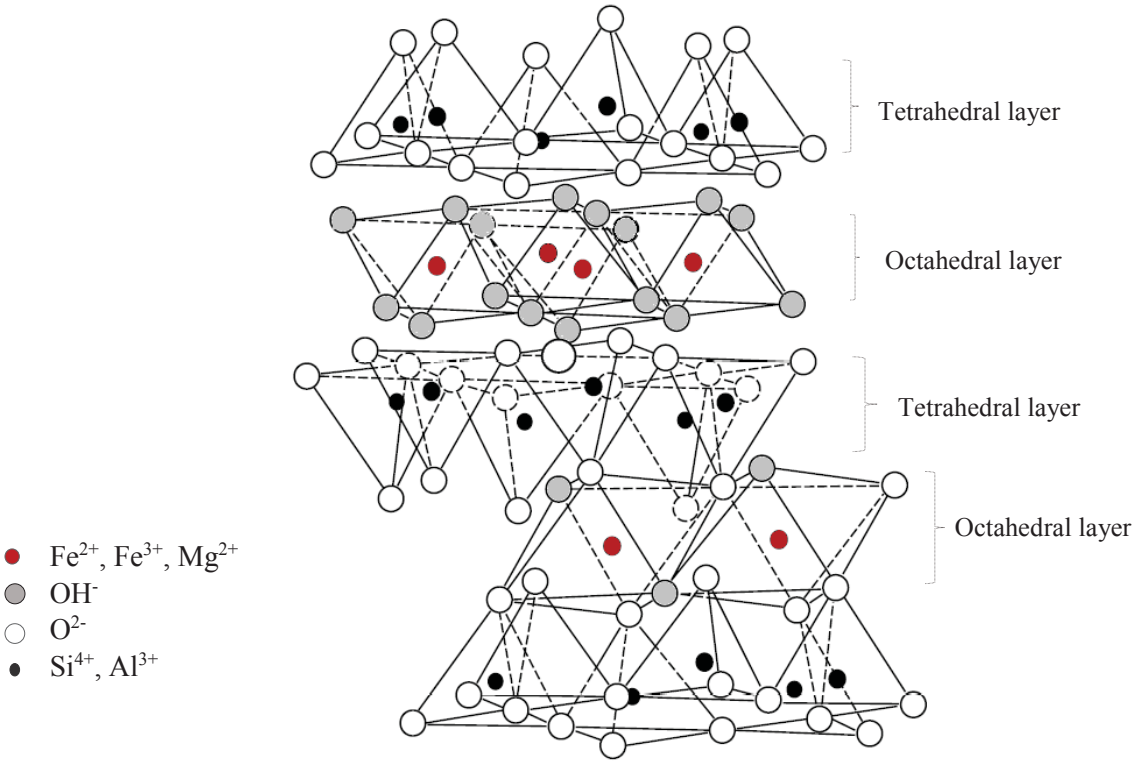

Figure 3.7: Illustration showing the basic chemical structure of chlorite (modified from Ballet et al., 1985; McLean and Gribble, 2003).

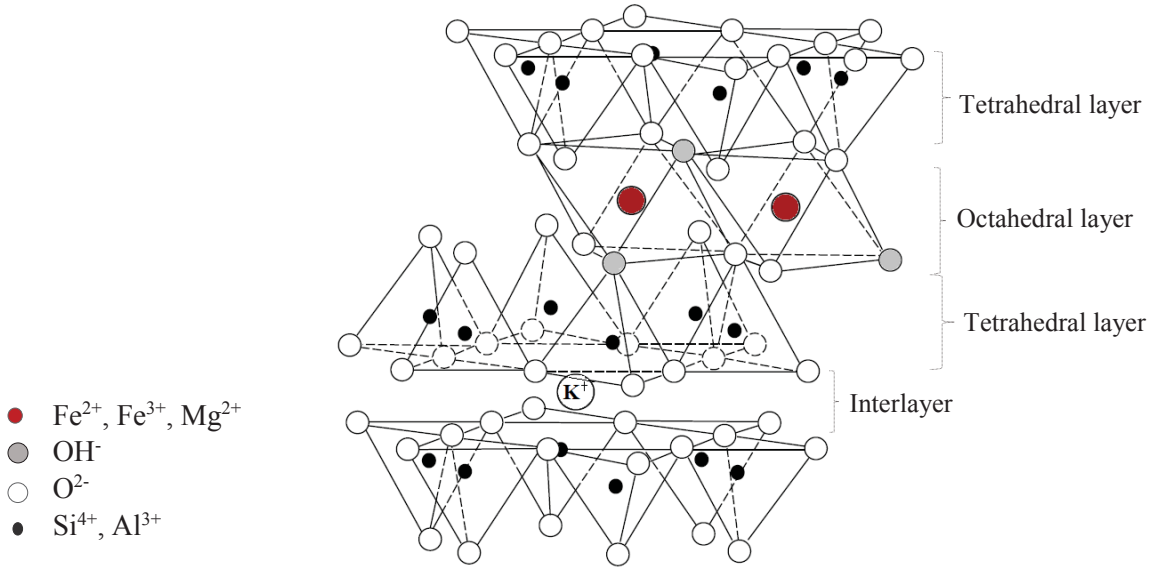

Figure 3.8: Illustration showing the basic chemical structure of illite (modified from Ballet and Coey, 1982; McLean and Gribble, 2003).

Table 3.1: Chemical formulas and magnetic susceptibilities of magnetic minerals common in shales and mudstones (Brace, 1965; Thompson and Oldfield, 1986; Carmichael, 1989; Deer et al, 1992; Tarling and Hrouda, 1993; Dunlop and Ozdemir, 1997).

Mineral	Chemical formula	Magnetic susceptibility ($10^{-8}m^3kg^{-1}$)
Paramagnetic		
Illite	$(K_{1-1.5}Al_4)[(Si_{7-6.5}Al_{1-1.5}O_{20}](OH)_4$	15
Chlorite group	$(Mg,Al,Fe)_{12}[(Si,Al)_8O_{20}](OH)_{16}$	2.5 – 55.4
Smectite group	$(½Ca, Na)\ 0.7(Al, Mg, Fe)_4[(Si, Al)_8O_{20}]\ nH_2O$	3.2
Pyrite	FeS_2	0.05 - 5
Diamagnetic		
Kaolinite	$Al_2Si_2O_5\ (OH)_4$	-2
Quartz	SiO_2	-0.5 to -0.6
Calcite	$CaCO_3$	-0.48
Dolomite	$CaMg\ (CO_3)_2$	-1.2
Ferrimagnetic		
Magnetite	Fe_3O_4	20000 - 110000

3.2 Anisotropy of Magnetic Susceptibility (AMS)

3.2.1 Theoretical background

If the magnetization, M, induced in a sample by an external magnetic field of constant strength H, is dependent on the direction in which the external field is applied, the sample is magnetically anisotropic. Anisotropy of magnetic susceptibility (AMS) is a measure of the variation of magnetic susceptibility with direction. It is described by a symmetric, second-rank tensor k_{ij} whose relationship with induced magnetization, M, and applied field strength, H, is described by the following set of linear equations:

$$\begin{bmatrix} M_1 \\ M_2 \\ M_3 \end{bmatrix} = \begin{bmatrix} K_{11} & K_{12} & K_{13} \\ K_{21} & K_{22} & K_{23} \\ K_{31} & K_{32} & K_{33} \end{bmatrix} \begin{bmatrix} H_1 \\ H_2 \\ H_3 \end{bmatrix} \quad (3.7)$$

The susceptibility tensor k_{ij} can be geometrically represented by an ellipsoid with three orthogonal principal axes (**Figure 3.5**). The eigenvectors of k_{ij} define the directions of maximum, intermediate, and minimum directions of susceptibility, while its corresponding eigenvalues (k_1, k_2 and k_3) are the values of magnetic susceptibilities in the three principal directions (Rochette et al. 1992).

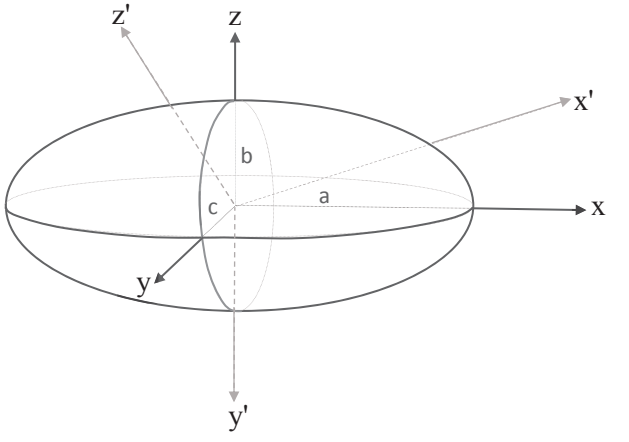

Figure 3.9: The magnetic susceptibility ellipsoid and its three orthogonal axes.

For any given sample, the susceptibility ellipsoid represents the average preferred orientation of grains or the average grain shape. It is spherical ($k_1 = k_2 = k_3$) when a sample is magnetically isotropic (consists of randomly oriented grains), and increasing prolate (rod shaped with $k_1 > k_2 = k_3$) or oblate (disk shaped with $k_1 = k_2 > k_3$) as the magnitude of the anisotropy of magnetic susceptibility increases (Hounslow, 1985).

3.2.2 Petrofabric controls on the anisotropy of magnetic susceptibility (AMS)

The degree of anisotropy of magnetic susceptibility of a sample and the shape of its susceptibility ellipsoid are dependent on the following:

1. The anisotropy of individual matrix components
2. The degree of alignment of matrix components

3.2.2.1 Anisotropy of individual matrix components

Intrinsic to each magnetic phase present in a sample is a crystalline and shape anisotropy. Crystalline anisotropy arises when because of lattice structure, a material's atomic moments preferentially align along an energetically favorable direction known as the easy axis. In an applied field, induced magnetization is highest in this direction and k_1 (k_{max}) is parallel to it. Shape anisotropy on the other hand is due to grain shape. For an elongate grain, k_1 (k_{max}) is parallel to the grain long axis and k_3 (k_{min}) is perpendicular to it. This would represent a **normal fabric**.

Where ferrimagnetic or ferromagnetic grains are present, depending on domain state and grainsize, the orientation of k_{max} and k_{min} for a grain with shape anisotropy will vary (Stephenson et al. 1986). In an applied field, small grains (typically ~1μm for magnetite) known as stable single domain (SD) grains are easily magnetized along the short axis i.e., k_1 (k_{max}) is perpendicular to the grain long axis. This would produce an **inverse fabric**. Larger grains known as multidomain (MD) grains have k_1 (k_{max}) parallel to grain long axis producing the more common normal fabric.

Magnetic domains

A magnetic domain is a volume in a ferromagnetic or ferrimagnetic material in which all magnetic moments are parallel and magnetized in the same direction. Magnetic domains form in order to reduce the self-demagnetizing energy (magnetostatic energy) associated with the distribution of

surface charges produced by magnetic dipoles. The number of domains decreases with decreasing grainsize. Large grains called multidomain (MD) grains have several domains separated by domain or Bloch walls while small grains known as single domain (SD) grains have only one domain (**Figure 3.10**). The SD grainsize is defined by the point where the energy required to build a domain wall exceeds the reduction in magnetostatic energy resulting from creating a new domain. Above the SD grainsize, the decrease in magnetostatic energy resulting from creating each domain exceeds the energy required to build the associated domain wall (Butler, 1992).

For a single domain grain dominated by crystalline anisotropy, magnetic susceptibility is minimum parallel to the easy axis and maximum parallel to the hard axis. This is because the grain is already magnetized to its saturation magnetization along its easy axis; any further application of a magnetic field in that direction induces no magnetization. If shape anisotropy dominates, minimum magnetic susceptibility is parallel to the grain's long axis and maximum susceptibility is parallel to the grain's short axis. Parallel to the long axis, magnetostatic energy is minimum (reduced surface area results in fewer surface charges (**Figure 3.11**)) so the grain is magnetized to its saturation (Tarling and Hrouda, 1993). For a multidomain (MD) grain dominated by shape anisotropy, maximum magnetic susceptibility, k_1 (k_{max}), is parallel to the grain's long axis since the moments of the different domains can still be forced into alignment with the applied field, i.e., saturation magnetization is yet to be achieved in this direction.

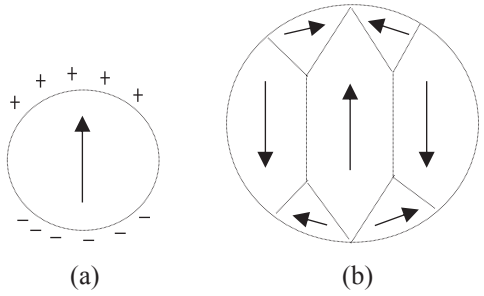

Figure 3.10: (a) A spherical single domain grain with magnetization direction shown by arrow. Surface charges are depicted by plus and minus signs. (b) A spherical multidomain grain with arrows showing the magnetization direction of different domains. Domains are separated by Bloch or domain walls (Butler, 1992).

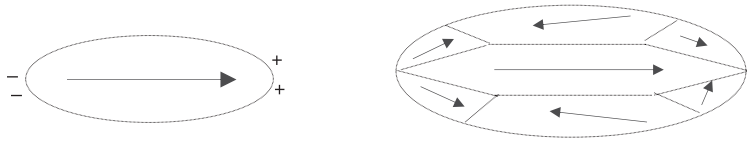

Figure 3.11: (a) Surface charge distribution for an elongate single domain grain. Arrow depicts the direction of magnetization. (b) An elongate multidomain grain with arrows showing the magnetization direction of different domains (Butler, 1992).

3.2.2.2 Degree of alignment of matrix components

The overall alignment of matrix components in a given volume of rock is another factor that determines the value of anisotropy of magnetic susceptibility and the nature of the susceptibility ellipsoid. Preferred orientation in sedimentary rocks is the product of a combination of forces acting during sediment deposition through to rock formation. The primary forces responsible are lithostatic compression or overburden pressure, tectonic stress and gravity.

Compaction due to lithostatic compression involves the rearrangement of grains, expulsion of interstitial water, plastic deformation, brittle deformation and pressure solution. The resulting reduction in porosity is accompanied by a closer packing of grains and increased alignment of matrix components perpendicular to the compression direction (Wilston and Stanton, 1994; Lander and Walderhaug, 1999). As burial progresses and the alignment of matrix components increase, the degree of AMS increases and the susceptibility ellipsoid becomes more oblate. Because the extent of grain reorientation, water expulsion and deformation produce the distribution and orientation of matrix components observed in sedimentary rocks, magnetic fabrics can be used in understanding the progression of diagenetic alterations (Reese, 1968; Hirt et al. 1995).

Tectonic stresses may also cause minerals and other matrix components to be preferentially aligned. Graham (1966) and Hrouda and Ježek (1999) observed that the principal axes of the susceptibility ellipsoid are coincident with the principal axes of the strain ellipsoid in tectonically deformed sedimentary rocks. Initially, when mineral alignment is due solely to compaction, the susceptibility ellipsoid is oblate, with minimum magnetic susceptibility (k_{min}) perpendicular to the bedding plane and maximum susceptibility (k_{max}) parallel to the bedding or deposition plane. When

a uniform compression or shear stress is applied parallel to the bedding plane, minerals and other matrix components are reoriented (rotate without changing shape) or change their shape such that their long axes become perpendicular to the shortening direction. Principal axes are also reoriented; maximum susceptibility axes become perpendicular to the direction of shortening (bedding plane) and minimum susceptibility becomes parallel to it (Richter et al., 1991). Oblate ellipsoids as a result become increasingly prolate as lateral shortening continues (Owens, 1974).

Gravitational settling of grains from suspension onto a depositional surface may also produce preferentially oriented grains with an oblate magnetic fabric. In the absence of any current, deposited grains lie with their long axes parallel to but randomly distributed on the depositional plane.

3.2.2.3 Stringing together of magnetic grains

An assemblage of closely packed magnetic grains lying on a plane will also possess an anisotropy of magnetic susceptibility (Bhathal, 1971). As with a grain with shape anisotropy, maximum magnetic susceptibility will be parallel to long axis of the assemblage if it consists primarily of multidomain grains and perpendicular to the long axis if the assemblage consists mainly of single domain grains.

3.2.3 Literature review: Magnetic susceptibility and anisotropy of magnetic susceptibility in mudrocks

The application of magnetic susceptibility and anisotropy of magnetic susceptibility (AMS) to the understanding of depositional and tectonic fabrics in a wide range of rock types has been well demonstrated since the 1950s and 1960s (Graham, 1954; Rees, 1961; Girdler, 1961; Khan, 1962; Hamilton, 1963; Reese, 1965a; Reese 1965b; Graham, 1966; King, 1966; Khan and Rees, 1968). AMS results have been used in the assessment of current and paleoflow directions (Galehouse, 1968; Ellwood, 1980; Schieber and Ellwood, 1993), in the determination of stress and deformation directions (Jackson et al. 1989), and in the detection of small mineralogical variations (Robion et al. 1995; Lehman et al. 1996). Most applications in mudrock sequences have so far focused mainly

on tectonically produced fabrics and determination of paleocurrent directions (Auboug et al., 1991; Schieber and Ellwood, 1993; Chadima et al., 2006). Detailed studies on the origin of planar magnetic fabrics and factors controlling the magnetic response of undeformed and weakly mudrocks is still lacking, hence, the application of magnetic susceptibility and anisotropy of magnetic susceptibility in determining the spatial distribution of minerals and other matrix components in mudrocks remains underutilized.

The general consensus of the few existing studies is that the magnetic susceptibility of mudrocks is controlled primarily by the concentration of paramagnetic clays, especially illite and chlorite (Jackson et al. 1989; Hirt et al. 1995; Parés et al., 2004). Reported low field bulk susceptibilities are typically between 10^{-4} and 10^{-5}SI, indication that the contribution of ferrimagnetic minerals such as magnetite is typically minimal (Auboug et al., 1991; Larrasoaña et al 2011; Pares, 2015). Where ferrimagnetic minerals, particularly magnetite, dominate, bulk magnetic susceptibilities typically exceed 2000 $\times 10^{-6}$ SI (Larrasoaña et al., 2011). Siderite, a high susceptibility paramagnetic, iron-bearing carbonate, has also been observed to significantly control magnetic susceptibility in mudrocks (Chadima et al., 2006).

Previous studies also conclude that the alignment and distribution of paramagnetic clay minerals is the primary control on the anisotropy of magnetic susceptibility of mudrocks (Hirt et al., 1995; Chadima et al., 2006). Individual clay grains, by virtue of their sheet-like morphology, possess significant shape anisotropy hence have distinctly oblate susceptibility ellipsoids with minimum susceptibility axes parallel to their c-axes and maximum susceptibility axes parallel to their basal planes (Parry, 1971). In the absence of significant tectonic deformation, the alignment of clays as a result of gravitational settling and lithospheric compression due to burial therefore produces a normal magnetic fabric. Normal magnetic fabrics are characterized by k_{max} (maximum susceptibility) parallel to the bedding plane (depositional plane) and minimum susceptibility (k_{min}) normal to the bedding plane (Hamilton and Rees, 1970). Hounslow (1985) observed that the percent anisotropy of magnetic susceptibility and hence, degree of alignment of clay minerals in mudstones, i.e., massive, siliceous/calcareous, non-fissile mudrocks, was consistently lower than that of shales (fissile, clay rich mudrocks). Since the studied shales were more organic rich than the mudstones, Hounslow (1985) proposes that organic carbon may be play a vital role in the preferred orientation of clay minerals and AMS in mudrocks, although no direct correlation with

total organic carbon (TOC) was noted. Hounslow (1985) also proposed that in some cases, the degree of preferred alignment of rigid grains like quartz may also control the preferred alignment of phyllosilicates which tend to wrap around them as compaction progresses.

The magnetic susceptibility and anisotropy of magnetic susceptibility of some mudrocks have also been reported to be controlled by the concentration and preferred orientation of siderite, a paramagnetic iron carbonate which exhibits significant crystalline anisotropy. These mudrocks have characteristically higher bulk susceptibilities than those whose bulk magnetic susceptibilities are dominated by paramagnetic clays and their principal axes orientations define an inverse magnetic fabric (Hirt et al., 1991; Chadima et al., 2006). Inverse fabrics are the opposite of normal magnetic fabrics. They are characterized by maximum susceptibility axes normal to the bedding/depositional plane and minimum susceptibility parallel to the bedding plane.

3.3 Chapter goals

This chapter aims to determine the controls on the magnetic susceptibility and anisotropy of magnetic susceptibility of the Horn River Group. The different types of magnetic fabrics present in the shales and mudstones of the Muskwa, Otter Park and Evie are identified, and results are interpreted in terms of the 3D distribution of minerals and other matrix components. The chapter is divided into two main sections: bulk volume magnetic susceptibility and anisotropy of magnetic susceptibility.

3.4 Bulk volume magnetic susceptibility

In this section, the magnetic classes present in the Muskwa, Otter Park and Evie members are determined based on experimentally determined bulk magnetic susceptibilities. In combination with elemental compositions, the minerals and matrix components controlling bulk susceptibility are also determined.

3.5 Anisotropy of Magnetic Susceptibility (AMS)

Using a set number of directional magnetic susceptibilities, the AMS tensors and ellipsoids for samples from the Muskwa, Otter Park and Evie are computed. The degree of AMS is calculated from principal magnetic susceptibility magnitudes, and the matrix components

controlling AMS are determined. Principal axes orientations are also used as a quantitative means of discerning mineral/grain orientations and alignments.

3.4 Bulk volume magnetic susceptibility

3.4.1 Sample preparation

No sample preparation was required for the measurement of bulk volume magnetic susceptibility. The method and equipment used required only a smooth sample surface, and the cut faces of core samples were suitable measurement surfaces.

3.4.2 Materials and method

Bulk volume magnetic susceptibility of slabbed core from the Imperial Komie well was measured using a Bartington MS2E logging sensor. The logging sensor consists of a surface scanning sensor with a flat sensing surface at the end of a ceramic tube. The sensor is connected to the MS2E meter by a coaxial cable.

To perform a measurement, the sensing surface is held in contact with the surface of interest and a low field of 80 A m^{-1} is applied to the sample. The MS2E meter computes the bulk magnetic susceptibility for approximately 0.04cm^3 of sample. The surface sensor is held to the sample surface for the entire measurement period which is between 1.3 and 1.5 seconds. For 182m of Horn River Group core from the Imperial Komie well, bulk volume magnetic susceptibility measurements were taken every 0.25m in two directions; parallel to the bedding plane and perpendicular to the bedding plane.

3.4.3 Results and discussion

Figure 3.12 shows the bulk volume magnetic susceptibility with depth for the Horn River Group sequence from the Imperial Oil Komie well. The Muskwa, Otter Park and Evie formations are easily distinguished on the basis of their bulk volume magnetic susceptibilities. The Otter Park can

also be separated into three distinct sections that are not apparent on the gamma ray log which is also shown in **Figure 3.12**.

Bulk volume magnetic susceptibilities are highest in the Otter Park and lowest in the Upper Muskwa and Evie Formations. Values in the Upper Muskwa range from -0.1×10^{-5} SI to 5.4×10^{-5} SI with a few peaks of 9.5×10^{-5} SI to 13.4×10^{-5} SI. In the Evie, values are lower than those of the Upper Muskwa. They range from -1.6×10^{-5} SI to 3.5×10^{-5} SI, with more diamagnetic (negative bulk susceptibility) intervals than the Upper Muskwa. In the Otter Park values range from 0.6×10^{-5}SI to 25.2×10^{-5}SI and in the Lower Muskwa, they are between 1.8×10^{-5}SI and 16×10^{-5}SI.

Low overall bulk susceptibilities in all three formations suggest that the contribution of ferrimagnetic minerals like magnetite to susceptibility is minimal. Where ferrimagnetic minerals dominate the magnetic susceptibility signal, susceptibility is typically between 1000×10^{-6} SI and 100000×10^{-5} SI (Ferré et al. 2004). Since the bulk volume magnetic susceptibility of the Upper Muskwa and Evie are very small and positive, and negative in some intervals, these members are dominated by diamagnetic minerals. Increased bulk volume magnetic susceptibilities in the Otter Park indicate increased contribution of paramagnetic minerals to bulk susceptibility. Without comparison with results from other techniques however, it is not possible to discern which diamagnetic and paramagnetic minerals control bulk volume magnetic susceptibility.

3.4.3.1 Effect of chemical composition on bulk magnetic susceptibility

The minerals and matrix components contributing to the bulk volume magnetic susceptibility signal can be determined when bulk volume magnetic susceptibilities are compared with the chemical composition of samples. **Table 3.2** shows the chemical compositions of representative samples from the Muskwa, Otter Park and Evie. Oxide concentrations were determined at Acme Analytical Laboratories using Inductively Coupled Plasma Mass Spectrometry (ICP-MS) and total organic carbon (TOC) was determined by Weatherford Laboratories using LECO combustion. The later process involves treating ground samples with hydrochloric acid to remove inorganic carbon (like carbonates), and then combusting the dried samples in an oxygen-rich atmosphere. The mass

of CO_2 released during the combustion of organic matter (organic carbon) is converted to percent total organic carbon (TOC) based on the dry sample weight (Spencer, 1993; Schumacher, 2002).

Figure 3.13 shows the relationship between oxide concentrations and bulk volume magnetic susceptibility. The concentrations of iron, manganese and chromium are of primary importance because all three have large magnetic moments capable of dominating magnetic properties (Biedermann et al. 2014). Strong positive correlations between bulk volume magnetic susceptibility and Fe_2O_3 ($R^2 = 0.8$) as well as MnO ($R^2 = 0.71$) are noted, but no correlation is observed with Cr_20_3 (**Figure 3.13**). Samples contain only small amounts of manganese (<0.1wt. % MnO), so iron (Fe_2O_3 concentrations between 0.32 and 6.66 wt. %) is most likely responsible for higher bulk volume magnetic susceptibilities in the Otter Park. In mudrocks, paramagnetic clays like illite and chlorite and ferrimagnetic iron oxides like magnetite are the main sources of iron. To determine which is mainly responsible for the paramagnetic behaviour of the Otter Park, the concentrations of Al_2O_3 and K_2O (contained mostly in clay minerals) are compared with the concentrations of Fe_2O_3. A strong positive correlation between Al_2O_3 and FeO ($R^2 = 0.72$) and between K_2O and Fe_2O_3 ($R^2 = 0.71$) (**Figure 3.14**) indicates that paramagnetic clays, and not ferrimagnetic minerals like magnetite, are the main source of iron in the Horn River Group, and thus responsible for higher bulk susceptibilities in the Lower Muskwa and Otter Park members.

The concentrations of SiO_2 and total organic carbon (TOC) also determine the value of bulk volume susceptibility. Moderate to strong negative correlations are observed between bulk volume magnetic susceptibility and SiO_2 ($R^2 = 0.62$) and between bulk volume susceptibility and Total Organic Carbon (TOC) ($R^2 = 0.72$) (**Figure 3.12**). Higher quartz and organic matter concentrations, particularly in the Upper Muskwa and Evie, are thus responsible for their low and sometimes negative bulk volume magnetic susceptibilities. High gamma ray readings in the Upper Muskwa and Evie (**Figure 3.12**) despite their low bulk magnetic susceptibility further indicate that TOC is a key control on bulk volume magnetic susceptibility. Where the gamma ray log responds to uranium adsorbed by organic matter, organic rich mudrocks such as the Upper Muskwa and Evie have high gamma ray readings. The correlation between TOC and bulk volume magnetic susceptibility has not, to our knowledge, been reported in any other studies.

.

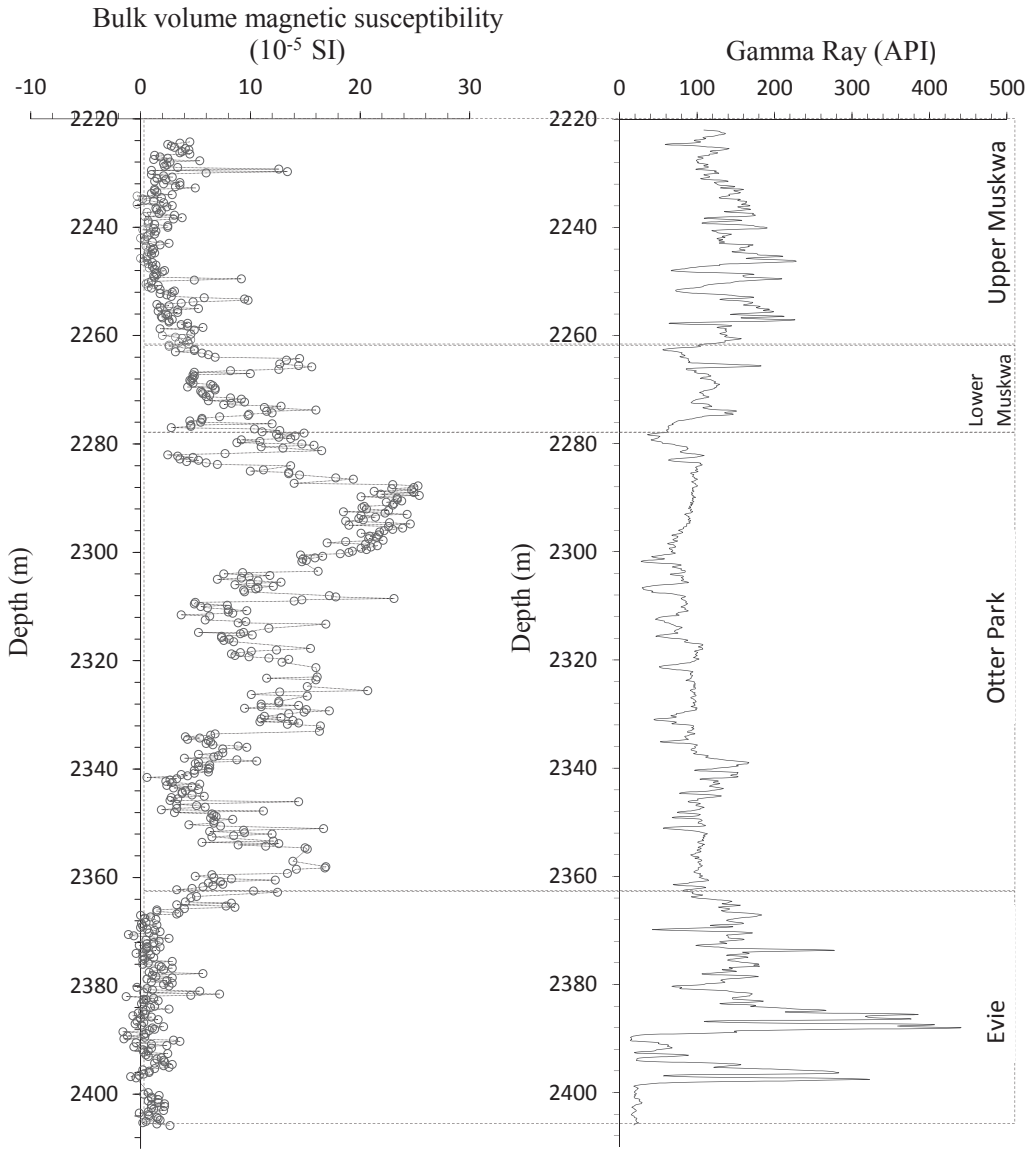

Figure 3.12: Gamma ray log and bulk volume magnetic susceptibility of the Horn River Group members from the Imperial Komie well.

Table 3.2: Geochemical compositions from mass spectrometry of representative Horn River Group samples from the Imperial Komie well.

	Depth (m)	TOC %	SiO_2 %	Al_2O_3 %	Fe_2O_3 %	MgO %	CaO %	Na_2O %	K_2O %	MnO %	Cr_2O_3 %
Muskwa											
	2233.13	3.075	74.49	9.75	2.82	0.8	0.63	0.57	1.83	0.01	0.008
	2235.03	4.54	84.46	4.33	1.43	0.5	0.59	0.23	0.82	0.005	0.013
	2251.55	6.85	75.43	5.01	2.39	0.85	2.14	0.5	0.91	0.01	0.008
	2253.53	2.535	46.23	7.59	3.14	6.2	12.77	0.65	1.5	0.09	0.008
	2265.55	0.492	53.52	15.26	5.34	3.14	5.65	0.62	3.18	0.05	0.013
	2267.53	2.27	73.39	7.25	3.56	0.96	3.17	0.46	1.39	0.02	0.007
	2269.545	3.09	70.1	9.01	3.66	1.11	3.4	0.48	1.75	0.02	0.007
	2271.55	2.55	64.9	12.05	4.48	1.42	3.23	0.6	2.35	0.02	0.012
Otter Park											
	2278.05	0.68	39.41	10.7	4.05	2.93	18.39	0.59	2.2	0.06	0.01
	2286.55	0.632	53.43	17.04	5.68	2.14	5.7	0.65	3.3	0.05	0.015
	2296.55	0.552	50.04	15.93	5.35	2.24	8.73	0.65	3.1	0.06	0.012
	2302.045	0.64	27.6	7.97	5.16	4.69	24.27	0.46	1.59	0.08	0.007
	2304.54	0.93	52.56	11.61	2.71	1.47	12.37	0.76	2.33	0.03	0.01
	2315.055	1.49	49.72	10.19	2.26	1.4	15.82	0.77	1.89	0.02	0.008
	2317.05	0.956	29.69	7.02	6.66	6.47	20.25	0.32	1.39	0.1	0.006
	2325.05	0.856	54.6	15.86	5.33	2.12	6.31	0.61	3.08	0.05	0.013
	2333	1.28	47.26	12.86	4.48	3.6	10.41	0.67	2.62	0.06	0.011
	2344.055	5.59	59	8.25	3.54	2.6	7.49	0.79	1.62	0.03	0.008
	2359.61	0.967	57.14	20.96	3.12	1.87	1.77	0.44	4.69	0.04	0.016
	2361.465	0.789	54.41	19.54	5.23	2.29	2.59	0.61	4.23	0.05	0.015
Evie											
	2377.035	4.73	67.8	7.3	2.37	0.85	5.19	0.76	1.51	0.01	0.016
	2383.045	4.28	52.47	7.51	2.81	1.8	14.14	0.63	1.46	0.02	0.011
	2396.05	3.05	7.58	0.61	0.32	0.85	48.54	0.02	0.11	0.005	0.001

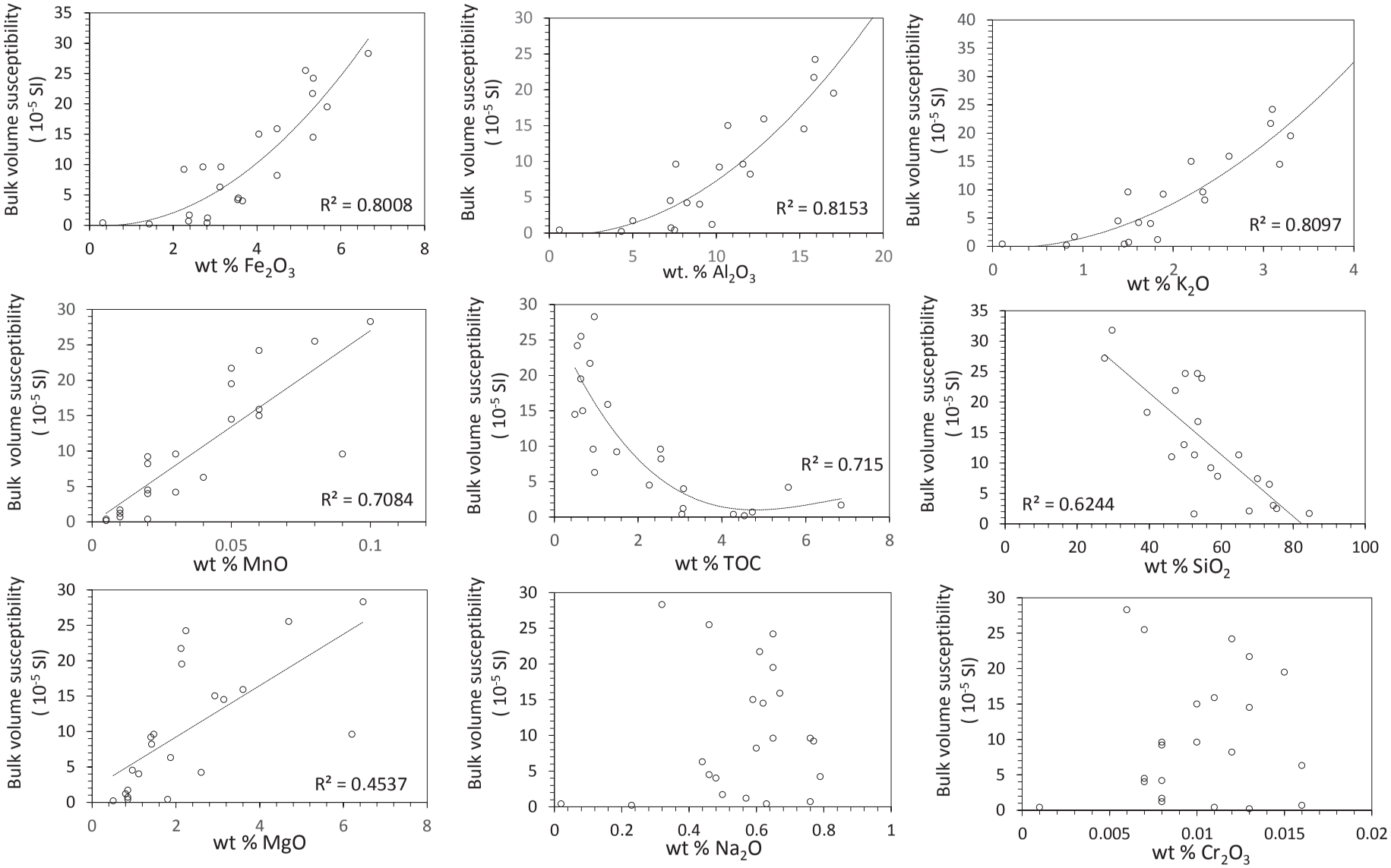

Figure 3.13: Relationship between chemical composition from mass spectrometry and bulk volume magnetic susceptibility measured using a hand-held probe sensor.

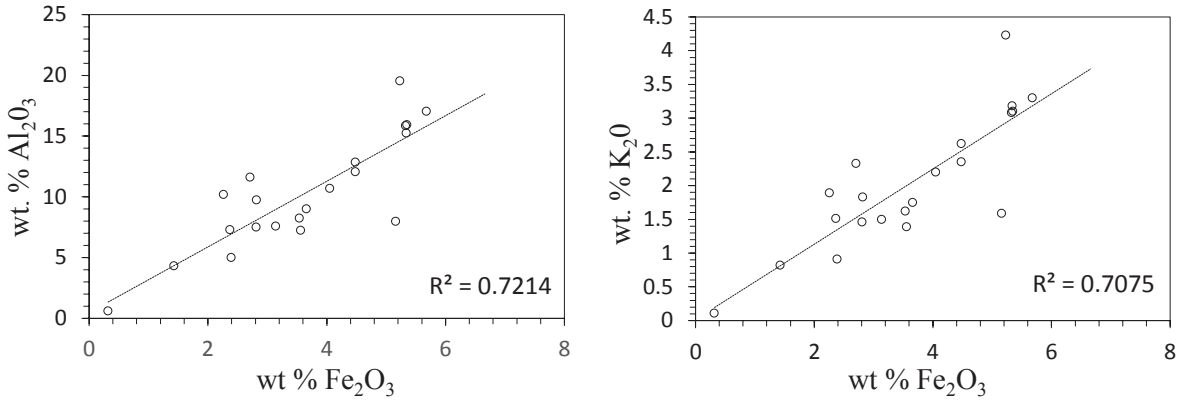

Figure 3.14: Relationship between iron oxide concentration and aluminium oxide and potassium oxide concentrations indicate that clays are the primary source of iron in the Horn River Group.

3.5 Anisotropy of Magnetic Susceptibility (AMS)

3.5.1 Sample preparation

Anisotropy of magnetic susceptibility tensors and ellipsoids were determined for cubic samples taken from the Imperial Komie slabbed core. To ensure that samples collected accurately portray the diverse lithofacies present in the Horn River Group at this location, sample selection was based on thin section observations and bulk volume magnetic susceptibility values discussed in section **3.4.3**. The following is a description of the sample preparation technique used.

Certain intervals of the Lower Muskwa and Upper Otter Park formations are extremely friable, hence did not allow for collection of standard plug samples. To minimize alteration of the original rock fabric prior to taking directional magnetic susceptibility measurements, a technique that involved impregnating samples with an adhesive before cutting was used. It was important that the adhesive chosen be fluid enough to sufficiently penetrate the sample but also that its magnetic properties not mask those due to the rock fabric. A number of paleomagnetic studies report coating poorly consolidated samples with weakly diamagnetic sodium silicate (Na_2SiO_3) prior to taking measurements (Hall and Sager, 1990). The Horn River samples in the present study were impregnated with Na_2SiO_3 by soaking for three to five minutes and left to dry overnight before

cutting. Initial attempts to cut samples under water proved futile since sodium silicate is water soluble. Cutting the samples under a jet of propylene glycol however, ensured the adhesive holding the samples together remained intact.

Fifty-eight 2.2cm × 2.2cm ×2.2cm cubes, such as are shown in **Figure 3.15**, were cut from the sodium silicate impregnated samples: 10 samples were from the Muskwa, 19 from the Upper Otter Park, 20 from the Lower Otter Park and 9 from the Evie.

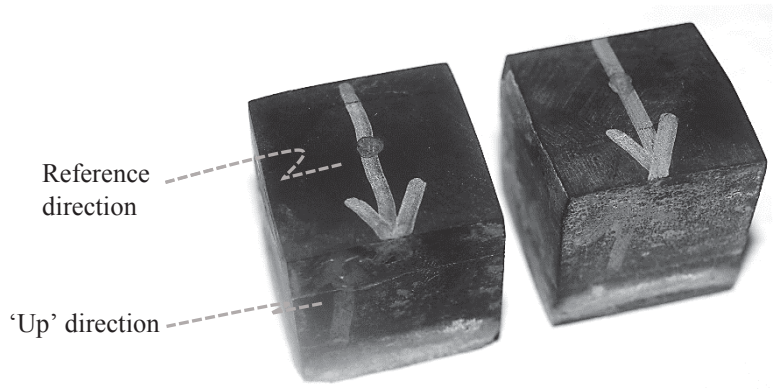

Figure 3.15: 2.2cm × 2.2cm ×2.2cm cubes cut from sodium silicate impregnated core.

3.5.2 Materials and method

To determine the anisotropy of magnetic susceptibility (AMS) tensor k_{ij}, magnetic susceptibility has to be measured in at least nine directions. Here, it is measured in the 18 directions shown in **Figure 3.16**. For each sample, these measurement directions were defined with respective to a bedding-parallel reference orientation, as shown in **Figures 3.15** and **3.16**. The direction of the orientation arrow in the bedding plane is defined by the cut surface of the slabbed core. Although the orientation of the cut surface in the bedding plane may vary between core intervals (runs), the variation of magnetic susceptibility in horizontal plane is expected to be minimal since shales and mudstones are typically well bedded/laminated and have a planar fabric. Moreover, each core run consists of 8 to 10m of core, so, the direction of the reference orientation in the bedding plane is consistent for every 8 to 10m run.

Directional susceptibilities were measured using the Bartington dual frequency MS2B AMS meter. This static AMS meter is unidirectional, measuring magnetic susceptibility in one direction for each application of a low alternating magnetic field of 80 Am^{-1}. It is capable of computing both mass magnetic susceptibility and volume magnetic susceptibility; mass magnetic susceptibility was measured here. The sample whose mass magnetic susceptibility is to be measured is placed in a $10cm^3$ cavity in the desired measurement direction, and following the application of the magnetic field, the instrument calculates the mass magnetic susceptibility using a previously inputted sample mass. The procedure is repeated for all 18 measurement directions. Using the 18 directional mass magnetic susceptibilities, the k_{ij} tensor is computed and used to compute the AMS ellipsoid with principal axes $k_1 \geq k_2 \geq k_3$.

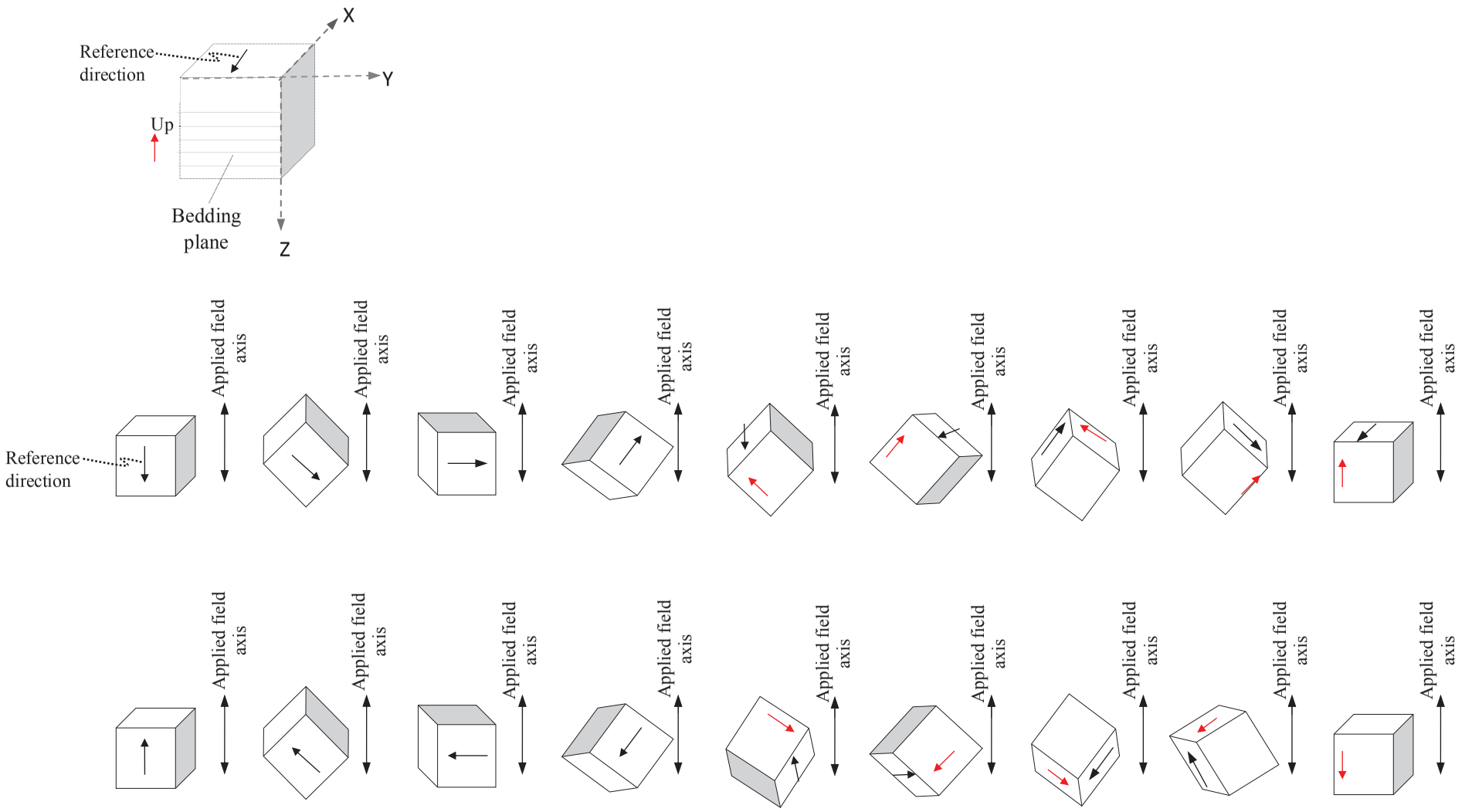

Figure 3.16: Schematic showing sample coordinate system, reference position and 18 measurement positions for which magnetic susceptibilities were measured.

3.5.3 Determining the anisotropy of magnetic susceptibility tensor and ellipsoid from 18 directional mass magnetic susceptibilities

In this section, a detailed description of how the k_{ij} tensors and their ellipsoids were determined from the 18 directional magnetic susceptibilities measured is presented. The relationship between the strength of an applied magnetic field, H, and the magnetization, M, it induces in each measurement direction is given by the expression:

$$M_i = K_{ij} H_j \tag{3.7}$$

For a magnetically anisotropic sample, the above expression can be expanded as follows:

$$M_1 = K_{11} H_1 + K_{12} H_2 + K_{13} H_3$$

$$M_2 = K_{21} H_1 + K_{22} H_2 + K_{23} H_3$$

$$M_3 = K_{31} H_1 + K_{32} H_2 + K_{33} H_3 \tag{3.8}$$

where K_{ij} are coefficients or elements of the second order AMS tensor.

Since the AMS tensor is symmetric ($K_{ij} = K_{ji}$), it has only six independent elements (b_1 to b_6).

$$b_1 = K_{11}$$

$$b_2 = K_{22}$$

$$b_3 = K_{33}$$

$$b_4 = K_{21} = K_{12}$$

$$b_5 = K_{23} = K_{23}$$

$$b_6 = K_{13} = K_{31} \tag{3.9}$$

The elements of b are related to the experimentally derived directional magnetic susceptibilities K_i by the following expression:

$$K_i = A_{ij} b_j \tag{3.10}$$

where A is called the design matrix and is dependent on the experimental design or measurement directions in which magnetic susceptibility is measured. The design matrix, A determined from the direction cosines for the directions shown in **Figure 3.16** is as follows:

$$\mathbf{A} = \begin{bmatrix} 1 & 0 & 0 & 0 & 0 & 0 \\ 0 & 1 & 0 & 0 & 0 & 0 \\ 0 & 0 & 1 & 0 & 0 & 0 \\ \frac{1}{\sqrt{2}} & \frac{1}{\sqrt{2}} & 0 & 0 & 0 & 1 \\ \frac{1}{\sqrt{2}} & 0 & \frac{1}{\sqrt{2}} & 0 & 1 & 0 \\ 0 & \frac{1}{\sqrt{2}} & \frac{1}{\sqrt{2}} & 1 & 0 & 0 \\ \frac{1}{\sqrt{2}} & \frac{1}{\sqrt{2}} & 0 & 0 & 0 & -1 \\ \frac{1}{\sqrt{2}} & 0 & \frac{1}{\sqrt{2}} & 0 & -1 & 0 \\ 0 & \frac{1}{\sqrt{2}} & \frac{1}{\sqrt{2}} & -1 & 0 & 0 \end{bmatrix}$$

The elements of b can then be calculated algebraically as follows:

$$b = (A^T A)^{-1} A^T K \tag{3.11}$$

$$b = BK \tag{3.12}$$

where A^T is the transpose of A, and $B = (A^T A)^{-1} A^T$

The elements of B for the experimental design shown in **Figure 3.16** are:

$$B = \begin{bmatrix} 0.4000 & -0.1000 & -0.1000 & 0.2121 & 0.2121 & -0.1414 & 0.2121 & 0.2121 & -0.1414 \\ -0.1000 & 0.4000 & -0.1000 & 0.2121 & -0.1414 & 0.2121 & 0.2121 & -0.1414 & 0.2121 \\ -0.1000 & -0.1000 & 0.4000 & -0.1414 & 0.2121 & 0.2121 & -0.1414 & 0.2121 & 0.2121 \\ 0 & 0 & 0 & 0 & 0 & 0.5 & 0 & 0 & -0.5 \\ 0 & 0 & 0 & 0 & 0.5 & 0 & 0 & -0.5 & 0 \\ 0 & 0 & 0 & 0.5 & 0 & 0 & -0.5 & 0 & 0 \end{bmatrix}$$

Using equation (3.12), the six independent elements (b_1 to b_6) of the susceptibility tensor K_{ij} can be calculated as follows:

$$\begin{bmatrix} b_1 \\ b_2 \\ b_3 \\ b_4 \\ b_5 \\ b_6 \end{bmatrix} = \begin{bmatrix} 0.4000 & -0.1000 & -0.1000 & 0.2121 & 0.2121 & -0.1414 & 0.2121 & 0.2121 & -0.1414 \\ -0.1000 & 0.4000 & -0.1000 & 0.2121 & -0.1414 & 0.2121 & 0.2121 & -0.1414 & 0.2121 \\ -0.1000 & -0.1000 & 0.4000 & -0.1414 & 0.2121 & 0.2121 & -0.1414 & 0.2121 & 0.2121 \\ 0 & 0 & 0 & 0 & 0 & 0.5 & 0 & 0 & -0.5 \\ 0 & 0 & 0 & 0 & 0.5 & 0 & 0 & -0.5 & 0 \\ 0 & 0 & 0 & 0.5 & 0 & 0 & -0.5 & 0 & 0 \end{bmatrix} \begin{bmatrix} k_1 \\ k_2 \\ k_3 \\ k_4 \\ k_5 \\ k_6 \\ k_7 \\ k_8 \\ k_9 \end{bmatrix}$$

where k_i (k_1 to k_9) are determined from the 18 experimental mass magnetic susceptibilities. For each direction shown in **Figure 3.16** (x, xy, y, -xy, yz, -yz, -zx, zx, z), two magnetic susceptibilities are measured for applied fields in two opposite directions. k_1 to k_9 are the average magnetic susceptibilities for each direction.

The coefficients of the symmetric, second rank AMS tensor K_{ij}, are determined from the column matrix b.

$$K_{ij} = \begin{bmatrix} b_1 & b_4 & b_6 \\ b_4 & b_2 & b_5 \\ b_6 & b_5 & b_3 \end{bmatrix} = \begin{bmatrix} k_{11} & k_{12} & k_{13} \\ k_{21} & k_{22} & k_{23} \\ k_{31} & k_{32} & k_{33} \end{bmatrix} \quad (3.13)$$

The determinant of K_{ij} gives a matrix, C whose off-diagonal terms are zero. The diagonal terms or eigenvalues k_1, k_2 and k_3 are the maximum (k_{max} or k_1), intermediate (k_{int} or k_2) and minimum (k_{min} or k_3) magnetic susceptibilities.

$$C = \begin{bmatrix} k_1 & 0 & 0 \\ 0 & k_2 & 0 \\ 0 & 0 & k_3 \end{bmatrix} \quad (3.14)$$

Using k_{max}, k_{int} and k_{min}, percent anisotropy of magnetic susceptibility is calculated as follows:

$$\frac{(k_{max} - k_{min})}{k_{int}} \times 100 \quad (3.15)$$

The eigenvectors of k_1, k_2 and k_3 define the orientations of the three orthogonal principal axes k_1, k_2 and k_3. The orientation (declination and inclination) of the principal axes are calculated as follows from the eigenvectors (x, y, z) of k_1, k_2 and k_3

$$\text{Declination} = \tan^{-1}(y/x) \quad (3.16)$$

$$\text{Inclination} = \sin^{-1}(z) \quad (3.17)$$

3.5.4 Results

As a first attempt to check how magnetically anisotropic the members of the Horn River Group are, room temperature bulk volume magnetic susceptibility of slabbed core samples measured parallel and perpendicular to the bedding plane were compared. **Figure 3.17** is a graphical comparison of both bulk volume magnetic susceptibilities. Despite the small sample volume measured by the Bartington 2E logging sensor, anisotropy in the Horn River Group is apparent from the obtained bulk volume magnetic susceptibilities. The bedding-parallel bulk volume magnetic susceptibility is consistently higher than the bedding perpendicular bulk volume magnetic susceptibility in all three formations. In **Figure 3.18**, the ratio of bedding parallel susceptibility to bedding perpendicular susceptibility gives an idea of how much both magnetic susceptibilities differ. Despite the low bulk volume susceptibilities, higher diamagnetic and lower paramagnetic concentrations of the Upper Muskwa and Evie, they have the greatest difference between horizontal and vertical bulk volume magnetic susceptibility, an initial indication that although higher concentration of paramagnetic clays result in higher bulk susceptibility, clays alone are not responsible for high anisotropy of magnetic susceptibility in the Horn River Group.

To apply anisotropy results in petrofabric analysis, an understanding of how magnetic susceptibility varies in 3D is necessary. From the 18 directional mass magnetic susceptibilities, the second rank anisotropy of magnetic susceptibility tensor K_{ij} and its ellipsoid defined by three orthogonal axes that are the maximum, intermediate and minimum susceptibility were computed.

Table 3.3 lists the determined k_1 (k_{max}), k_2 (k_{int}) and k_3 (k_{min}) magnitudes and directions for the Muskwa, Otter Park and Evie samples. A measure of the variation in the magnitudes of these principal axes is the percentage anisotropy of magnetic susceptibility. **Figure 3.18** shows the variation in %AMS with depth. This variation with depth is compared to the anisotropy degree derived from just one horizontal and perpendicular magnetic susceptibility measured with a surface MS probe. Although using magnetic susceptibilities from only two directions overestimates susceptibility anisotropy, both the surface probe derived anisotropies and 18-direction derived AMS have the same trend**.** Henceforth, unless otherwise mentioned, percent AMS values mentioned will refer to those calculated from the principal magnetic susceptibilities.

AMS is highest in the Evie with values between 13% and 35%. In the Upper Muskwa, it is between 7% and 13%, and in the Lower Muskwa and Otter Park formations, values are between 1.1% and 14.3%.

AMS ellipsoid principal axes orientations

Principal axes orientations in the Horn River Group define normal, inverse and intermediate magnetic fabrics (**Figure 3.19**). Observed magnetic fabrics are not specific to any formation, all three types are present in the three formations. Fabric types are defined according to the relationship of principal directions to the bedding plane. A normal magnetic fabric is characterized by k_1 direction parallel/subparallel to the bedding plane and k_3 direction normal to the bedding plane while an inverse magnetic fabric has k_1 normal to the bedding plane and the k_3 is parallel/subparallel to the bedding plane. Of 58 samples, 27 have normal fabrics, 16 have inverse fabrics and 15 have intermediate fabrics. In this study, k_1 inclinations less than 20° and k_3 inclinations greater than 50° define a normal fabric and k_1 inclinations greater than 50° and k_3 inclinations less than 20° define an inverse magnetic fabric. Samples with intermediate fabrics have either k_1 or k_3 inclinations between 21° and 49°or both k_1 and k_3 inclinations between 21° and 49°. **Table 3.3** lists the calculated AMS principal axes orientations for the Horn River Group samples.

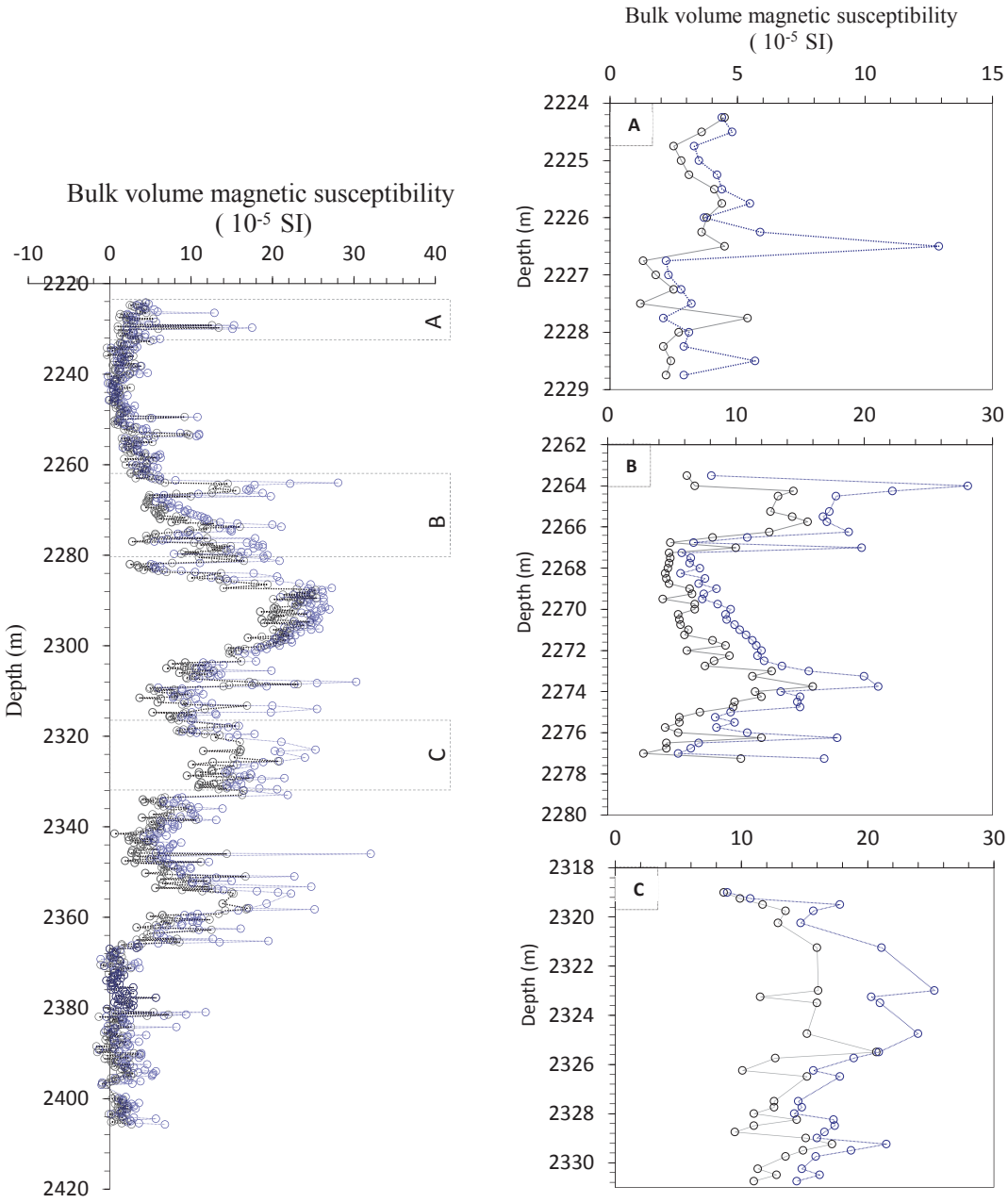

Figure 3.17: Comparison of bedding parallel (blue plot) and bedding perpendicular (black plot) bulk volume magnetic susceptibilities measured using a Bartington MS2E hand-held surface probe. AMS is therefore apparent even from these direct susceptibility measurements on unprepared core samples.

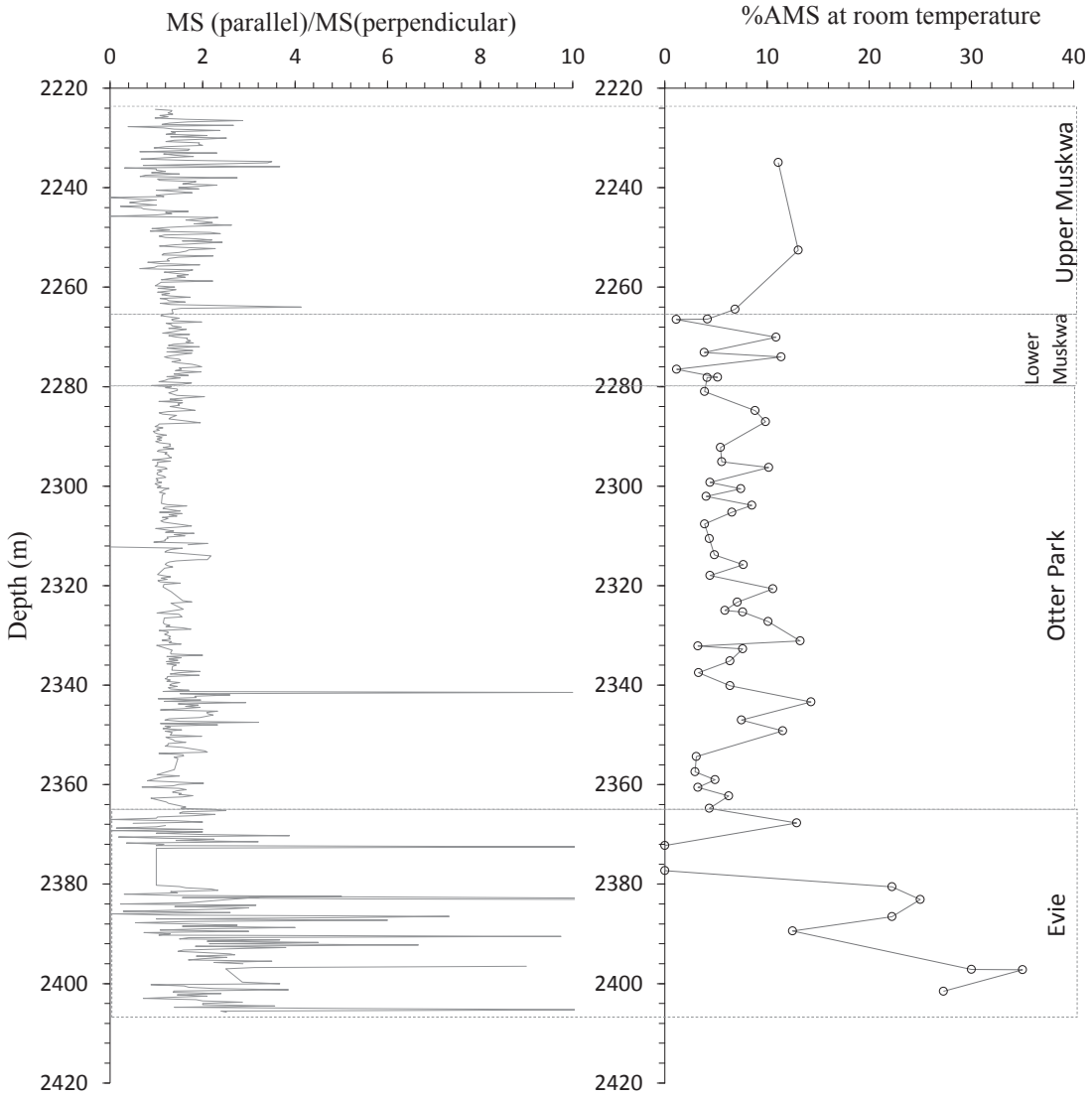

Figure 3.18: Comparison of the ratio of bedding parallel to bedding perpendicular bulk volume magnetic susceptibilities from the probe MS2E sensor measurements of **Figure 3.17** and % Anisotropy of Magnetic Susceptibility derived from 18 directional susceptibilities using the scheme shown in **Figure 3.16** with measurements in a Bartington MS2B sensor.

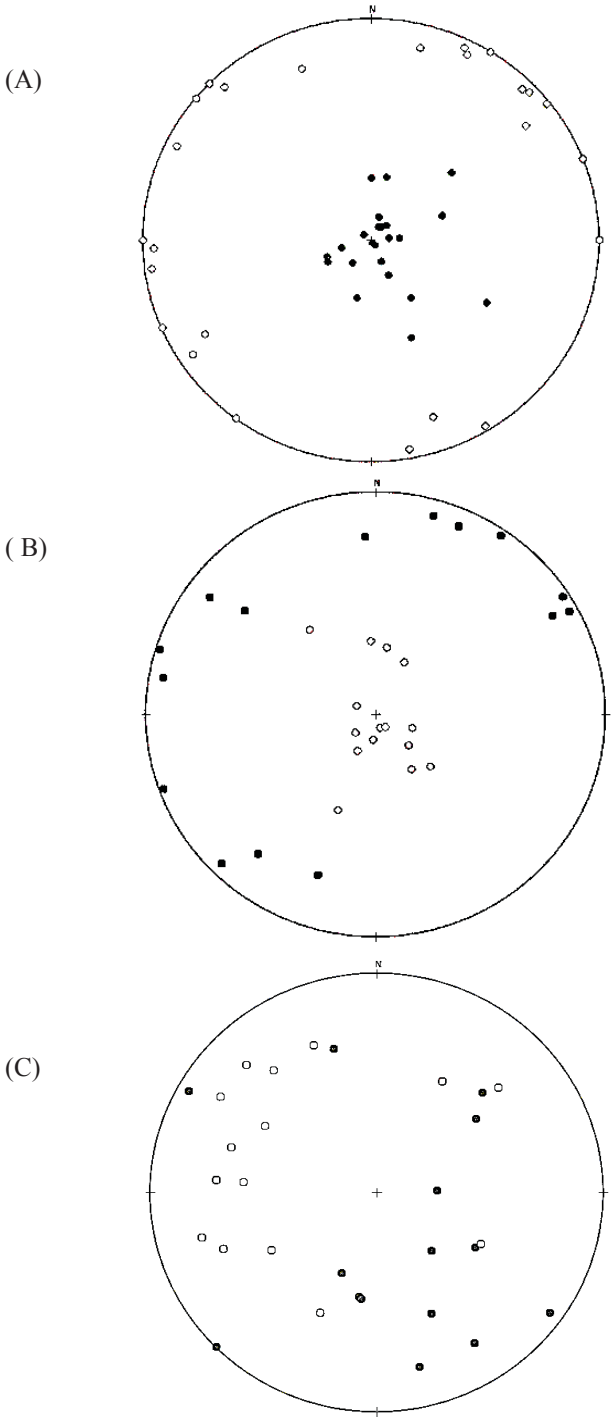

Figure 3.19: Equal-area projection showing the three room temperature anisotropy of magnetic susceptibility fabrics in the Horn River Group. (A) Samples with normal magnetic fabrics have minimum magnetic susceptibility (closed squares) normal to the bedding plane and maximum susceptibility (open circles) sub-parallel to the bedding plane. (B) Samples with inverse magnetic fabrics have principal axes that are opposite those with normal fabrics. (C) Samples with intermediate magnetic fabrics are between inverse and normal.

Table 3.3: Principal magnetic susceptibilities and principal axes orientations (continued on next page).

Formation	Directions						Magnitudes		
	k_{max}		k_{int}		k_{min}		k_{max}	k_{int}	k_{min}
	Declination (°)	Inclination (°)	Declination (°)	Inclination (°)	Declination (°)	Inclination (°)			
Muskwa	134.1	62.7	40.5	1.8	309.5	27.3	1	0.9	0.9
	338.5	18	72.5	11.6	193.7	68.4	0.4	0.3	0.2
	320.7	28.7	65.5	24.9	189.5	50.3	2.5	2.3	2.2
	147.5	66.3	262.5	10.5	356.6	21	10.7	10.2	10
	274.6	40.8	57.7	42.8	166.8	19.5	7.3	7.2	7
	133.9	73.7	283.8	14.2	15.6	7.9	9	8.9	8.9
	356.1	63	122.9	16.8	219.3	20.4	4.9	4.6	4.4
	68.3	0.1	338.2	38.8	158.4	51	10.8	10.4	10.4
	239.9	16.9	144.8	16.4	13.1	66.1	8	7.9	7.1
Otter Park	288	33	168	37.6	45.4	35	8.8	8.7	8.7
	110.4	76.3	316.3	12.3	225	5.8	9.9	9.7	9.4
	205.4	75.3	328.2	8.1	60	12.2	10	9.7	9.6
	162.2	84.9	303.8	4	34	3.1	10.5	10.3	10.1
	309.9	0.3	39.8	10.5	218.4	79.5	6.8	6.8	6.2
	317.1	6.3	226.3	7.9	85.1	79.9	13.4	13.2	12.1
	255.2	21.2	346.8	4.1	87.4	68.3	5.7	5.5	5.4
	267.7	5.4	115.3	84.1	358	2.7	12.8	12.6	12.1
	246.7	0.6	336.7	2.2	142.5	87.7	13.2	12.8	11.9
	236.6	7.2	145.9	5.7	18	80.9	11.5	11.3	11
	29.7	41.3	223	48	125.6	6.6	9.8	9.4	9.1
	142.3	84.3	340.3	5.4	250.1	1.8	15.2	14.8	14.6
	51.4	1.7	320.8	8.2	154.5	81.6	13	12.9	11.9
	46	4.2	314.8	13.4	153.8	75.9	6.1	6.1	5.7
	302.5	19.4	47.3	32.7	188.2	49.5	7.7	7.7	7.4
	216.3	0.4	126.3	3	312.4	86.7	7	6.9	6.7
	25.1	4.4	290.2	48	119.1	41.6	6.5	6.2	6.2
	48.2	29.1	310.9	11.3	202.7	57.3	5.4	5.2	5

Formation	Directions						Magnitudes		
	k_{max}		k_{int}		k_{min}		k_{max}	k_{int}	k_{min}
	Declination (°)	Inclination (°)	Declination (°)	Inclination (°)	Declination (°)	Inclination (°)			
Otter Park	262.3	3.3	172.1	4.7	27.1	84.3	10.7	10.4	9.6
	169.8	4.8	262.3	26.6	70.3	62.9	11.7	11.3	10.9
	149.1	2.5	239.7	6.2	36.8	83.7	12	11.9	11.3
	296.6	5.3	206.2	3.5	82.7	83.6	13.3	13.1	12.3
	31.6	0.4	301.6	1.1	145.6	88.9	11.4	10.9	10.3
	315.4	19.3	134.7	70.2	225.4	0.3	8.9	8.3	7.8
	337.5	27.9	242.8	9.1	137.8	60.7	3.1	3.1	3
	28	68.3	187.4	20.4	280.2	6.9	12.5	11.8	11.6
	315	0	225	7.8	45	82.4	4.8	4.7	4.5
	294.8	82.7	151.7	5.8	61.3	4.3	9.2	9.1	8.9
	44.2	5.5	311.4	24.7	146.2	64.5	4.8	4.7	4.5
	116.9	47.2	236.8	24.8	343.8	32.3	2.9	2.8	2.5
	249.2	28.5	27.8	54.1	147.8	19.9	4.2	4	3.9
	26.7	7	118.3	7.9	255.9	79.2	5.3	5.2	4.7
	185.6	80.9	17.5	8.9	287.2	1.8	9.7	9.7	9.4
	200.8	52.2	43.9	35.6	306.1	11.6	13.8	13.5	13.4
	274.6	29.5	28.3	36.2	156.4	39.8	10.4	10.2	9.9
	301.8	41.5	211	1.4	119.9	48.4	9.3	9.3	9
Evie	270	0	179.9	23.1	360	67	3.2	3.2	3
	204.6	39.7	36	49.8	299.3	5.7	4.7	4.6	4.5
	323	50.4	149.4	38.9	56.9	3.1	3.2	3.1	2.8
	90	0	176.1	28.1	270	0	0.3	0.3	0.3
	90	0	176.1	28.1	270	0	0.3	0.3	0.3
	9.1	65.1	107.8	3.3	199.3	24.6	1.9	1.8	1.5
	52.6	15.9	143.6	4.7	248.9	73.3	1.2	1.2	0.9
	9.1	65.1	107.8	3.3	199.3	24.6	1.9	1.8	1.5
	240.5	45.6	146.3	4.1	52.5	44.1	0.9	0.8	0.8
	14	11.5	106.7	12.5	242.8	72.8	1.1	1	0.8
	161.2	16.8	263.3	33.4	49.1	51.4	0.2	0.1	-0.1
	227.4	80.3	113.8	3.9	23.1	8.8	4.1	3.3	3.2

3.5.5 Discussion

3.5.5.1 Room temperature AMS controls and fabric implications

Geochemical composition results indicate that the concentrations of clay minerals, TOC and quartz are primarily responsible for the bulk magnetic susceptibility trend observed in the Horn River Group. Although the lowest susceptibility member (the Evie) has the highest anisotropy of magnetic susceptibility, no apparent correlation is observed between magnetic susceptibility and the degree of room temperature anisotropy of magnetic susceptibility (**Figure 3.20**). The primary control on bulk susceptibility is therefore different from the primary control on AMS. Little to no correlation between clay content and AMS (**Figure 3.21**) confirms that increasing concentration of clay minerals does not result in an increase in matrix/mineral preferred orientation or alignment in the Horn River Group members. Clay rich shales in the Lower Muskwa and Otter Park have comparable AMS values, and hence comparable degrees of bulk mineral alignment as the siliceous, clay poor mudstones in the Upper Muskwa. They also have lower AMS values (lower alignment of matrix components) than the calcareous clay poor mudstones of the Evie.

A correlation is instead noted between organic matter concentration and AMS. Weight percent Total Organic Carbon (TOC) is used as a proxy for organic matter concentration. Since the graph of bedding parallel susceptibility to bedding perpendicular susceptibility has a similar trend as the percent anisotropy of magnetic susceptibility (AMS) determined from 18 directional mass magnetic susceptibilities, a comparison of both anisotropy results and % TOC is made. In **Figure 3.22,** normalized TOC values are compared to normalized AMS values and normalized bedding parallel MS/bedding perpendicular MS values. The gamma ray log of this succession is an indicator of Total Organic Carbon (TOC) and not clay content, so percent AMS derived from 18 directional susceptibilities is also compared with the gamma ray log in **Figure 3.22**. **Figure 3.23** shows the cross-plots comparing TOC and both anisotropy results. Low regression coefficients in some formations may be due to the fact that since TOC data was not available for all depths sampled for AMS measurements, %AMS values are compared to %TOC of samples at the nearest depth.

In the Muskwa and Otter Park formations, a positive correlation between TOC and the ratio of bedding parallel to bedding perpendicular magnetic susceptibility is observed ($R^2 = 0.91$) (**Figure 3.23**). Total organic carbon data was not available for most of the samples for which 18 directional AMS values were determined so TOC values for samples at a similar depth was used. The

correlation is strongest in the clay rich Lower Muskwa ($R^2 = 0.76$) and Otter Park ($R^2 = 0.67$) and weakest in the siliceous, clay poor Upper Muskwa and carbonate-rich Evie. Two possible explanations for the observed correlation are as follows:

1. Organic matter is more preferentially oriented than other matrix constituents, hence despite being diamagnetic (Basavaiah, 2011), shows greater variation in directional susceptibility than higher susceptibility paramagnetic minerals in the matrix. Given that organic matter only makes up a small portion of total composition (TOC is between 0.46wt % and 6.85wt %), this explanation is less likely.
2. Organic matter influences the extent of preferred orientation of other matrix minerals, especially clays. Although no work showing the effect of organic matter on the anisotropy of magnetic susceptibility of shale and mudstones was found, a few studies have reported that the presence of organic matter may enhance the preferred orientation of clay minerals in the mudrock matrix (O'Brien, 1963; Odom, 1964; Odom, 1967; Meade, 1968). Moon and Hurst (1984) and Hounslow (1985) suggest that organic carbon acts to minimize clay flocculation, allowing for better alignment of individually dispersed clay platelets. **Figure 3.24** shows the SEM images of three Horn River samples with relatively high TOC values and **Figure 3.25** shows the SEM image for one with a low TOC value. Generally, high AMS, high TOC samples show better alignment of minerals. Even the Evie sample, with its low concentration of clays, shows good alignment of the little clay minerals present. The low TOC, low AMS sample on the other hand, has more randomly oriented clay minerals.

Of the three Horn River Group formations, the Evie has the highest AMS despite having TOC values comparable to the Upper Muskwa (**Table 3.2**). Although unlike the Muskwa and Otter Park, a negative correlation is observed between bedding parallel MS/bedding perpendicular MS and TOC (**Figure 3.23A**), a weak positive correlation is observed with AMS. The similar trends of the TOC, gamma ray log and %AMS plots suggest an incorrect matching of depths in the Evie. If a downward depth shift of 5m is applied to parallel MS/perpendicular MS values between 2373m and 2383m, the correlation between bedding parallel MS/bedding perpendicular MS and percent TOC becomes positive. The correlation is however not as strong as in the clay rich Lower Muskwa and Otter Park members, an indication that organic matter concentration alone does not explain the high AMS of the Evie. Thin section photomicrographs indicate that a stress other that lithostatic compression contributes to matrix preferred orientation and anisotropy of magnetic susceptibility

in the Evie. A notable characteristic of certain Evie intervals in the Imperial Komie well is the presence of elongate bioclasts some of which are twinned (**Figure 3.26**). Under shear stresses, calcite typically deforms by forming twin lamellae. A twin lamella results from the homogeneous simple shear of one part of a crystal along certain crystallographic planes (Carter and Raleigh, 1969; Tourneret and Lauarent, 1990; De Bresser and Spiers, 1997*).* It consists of an undeformed (host) part separated by a twin plane from a deformed part that is a mirror reflection of the host (**Figure 3.27**); each atom in the deformed portion having been translated by a fixed amount in the shear direction. The orientation of the twin plane is roughly parallel to the maximum shear stress axis. The analysis of calcite twin orientations have as a result been widely applied in tectonic studies for the determination of stress orientations (Turner et al. 1954; Jamison and Spang 1976, Tullis 1980; Borradaile and McArthur, 1990; Hamilton et al., 2004; Borradaile and Jackson, 2004; de Wall et al., 2000; Schmidt et al., 2006). In the Evie, twin orientations suggest an E-W extension axis (**Figure 3.26**). If matrix preferred orientation is in part attributable to tectonic stress, it is expected that the AMS ellipsoid axes be coaxial with principal strain directions (Borradaile and Henry, 1997). In the thin section images shown in **Figure 3.26**, the twin planes have the same inclination as the maximum susceptibility axis which is also coincident with the long axis of calcite bioclasts. It is the strong preferred orientation of these elongate calcite bioclasts that makes the anisotropy of magnetic susceptibility in the Evie significantly higher than the AMS in the Muskwa and Otter Park.

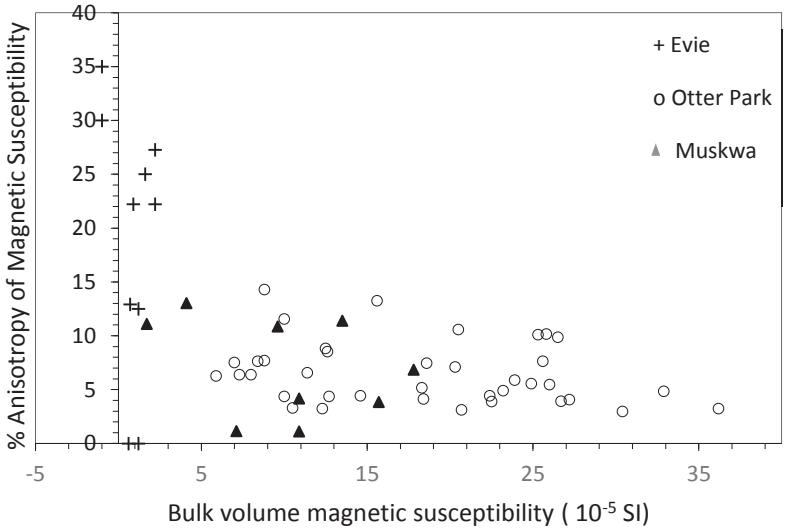

Figure 3.20: Relationship between bulk volume magnetic susceptibility and room temperature anisotropy of magnetic susceptibility.

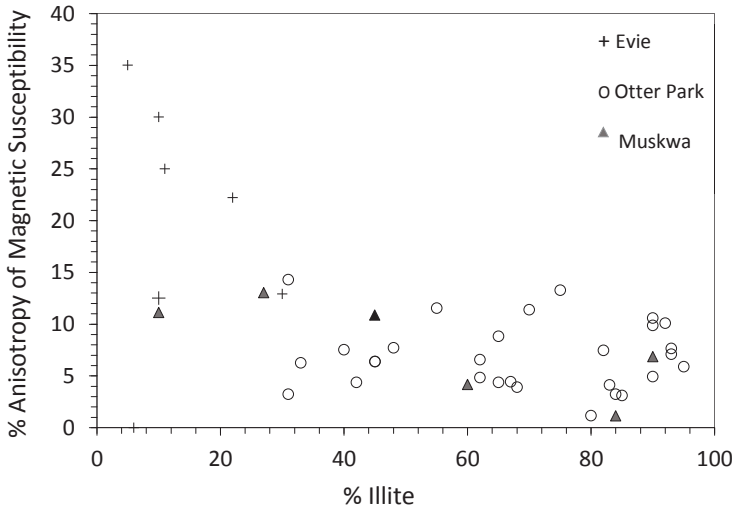

Figure 3.21: Relationship between illite content (determined from low temperature magnetic susceptibility measurements detailed in **Chapter 4**) and room temperature anisotropy of magnetic susceptibility.

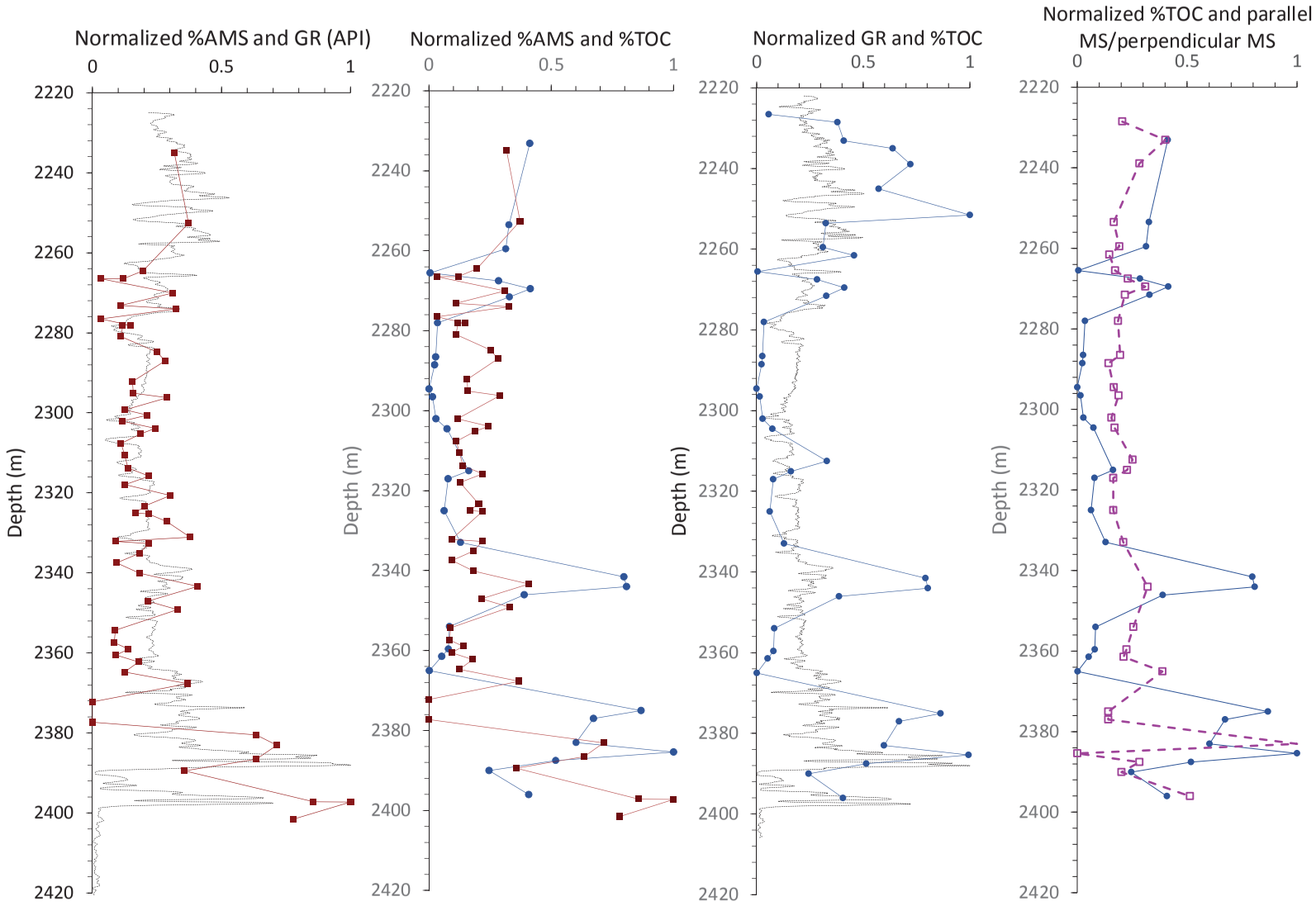

Figure 3.22: Relationship between normalized Gamma ray readings (black dashed graph), normalized room temperature %AMS (red graph), normalized % TOC (blue graph) and normalized bedding parallel MS/bedding perpendicular MS (pink dashed graph) suggests that organic matter is a primary control on anisotropy of magnetic susceptibility in the Horn River Group.

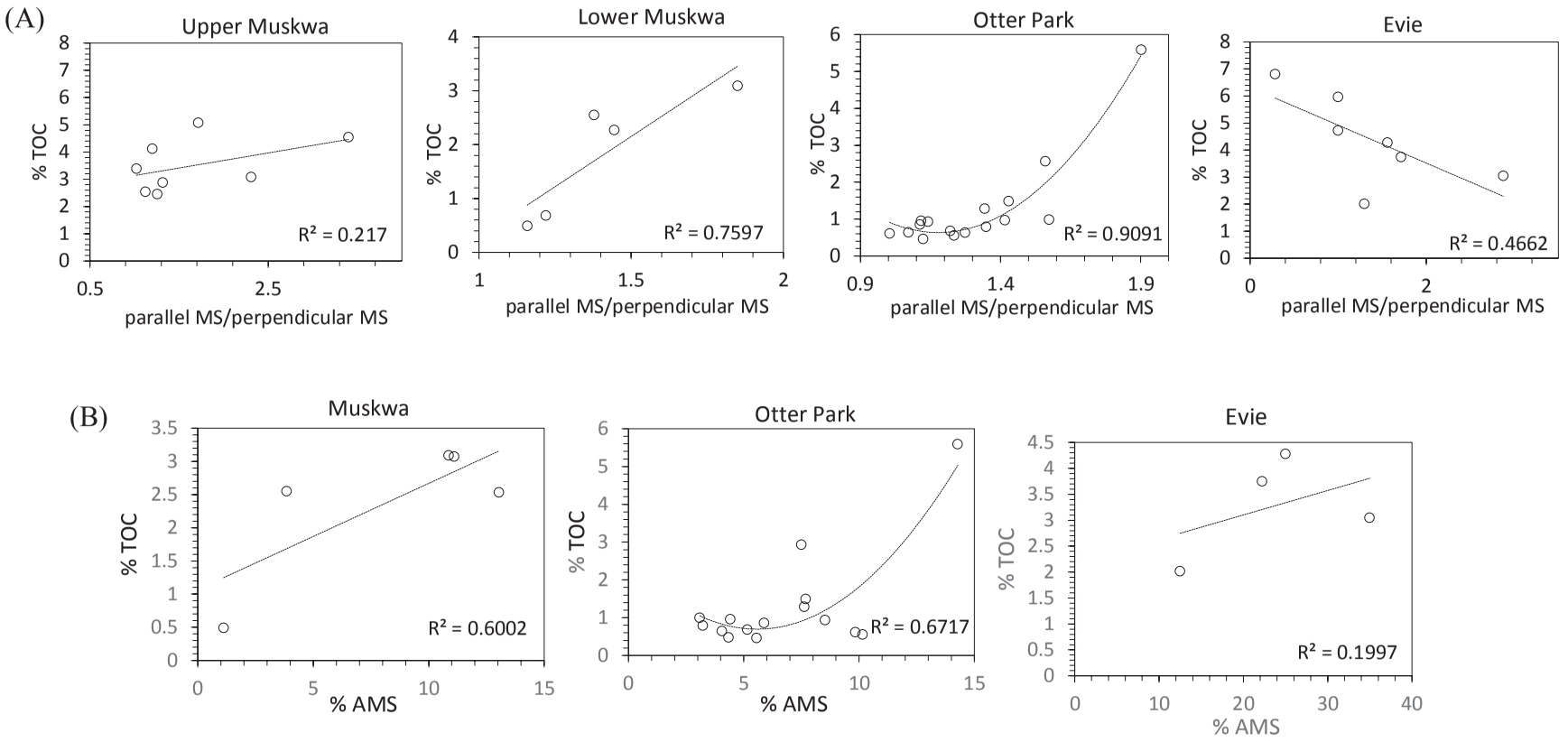

Figure 3.23: Cross-plots showing the relationship between (A) bedding parallel MS/bedding perpendicular MS and Total Organic Carbon and (B) AMS and Total Organic Carbon in the three Horn River Group Formations.

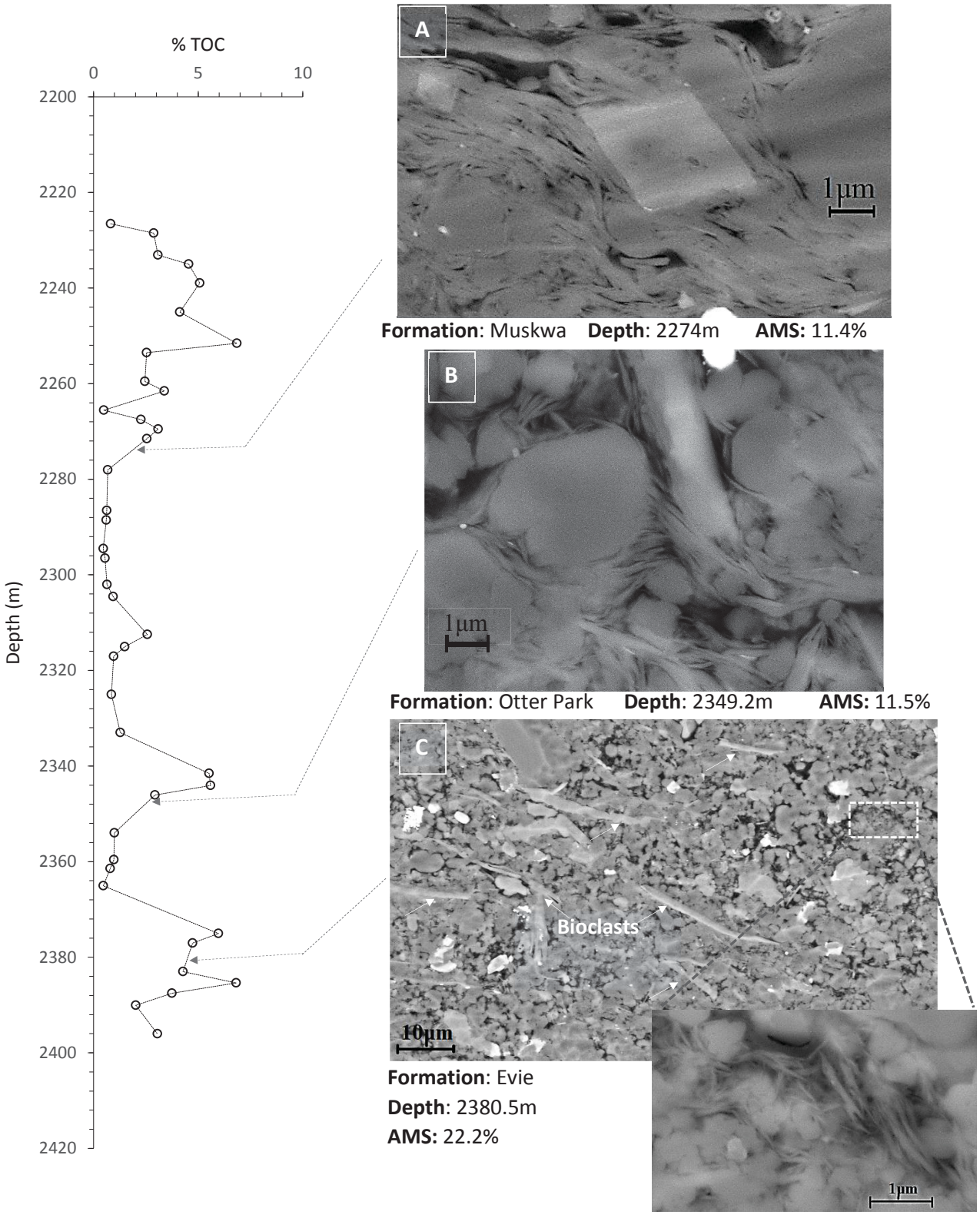

Figure 3.24: Comparison of AMS, TOC and matrix alignment in SEM images for Horn River Group samples with relatively high TOC.

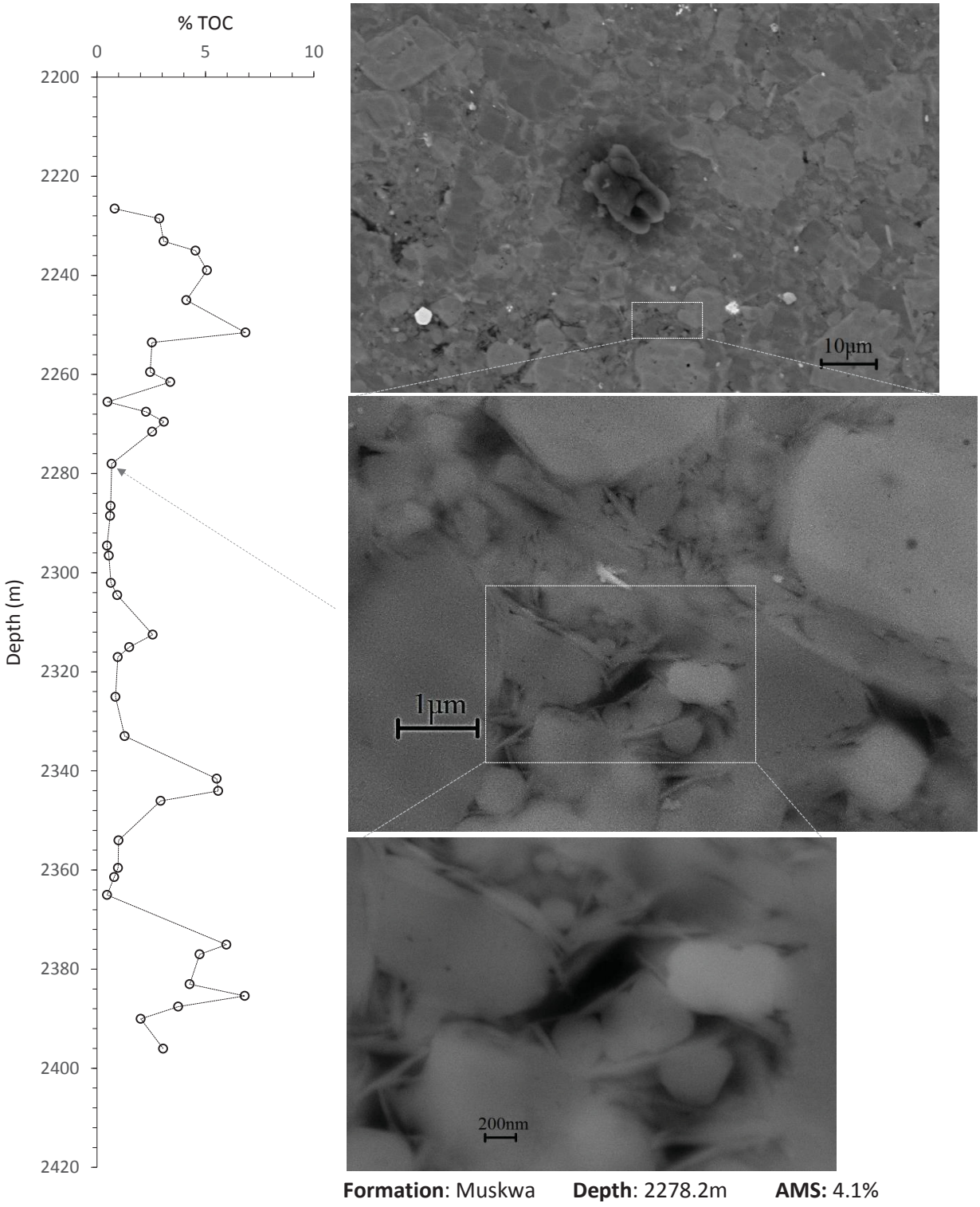

Figure 3.25: Comparison of AMS, TOC and matrix alignment in SEM images for a Horn River Group sample with low TOC.

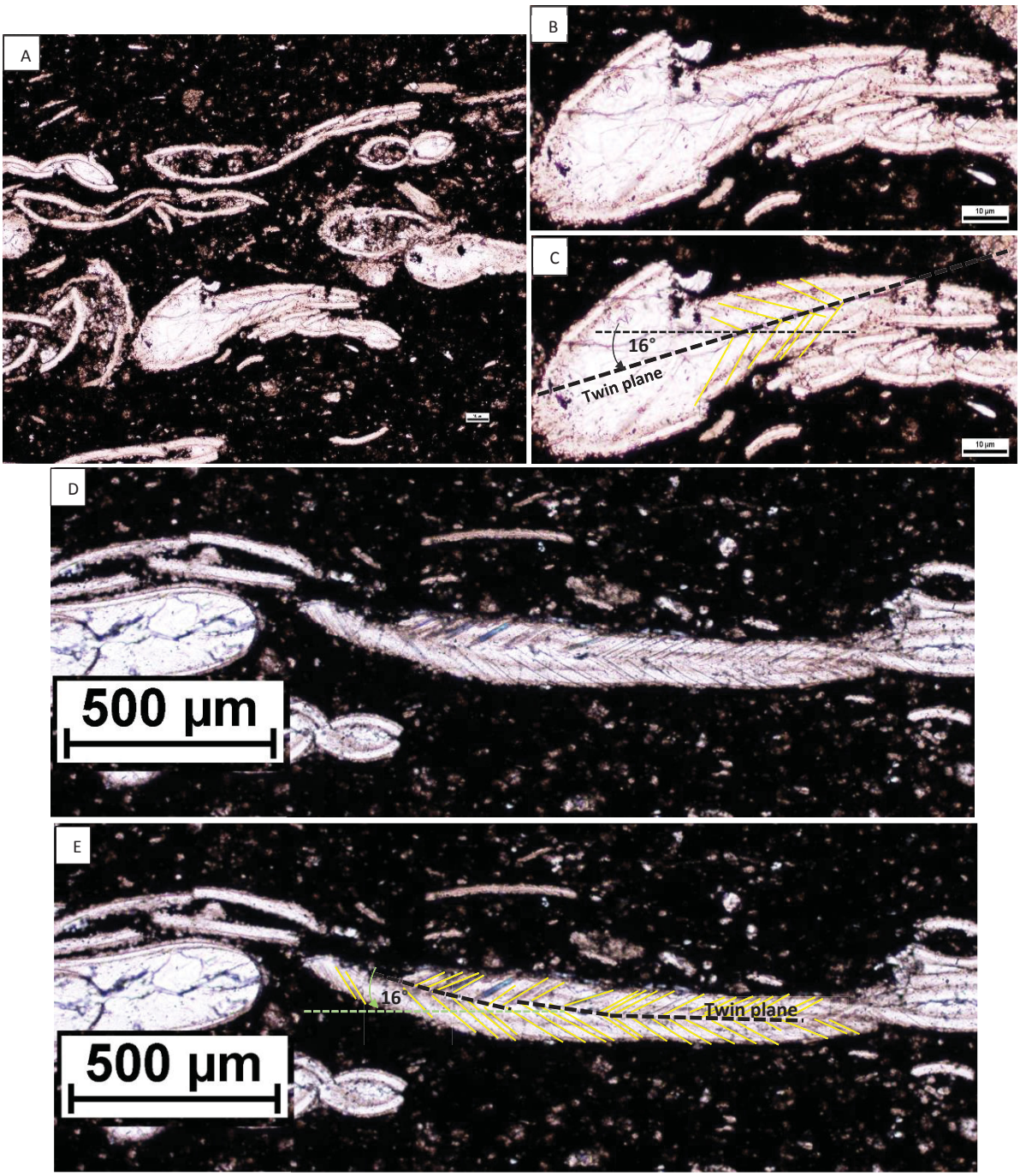

Formation	k_{max} Declination (°)	k_{max} Inclination (°)	k_{min} Declination (°)	k_{min} Inclination (°)	k_{int} Declination (°)	k_{int} Inclination (°)
Evie	52.6	15.9	248.9	73.3	143.6	4.7

Figure 3.26: Calcite twins with twin plane inclination coincident with the maximum susceptibility axes.

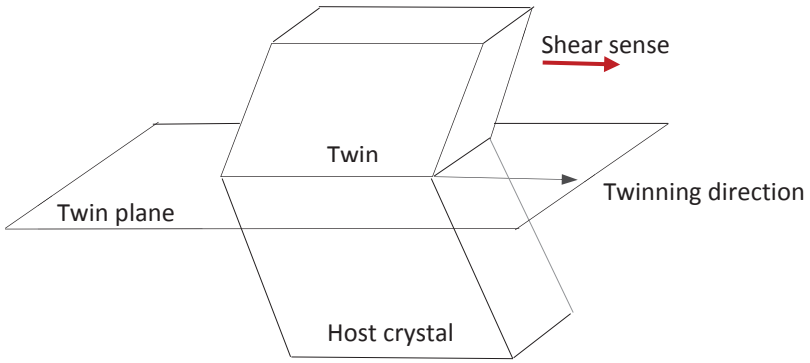

Figure 3.27: Schematic of a twin lamellae. The translation of atoms in the deformed portion of the crystal (twin) is in the twinning direction (modified from Carter and Raleigh, 1969).

3.5.5.2 The origin of normal, intermediate and inverse magnetic fabrics

The dominance of normal magnetic fabrics is confirmation that matrix preferred orientation is primarily due to lithospheric compression or compaction. The stereographic projection shown in **Figure 3.19** shows that although matrix components have long axes that are parallel to the bedding plane, they do not define a lineation direction (their maximum susceptibility axes have declinations ranging to 9° to 356°). This indicates that the Horn River Group was deposited in a quiet setting with little to no current influence. If currents contributed to the observed fabric, there would be a clustering of maximum magnetic susceptibility axes.

Reports of inverse magnetic fabrics in shales and mudstones are sparse; only one paper describing inverse fabrics in siderite bearing black shales was found (Chadima et al. 2006). Potter and Stephenson (1988) first described them in igneous/metamorphic samples where they were due to the presence of uniaxial stable single domain magnetite. We will identify such inverse fabrics in shales for the first time to our knowledge (see **Chapter 6**). They have also been recognized in igneous and metamorphic samples containing tourmaline (Rochette et al. 1994). It is not possible to discern which of these applies with room temperature AMS results alone so in **Chapters 4** and **7,** magnetic techniques which allow for the isolation of specific magnetic sub-fabrics are used to determine which scenario applies in the Horn River Group mudrocks.

Intermediate fabrics have been modeled by mixing together normal and inverse fabrics. Different types of intermediate fabrics are produced depending on the degree of anisotropy and amounts of normal and inverse fabrics mixed (Rochette et al. 1992; Ferré, 2002; Chadima et al. 2006). For Horn River samples with both minimum and maximum susceptibility axes inclined at 20° to 49°, intermediate fabrics may be due to the presence of grains that show some preferred orientation but have some grain long axes that are randomly oriented. **Figure 3.26** compares the thin section photomicrograph and principal axes orientations of such a sample. Compared to other Evie samples, bioclasts in this sample are not strongly aligned. The 45° and 44° inclinations of the maximum and minimum susceptibility axes may be because, although bioclasts clearly define a bedding parallel fabric, their long axes are randomly oriented. Since the bulk AMS tensor and ellipsoid of a sample are composites of the individual tensors and ellipsoids of its constituent grains, the obtained principal orientations are not reflective of actual rock fabric.

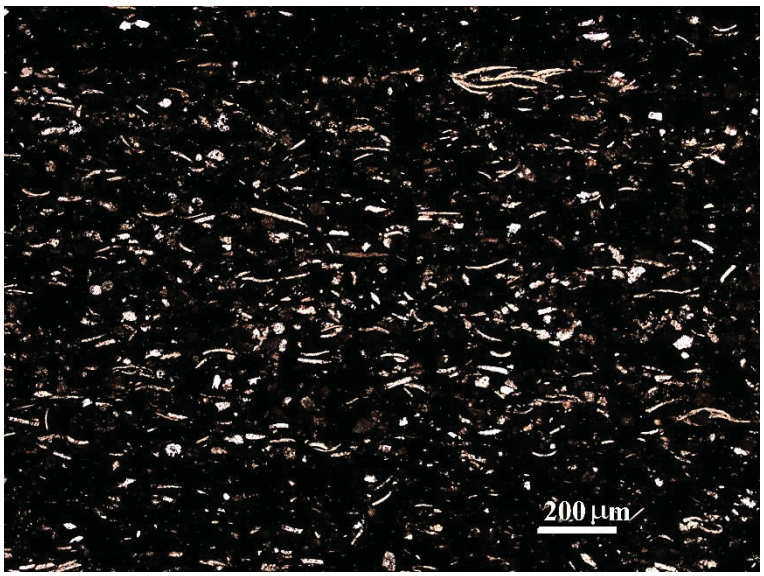

k_1		k_2		k_3	
Declination (º)	Inclination (º)	Declination (º)	Inclination (º)	Declination (º)	Inclination (º)
240.5	45.6	146.3	4.1	52.5	44.1

Figure 3.28: Thin section photomicrograph and principal susceptibility axes orientations of a Horn River Group sample with intermediate AMS fabric.

3.6 Conclusions

Magnetic susceptibility of cubic, sodium silicate impregnated mudstone and shale samples were measured in 18 directions and used to compute AMS tensors and ellipsoids. From the bulk susceptibility and AMS results of Horn River Group mudrocks from the Imperial Komie well, the following conclusions are reached:

1. Anisotropy of magnetic susceptibility techniques can successfully be utilized as a fabric analysis tool in fissile shales. When argillaceous samples are impregnated with viscous sodium silicate and cut in a jet of propylene glycol, there is little to no alteration of their original fabric.
2. Bulk magnetic susceptibility was controlled by the concentration of paramagnetic clay minerals and diamagnetic quartz and organic matter. It is lowest in the siliceous Upper Muskwa and calcareous Evie and highest in the clay rich Otter Park and Lower Muskwa.
3. There is a strong correlation between total organic content (TOC) and bulk volume magnetic susceptibility. There was also a strong correlation between TOC and anisotropy of magnetic susceptibility. No prior studies to our knowledge have shown these relationships.
4. The concentration of organic matter is the primary control on anisotropy of magnetic susceptibility, and hence, preferred orientation of minerals. Organic rich mudstones of the Evie have the highest AMS of all three formations studied and organic rich mudstones of the Upper Muskwa have AMS values comparable to those of clay rich Otter Park. Increasing concentration of clay minerals does not therefore appear to be the primary control on anisotropy from these room temperature measurements. This study identified this effect of organic richness in shales and mudstones for the first time to our knowlege.
5. The prevalence of normal fabrics with an absence of a defined lineation indicated that mineral preferred orientation was primarily due to lithospheric compression or compaction. Inverse fabrics were also identified. We suspected that some of these were due to the presence of stable single domain magnetite. This was confirmed using the anisotropy of magnetic remanence (AMR) detailed in **Chapter 6**. To our knowledge, this is the first time that such inverse fabrics due to stable single domain particles have been reported in shales.

6. Some Evie samples show evidence that anisotropy could also be the result an extensional stress. In such samples, the orientations of twin planes are coincident with the principal AMS directions.

3.7 References

Aruldhas, G., 2010. Engineering physics. PHI Learning Pvt. Ltd., p. 295-296.

Aubourg, C., Rochette, P., and Vialon, P., 1991. Subtle stretching lineation revealed by magnetic fabric of Callovian-Oxfordian black shales (French Alps). Tectonophysics, 185(3), 211-223.

Ballet, O., and Coey, J.M.D., 1982. Magnetic properties of sheet silicates; 2:1 layer minerals. Phys. Chem. Minerals, 8, 218-229.

Ballet, O., Coey, J.M.D., and Burke, K.J., 1985. Magnetic properties of sheet Silicates; 2:1:1 layer minerals. Phys. Chem. Minerals, 12, 370-378.

Basavaiah, N., 2012. Geomagnetism: solid earth and upper atmosphere perspectives. Springer Science and Business Media, pp. 468.

Bhathal, R.S., 1971. Magnetic anisotropy in rocks. Earth Science Reviews, 7(4), 227-253.

Biedermann, A.R., Koch, C.B., Lorentz, W.E.A., and Hirt, A.M., 2014. Low-temperature magnetic anisotropy in micas and chlorite. Tectonophysics, 629, 63-74.

Bjorlykke, K., 2010. Petroleum Geoscience: From sedimentary environments to rock physics. Springer Science and Business Media, pp. 662.

Bødker, F., Hansen, M.F., Koch, C.B., Lefmann, K., and Møru P, S., 2000. Magnetic properties of hematite nanoparticles. Phys. Rev., B 61, 6826.

Borradaile, G.J., and McArthur, J., 1990. Experimental calcite fabrics in a synthetic weaker aggregate by coaxial and non-coaxial deformation. Journal of Structural Geology, 12(3), 351-363.

Borradaile, G.J., and Jackson, M., 2004. Anisotropy of magnetic susceptibility (AMS): magnetic petrofabrics of deformed rocks. In: Martin-Hernández, F.,Lüneburg, C.M., Aubourg, C., Jackson, M. (Eds.), magnetic fabric methods and applications. The Geological Society of London, Special Publications, 238, 299 - 360.

Butler, R.F., 1992. Paleomagnetism: magnetic domains to geologic terranes. Blackwell Scientific Publications, pp. 319.

Brace, W. F., 1965. Some new measurements of linear compressibility of rocks, J. Geophysics Res., 70, 391-398.

Carmichael, R. S., 1989. Practical handbook of physical properties of rocks and minerals. CRC Press, Boca Raton, pp. 345.

Carter, N.L., and Raleigh, C.B., 1969. Principal stress directions from plastic flow in crystals. Geological Society of America Bulletin, 80, 1231-1264.

Chadima, M., Pruner, P., Šlechta, S., Grygar, T., and Hirt, A.M., 2006. Magnetic fabric variations in Mesozoic black shales, Northern Siberia, Russia: Possible paleomagnetic implications. Tectonophysics, 418, 145-162.

Cornell, R. M., and Schwertmann, U., 2006. The Iron oxides: Structure, properties, reactions, occurrences and uses. John Wiley and Sons, p. 32-33.

De Bresser J.H.P., and Spiers C.J., 1997. Strength characteristics of the r, f and c slip systems in calcite. Tectonophysics, 272, 1-23.

Deer, W.A., Howie, and R.A., Zussman, J., 1992. An introduction to the rock forming minerals. Longman Group UK Limited, pp. 498.

de Wall, H., Bestmann,. M., and Ullemeyer, K., 2000. Anisotropy of diamagnetic susceptibility in Thassos marble: a comparison between measured and modeled data. J. Struct. Geol., 22, 1761-1771.

Dunlop, D. J., Ozdemir, O., 1997. Rock magnetism: Fundamentals and frontiers. Cambridge University Press, Cambridge, p. 573.

Ellwood, B.B., 1980. Application of the anisotropy of magnetic susceptibility method as an indicator of bottom-water flow direction. Marine Geology, 34, 783-790.

Ferré, E.C., 2002. Theoretical models of intermediate and inverse AMS fabrics. Geophysical Research Letters. 29(7).

Ferré E.C., Martin-Hernández, F., Teyssier, C., and Jackson, M., 2004. Paramagnetic and ferromagnetic magnetic susceptibility in migmatites: measurements in high and low fields and kinematic implications. Geophys. J. Int., 157, 1119-1129.

Galehouse, J. S., 1968. A test of the method using the anisotropy of magnetic susceptibility as a paleocurrent indicator. Geol. Soc. Amer. Bull., 79, 887-890.

Girdler, R. W., 1961. The measurement and computation of anisotropy of magnetic susceptibility in rocks. Geophys. J. R. Astron. Soc., 5, 34–44.

Graham, J. W., 1966. Significance of magnetic Anisotropy in Appalachian Sedimentary rocks, In: Steinhart, S., and Smith, T.J., The earth beneath the continents, Geophysical Monograph Series 10, eds ,Washington, DC: American Geophysical Union, 627-648.

Graham, J. W., 1954. Magnetic susceptibility anisotropy, an unexploited petrofabric element. Bulletin of the Geological Society of America, 65, 1257-1258.

Gornitz, V., 2008. Encyclopedia of paleoclimatology and ancient environments, Springer Science and Business Media, p. 580.

Grim, R. E., Bray, R. H., and Bradley, W. F., 1937. The mica in argillaceous sediments. Amer. Mineral, 22, 813- 829.

Hall, S., and Sager, W.W., 1990. Paleomagnetic and rock magnetic properties of sediment samples from ocean drilling program leg 116, central Indian Ocean. Proceedings of the Ocean Drilling Program, Scientific Results, 116.

Hamilton N., 1963. Susceptibility anisotropy measurements on some Silurian siltstones. Nature, 197, 170-171.

Hamilton, N., Rees, A.I., 1970. Magnetic fabric of sediments from the shelf at La Jolla (California). Marine Geology, 9, M6-M11.

Hamilton, T.D., Borradaile, G.J., and Lagroix, F., 2004. Sub-fabric identification by standardization of AMS: an example of inferred neotectonic structures from Cyprus. In: Geological Society, London, Special Publications, 238, 527-540.

Hill, R.J., Craig, J.R., and Gibbs, G.V., 1979. Systematics of the spinel structure type. Physics and Chemistry of Mineral, 4(4), 317-339.

Hirt, A.M., Evans, K.F., and Engelder, T., 1995. Correlation between magnetic anisotropy and fabric for Devonian shales on the Appalachian Plateau. Tectonophysics, 247, 121-132.

Hirt, A. M., and Gehring, A. U., 1991. Thermal alteration of the magnetic mineralogy in ferruginous rocks. J. Geophys. Res., 96, 9947-9953.

Hounslow, M. W., 1985. Magnetic fabric arising from paramagnetic phyllosilicate minerals in mud rocks. J. Geol. Soc. London, 142**,** 995-1006.

Hounslow, M. W., 2001. The crystallographic fabric and texture of siderite in concretions: implications for siderite nucleation and growth processes. Sedimentology, 48, 533-557.

Hrouda, F., and Ježek, J., 1999. Magnetic anisotropy indications of deformations associated with diagenesis. In: Tarling, U. H., and Turner, P. (eds), Palaeornagnetisrn and Diagenesis in Sediments, Geological Society, London, Special Publications, 151, 127-137.

Ihmlé, P. F., Hirt, A. M., Lowrie, W., and Dietrich, D., 1989. Inverse magnetic fabric in deformed limestones of the Morcles Nappe, Switzerland. Geophys. Res.Lett., 16, 1383-1386.

Jackson, M., Sprowl, D., and Ellwood, B., 1989. Anisotropies of partial anhysteretic remanence and susceptibility in compacted black shales: Grainsize and composition dependent magnetic fabric. Geophysics Research Letters, 16, 1063-1066.

Jackson, M., 1991. Anisotropy of magnetic remanence: a brief review of mineralogical sources, physical origins, and geological applications, and comparison with susceptibility anisotropy. Pure Appl. Geophys*,* 136, 1-28.

Jain, M., Gupta, R., Gupta, A., and Kumar, M., 2007. Diamagnetic susceptibility and anisotropy of organic and organometallic compounds. Springer Science and Business Media, 27(A), 3-4.

Jamison, W. R., and Spang, J. H., 1976. Use of calcite twin lamellae to infer differential stress. Bull. Geol. Soc. Am., 87, 868-872.

Khan, M. A., 1962. Anisotropy of magnetic susceptibility of some igneous and metamorphic rocks. J. Geophys. Res., 67, 2873-2885.

Khan, M. A., and Rees, A. I., 1968. Magnetic analysis of rock fabric. In: Runcorn, S. K. ed., International Dictionary of Geophysics, Pergamon.

King, R. F., 1966. The magnetic fabric of some Irish granites. Geol. J., 5, 43-46.

Lander, R.H., and Walderhaug, O., 1999. Predicting porosity through simulating sandstone compaction and quartz cementation. AAPG Bulletin, 83(3), 433-449.

Larrasoaña, J.C., Gómez-Paccard, M., Giralt, S., and Roberts, A.P., 2011. Rapid locking of tectonic magnetic fabrics in weakly deformed mudrocks. Tectonophysics, 507, 16-25.

Lee, T.Q., and Angelier, J., 2000. Tectonic significance of magnetic susceptibility fabrics in Plio-Quaternary mudstones of southwestern foothills, Taiwan. Earth, Planets, Space, 52, 527-538.

Lehman, B., Sagnotti, L., Winkler, A., Lo Cascio, C., 1996. Magnetic mineralogy changes in the Pleistocene marine sequence of Montalto di Castro (central Italy) and influence on the magnetic anisotropy. Geophys. J. Int. 127, 529-541.

McLean, A., and Gribble, C., 2003. Geology for civil engineers. CRC Press, pp.336.

Merrill, R.T., 2010. Our magnetic earth. University of Chicago Press, p. 12.

Owens, W. H., 1974. Mathematical model studies on factors affecting the magnetic anisotropy of deformed rocks. Tectonophysics, 24, 115-131.

Parés, J.M., 2004. How deformed are weakly deformed mudrocks? Insights from magnetic anisotropy. Geological Society, London, Special Publication, 238, 191-203.

Parés, J.M., 2015. Sixty years of anisotropy of magnetic susceptibility in deformed sedimentary rocks. Frontiers in Earth Science: Geomagnetism and Paleomagnetism, 3(4).

Potter, D.K., and Stephenson, A., 1988. Single-domain particles in rocks and magnetic fabric analysis. Geophysical Research Letters, 15(10), 1097-1100.

Rees, A. I., 1961. The effect of water currents on the magnetic remanence and anisotropy of susceptibility of some sediments. Geophys. J. R. Astron. Soc., 5, 235-251.

Rees, A. I., 1965a. The use of anisotropy of magnetic susceptibility in the estimation of sedimentary fabric. Sedimentology, 4, 257-271.

Rees, A. I., 1965b. Preliminary measurements of the anisotropy of magnetic susceptibility of the Franciscan formation of central California. Geol. Soc. Amer. Bull., 76, 975-980.

Rees, A. I., 1968. The production of preferred orientation in a concentrated dispersion of elongated and flattened grains. Jour. Geology, 76, 457 - 465.

Richter, C., Frisch, W., Ratschbacher, L., and Schwarz, H.U., 1991. The magnetic fabrics of experimentally deformed artificial clays-water dispersions. Tectonophysics, 200, 143-155.

Robion, P., Delamotte, D.F., Kissel, C., and Aubourg, C., 1995. Tectonic versus mineralogical contribution to the magnetic fabric of epimetamorphic slaty rocks–an example from the Ardennes Massif (France–Belgium). J. Struct. Geol., 17, 1111-1124.

Rochette, P., and Fillion, G., 1988. Identification of multicomponent anisotropies in rocks using various field and temperature values in a cryogenic magnetometer. Phys. Earth Planet. Inter., 51, 379-386.

Rochette, P., Jackson, M. and Aubourg, C., 1992. Rock magnetism and the interpretation of anisotropy of magnetic susceptibility. Review of Geophysics, 30, 209-226.

Rochette, P., Scaillet, B., Guillot, S., Le Fort, P., Pecher, A., 1994. Magnetic properties of the High Himalayan leucogranites: structural implications. Earth Planet. Sci. Lett., 126, 217-234.

Schieber, J., and Ellwood, B., 1993. Determination of basinwide paleocurrent patterns in a shale succession from anisotropy of magnetic susceptibility (AMS): a case study of the Mid Proterozoic Newland Formation, Montana. Journal of Sedimentary Petrology, 63, 874-880.

Schmidt, V., Günther, D., Hirt, A.M., 2006. Magnetic anisotropy of calcite at room temperature. Tectonophysics, 418, 63-73.

Schumacher, B.A., 2002. Methods for the determination of total organic carbon (TOC) in soils and sediments. US. Environmental Protection Agency, NCEA-C- 1282 EMASC-00.

Smith, D.O., 1956. Magnetization of a magnetite single crystal near the Curie point. Phys. Rev., 102, 959.

Spencer, A.M., 1993. Generation, accumulation and production of Europe's hydrocarbons III. Special Publication of the European Association of Petroleum Geoscientists, No. 3, p. 101.

Stephenson, A., Sadikun, S., and Potter, D.K., 1986. A theoretical and experimental comparison of anisotropies of magnetic susceptibility and remanence in rocks and minerals. Geophysics J. R. Astr. Soc. 84, 185-200.

Tarling, D. H., and Hrouda, F., 1993. The magnetic anisotropy of rocks. Chapman and Hall, London, p. 217.

Thompson, R. and Oldfield, F., 1986. Environmental Magnetism. Allen and Unwin, London, pp. 243.

Tourneret, C., and Laurent, P., 1990. Paleo-stress orientations from calcite twins in the North Pyrenean foreland, determined by the Etchecopar inverse method. Tectonophysics, 180, 287-302.

Tullis, T. E., 1980. The use of mechanical twinning in minerals as a measure of shear stress magnitude. J. Geophys. Res., 85, 6263-6268.

Turner, F.J., Griggs, D.T., and Heard, H., 1954. Experimental deformation of calcite crystals. Geol. Soc. Am. Bull., 65, 883-934.

Wilson, M. D., and Stanton, P.T., 1994, Diagenetic mechanisms of porosity and permeability reduction and enhancement, in M. D. Wilson, ed., Reservoir quality assessment and prediction in clastic rocks: SEPM Short Course 30, p. 59–119.

Yaalon, D.H., 1962. Mineral composition of the average shale. Clay Minerals, 5(27), 31-36.

Chapter 4

Quantifying shale and mudstone mineralogy and anisotropy from low temperature magnetic susceptibility measurements

4.1 Introduction

In this chapter, the low field temperature dependence of paramagnetic susceptibility and anisotropy of magnetic susceptibility (AMS) are applied in quantifying mineralogy and understanding the petrofabric of shales and mudstones from the Horn River Basin. Although the variation of magnetic susceptibility with temperature has been used in some studies to enhance bulk magnetic susceptibility (Ihmlé et al., 1989), only a few studies have measured the variation of AMS with temperature (Richter and van der Pluijm, 1994; Hirt et al., 1995; Schmidt et al., 2007). All of these measured AMS at only two temperatures, room temperature and liquid nitrogen temperature, and only one (Hirt et al., 1995) studied shales.

Room temperature bulk magnetic susceptibility and anisotropy of magnetic susceptibility are dependent on the magnetic susceptibility and preferred orientation of all matrix components respectively. They therefore include contributions from the diamagnetic, paramagnetic, antiferromagnetic and ferrimagnetic minerals within a sample. In certain applications, it may be necessary to isolate or exclude the contributions to the bulk magnetic signal of certain magnetic phases or minerals. If, for example, ferrimagnetic minerals dominate a sample's magnetic signal despite their low concentrations, a method to exclude the ferrimagnetic subfabric is necessary, especially if AMS ellipsoids are to be accurately used to determine the preferred orientation of the matrix minerals. Where magnetic phases within a sample all have different preferred orientations

and the AMS ellipsoid is not representative of actual petrofabric, methods that isolate individual subfabrics are necessary. Several methods of isolating or separating the contributions of different magnetic phases have been advanced. The following is a brief description of the most common ones.

Comparison of low field and high field anisotropy of magnetic susceptibility

High field susceptibility methods allow for the separation of diamagnetic and paramagnetic AMS from ferrimagnetic AMS (Rochette and Fillion, 1988; Hrouda and Jelinek, 1990). Magnetic susceptibilities measured in low fields (0.1mT - 0.5mT) are the sum of magnetic susceptibilities of all magnetic phases within a sample. In high magnetic fields (> 1 T), all ferrimagnetic minerals are saturated, leaving only the diamagnetic and paramagnetic contributions.

Anisotropy of magnetic remanence (AMR)

Anisotropy of magnetic remanence methods measure the anisotropy of only matrix minerals capable of retaining a remanent magnetization (ferrimagnetic and antiferromagnetic minerals). The most common techniques are the anisotropy of isothermal remanent magnetization (AIRM) and the anisotropy of anhysteretic remanent magnetization (AARM) (Rochette et al., 1992; Borradaile and Henry, 1997). These methods are useful for determining the petrofabric of ferrimagnetic and antiferromagnetic minerals, but because remanent magnetization is magnetization retained in the absence of a previously applied magnetic field, AMR results cannot be directly compared to anisotropy of magnetic susceptibility (AMS) results or used in the separation of AMS components (Martin-Hernández and Ferré, 2007).

Low and high temperature methods

Temperature methods take advantage of the temperature dependence of paramagnetic susceptibility described by the Curie law (Biedermann et al., 2014; Hirt and Gehring, 1991; Ihmlé et al. 1989). With decreasing temperature, paramagnetic susceptibility and paramagnetic

anisotropy of magnetic susceptibility increase. This enhancement of the paramagnetic contribution can be used to quantify the contribution of paramagnetic minerals to bulk magnetic susceptibility and AMS (Richter and van der Pluijim, 1994), and to determine the orientation of paramagnetic minerals especially where they differ from those of other matrix minerals. Low temperature methods are particularly useful in the study of magnetic fabrics in mudrocks because at room temperature, mudrocks generally have low magnetic susceptibilities that may result in weakly defined magnetic fabrics. Increasing bulk magnetic susceptibility potentially allows for easier analysis of magnetic fabrics.

High temperature or heating methods may be used to determine the ferrimagnetic or antiferromagnetic minerals present in a sample. This is because above a mineral specific critical temperature known as the Curie temperature (T_c) in ferrimagnetic minerals and Neèl temperature (T_N) in antiferromagnetic minerals, ferrimagnetic and antiferromagnetic minerals behave like paramagnets (Hrouda et al., 1997). Heating methods are however unsuitable for understanding original rock fabrics because of the possibility of irreversible chemical changes that introduce new magnetic minerals with fabrics that differ from that of the original matrix minerals (Henry et al., 2003). We therefore decided to concentrate on a low temperature methodology to quantify shale and mudstone mineralogy and anisotropy in several Horn River Group samples.

4.1.1 Theoretical background of the low temperature magnetic method: The Curie-Weiss law

As previously mentioned, the low temperature technique is based on the Curie-Weiss law. In the absence of an external magnetic field, the unpaired electrons in a paramagnetic material are randomly oriented; their net moments cancel out resulting in zero net magnetization. When a field is applied, moments partially align producing a small positive net magnetization parallel to the external field. Thermal agitation or excitement of atoms works to reduce the alignment of atomic moments, hence, with decreasing temperature, moments become more aligned and net magnetization increases. This increase in paramagnetic susceptibility, χ_{para}, with decreasing temperature is described by the Curie-Weiss law as follows:

$$\chi_{para} = \frac{C}{T} \tag{4.1}$$

where T is the absolute temperature in Kelvin and C is the mineral specific Curie constant.

Diamagnetic susceptibility is independent of temperature. Also, assuming magnetite is the primary ferrimagnetic mineral present in the mudrocks studied here, ferrimagnetic susceptibility is also approximately independent of temperature between 120K and room temperature (Richter and Pluijm, 1994; Özdemir et al. 2009). **Figure 4.1** shows the magnetic susceptibility-temperature behaviour of magnetite in magnetic fields of different intensities. At 120K, the crystal structure of magnetite changes from cubic to monoclinic (Verwey, 1939).

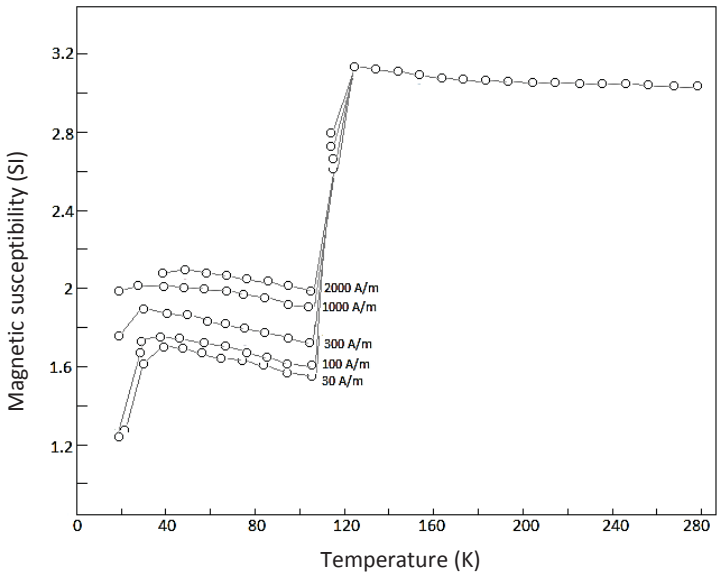

Figure 4.1: Variation of the magnetic susceptibility of magnetite with temperature at different magnetic field strengths. Above the Verwey transition (~120K), the magnetic susceptibility of magnetite is approximately independent of temperature (modified from Özdemir et al., 2009).

4.1.2 Literature review: the application of the Curie-Weiss law in mudrocks

Only one study applying the low temperature method to the study of mudrock petrofabric was found (Hirt et al., 1995). They concluded that paramagnetic clay minerals (especially chlorite) are responsible for the low temperature enhancement of bulk magnetic susceptibility and anisotropy of magnetic susceptibility in Devonian shales from the Appalachian Plateau. They also observed

that low temperature anisotropy of magnetic susceptibility correlated with percent compaction; which indicated that preferred orientation of clay minerals in the studied mudrocks was primarily due to compaction. All their samples contained over 90% clays, so lack of mineralogical and textural variability in their mudrocks mean that many aspects of the low temperature magnetic susceptibility and AMS behaviour of mudrocks remain poorly understood. In samples containing multiple paramagnetic minerals, for example, the impact of paramagnetic minerals other than clays on the temperature dependent bulk susceptibility and AMS have not been studied. Pyrite, for example can make up as much as 15% of a mudrock's composition, and paramagnetic carbonate minerals like siderite may be present in appreciable quantities, particularly in calcareous mudrocks. Additionally, even in mudrocks with clays as the dominant or only paramagnetic minerals, there is a lack of work on the differences between the temperature dependent behaviors of varying concentrations of diamagnetic and paramagnetic minerals. The application in isolating the fabric of paramagnetic minerals from low temperature susceptibility ellipsoids also remains unexplored.

4.1.3 Chapter goals

This chapter comprises three main sections. In each section a different application of the low temperature enhancement of paramagnetic susceptibility or AMS is investigated.

4.2 Temperature-susceptibility (k(T)) curves

In this section the variation of magnetic susceptibility with decreasing temperature for the siliceous mudstones from the Upper Muskwa, calcareous mudstones from the Evie and laminated argillaceous shales from the Lower Muskwa and Otter Park are compared. The comparison of k(T) curves gives an idea of the relative concentrations of paramagnetic and diamagnetic minerals in the studied samples.

4.3 Quantifying mineral concentrations in the Horn River Group

By comparing k (T) curves determined in section **4.2** to k (T) curves of theoretical mineral mixtures of known concentrations, absolute mineral concentrations for the shales and mudstones of the Horn River Group are determined.

4.4 Low temperature Anisotropy of Magnetic Susceptibility (LTAMS)

In this section the low temperature enhancement of paramagnetic AMS associated with the enhancement of paramagnetic susceptibility is investigated. The fabric elements controlling the variation in AMS with decreasing temperature are discussed, and the orientations of the LTAMS ellipsoids are used to determine the orientation of paramagnetic phases in representative samples from sections **4.2** and **4.3.** The LTAMS technique is particularly useful where paramagnetic minerals have orientations different from other matrix components**.**

4.2 Temperature-susceptibility (k (T)) curves

4.2.1. Sample preparation

Fifty-four of the 2.2cm × 2.2cm ×2.2cm sodium silicate impregnated cubic samples used in **Chapter 3** were used here. 10 samples were from the Muskwa, 18 from the Upper Otter Park, 20 from the Lower Otter Park and 6 from the Evie.

4.2.2 Method

Magnetic susceptibilities were measured between approximately 173K (-100°C) and room temperature 294.15K (21°C). Measurements were taken above 120K to ensure that ferrimagnetic (magnetite) susceptibility was independent of temperature and any increase in susceptibility was solely due to the paramagnetic minerals. First, each sodium silicate impregnated sample was cooled to approximately 173 K (-100°C) by full immersion in liquid nitrogen for 45 minutes. Magnetic susceptibility and temperature could not be measured simultaneously, so the temperature as a function of time, T (t), as the sample warmed up from 173K to room temperature was first measured using a thermocouple placed in a small hole drilled on the surface of the sample. The sample was then cooled a second time by full immersion in liquid nitrogen for 45 minutes. Following this second cooling, the mass magnetic susceptibility with time, k (t), was measured as the sample warmed up to room temperature using a Bartington dual frequency MS2B AMS sensor.

Mass magnetic susceptibility was measured in a low alternating field of 80A/m. The T (t) and k (t) graphs were combined to get k (T) (mass magnetic susceptibility as a function of temperature).

4.2.3 Results

Figure 4.2 shows the temperature profiles for two of the 54 samples whose temperature-susceptibility curves were determined. On average, it took 50 minutes to 55 minutes for samples to warm up to room temperature from 173K. **Figures 4.3A-D** show how magnetic susceptibility varies with temperature in the three formations. In all three, there is an inverse relationship between magnetic susceptibility and temperature as described by the Curie law. Since diamagnetic susceptibility is independent of temperature, and magnetite's susceptibility above the Verwey transition (120 K) is also approximately constant with temperature, the progressive increase in susceptibility with decreasing temperature is due to the presence of paramagnetic minerals.

A comparison of the susceptibility-temperature curves gives an idea of relative paramagnetic versus diamagnetic mineral concentrations. The largest percentage increase in magnetic susceptibility with decreasing temperature is noted in the lowest susceptibility, more diamagnetic intervals of the Upper Muskwa and Evie Formations. Note however, that these give the smallest absolute changes. The slope of the inverse susceptibility with temperature line may also be used as a measure of relative paramagnetic and diamagnetic concentrations; slope increases with decreasing paramagnetic/increasing diamagnetic concentration. **Figures 4.4A-D** are the (1/susceptibility) - temperature lines for the Muskwa, Otter Park and Evie samples.

In the Muskwa, two groups are identified: a paramagnetic poor (diamagnetic rich) Upper Muskwa with steeper 1/susceptibility –temperature plots and a paramagnetic rich Lower Muskwa. Below a certain paramagnetic concentration, as the diamagnetic component(s) susceptibility begin to dominate, the relationship between 1/susceptibility and temperature becomes more exponential than linear (**Figure 4.4A**).

In the Otter Park, there is no clear distinction between the Upper and Lower Otter Park on the basis of susceptibility-temperature and 1/susceptibility-temperature profiles. Upper Otter Park samples do however, generally have less steep 1/susceptibility-temperature plots, and are thus richer in paramagnetic components. The Evie and Upper Muskwa have the steepest 1/susceptibility-

temperature plots, and hence have significantly less paramagnetic minerals than the Lower Muskwa and Otter Park.

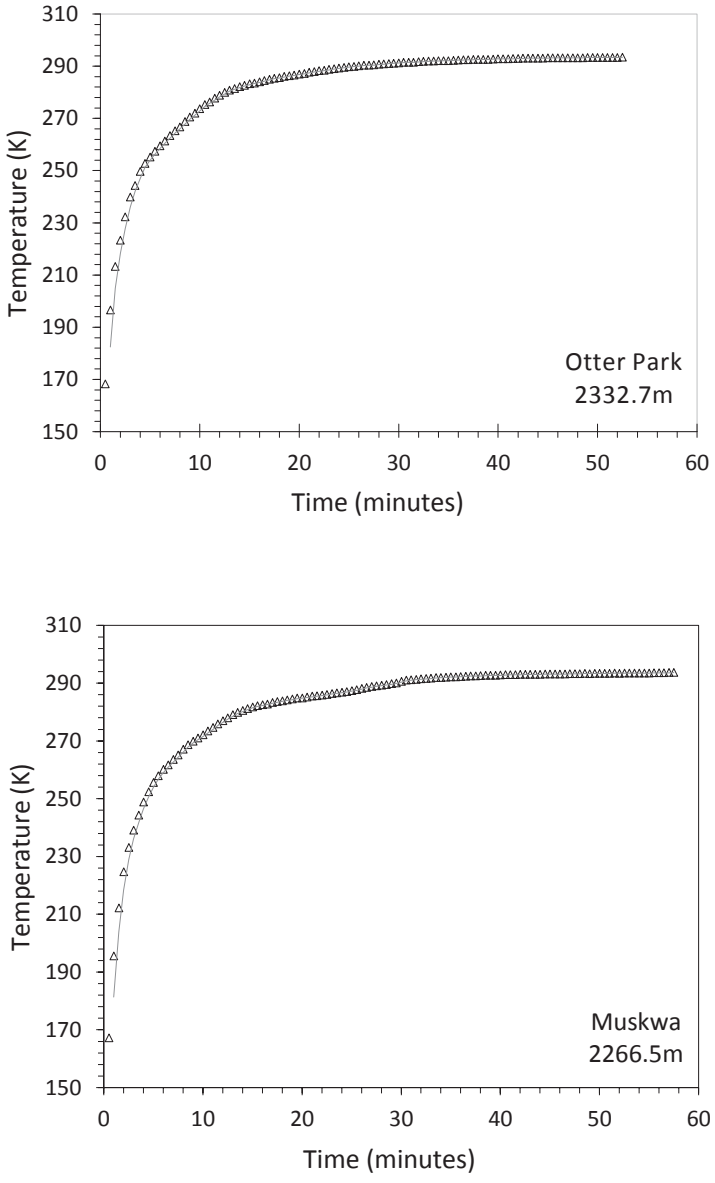

Figure 4.2: Warming profiles for two Horn River Group samples. It took approximately 50 – 55 minutes for samples to warm up to room temperature from approximately 170K.

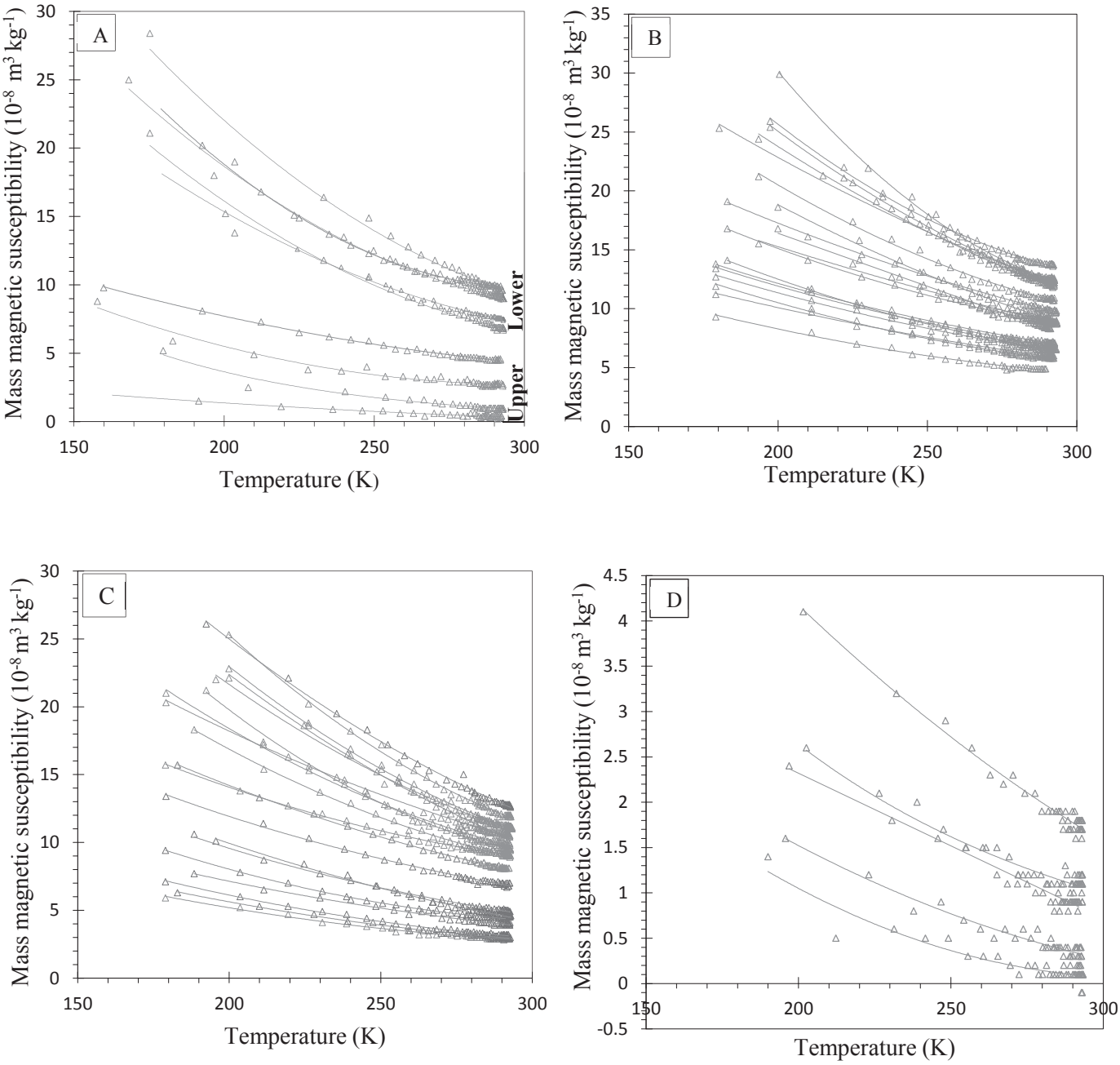

Figure 4.3: Low temperature magnetic susceptibility curves for a) the Muskwa b) Upper Otter Park c) Lower Otter Park and d) Evie Formations.

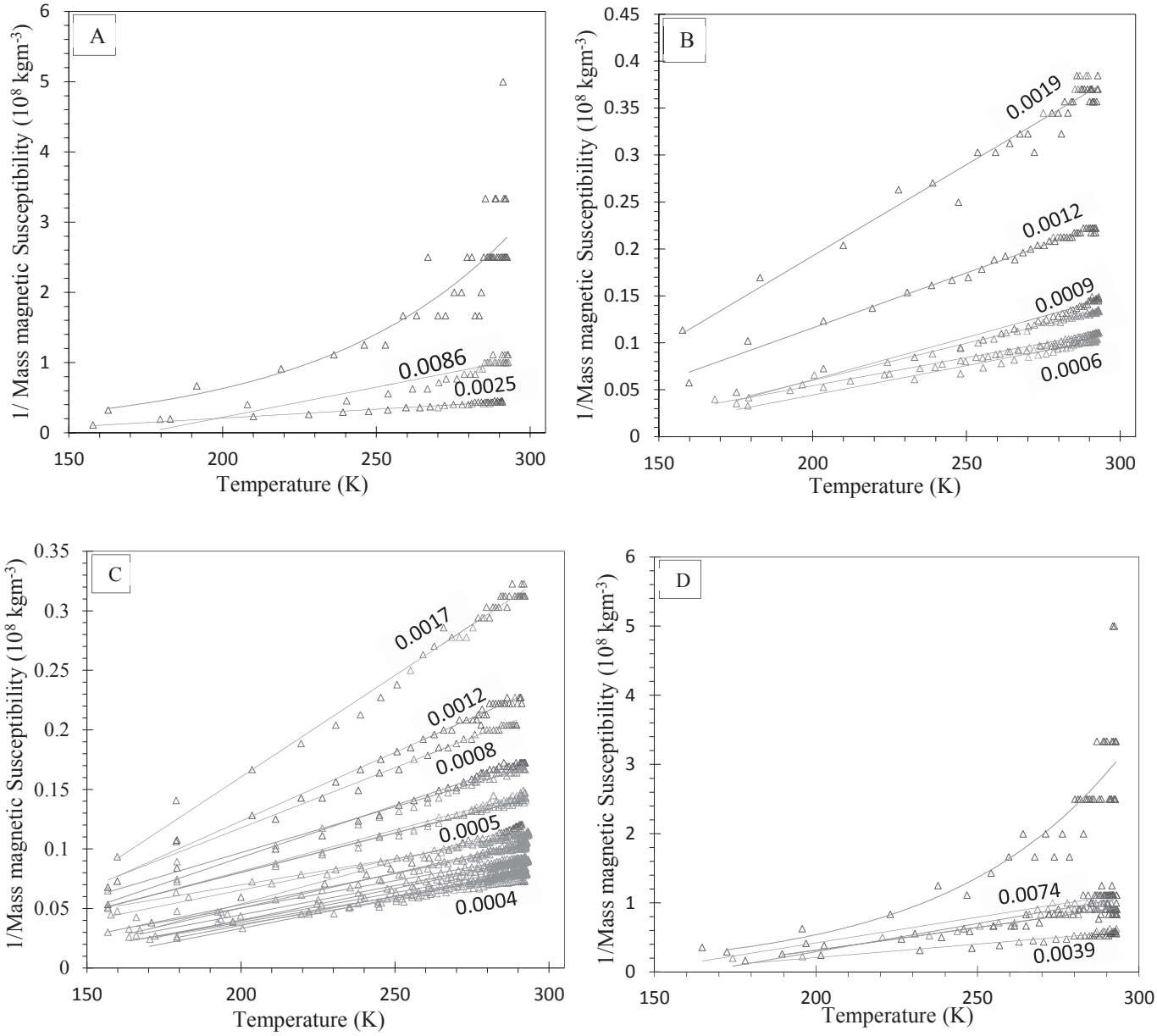

Figure 4.4: 1/magnetic susceptibility plots with temperature for (a) Upper Muskwa (b) Lower Muskwa (c) select samples from the Otter Park and (d) Evie Formations.

4.3 Mineral quantification using low temperature magnetic susceptibility curves

4.3.1 Theoretical susceptibility-temperature curves for illite-quartz mixtures

Comparing low temperature susceptibility curves only gives an idea of the relative concentrations of paramagnetic and diamagnetic minerals in a sample. To determine absolute mineral concentrations of Horn River Group samples, theoretical k (T) curves for known quartz and illite mixtures were compared to those of the Horn River formations determined in section **4.2**. The theoretical curves were determined for mixtures of quartz and illite because XRD results from Makhanov (2013) (**Table 4.1**) show that they are the primary paramagnetic and diamagnetic minerals in the Horn River Group. Although calcite is the dominant diamagnetic mineral in the Evie formation, calcite was not modelled separately since quartz and calcite have similar magnetic susceptibilities.

To determine the variation with temperature of magnetic susceptibility, the Curie law was used as follows:

$$\chi_T = C / T \tag{4.1}$$

where T is absolute temperature and C is the Curie constant. At any given temperature, the bulk magnetic susceptibility for a sample is the sum of the contributions of all of its individual components. For a sample consisting of illite and quartz, the magnetic susceptibility per unit mass χ_T is given by the expression:

$$\chi_T = \{(F_I)\,(\chi_I)\} + \{(1 - F_Q)(\chi_Q)\} \tag{4.2}$$

where F_I is the fraction of illite, $(1 - F_I)$ is the fraction of quartz and χ_I and χ_Q are the mass magnetic susceptibilities of the illite and quartz respectively (Potter et al, 2004). Using equation (4.2), the mass magnetic susceptibility of a particular combination of illite and quartz at room temperature is first calculated. For illite, a room temperature mass magnetic susceptibility of 15 $\times 10^{-8} m^3 kg^{-1}$ was used and for quartz, -0.55 $\times 10^{-8} m^3 kg^{-1}$ was used. Using equation (4.1), the calculated χ_T is then used to calculate the mixture's Curie constant C, which is in turn used to calculate χ_T for progressively reduced temperatures.

Eleven theoretical magnetic susceptibility-temperature template curves where determined for eleven mixtures of illite and quartz. Mass magnetic susceptibilities were calculated for temperatures between 80K (-193.15°C) and 294.15K (21°C). The illite-quartz combinations for which k (T) curves were determined are as follows:

3 wt. % illite 97wt. % quartz 10wt. % illite 90wt. % quartz 20wt. % illite 80wt. % quartz

30wt. % illite 70wt. % quartz 40wt. % illite 60wt. % quartz 50wt. % illite 50wt. % quartz

60wt. % illite 40wt. % quartz 70wt. % illite 30wt. % quartz 80wt. % illite 20wt. % quartz

90wt. % illite 10wt. % quartz 100wt. % illite

Table 4.1: XRD derived mineral compositions for Horn River Group mudrocks (Makhanov, 2013).

Formation	Quartz (wt. %)	Feldspar (wt. %)	Calcite (wt. %)	Dolomite (wt. %)	Pyrite (wt. %)	Kaolinite (wt. %)	Chlorite (wt. %)	Illite (wt.%)	Mixed layer (wt. %)	Total Clay (wt.%)
Muskwa	43	2	0	0	4	1	13	36	1	51
Muskwa	61	3	0	0	7	0	0	29	0	29
Otter Park	50	3	5	9	10	0	0	23	0	23

4.3.2 Results

4.3.2.1 Theoretical susceptibility-temperature curves for illite-quartz mixtures

The theoretical susceptibility temperature (k (T)) curves for the 11 mixtures of quartz and illite are shown in **Figure 4.5A**. The curves are used as templates for determining illite and quartz concentrations in the Horn River Group as shown in **Figure 4.5B**. Note that the "quartz" content may in fact be a "quartz + calcite" content in some samples. The concentrations of illite and quartz obtained are shown in **Figure 4.6** and **Table 4.2** provides a summary of the range of concentrations for each formation. To correct illite concentrations for anisotropy effects, the k(T) curves derived by taking an average of 9 directional susceptibilities for each measurement temperature were also used to determine illite concentration. **Figure 4.7** compares the illite concentrations determined using x axes k(T) curves and illite concentrations determined using an average of 9 directional

k(T) curves for 19 samples. The 9-axis determinations (which take account of the anisotropy) give illite contents that are, generally, slightly higher (up to about 10%) than those derived from the single x-axis determinations.

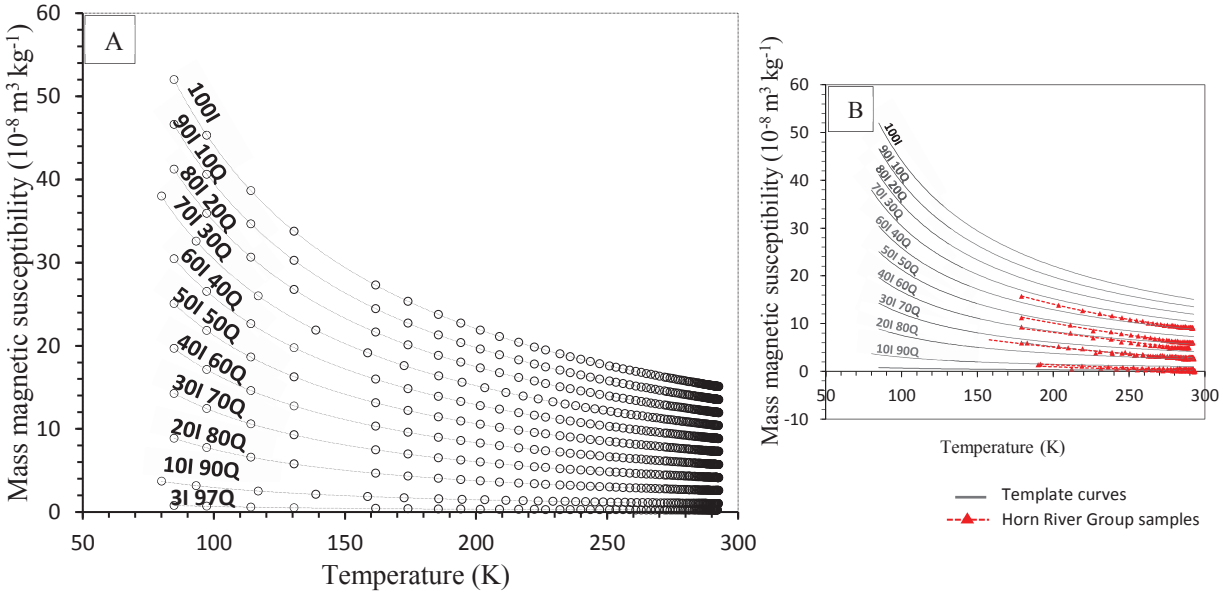

Figure 4.5: (A) Theoretical mass magnetic susceptibility-temperature curves for eleven mixtures of quartz and illite. The amounts of illite and quartz in each mixture are labelled 'I' and 'Q' respectively (e.g., 90I 10Q is 90% illite and 10% quartz). (B) Using theoretical mass magnetic susceptibility-temperature curves as templates for determining illite and quartz in the Horn River Group. Some experimental results are shown superimposed on the template curves.

As an independent check on the validity of the magnetically derived concentrations, we compared our results with those from a standard geochemical technique. The general formula for illite is $(K,H_3O)(Al,Mg,Fe)_2(Si,Al)_4O_{10}[(OH)_2,(H_2O)]$ and its aluminium oxide concentration varies from 25% to 45% (Manning, 1995). Since most of the aluminium oxide (Al_2O_3) in mudrocks is found in clays, Al_2O_3 concentrations were used to confirm the magnetic susceptibility derived clay (illite) concentrations. The Al_2O_3 concentrations were determined from Inductively Coupled Plasma Mass Spectrometry (ICP-MS). **Figure 4.8** shows a comparison of percent aluminium oxide and percent illite with depth, and **Figure 4.9** is the corresponding cross plot of percent Al_2O_3 and illite. Geochemical data was not available for all depths sampled for low temperature susceptibility

measurements, so only illite contents at depths close to those for which Al_2O_3 data are available are compared in **Figures 4.8** and **4.9** A Good correlation between the percent illite derived from low temperature magnetic susceptibility curves and the percent aluminium oxide suggests that illite content determined from low temperature magnetic susceptibility measurements are meaningful. For most samples, we determined the illite content from the temperature magnetic susceptibility in just one direction (open circles in **Figures 4.6**, **4.7**, **4.8** and **4.9**), the x-axis. For the samples whose illite content were also determined from an average of 9 orientations (solid squares in **Figures 4.8** and **4.9**), a slightly better correlation with the Al_2O_3 data is observed in **Figure 4.9 (**regression coefficient R^2=0.86 compared to R^2=0.84 for the single x-axis results).

.

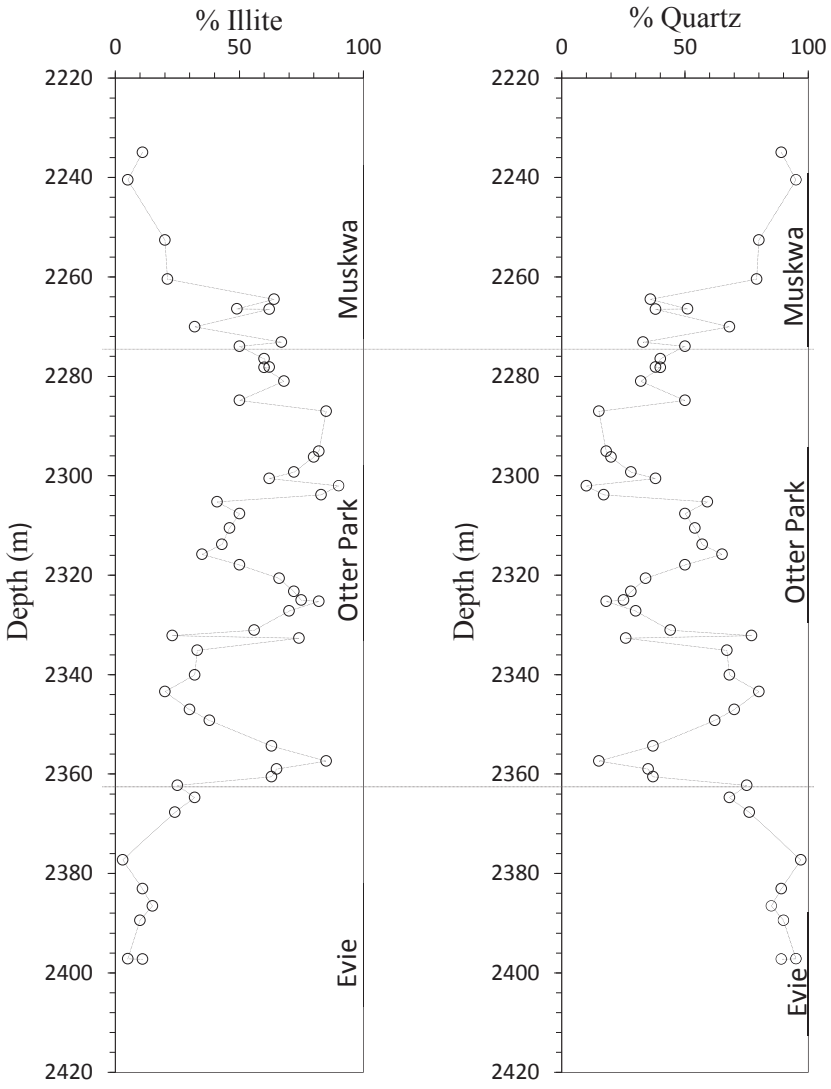

Figure 4.6: Percent illite and percent quartz with depth derived from k (T) curves of Horn River Group samples.

Table 4.2: Magnetic susceptibility derived clay and quartz concentration ranges for the Muskwa, Otter Park and Evie Formations.

Formation	Illite (wt. %)	Quartz (wt. %)
Upper Muskwa (top 30m)	11 - 21	79 - 95
Lower Muskwa (lower 20m)	32 - 67	33 - 68
Upper Otter Park (top 48m)	23 - 90	10 - 77
Lower Otter Park (lower 30m)	20 - 85	15 - 80
Evie	3 - 15	85 - 97

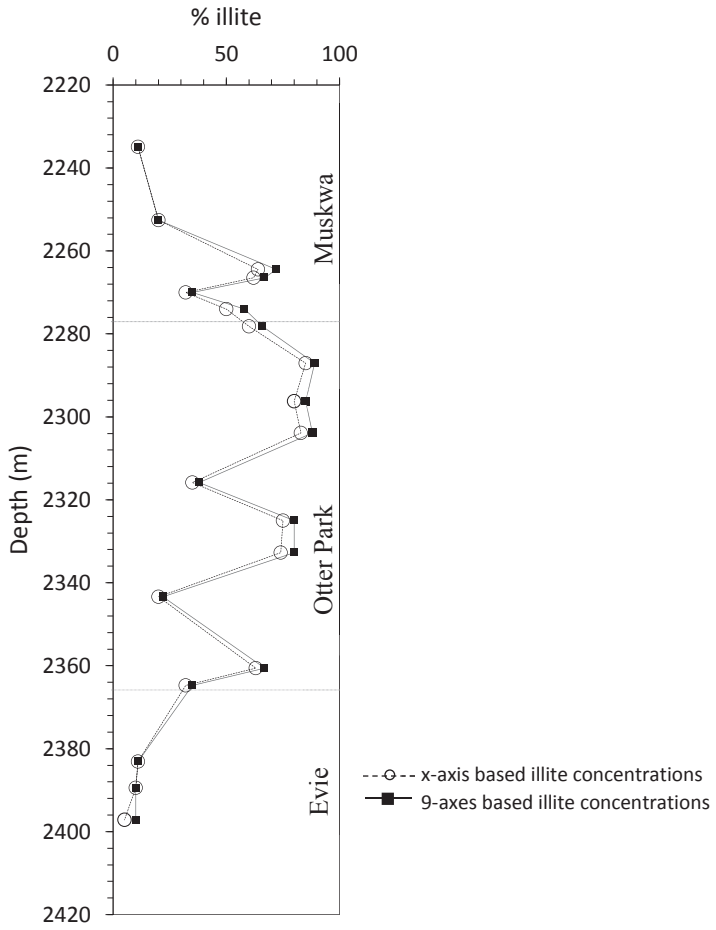

Figure 4.7: Comparison of percent illite from x-axes k(T) curves (open circles) and percent illite from an average of 9 k(T) curves (closed squares).

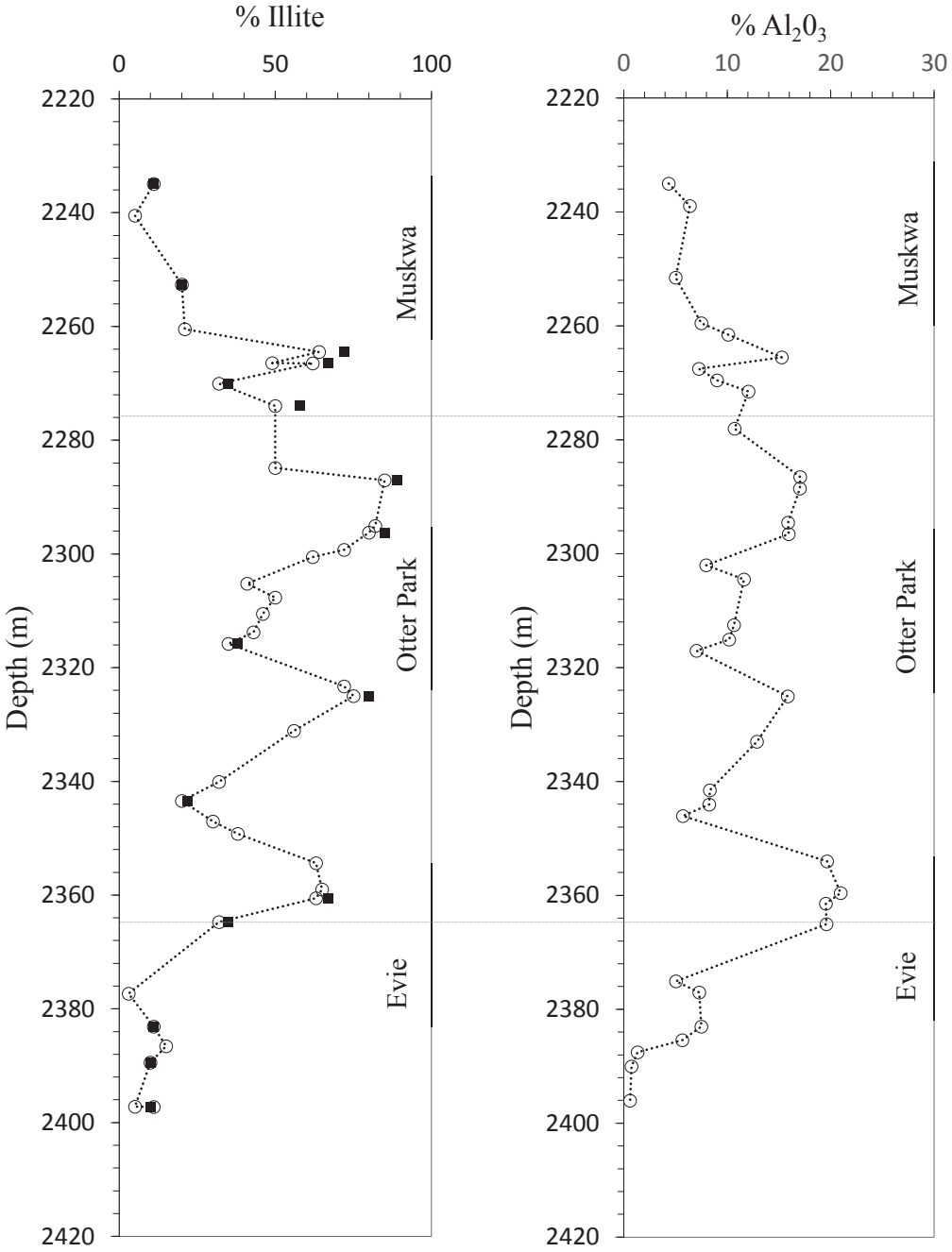

Figure 4.8: Percent illite derived from k (T) curves and percent Al_2O_3 from mass spectrometry in the Horn River Group. Similar trends with depth suggest that the low temperature magnetic technique can provide meaningful illite content in the Muskwa, Otter Park and Evie formations. For the illite content, closed squares are percent illite determined from an average of 9 directional susceptibilities, and open circles are illite concentrations derived using just one directional susceptibility (along the x-axis).

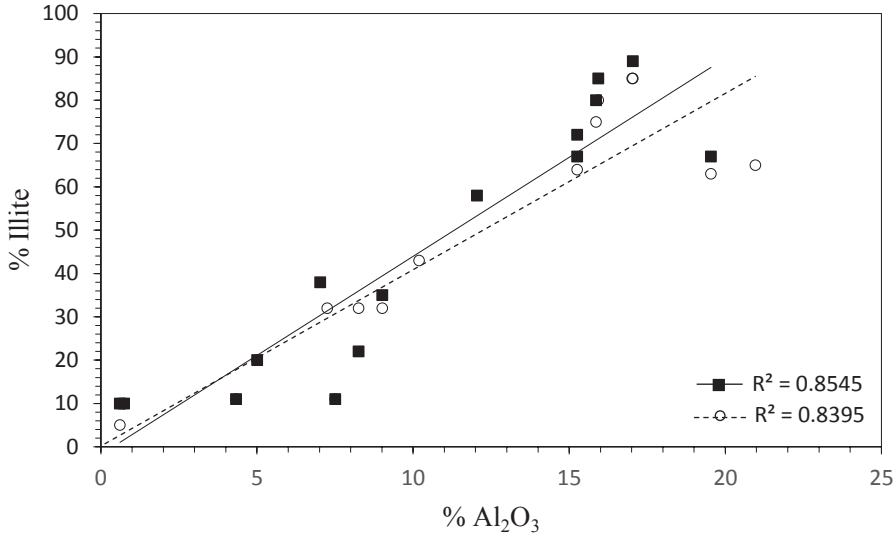

Figure 4.9: Cross plot of % Illite and % Al_2O_3. Closed squares are for illite concentrations derived using an average of 9 k(T) curves and open circles are for illite concentrations derived using x-axes k(T) curves. Good correlation demonstrates that illite concentrations can be accurately determined from susceptibility-temperature curves.

4.4 Low temperature Anisotropy of Magnetic Susceptibility (LTAMS)

4.4.1 Materials and method

At progressively lower temperatures, the orientations and magnitudes of the orthogonal principal axes that define the susceptibility ellipsoid increasingly reflect the petrofabric of paramagnetic minerals present in a sample. In sections **4.2.2** and **4.3.2**, low temperature mass magnetic susceptibility is measured in one direction. To determine the susceptibility tensor and its ellipsoid with decreasing temperature, at each temperature, at least 9 directional susceptibility measurements are required. For 19 of the 54 sodium silicate impregnated Horn River Group samples, the nine directions measured are shown **Figure 4.10**. Nine k (T) curves, one for each direction shown in **Figure 4.10**, were determined for each sample using the same procedure as in sections **4.2.2** and **4.3.2**. Each of the nine curves were determined in a consistent manner in terms of the timing of measurements. Principal values, directions and percent anisotropy of magnetic susceptibility were calculated for each measurement temperature.

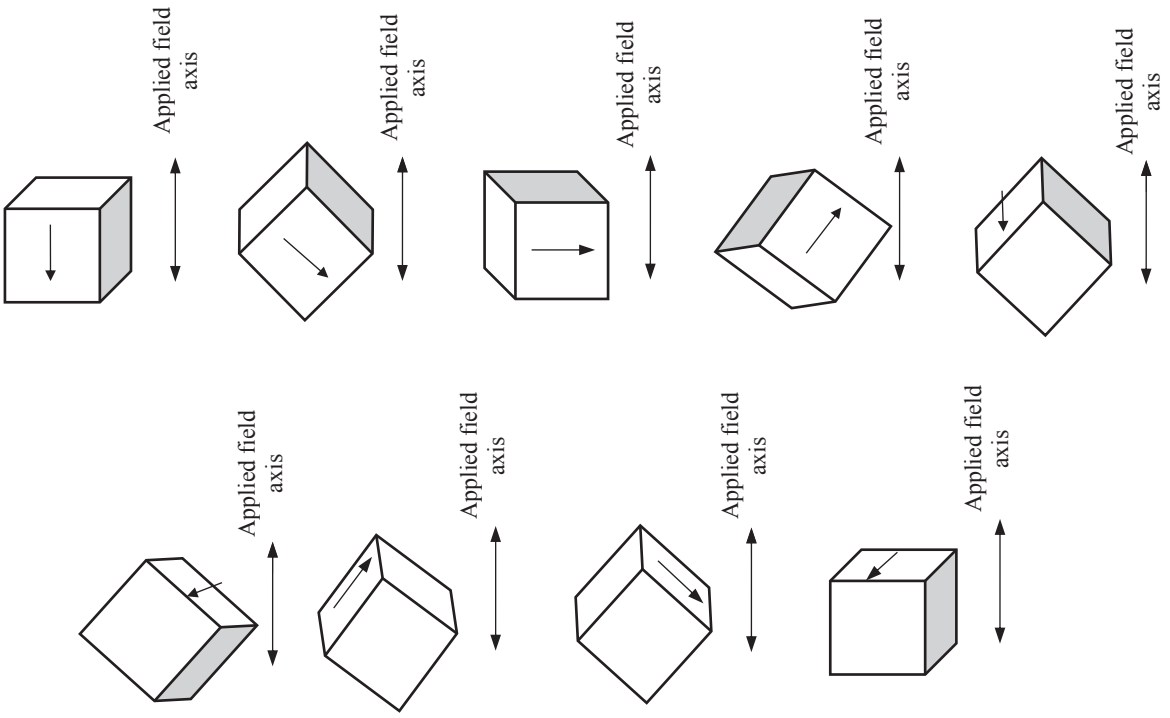

Figure 4.10: Nine directions for which susceptibilities where measured during warming from low temperature to room temperature. Directional susceptibilities are used to determine the susceptibility tensor kij.

4.4.2 Results

4.4.2.1 Anisotropy of magnetic susceptibility with temperature behaviour

For all 19 samples from the Muskwa, Otter Park and Evie formations whose AMS with temperature was determined, mass magnetic susceptibility increased with decreasing temperature in all nine measurement directions. At each temperature, anisotropy of magnetic susceptibility ellipsoids and percent anisotropy were calculated. **Figure 4.11** compares room temperature AMS and AMS at 200K for the 19 samples. Between room temperature and 200K, AMS increases by <1% to 158%. **Figures 4.12**, **4.13 a**nd **4.14** show the progressive changes in percent AMS with temperature for individual samples. The difference between room temperature AMS and AMS at a lower temperature is due solely to the paramagnetic phases in a sample. Note that some samples

exhibit negligible AMS at room temperature, but significant AMS at low temperature. This shows the usefulness of the low temperature measurements in identifying anisotropy. For Horn River Group samples with illite content between 10% and 74%, there is a general increase in the difference between lower temperature and room temperature AMS with increasing illite concentration. **Figure 4.15B** shows a good correlation between the difference between AMS at 200K and room temperature AMS {AMS (200K) −AMS (RT)} and illite concentration ($R^2 = 0.79$). The concentration of the primary paramagnetic phase (illite) therefore appears to be the principal control on the AMS (T) response of these samples. However, three Horn River Group samples with illite concentrations above 74% have {AMS (200K) −AMS (RT)} values similar to samples with 30% to 40% illite (**Figure 4.15A**). The lower difference between low temperature AMS and room temperature AMS despite high concentrations of illite indicates that illite concentration may not be the only control on the AMS (T) response of these samples.

One sample from the Evie, despite its low clay content (11%), had percent AMS that decreased with increasing temperature in a profile similar to that of a sample with 60% to 70% illite (**Figure 4.16**). This suggests that a paramagnetic mineral other than illite dominates the paramagnetic anisotropy of magnetic susceptibility at this depth.

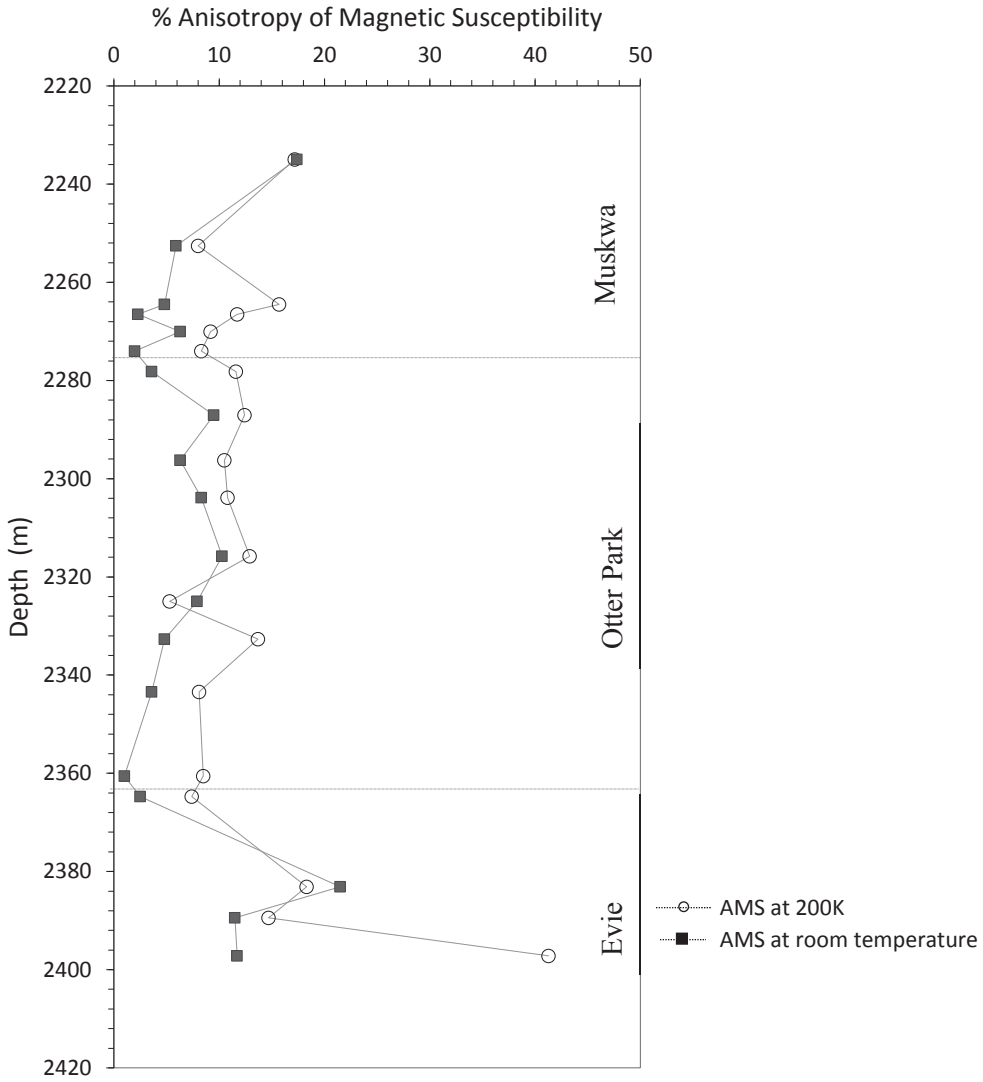

Figure 4.11: Comparison of AMS at room temperature and AMS at 200K. The closed square symbols represent the room temperature AMS and the open circle symbols represent the AMS at 200K.

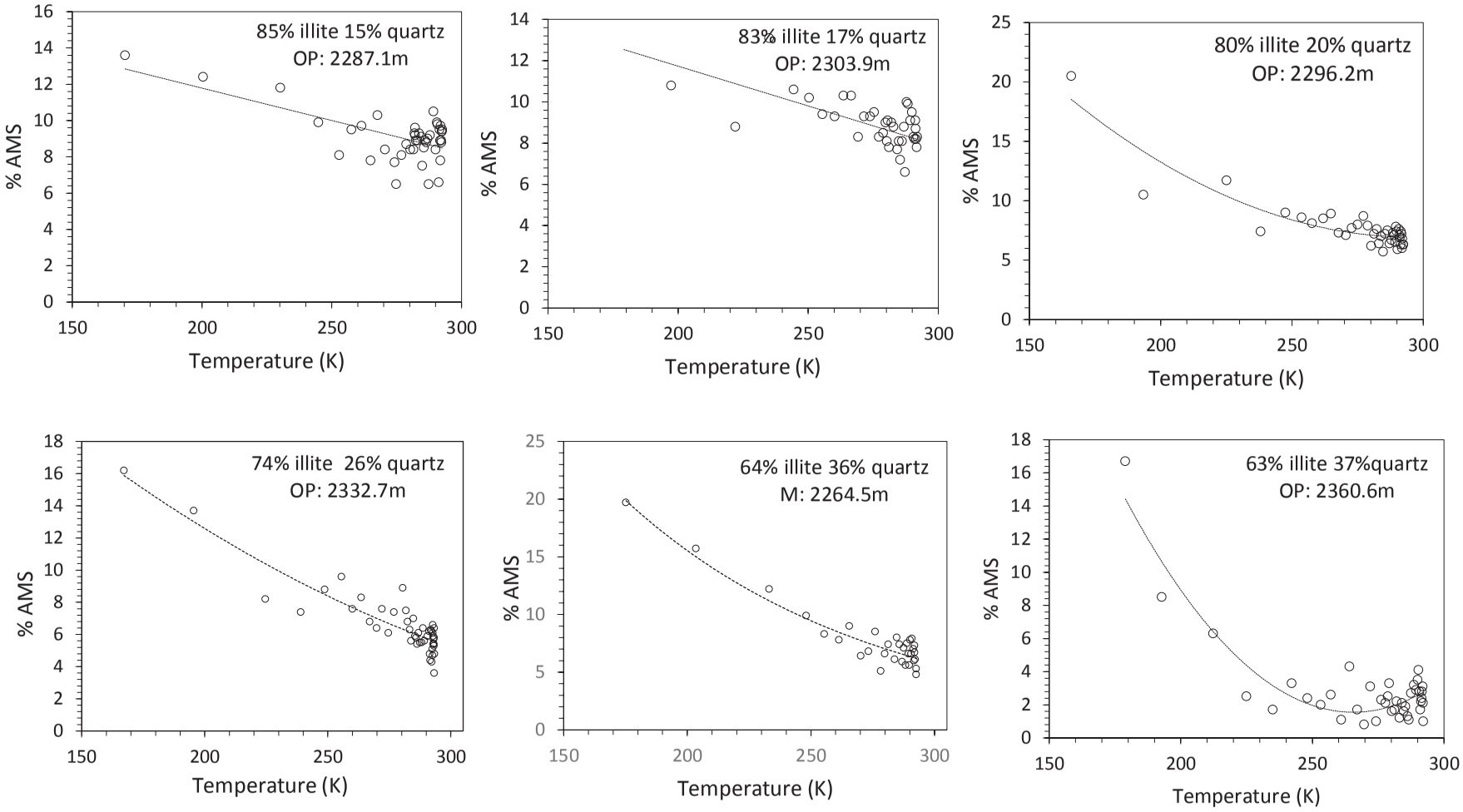

Figure 4.12: Variation of percent AMS with temperature for Horn River Group samples. Samples labelled 'M' are from the Muskwa, and those labelled 'OP' are from the Otter Park.

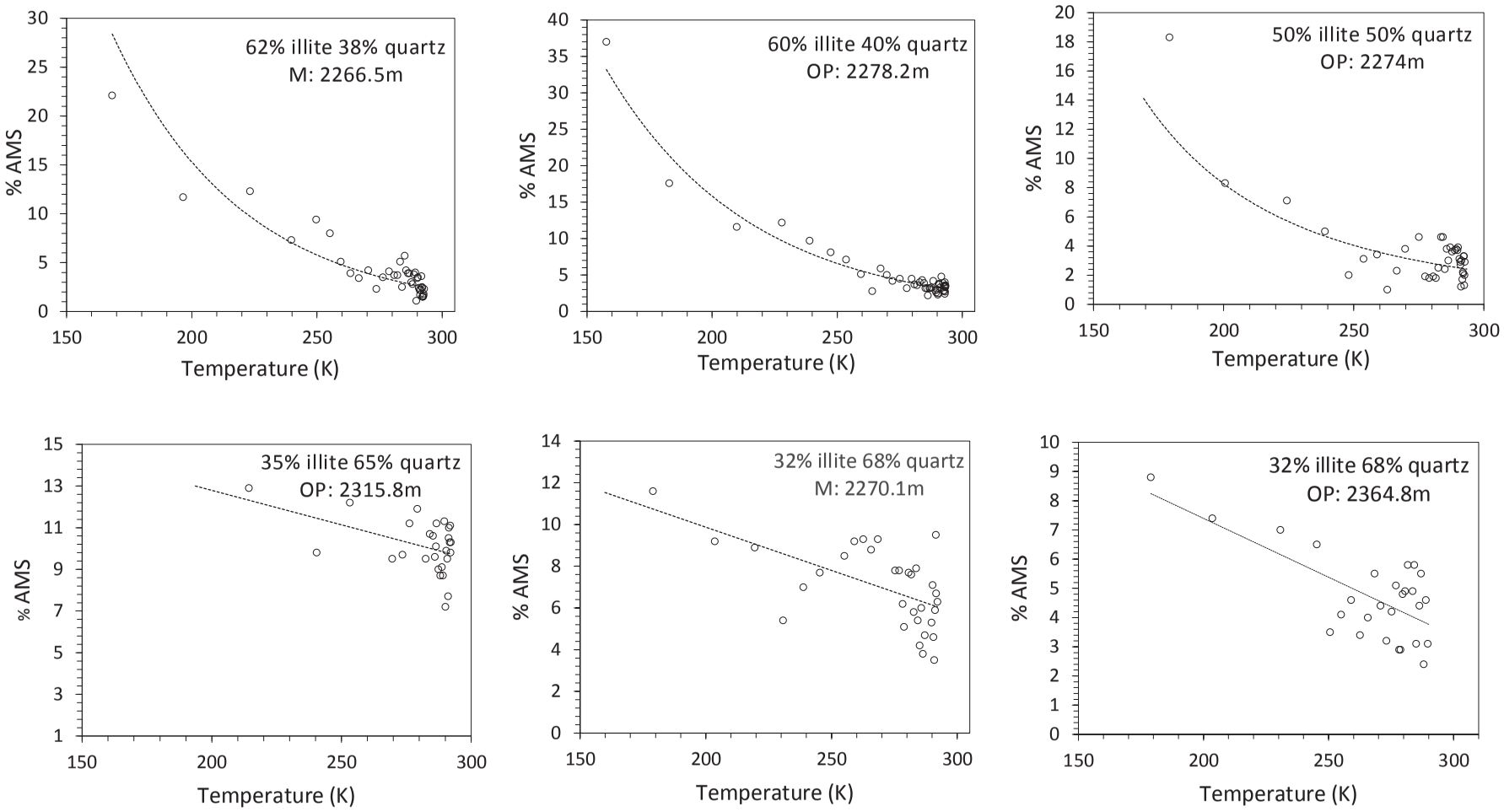

Figure 4.13: Variation of percent AMS with temperature for Horn River Group samples. Samples labelled 'M' are from the Muskwa, and those labelled 'OP' are from the Otter Park.

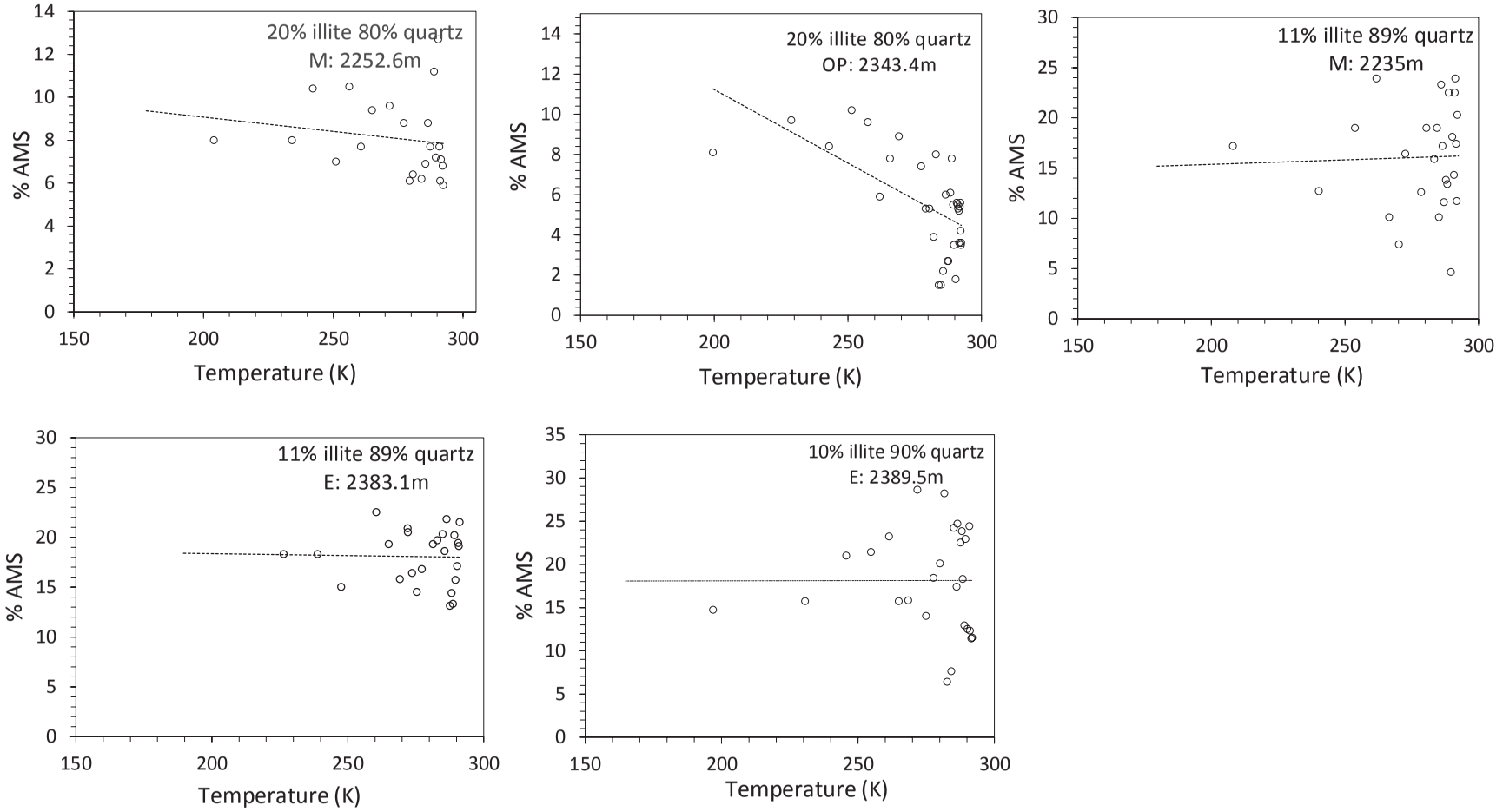

Figure 4.14: Variation of percent AMS with temperature for Horn River Group samples. Samples labelled 'M' are from the Muskwa, those labelled 'OP' are from the Otter Park, and those labelled 'E' are from the Evie.

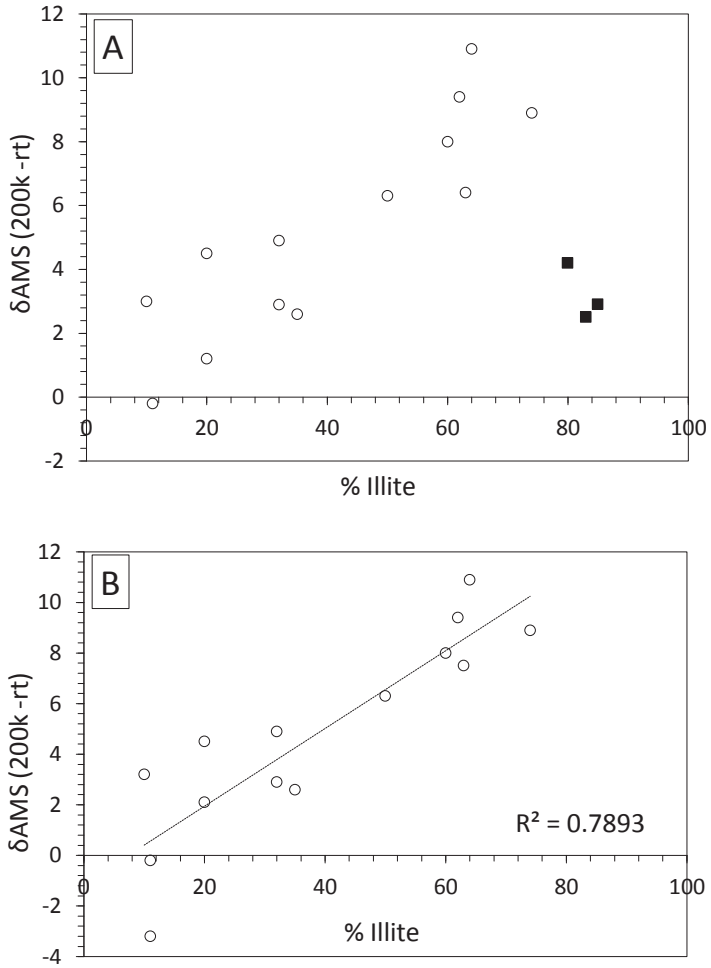

Figure 4.15: Relationship between (AMS 200K – room temperature AMS) and illite content for (A) all 19 Horn River Group samples whose susceptibility ellipsoids were determined and (B) for Horn River Group samples with illite concentration less than 74%.

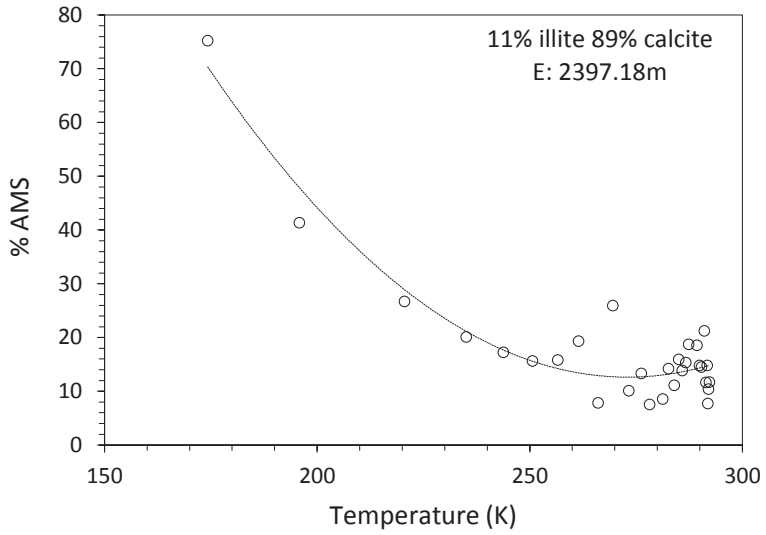

Figure 4.16: AMS (T) profile for a calcareous sample from the Evie formation. Despite a low illite concentration, the sample has a significant increase in AMS with decreasing temperature. This shows the usefulness of low temperature measurements in identifying anisotropy.

4.4.2.2 Orientations of the principal AMS axes with decreasing temperature

Where paramagnetic minerals have orientations different from those of other minerals in a sample, the orientations of the orthogonal principal axes that comprise the 3D ellipsoid will increasingly reflect the orientations of paramagnetic phases with decreasing temperature. In the Horn River formations, four distinct fabrics were distinguished on the basis of changes in principal axes orientations with decreasing temperature. The following are the cases observed in the Horn River Group from Imperial Komie D-069-K/094-O-02:

1. *Normal fabric with k_{min} (k_3) and k_{max} (k_1) retaining a constant orientation with decreasing temperature*

   These samples have k_{max} subparallel to and k_{min} perpendicular to the bedding plane irrespective of temperature (**Figure 4.17**). K_{max} declinations show some variability (as one would expect for a planar fabric where the k_{max} inclinations are low), but for the most part, remain fairly consistent with temperature. These ellipsoid orientations suggest that the paramagnetic

minerals have the same or similar orientation as the matrix component(s) controlling room temperature AMS.

Significantly, a northeast-southwest clustering of principal AMS axes with decreasing temperature is observed in some samples (**Figure 4.17b – 4.17e**). **Figures 4.18a** and **4.18b** show expanded stereonets (with the corresponding temperatures for k_{max} axes) of two such samples in **Figure 4.17**. At higher temperatures (280K to 293K), k_{max} has a range of declinations for the sample shown in **Figure 4.18a**. However, at lower temperatures (<270K) a tight clustering of k_{max} axes suggests a possible subtle structural feature (e.g lineation) not observed at room temperature. At room temperature % AMS for this sample is approximately 6 to 8%, while at 200K it is approximately 12.4%. The tight clustering of k_{max} at low temperature may therefore be due to the 40% to 70% increase in anisotropy with decreasing temperature. For the sample whose expanded stereonet is shown in **Figure 4.18b**, there is a clustering of both room temperature and low temperature k_{max} axes. Since this lineation is observed in four of six Type 1 samples shown in **Figure 4.17**, the low temperature clustering of k_{max} axes can potentially be used for re-orienting core samples.

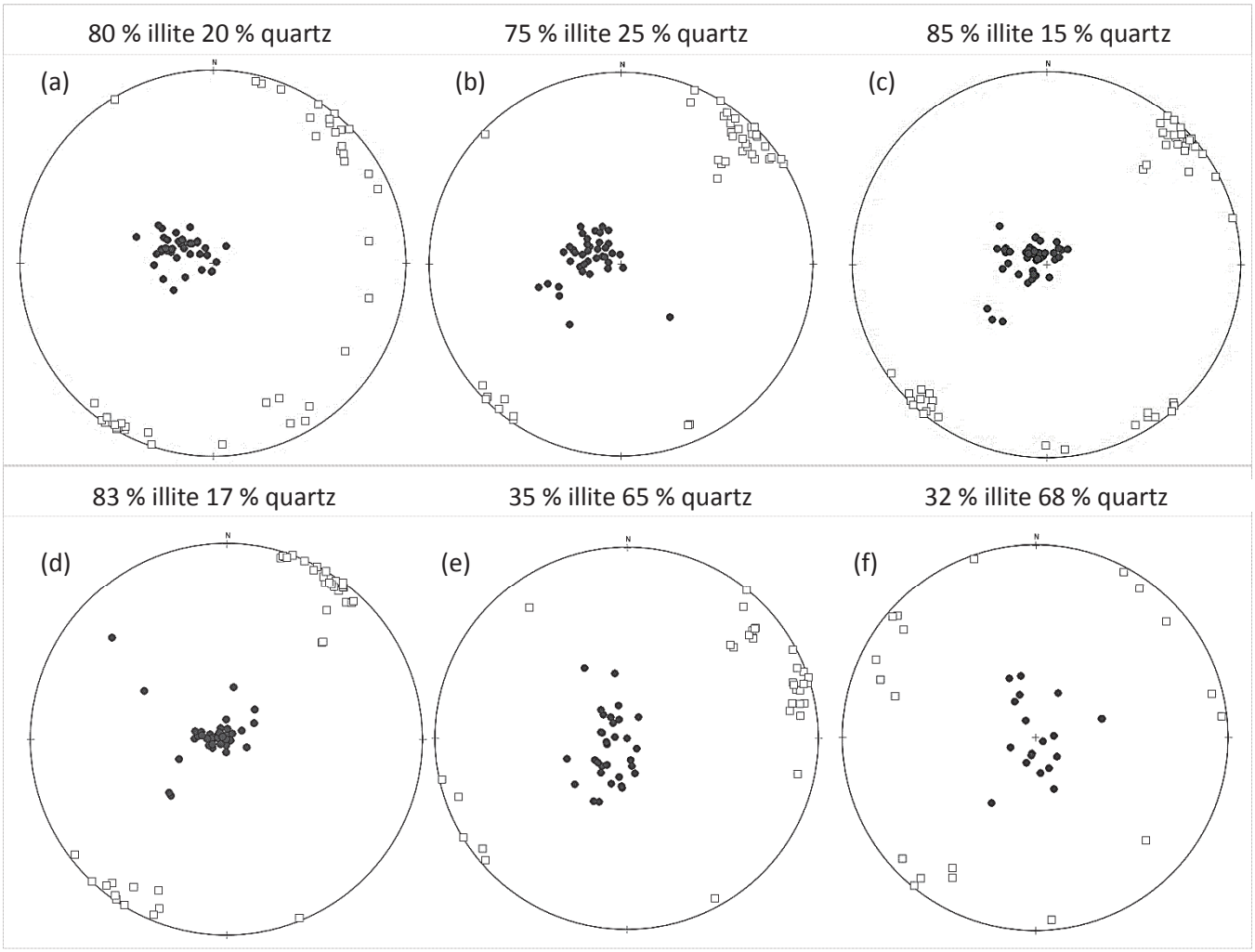

Figure 4.17: Stereographic projections showing variation in magnetic fabric type with temperature for the Horn River Group Type 1 samples that have normal magnetic fabrics irrespective of temperature i.e. minimum magnetic susceptibility (solid circles) is normal to the bedding/deposition plane and maximum magnetic susceptibility (open squares) is parallel to it. Each stereonet shows results from low temperature to room temperature for one sample (temperature values have been omitted for clarity).

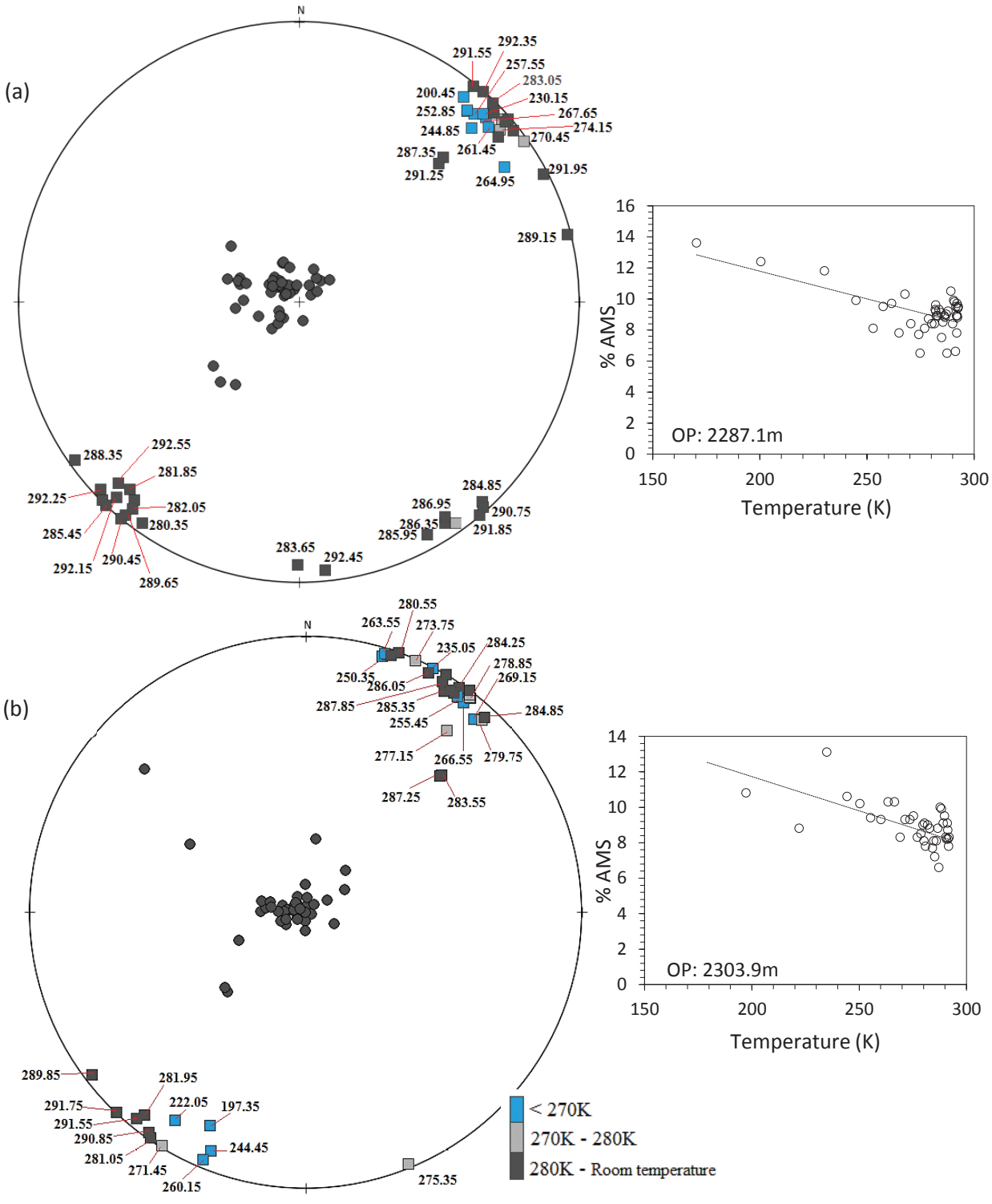

Figure 4.18: Expanded stereographic projections of Type 1 samples with a clustering of k_{max} principal orientations (closed squares) with decreasing temperature. K_{max} axes are colored to clearly show their variation with decreasing temperature.

2. *Inverse fabric with k_{min} and k_{max} retaining a constant position with decreasing temperature*

   Room temperature ellipsoid results showed that some Horn River samples have an inverse magnetic fabric with k_{min} parallel/subparallel to the bedding plane and k_{max} perpendicular to it. Stephenson et al. (1986) found that such fabrics may be due to the presence of stable single domain (SSD) magnetite, while Rochette and Fillion (1988), Ihmlé et al. (1989) and Schmidt et al. (2007) found that they may also be due to the presence of paramagnetic ferroan calcite or siderite whose c-axis is its maximum susceptibility axis (Jacobs, 1963). In the second group of Horn River samples, an inverse fabric is sustained (and in fact enhanced) between room temperature and 200K (-73°C) (**Figure 4.19**). This suggests that iron-bearing carbonates are present and contribute to the paramagnetic behaviour in these samples. It also suggests that stable single domain (SSD) magnetite is not solely responsible for the inverse fabric observed at room temperature in these samples. This is because magnetite susceptibility is temperature independent between 120K and room temperature, and so the inverse fabric would not be enhanced at low temperature if SSD magnetite was responsible. Scanning electron microscope images of two of these samples (**Figure 4.20**) confirm that samples in this class are rich in carbonates. EDX (Energy Dispersive X-ray) spectra of both samples confirmed that the carbonates are iron bearing (**Figure 4.21** and **Figure 4.22**).

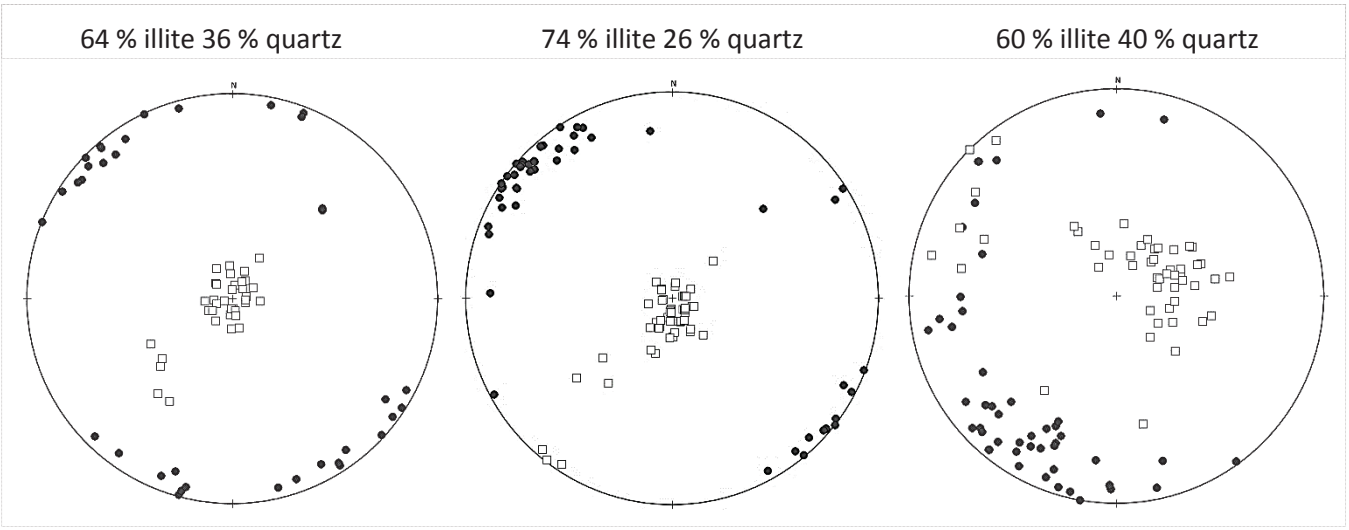

Figure 4.19: Stereographic projections showing variation in magnetic fabric type with temperature for the Horn River Group Type 2 samples that have inverse magnetic fabrics irrespective of temperature i.e. maximum magnetic susceptibility (open squares) is normal to the bedding/deposition plane and minimum magnetic susceptibility (closed circles) is parallel to it.

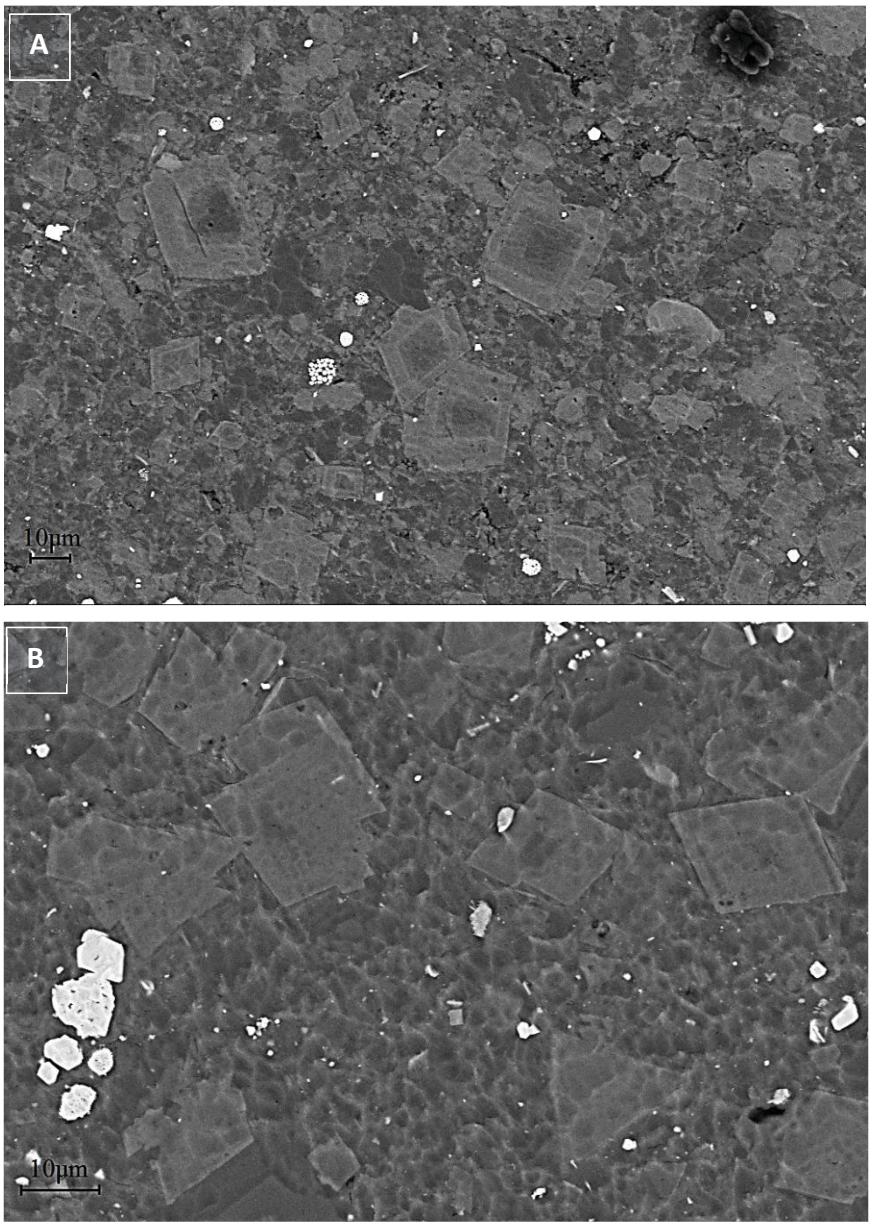

Figure 4.20: Scanning electron microscope images of two samples with inverse magnetic fabrics at room temperature and progressively lower temperatures. Samples are carbonate rich so illite is not primarily responsible for the observed variation of susceptibility with temperature.

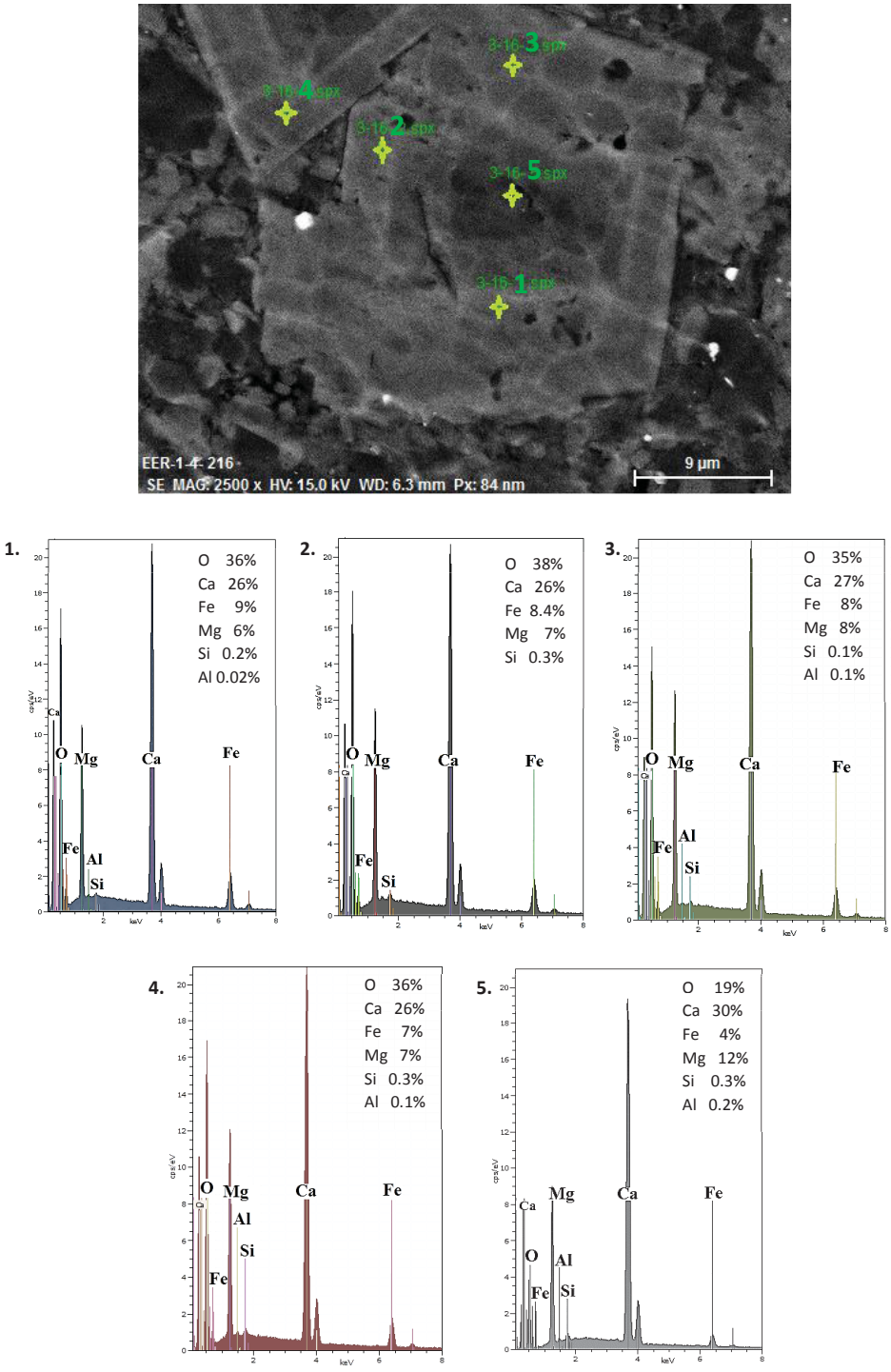

Figure 4.21: EDX spectra for samples that retain an inverse magnetic fabric irrespective of temperature confirm the presence of iron-carbonates. Spectra are for sample A in **Figure 4.20** and elemental compositions are semi-quantitative.

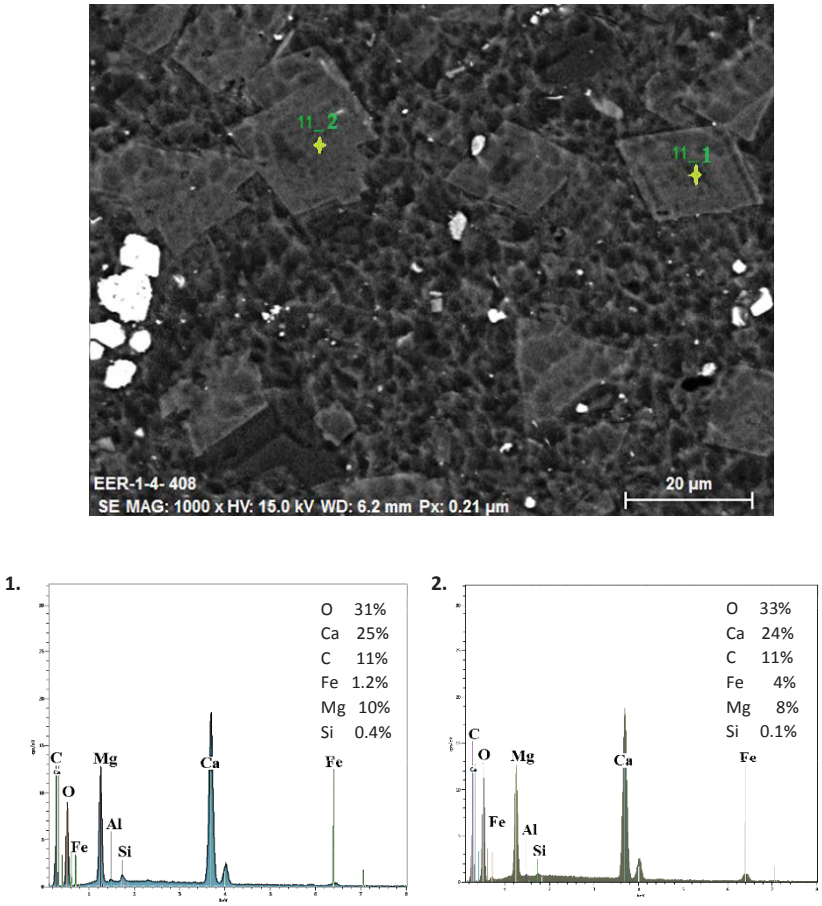

Figure 4.22: EDX spectra for samples that retain an inverse magnetic fabric irrespective of temperature confirm the presence of iron-carbonates. Spectra are for sample B in **Figure 4.20** and elemental compositions are semi-quantitative.

3. *Normal to inverse type fabric with decreasing temperature*

In this group, two cases are observed. In the first, a sample's k_{max} axis becomes more inclined with decreasing temperature and its k_{min} axis becomes more horizontal. **Figures 4.23** and **4.24** show the stereographic projections of two such samples. In **Figure 4.23**, k_{min} is inclined at 65° to 70° at room temperature and between 7° and 12° between 200K and 250K. K_{max} is inclined at 10° to 25° at room temperature increasing to 35°- 46° between 200K and 250K. For another sample (**Figure 4.24**), k_{min} inclinations increase from 0.2° at 200K to 45°- 60° between 280K and 285K. Above 285K, inclinations slightly decrease to 30° and 50°. K_{max} inclination

increases to 40°-50° between 200K and 260K. K_{min} declinations in this sample also progressively shift towards a more eastward direction with decreasing temperature.

In the second case (**Figure 4.25),** the k_{min} axis remains subparallel to bedding while k_{max} inclination increases from 16° at 290K to 70° at 200K.

The presence of an inverse type fabric at low temperature but not at room temperature indicates that paramagnetic minerals such as siderite or ferroan calcite are responsible for inverse fabrics in this group of samples. Samples consisting of a mixture of multidomain ferrimagnetic minerals and/or paramagnetic clays and ferroan calcite or siderite will have such a fabric. The multidomain ferromagnetic minerals and /or paramagnetic clays give a dominant normal fabric at room temperature, while the ferroan calcite or siderite give a dominant inverse fabric at low temperature.

4. *Inverse to normal fabric with decreasing temperature*

   An example of this group is shown in **Figure 4.26** where k_{min} shifts from sub-parallel to bedding (inclinations between 22° and 23°) at 292K to almost perpendicular to bedding plane at 196K (inclination ~85°). The maximum susceptibility direction also shifts from higher inclinations (65° at 292K) to subparallel to bedding plane with decreasing temperature. The orientations at progressively lower temperatures increasingly reflect the normal orientation of paramagnetic clay (illite) phases. The shift from inverse to normal fabric is an indication that the inverse fabric observed at room temperature is most likely due to the presence of stable single domain (SSD) magnetite and not paramagnetic iron- bearing carbonates. Subsequent anisotropy of magnetic remanence (AMR) measurements (see **Chapter 6**) confirmed the presence of SSD magnetite.

Fabric Types 1 and 2 occur only in the Muskwa and Otter Park Formations. Type 3 fabrics are primarily noted in the lower 25m of the Otter Park Formation, and type 4 is only found in the Evie.

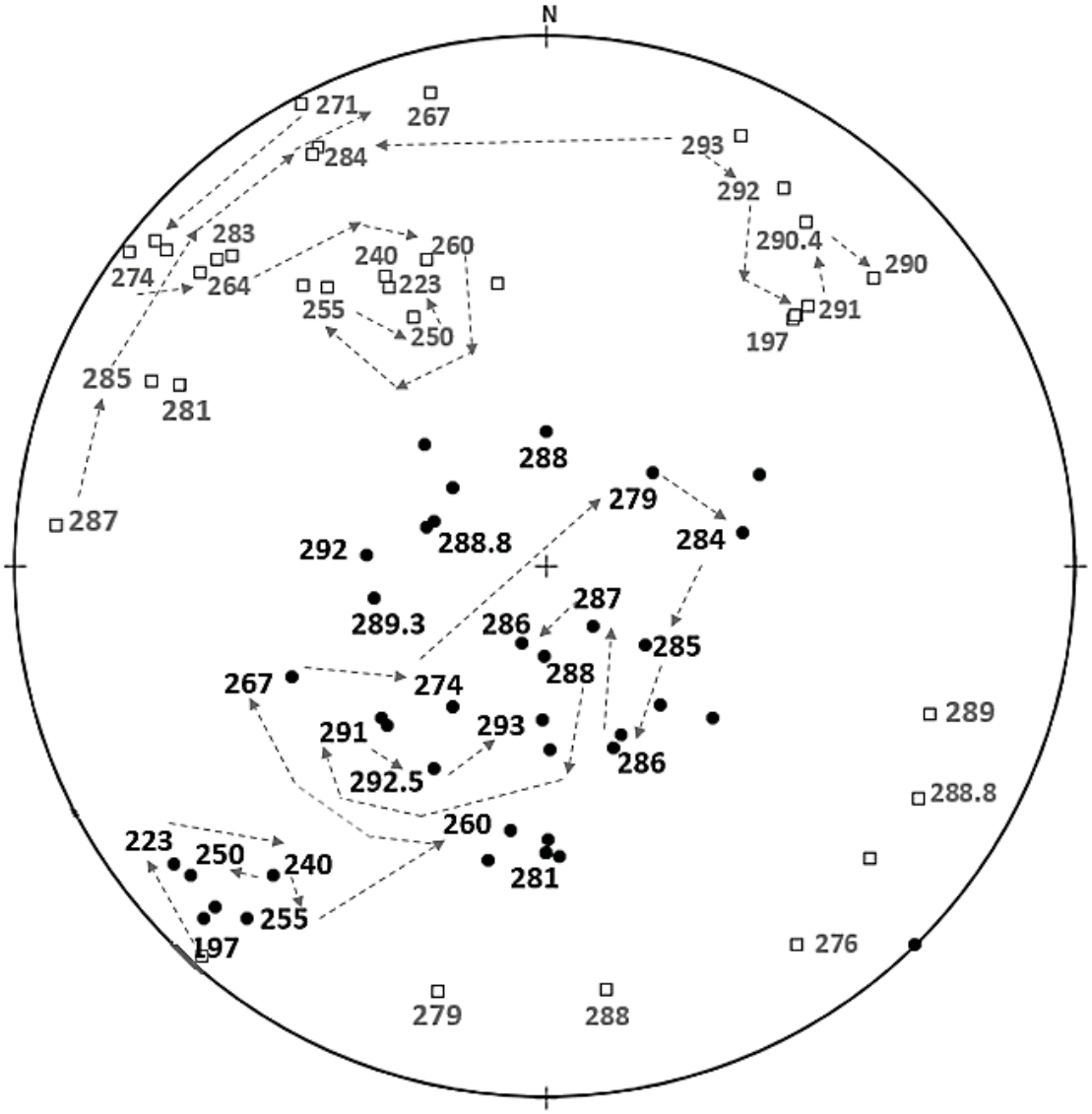

Figure 4.23: Stereographic projection showing the variation of maximum and minimum susceptibility axes with temperature in a Type 3 sample. Solid circles are minimum susceptibility directions and open squares are maximum susceptibility directions. Magnetic fabric is normal at room temperature and becomes inverse with decreasing temperature.

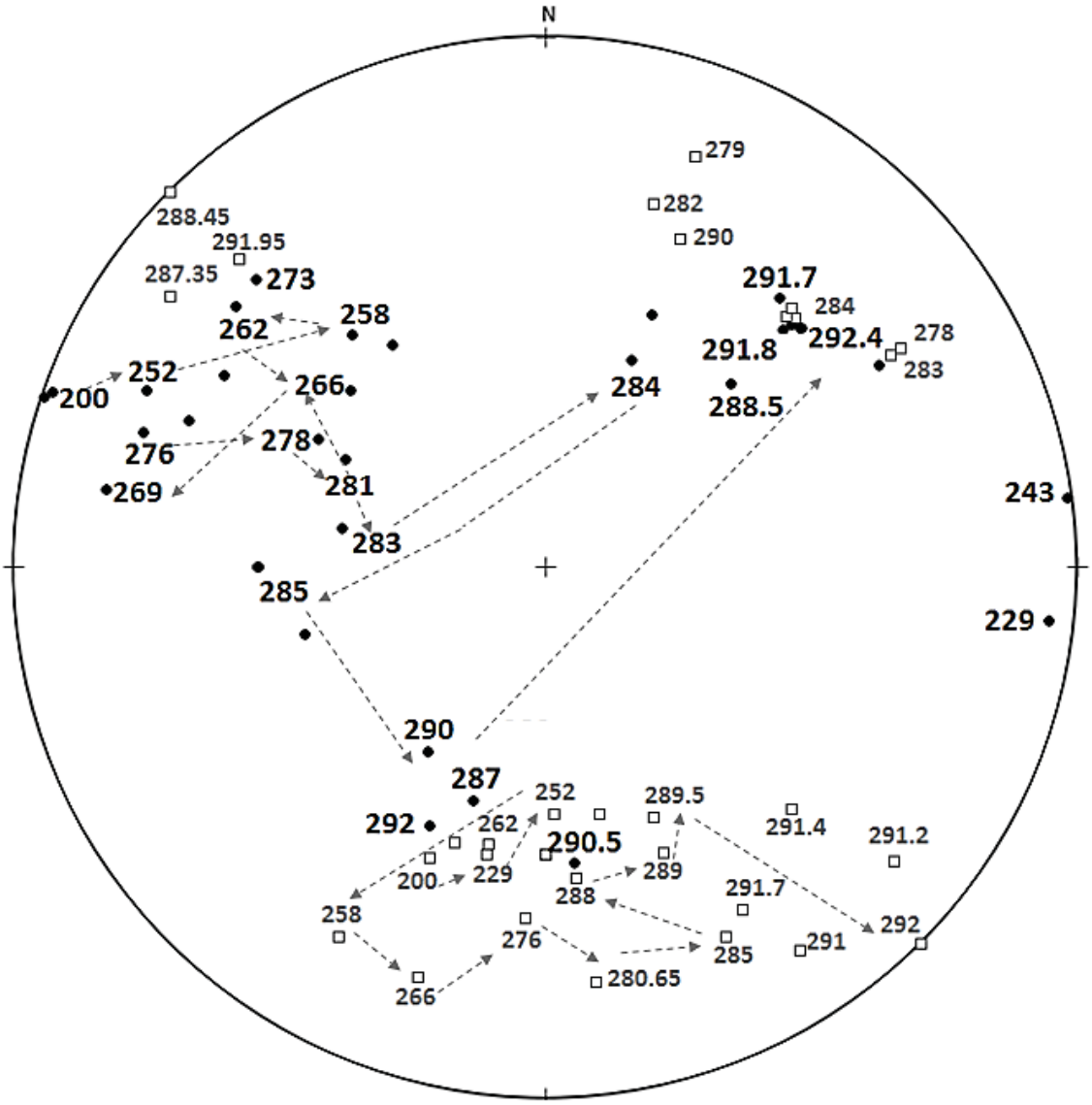

Figure 4.24: Stereographic projection showing the variation of maximum and minimum susceptibility axes with temperature in a Type 3 sample. Solid circles are minimum susceptibility directions and open squares are maximum susceptibility directions. Magnetic fabric is normal at room temperature and becomes inverse with decreasing temperature.

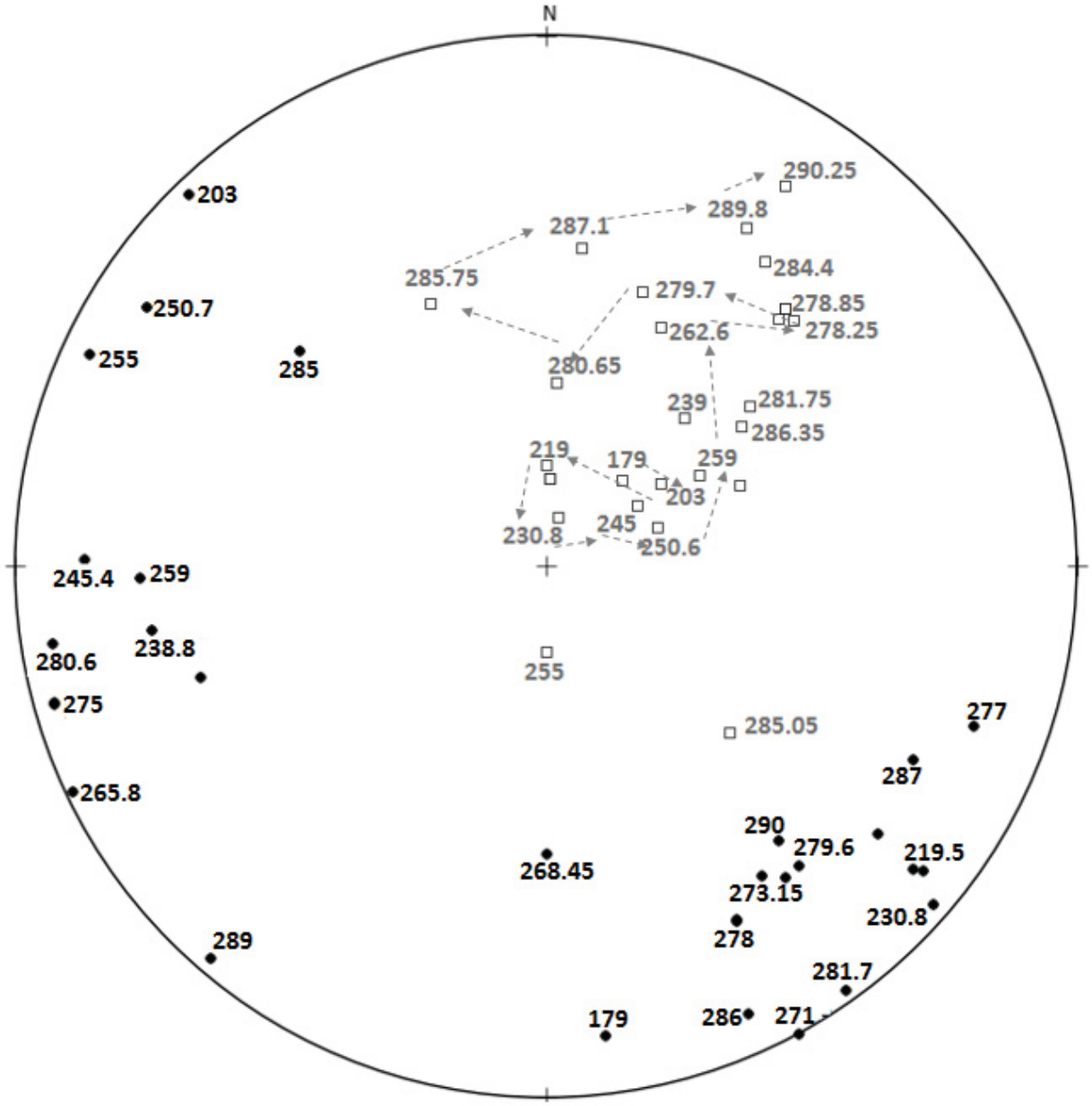

Figure 4.25: Stereographic projection showing the variation of maximum and minimum susceptibility axes with temperature in a Type 3 sample. Solid circles are minimum susceptibility directions and open squares are maximum susceptibility directions. Magnetic fabric is normal at room temperature and becomes inverse with decreasing temperature. K_{min} remains sub-parallel to bedding and k_{max} inclination increases from 16° at 290K to ~70° at 200K.

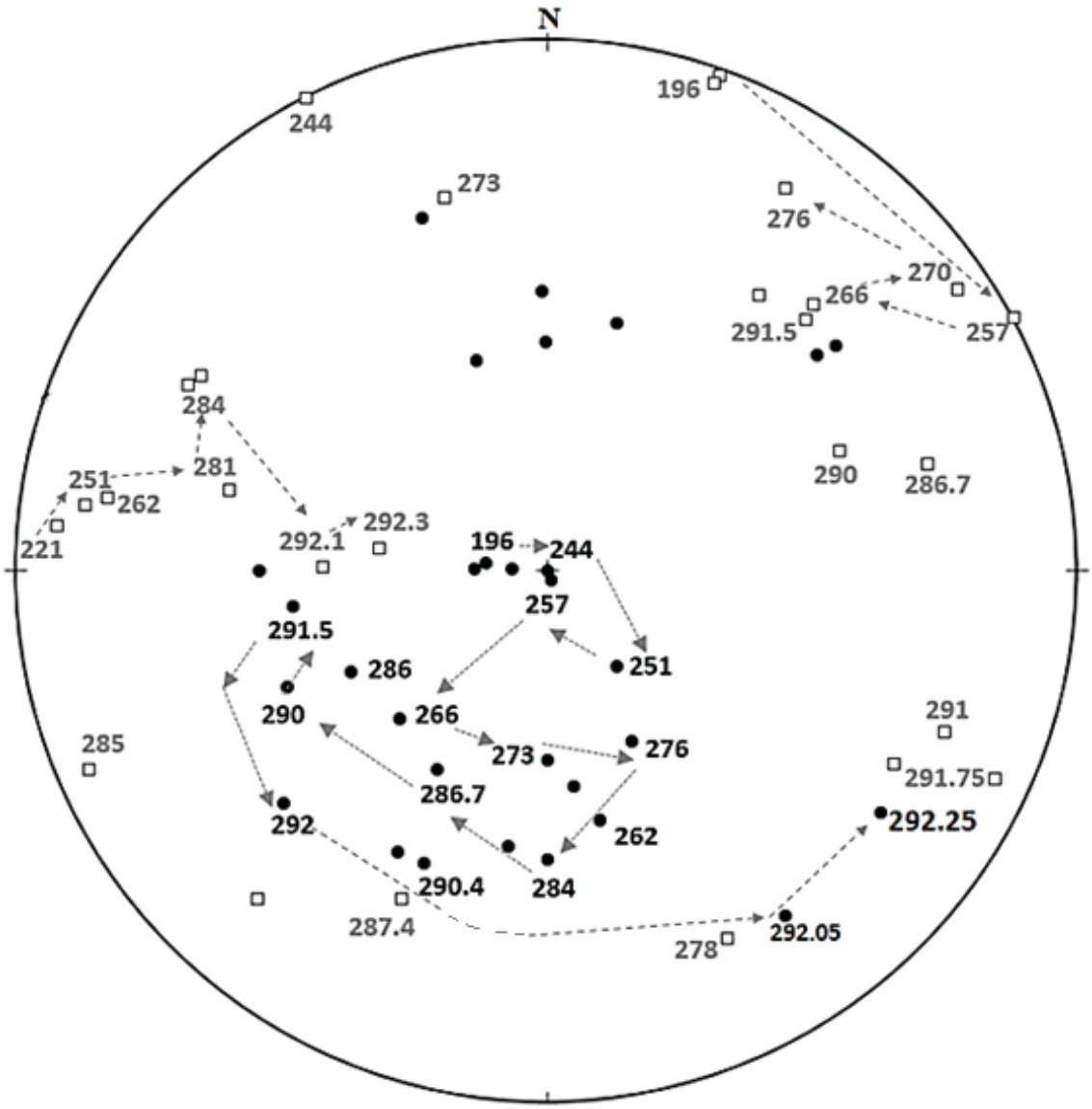

Figure 4.26: Stereographic projection showing the variation of maximum and minimum susceptibility axes with temperature in a Type 4 sample. Solid circles are minimum susceptibility directions and open squares are maximum susceptibility directions. Magnetic fabric is inverse at room temperature and becomes normal with decreasing temperature.

4.5 Discussion

Although clays are thought to be the primary control on anisotropy in mudrocks because of their sheet-like morphology, room temperature anisotropy of magnetic susceptibility results (discussed in **Chapter 3**) for Horn River Group samples from the Imperial Komie well showed little correlation with clay content. The temperature dependence of AMS, however, shows that illite contributes to the AMS and dominates the paramagnetic AMS in most of the Horn River Group mudrocks. There is also a good correlation between the illite content and the difference between magnetic susceptibility at 200K and room temperature (**Figure 4.27**). This suggests that illite is primarily responsible for the observed increase in magnetic susceptibility with decreasing temperature.

Results also indicate that in the calcite rich Evie member, composed of at least 70% calcite, the preferred orientation of calcite also contributes to paramagnetic AMS when there is substitution of iron for calcium in the calcite or dolomite lattice. **Figure 4.16** shows the AMS (T) curve for an Evie sample with approximately 11% illite and 90% calcite. Between room temperature and 174K, there is a 162% increase in AMS. Samples whose paramagnetic AMS are dominated by illite (between 60% and 70% illite) have an increase of 148% to 167% between room temperature and 174K, and samples in the Upper Muskwa with approximately 10% illite, but with quartz instead of calcite as the primary diamagnetic mineral, show little to no increase in AMS with decreasing temperature. In the quartz rich Upper Muskwa and calcite rich Evie, iron oxide concentration varies from 0.32wt% to 3wt%. When there is partial substitution of Fe^{2+} or Mn^{2+} for Ca^{2+} in calcite, calcite behaves like siderite, a paramagnetic carbonate mineral (Schmidt et al., 2006; Levi and Weinberger, 2011), and given that pure calcite is considerably anisotropic (Owens and Bramford, 1976; Hrouda et al., 2000; Hrouda, 2004*)*, with decreasing temperature, both the magnetic susceptibility and AMS of an iron-rich calcite will increase.

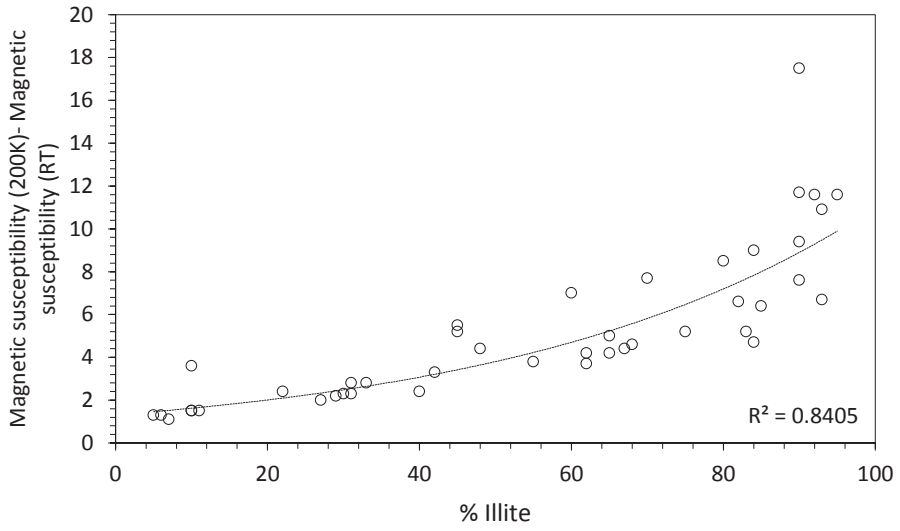

Figure 4.27: Relationship between (MS at 200K – MS at room temperature) and illite concentrations derived from k(T) curves. The good correlation indicates that the enhancement of magnetic susceptibility with decreasing temperature of Horn River Group samples is due primarily to the concentration of paramagnetic illite.

4.6 Conclusions

This chapter was in two main sections. In each, a different application of the increase in paramagnetic susceptibility and anisotropy of magnetic susceptibility with decreasing temperature was investigated. In the first section, clay and quartz concentrations of Horn River Group samples where determined by comparing theoretical susceptibility-temperature curves for mineral mixtures of known concentrations and susceptibility-temperature curves for Horn River Group samples. In the second section, the variation of AMS with decreasing temperature was used to distinguish the different types (especially paramagnetic and ferrimagnetic) minerals present and their orientations. The following key conclusions are reached from the results obtained:

1. Where clays such as illite are the primary paramagnetic mineral, k(T) curves can be used to determine clay concentrations.
2. Good agreement between illite concentrations derived from k(T) curves and independent geochemical data (Al_2O_3) from mass spectrometry confirmed that low temperature magnetic results are reliable.

3. Good correlation between illite content and the difference between magnetic susceptibility at 200K and room temperature suggests that clay minerals are primarily responsible for the observed increase in magnetic susceptibility with decreasing temperature.
4. On the basis of the variation in principal axes orientation with temperature, four classes of Horn River samples were identified: Type 1 samples with normal AMS fabric irrespective of temperature, Type 2 samples with inverse AMS fabric irrespective of temperature, Type 3 samples with normal fabric at room temperature and inverse fabric at low temperature, and Type 4 samples with inverse fabric at room temperature and normal fabric at low temperature.
    - For Type 1 samples with normal AMS fabric orientations that did not change significantly with temperature, the paramagnetic signal is dominated by paramagnetic clays (mainly illite).
    - For Type 2 samples with inverse AMS fabrics that did not change with temperature, the paramagnetic signal is dominated by iron bearing carbonates.
    - Type 3 samples with a normal AMS fabric at room temperature and an inverse AMS fabric at low temperature contain a mixture of clay, small amounts of multidomain ferrimagnetic material, and iron bearing carbonate. Iron carbonates dominate the paramagnetic signal at low temperature, leading to an inverse fabric, while the paramagnetic clays and multidomain ferrimagnetic material dominate the signal at room temperature, leading to a normal fabric.
    - For Type 4 samples with an inverse AMS fabric at room temperature and a normal AMS fabric at low temperature, the room temperature signal was dominated by the presence of uniaxial stable single domain ferrimagnetic particles (inverse fabric), whereas at low temperature the enhanced paramagnetic signal of the illite clay dominated (normal fabric).
5. Enhanced AMS at low temperature meant that subtle structural features (like lineations) not defined by the k_{max} axis at room temperature are clearly defined at low temperatures. AMS (T) measurements could therefore be extremely useful for identifying subtle features (like lineations related to flow or stress axes) not only in shales but also in other geological samples containing paramagnetic minerals.

4.7 References

Biedermann, A. R., Koch, C. B., Lorenz, E.A., and Hirt, A.M., 2014. Low-temperature magnetic anisotropy in micas and chlorite. Tectonophysics, 629, 63-74.

Borradaile, G. J., and Henry, B., 1997. Tectonic applications of magnetic susceptibility and its anisotropy. Earth Sci. Rev., 42, 49-93.

Rochette, P., and Fillion, G., 1988. Identification of multicomponent anisotropies in rocks using various field and temperature values in a cryogenic magnetometer. Phys. Earth Planet. Inter., 51, 379-386.

Hirt, A.M., and Gehring, A.U., 1991. Thermal alternation of the magnetic mineralogy in ferruginous rocks. J. Geophys. Res., 96 (B6), 9947-9953.

Hirt, A.M., Evans, K.F., Engelder, T., 1995. Correlation between magnetic anisotropy and fabric for Devonian shales on the Appalachian Plateau. Tectonophysics, 247, 121-132.

Henry, B. D., Jordanova , N., Souque, C., and Robion, P., 2003. Anisotropy of magnetic susceptibility of heated rocks. Tectonophysics, 366, 241-258.

Hrouda, F. and Jelinek,V., 1990. Resolution of ferrimagnetic and paramagnetic anisotropies in rocks, using combined low-field and high-field measurements. Geophys. J. Int., 103, 75-84.

Hrouda, F., Jelinek, V., and Zapletal K., 1997. Refined technique for susceptibility resolution into ferromagnetic and paramagnetic components based on susceptibility temperature variation measurement. Geophys. J. Int., 129, 715– 719.

Hrouda, F., Henry, B., and Borradaile, G., 2000. Limitations of tensor subtraction in isolating diamagnetic fabrics by magnetic anisotropy. Tectonophysics, 322, 303-310.

Hrouda, F., 2004. Problems in interpreting AMS parameters in diamagnetic rocks. In: Geol. Soc., London, Special Publications, 238, 49-59.

Ihmle, P.F., Hirt, A.M., Lowrie, W., and Dietrich, D., 1989. Inverse magnetic fabric in deformed limestones of the Morcles Nappe, Switzerland. Geophys. Res. Lett., 16, 1383–1386.

Jacobs, I. S., 1963. Metamagnetism of siderite. J. Appl. Phys., 34, 1106-1107.

Levi, T., and Weinberger, R., 2011. Magnetic fabrics of diamagnetic rocks and the strain field associated with the Dead Sea Fault, northern Israel. J. Struct. Geol., 33, 566-578.

Makhanov, K.K., 2013. An experimental study of spontaneous imbibition in Horn River shales. Master's thesis, University of Alberta, Edmonton, Canada. Retrieved from http://hdl.handle.net/10402/era.32660.

Manning, D.A.C., 1995. Introduction to industrial minerals. Chapmann and Hall publishing, p. 192.

Martin-Hernández, F., and Ferré, E.C., 2007. Separation of paramagnetic and ferrimagnetic anisotropies: a review. J. Geophys. Res., 112 (B03105).

Owens W. H., and Bamford, D., 1976. Magnetic, seismic, and other anisotropic properties of rock fabric. Philosophical Transactions of the Royal Society of London, Series A, 283, 55-68.

Özdemir, Ö., Dunlop, D.J., and Jackson, M., 2009. Frequency and field dependent susceptibility of magnetite at low temperature. Earth Planets Space, 61, 125-131.

Parés, J.M., and van der Pluijm, B.A., 2014. Low temperature AMS and the quantification of subfabrics in deformed rocks. Tectonophysics, 629, 55-62.

Potter, D.K., Corbett, P.W.M., Barclay, S.A., and Haszeldine, R.S., 2004. Quantification of illite content in sedimentary rocks using magnetic susceptibility - a rapid complement or alternative to x-ray diffraction. J. Sed. Res., 74(5), 730-735.

Richter, C., and van der Pluijm, B. A., 1994. Separation of paramagnetic and ferrimagnetic susceptibilities using low temperature magnetic susceptibilities and comparison with high field methods. Phys. Earth and Planet. Inter., 82, 113-123.

Rochette, P., and Fillion, G., 1988. Identification of multicomponent anisotropies in rocks using various field and temperature values in a cryogenic magnetometer. Phys. Earth Planet. Inter., 51, 379– 386.

Rochette, P., Jackson, M., and Aubourg, C., 1992. Rock magnetism and the interpretation of anisotropy of magnetic susceptibility. Rev. Geophys., 30, 209-226.

Schmidt, V., Günther, D., Hirt, A.M., 2006. Magnetic anisotropy of calcite at room temperature. Tectonophysics, 418, 63-73.

Schmidt, V., Hirt, A.M., Hametner, K., Günther, D., 2007 Magnetic anisotropy of carbonate minerals at room temperature and 77 K. American Mineralogist, 92, 1673–1684.

Stephenson, A., Sadikun, N. and Potter, D.K., 1986. A theoretical and experimental comparison of the magnetic susceptibility and remanence in rocks and minerals. Geophys. J. R. Astron. Soc., 84, 185-200.

Verwey, E. J., 1939. Electronic conduction of magnetite (Fe3O4) and its transition point at low temperature. Nature, 144, 327–328.

Witkowsky, J.M., Galford, J.E., Quirein, J.A., and Truax, J.A., 2012. Predicting pyrite and total organic carbon from well logs for enhancing shale reservoir interpretation. Conference paper: SPE Eastern Regional Meeting, 3-5 October.

Chapter 5

Electrical Resistivity and Anisotropy of Electrical Conductivity (AEC)

5.1 Introduction

5.1.1 Current flow in earth materials

Electrical resistivity, ρ, measures the opposition of a material to the flow of electric current. It is an intrinsic material property given by the expression:

$$\rho = \frac{RA}{L} \tag{5.1}$$

where R, the electrical resistance, is dependent on the cross sectional area A, and length L, across which current flows. Electrical resistivity is given in ohm meter (Ωm) while its inverse, electrical conductivity, which is a measure of a material's ability to conduct current, is in Siemens per meter (S/m).

Current flows through earth materials in one or a combination of two ways: electronic conduction or electrolytic conduction. The type of conduction, and hence resistivity of a material, is dependent on the density and mobility of charge carriers. In pure metals like copper, current flow is by electronic conduction. Charge carriers (electrons) are abundant and move freely from areas of higher negative potential to areas of lower negative potential. In electrolytic conduction current

flow is the result of the movement of ions (charge carriers), such as potassium or chlorine, within an electrolyte (Negi and Anand, 1985; Lowrie, 2007). Since ions have lower mobility than electrons, materials dominated by electrolytic conduction are usually more resistive than those dominated by electronic conduction.

Although some rock forming minerals like pyrite and galena are semiconductors, most are insulators with resistivities that vary over orders of magnitude (**Figure 5.1**). Given that a rock is an assemblage of resistive minerals, current flow is primarily by the movement of dissolved ions contained in connected pores. The resistivity/conductivity of a rock is therefore, at its simplest, dependent on the nature of pore spaces (distribution and connectedness) and the concentration and saturation of pore fluid/saturating electrolyte (Vinegar and Waxman, 1982; McCarter, 1984; McCarter et al. 2005; Ghorbani et al. 2008). The relationship between resistivity, porosity and saturation in porous media was first advanced by Archie (1942). He observed that the bulk resistivity, ρ_{bulk}, of clean, electrolyte-saturated sandstones from the Gulf of Mexico, was linearly proportional to the resistivity of the saturating electrolyte, $\rho_{w,}$ and inversely proportional to the degree of saturation, S, and porosity, ø, as follows:

$$\rho_{bulk} = \frac{a\,\rho_w}{ø^m\,S_w^{\,k}} \tag{5.2}$$

where a is the tortuosity factor, m is the cementation factor, and k is the saturation exponent. Archie's equation is, however, only valid for shale-free rocks with current flow restricted to connected pore spaces, that is, it assumes no movement of charges along grain surfaces (surface conductance) or through grains. Clays, one of the primary minerals in mudrocks, exhibit significant surface conductance due the presence of unbalanced negative charges on their grain surfaces. When placed in a solution, to attain electrical neutrality, negative surface charges attract exchangeable cations or counter-ions from the pore saturating electrolyte causing the concentration of cations to decrease with increasing distance from the clay surface (**Figure 5.2**). As distance from the surface increases, the force of attraction between the negatively charged clay surface and cations also decreases. The region of attracted cations/counterions (adsorbed water) and negatively charged clay surface constitute the electrical double layer. The layer of cations closest to the clay surface and held most strongly to it is known as the Stern layer. Beyond the Stern layer, but still within the electrical double layer, cations weakly held by the negatively charged clay surface make

up the diffuse layer (**Figure 5.2**). Past the diffuse layer is the bulk solution (Waxman and Smits, 1968; Revil et al. 1997; Leroy et al. 2004). The flow of ions near the surface of clay minerals significantly reduces the resistivity of clay bearing rocks and provides a second mode of conduction in such rocks. Current flow in shales and mudstones is therefore by a combination of surface conductance and electrolytic conduction.

Several models exist that attempt to include the contribution of surface conductance to bulk conductivity. Patnode and Wyllie (1950) proposed a model for electrical conductivity where bulk electrical conductivity or resistivity is the sum of electrolytic conduction (C_w) and surface conductance (C_z) through the electrical double layer of clays. Each current flow path is treated as a resistor, both resistors are in parallel and bulk conductivity C_{bulk} is given by:

$$C_{bulk} = \frac{1}{F} (C_w + C_z) \tag{5.13}$$

where F is the formation factor. C_w is determined from brine conductivity and C_z is approximated from the cation exchange capacity (CEC) of clay minerals present in the sample of interest. Waxman and Smits (1968) proposed a slight modification to the Patnode and Wyllie model by determining the electrolytic conduction component C_w from counterion conductance and concentration. Modifications to the Waxman and Smits model include attempts by Revil et al. (1998) to separate cation and anion flow paths. They propose that anions preferentially flow through connected pore spaces while cations flow through both pore spaces and along grain surfaces. The dual-water model of Clavier et al. (1984) attempts to differentiate between pore water surrounding clay particles (clay water) and water that fills the rest of the pores with conductivity, and salinity corresponding to that of the of the bulk formation water. Other modifications include those of Juhász (1981) and Bourlange et al (2003).

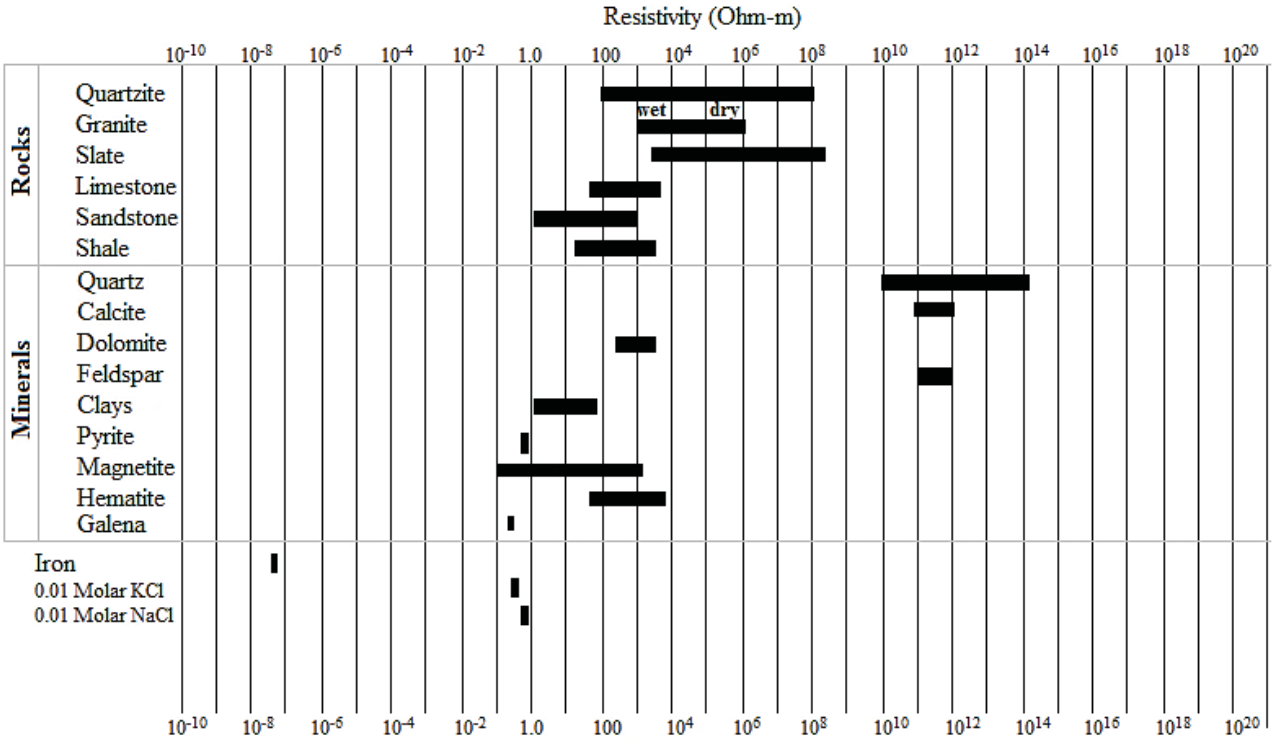

Figure 5.1: Typical ranges of electrical resistivities of common rocks and minerals common in mudrocks (Keller and Frischknecht, 1966; Mares, 1984; Telford et al. 1990).

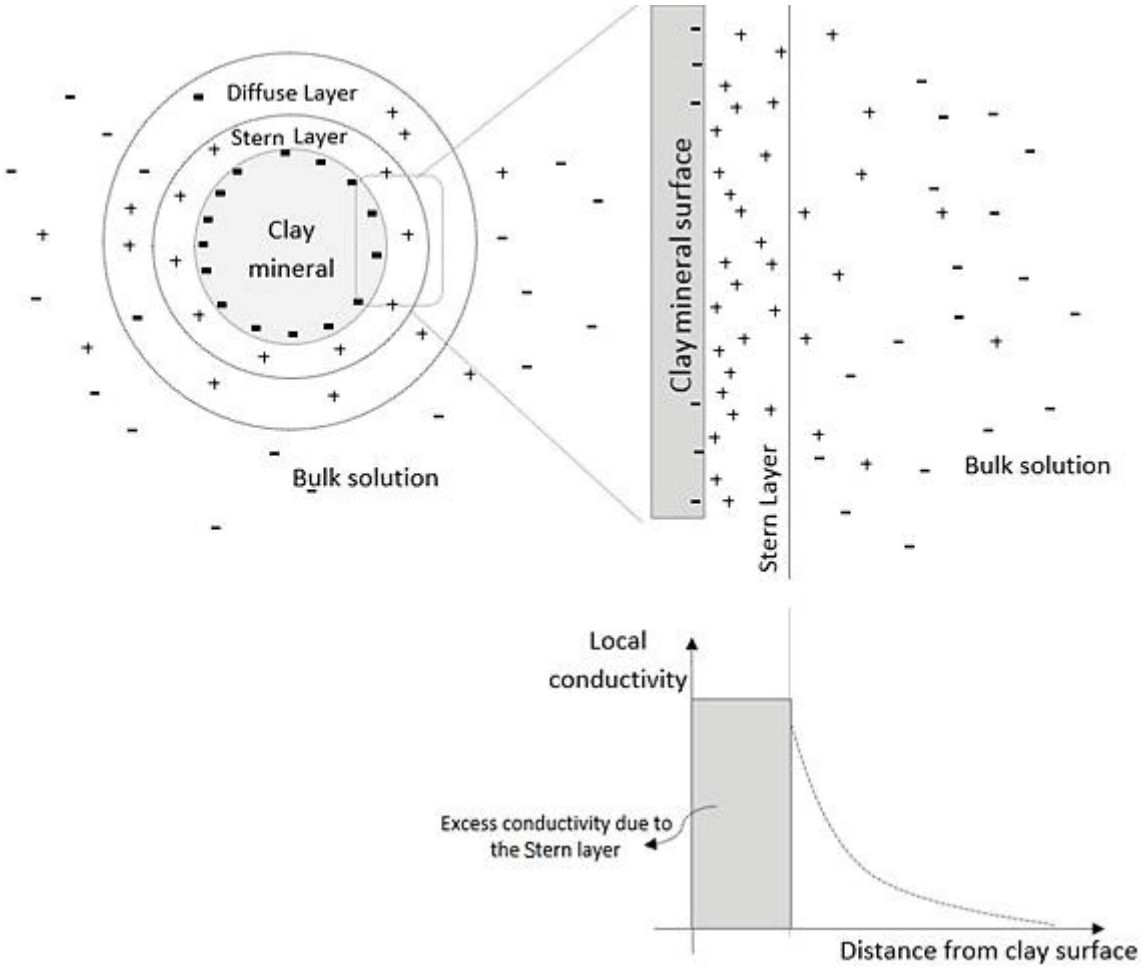

Figure 5.2: Schematic showing the electrical double layer (EDL) at the pore water interface for a fully brine saturated sample. The EDL is made of the Stern layer, with mobile counterions strongly attracted to the mineral surface, and the diffuse layer with counterions loosely attracted to the grain surface (modified from Mitchell, 1993).

5.1.2 Electrical anisotropy

The relationship between current density J and the electric field E it produces is given by Ohm's law as follows:

$$J = \sigma E \tag{5.3}$$

where σ is the electrical conductivity. When the relationship between J and E varies with direction, i.e., when conductivity/resistivity vary with direction, a material is said to be electrically anisotropic. Components of current density J_i in an anisotropic medium are related to components of the electric field E_i by the following expressions:

$$\begin{bmatrix} J_1 \\ J_2 \\ J_3 \end{bmatrix} = \begin{bmatrix} \sigma_{11} & \sigma_{12} & \sigma_{13} \\ \sigma_{21} & \sigma_{22} & \sigma_{23} \\ \sigma_{31} & \sigma_{32} & \sigma_{33} \end{bmatrix} \begin{bmatrix} E_1 \\ E_2 \\ E_3 \end{bmatrix} \tag{5.4}$$

where σ_{ij} are the coefficients of the conductivity tensor.

Alternatively, equation (5.4) can be written in terms of the resistivity tensor ρ_{ij}

$$\begin{bmatrix} E_1 \\ E_2 \\ E_3 \end{bmatrix} = \begin{bmatrix} \rho_{11} & \rho_{12} & \rho_{13} \\ \rho_{21} & \rho_{22} & \rho_{23} \\ \rho_{31} & \rho_{32} & \rho_{33} \end{bmatrix} \begin{bmatrix} J_1 \\ J_2 \\ J_3 \end{bmatrix} \tag{5.5}$$

The conductivity and resistivity tensors consist of nine coefficients, but since $\rho_{ij} = \rho_{ji}$ and $\sigma_{ij} = \sigma_{ij}$, only six independent elements define each tensor. They can be diagonalized to obtain the principal conductivity (or resistivity) values, σ_1, σ_2 and σ_3 (or ρ_1, ρ_2 and ρ_3) that are the maximum, intermediate and minimum conductivities/resistivities along the principal axes whose directions are defined by corresponding eigenvectors.

$$\boldsymbol{\sigma} = \begin{bmatrix} \sigma_1 & 0 & 0 \\ 0 & \sigma_2 & 0 \\ 0 & 0 & \sigma_3 \end{bmatrix} \tag{5.6}$$

The three orthogonal principal axes describe the conductivity/resistivity ellipsoid **(Figure 5.3**). The Euler angles ϑ, φ, and γ rotate the ellipsoid from the Cartesian reference frame to the principal axes frame.

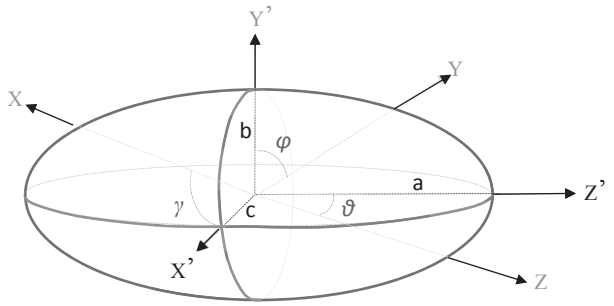

$a = 1/\sqrt{\sigma_1}$ $b = 1/\sqrt{\sigma_2}$ $c = 1/\sqrt{\sigma_3}$

Figure 5.3: The conductivity ellipsoid with three orthogonal principal axes (modified from Duan et al., 2006).

5.1.3 Petrofabric significance of the conductivity tensor

Electrical anisotropy in rocks can be due to the crystal structure of constituent minerals, the alignment or preferred orientation of fracture and pore networks, or layering (Herwanger et al., 2004). The eigenvalues and eigenvectors of the conductivity and resistivity tensors are related to the three dimensional orientations of whichever petrofabric element(s) control(s) the electrical anisotropy of a given sample. Where mineral alignments are the principal control, the maximum conductivity axis (minimum resistivity axis) will be parallel to the bedding plane or preferred orientation direction and minimum conductivity axes will be normal to it. Likewise, where electrical anisotropy is due to the distribution or alignment of fracture and pore networks, the maximum conductivity is parallel to the strike of the fracture network. Low electrical anisotropies are characteristic of minimally fractured rocks with sub-rounded to spherical grains or randomly oriented elongate grains.

5.1.4 Literature review: Electrical anisotropy in mudrocks

5.1.4.1 Transversely isotropic media

Shales and mudstones have long been known to be electrically anisotropic (Mousseau and Trump, 1967; Chemali et al., 1987). Recently, however, interest in the accurate interpretation of resistivity data for fluid saturation computations and subsurface structure mapping have led to increased interest in the study of their electrical anisotropy (Klein et al., 1997; Clavaud, 2008; Bachrach, 2011; Ellis et al., 2011).

Since mudrocks typically consist of alternations of organic-clay rich intervals and silty intervals, most studies treat them as transversely isotropic with a vertical axis of symmetry (VTI) as shown in **Figure 5.4**. Each layer in the laminated sequence is treated like an isotropic medium and an independent resistor. A given sample or section of mudrock of interest thus consists of a set of resistors, each with resistivity ρ_i. Bulk electrical resistivity does not vary in the horizontal plane but may vary in all other directions and the degree of electrical anisotropy, λ, is calculated as:

$$\lambda = \rho_v / \rho_h \quad = \sigma h / \sigma_v \tag{5.7}$$

where ρ_v, the transverse resistivity (resistivity normal to the lamination plane), is the maximum resistivity or minimum conductivity direction and ρ_h, the longitudinal (lamination parallel) resistivity, is the minimum resistivity or maximum conductivity direction.

Under the assumption of transverse isotropy, the total resistance R_{total} used to calculate ρ_h is obtained by treating the parallel laminations in a sample as a network of resistors in parallel. Current applied parallel to the lamination plane distributes itself through each layer and the total resistance is given by:

$$1/R_{total} = \Sigma\ (1 / R_i)$$

$$R_{total} = \frac{R_1\ R_2 \ldots\ R_n}{\sum R_i} \tag{5.8}$$

where R_i are the resistances of each layer (resistor).

In the transverse direction, current flows through a stack of layers arranged like a set of resistors in series and the total resistance is given by:

$$R_{total} = \Sigma R_i \quad (5.9)$$

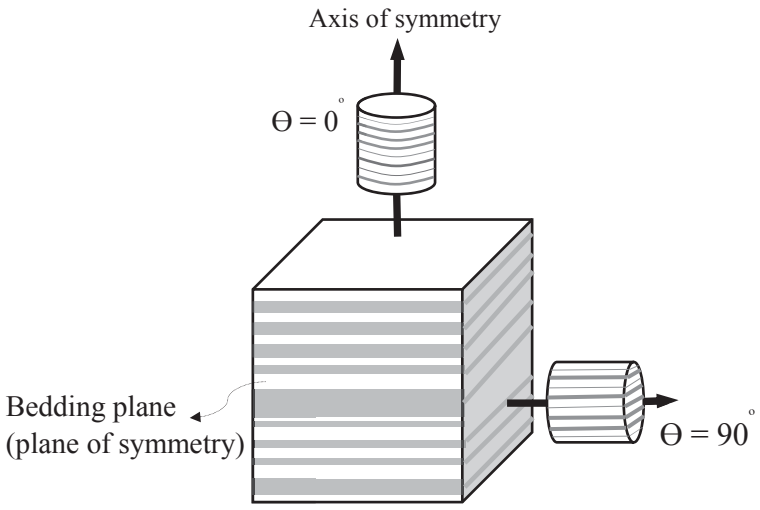

Figure 5.4: Schematic showing a transversely isotropic medium with a vertical axis of symmetry.

5.1.5 Chapter goals

The majority of the few available studies on electrical anisotropy in mudrocks determine the degree of electrical anisotropy from wireline log derived resistivities. The vertical resolution of standard induction logging tools is between 2ft and 6ft (Clavaud, 2008; Lyons et al., 2015). At such macroscopic scales electrical anisotropy due to microstructural fabric elements like grain alignment and fracture or pore distribution cannot be resolved. Higher resolution laboratory techniques traditionally measure horizontal and vertical resistivities in cubic samples or core plugs. Both resistivities are either measured in one sample or on two core plugs taken perpendicular and parallel to the bedding plane (**Figure 5.4**). Since at least nine directional resistivities are needed to determine the six coefficients of the 3D conductivity/resistivity tensor, the petrofabric implications of electrical anisotropy cannot be fully understood with only two directional resistivities. In this

chapter, a novel method of determining the conductivity tensor and ellipsoid from 18 directional resistivity measurements on each sample of interest is presented. The primary goals of the chapter are to:

1. Identify the petrofabric elements that control electrical anisotropy in mudrocks of the Horn River Basin.
2. Define the three-dimensional orientations and distribution of the primary electrical conductivity control(s) from conductivity tensors and ellipsoids.
3. Test the suitability of the VTI assumption on a microscopic scale.

5.2 Sample preparation

Thirty-three cubic to cuboid samples were trimmed and polished into eighteen sided samples (**Figure 5.5)**. 9 samples were from the Muskwa, 17 from the Otter Park and 7 from the Evie. Samples were oven dried at 40°C for 48 hours to remove water held in pore spaces prior to saturation with 20wt% potassium chloride (KCl) solution. To ensure full saturation, samples were fully immersed in the electrolyte for one week before taking resistance measurements. Although experimental resistivities were not corrected for the potential effects of reservoir salts left over after samples were oven dried, the small size of samples with respect to the volume of KCl electrolyte they were soaked in means that small amounts of residual reservoir salts have little to no effect on measured resistivities.

Figure 5.5: Core samples were polished into 18 sided prisms for electrical resistance measurements. Ag-AgCl electrodes placed on opposite faces of the desired measurement direction serve as current and potential electrodes. The ‘x’ arrow is a bedding parallel reference direction and the other is an ‘up’ arrow.

5.3 Method

5.3.1 Directional resistance measurement in multifaceted samples

Determination of the conductivity tensor σij and ellipsoid requires that electrical resistance be measured in at least nine directions for each sample. For each of 33 samples saturated in a KCl solution, electrical resistance was measured in nine directions (x, xy, y, -xy, yz, -yz, -zx, zx, z shown in **Figure 5.6**). In each direction, two resistivities are measured for two opposite directions of current flow. Both are averaged to determine the electrical resistivity in that direction. Nine directional resistivities are therefore produced from 18 electrical resistances measured. The same measurement directions that were used for determining anisotropy of magnetic susceptibility (AMS) in **Chapter 3** and **4** were also used here for determining electrical resistance, which was later converted to electrical resistivity and then used to calculate anisotropy of electrical conductivity (AEC). Having identical measurement directions meant that the magnetic anisotropy could be directly compared with the electrical anisotropy.

Figure 5.7 is a circuit diagram showing the set-up used to measure electrical resistance. A potential drop of 10V is applied across a circuit consisting of a resistor of known resistance in series with a Horn River Group sample whose resistance is unknown. Voltage is applied by an AFG320 function generator connected to the sample via Ag-AgCl disc electrodes attached to opposite faces of the sample in the direction of current flow. The magnitude of the voltage drop across the sample and test resistor are measured using a Tektronix TD3054B digital oscilloscope.

Electrical resistance of each direction is calculated as follows using Ohm's law (V = IR)

$$R_{sample} = \frac{R_{test}\,(V_1 - V_2)}{V_2} \qquad (5.11)$$

where R_{test} is the resistance of the test resistor, R_{sample} is the resistance of the sample, V_1 is the voltage drop across the sample and V_2 is the voltage drop across the test resistor. All measurements were done at room temperature and pressure.

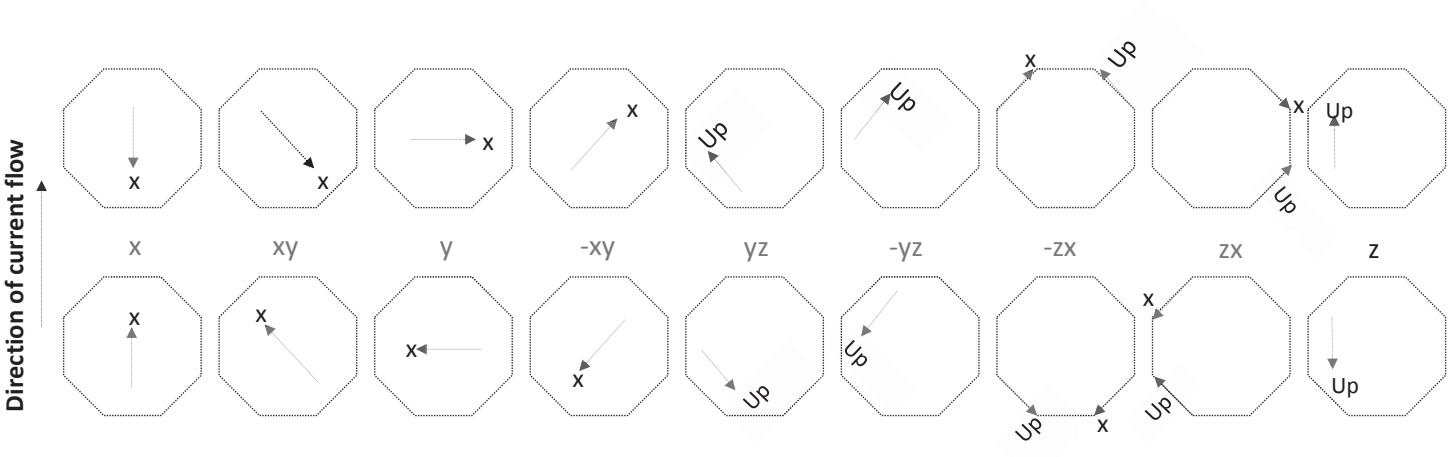

Figure 5.6: Plan view of 18 directions in which electrical resistance is measured.

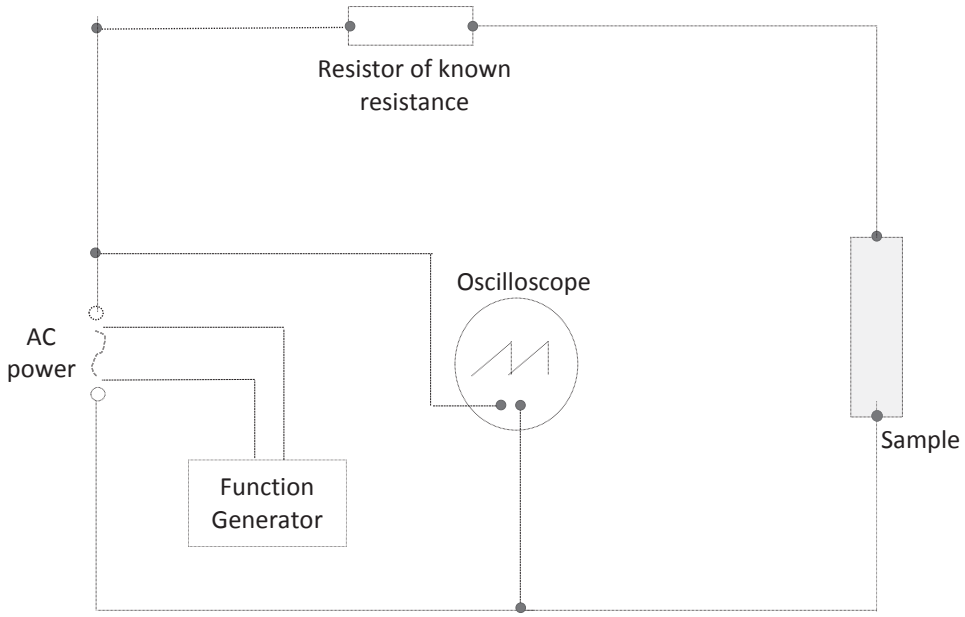

Figure 5.7: Circuit diagram of the set-up used to measure electrical resistance.

5.3.2 Converting directional resistances to resistivities in multifaceted samples

Electrical resistance is dependent on the cross-sectional area and length of the sample through which current flows. Resistivity on the other hand is an intrinsic material property, not varying with the shape of the material. The 18 directional resistances measured as described in the previous section are thus converted to resistivities. The following procedure applies for resistance to resistivity conversion for a multifaceted sample as shown in **Figure 5.5.**

Consider the eighteen-sided sample shown in **Figure 5.5**. Assuming current flow in one of eighteen directions shown in **Figure 5.6,** electrical resistance is given by:

$$R = \frac{\rho L}{A} \tag{5.12}$$

where ρ is the electrical resistivity, A is the cross-sectional area and *L* is the length across which current travels.

In the direction of current flow, assuming the sample consists of a series of thin sheets/slices with heights h and cross-sectional area A= hk, (where k is the length across the sample in the direction perpendicular to current flow as shown in **Figure 5.8**), k varies for each thin slice and is given by:

$$k = 2\,(L \tan 45) \tag{5.13}$$

where *L* is the length of the thin slice parallel to the direction of current flow as shown in **Figure 5.8**.

The contribution to total resistance of each thin rectangular slice is given by:

$$\delta R = \rho \frac{\delta L}{hk} \qquad \rho = \frac{\delta L}{2h\,(L \tan 45)} \tag{5.14}$$

Integrating the above expression across the length of the sample, from L_a to L'_a, yields the total resistance R of the sample.

$$R = \int_{L_a}^{L_m} \rho \frac{\delta L}{2h\,(L \tan 45)} + \int_{L'_a}^{L_m} \rho \frac{\delta L}{2h\,(L \tan 45)} \tag{5.15}$$

R is experimentally determined, h and *L* are measured for each sample and the integration is computed in MATLAB, allowing sample resistivity to be determined as follows:

$$R = A\rho + B\rho$$
$$\rho = R / (A+B) \quad (5.16)$$

where A is the solution to $\int_{La}^{Lm} \frac{\delta L}{2h\,(L \tan 45)}$ and B is the solution to $\int_{La}^{Lm} \frac{\delta L}{2h\,(L \tan 45)}$

Since each sample consists of different lithologies and layers with distinct resistivities, and current flow lines are as a result not uniformly distributed within samples, each computed resistivity is an apparent resistivity.

Eighteen directional apparent resistivities are calculated for each sample, converted to eighteen apparent electrical conductivities (by taking the reciprocal of each apparent resistivity value and used to determine the conductivity tensor σ_{ij} tensor. The conductivity tensor was computed instead of the resistivity tensor because the relationship between current density (J) and electric field (E) is traditionally expressed with respect to electrical conductivity.

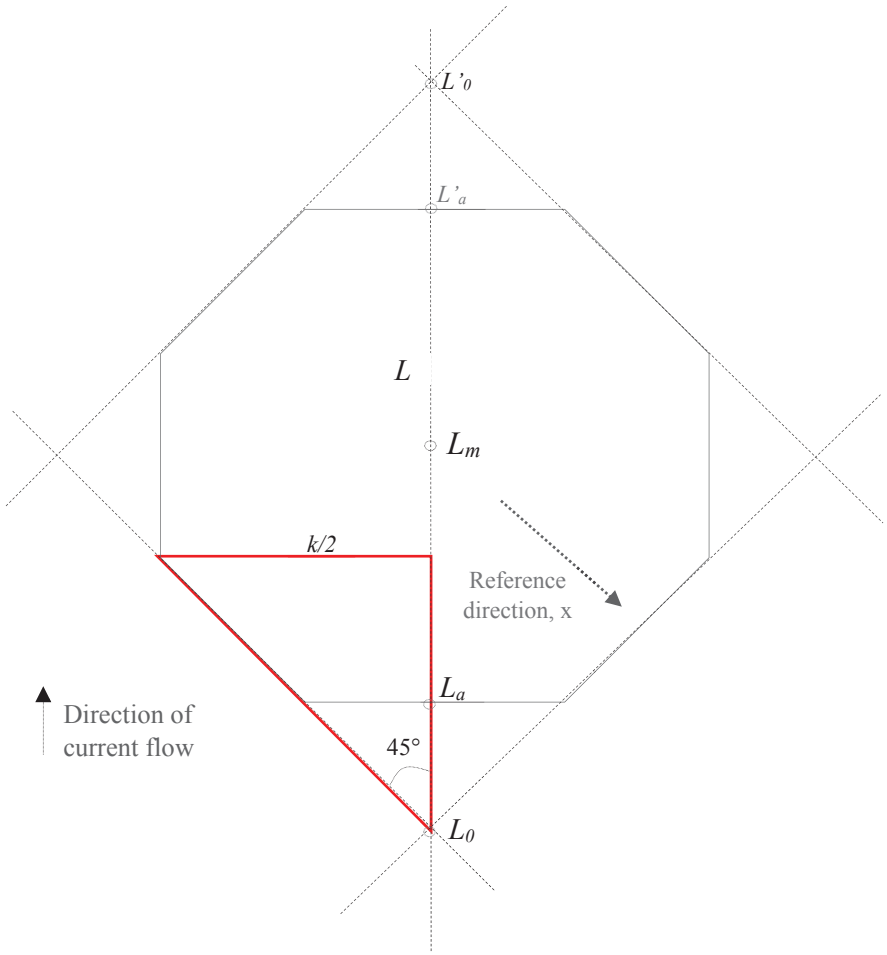

Figure 5.8: Schematic showing the relationship between variables used in the conversion of electrical resistance to resistivity for a multifaceted sample.

5.3.3 Determining the electrical conductivity tensor

The six coefficients of the symmetric, second order conductivity tensor in the Cartesian reference frame is the product of three matrices:

$$\sigma' = A^T \boldsymbol{\sigma}'' A \tag{5.17}$$

where $\boldsymbol{\sigma}''$ is a column matrix containing the six independent coefficients ($\sigma_{11}, \sigma_{12}, \sigma_{13}, \sigma_{22}, \sigma_{23}, \sigma_{33}$), σ' is a column matrix containing the measured directional conductivities, A is the design matrix for the experimental design shown in **Figure 5.6**, and A^T is the transpose of A**.** The same measurement scheme is used for computing the magnetic susceptibility tensor so A is also given by:

$$A = \begin{bmatrix} 1 & 0 & 0 & 0 & 0 & 0 \\ 0 & 1 & 0 & 0 & 0 & 0 \\ 0 & 0 & 1 & 0 & 0 & 0 \\ \frac{1}{\sqrt{2}} & \frac{1}{\sqrt{2}} & 0 & 0 & 0 & 1 \\ \frac{1}{\sqrt{2}} & 0 & \frac{1}{\sqrt{2}} & 0 & 1 & 0 \\ 0 & \frac{1}{\sqrt{2}} & \frac{1}{\sqrt{2}} & 1 & 0 & 0 \\ \frac{1}{\sqrt{2}} & \frac{1}{\sqrt{2}} & 0 & 0 & 0 & -1 \\ \frac{1}{\sqrt{2}} & 0 & \frac{1}{\sqrt{2}} & 0 & -1 & 0 \\ 0 & \frac{1}{\sqrt{2}} & \frac{1}{\sqrt{2}} & -1 & 0 & 0 \end{bmatrix} \tag{5.18}$$

The six independent elements of the conductivity tensor are calculated as follows using equation (5.17):

$$\boldsymbol{\sigma}'' = (A^T A)^{-1} A^T \sigma' \tag{5.19}$$

$$\begin{bmatrix} \sigma_{11} \\ \sigma_{22} \\ \sigma_{33} \\ \sigma_{21} \\ \sigma_{23} \\ \sigma_{31} \end{bmatrix} = \begin{bmatrix} 0.4000 & -0.1000 & -0.1000 & 0.2121 & 0.2121 & -0.1414 & 0.2121 & 0.2121 & -0.1414 \\ -0.1000 & 0.4000 & -0.1000 & 0.2121 & -0.1414 & 0.2121 & 0.2121 & -0.1414 & 0.2121 \\ -0.1000 & -0.1000 & 0.4000 & -0.1414 & 0.2121 & 0.2121 & -0.1414 & 0.2121 & 0.2121 \\ 0 & 0 & 0 & 0 & 0 & 0.5 & 0 & 0 & -0.5 \\ 0 & 0 & 0 & 0 & 0.5 & 0 & 0 & -0.5 & 0 \\ 0 & 0 & 0 & 0.5 & 0 & 0 & -0.5 & 0 & 0 \end{bmatrix} \begin{bmatrix} \sigma'_1 \\ \sigma'_2 \\ \sigma'_3 \\ \sigma'_4 \\ \sigma'_5 \\ \sigma'_6 \\ \sigma'_7 \\ \sigma'_8 \\ \sigma'_9 \end{bmatrix}$$

From the diagonalized σ_{ij} matrix, the eigenvalues σ_1, σ_2 and σ_3 that are the maximum, intermediate and minimum conductivities are determined.

Percent anisotropy of electrical conductivity was calculated as follows:

$$\% \text{ Anisotropy of Electrical Conductivity (AEC)} = (\sigma_1 - \sigma_3) / (\sigma_2) \quad (5.20)$$

The orientation (declination and inclination) of the principal axes are calculated as follows from the eigenvectors (x, y, z) of σ_1, σ_2 and σ_3

$$\text{Declination} = \tan^{-1} (y/x) \quad (5.21)$$

$$\text{Inclination} = \sin^{-1} (z) \quad (5.22)$$

5.4 Results

5.4.1 Directional resistivities

At atmospheric conditions and in 20wt% KCl, electrical resistivity in all directions is highest in the Evie member and lowest in the Otter Park and Lower Muskwa. **Table 5.1** shows the measured electrical resistivities. Parallel to the bedding plane (x, xy, y, and -xy), resistivities in the Evie range from 142 Ωm to 2367 Ωm. Perpendicular to the bedding plane (z), its resistivities range from 371Ωm to 3369 Ωm and in the off diagonal directions (yz, -yz, -zx, zx), they are between 251 Ωm and 3206 Ωm. The less resistive Otter Park and Lower Muskwa formations have resistivity values

between 22 Ωm and 323 Ωm parallel to the bedding plane, 134 Ωm to 906 Ωm perpendicular to it and 71 Ωm to 635 Ωm in off diagonal directions.

5.4.2 Anisotropy of Electrical Conductivity (AEC)

The preferred orientation and distribution of matrix constituents and pore spaces that define the fabric of mudrocks are typically assumed to result in transversely isotropic behaviour with a vertical axis of symmetry (VTI) (Tsvankin, 1997; Saeidi et al., 2014). Two anisotropy results will be compared herein, one treating the Horn River Group formations as transversely isotropic and the other incorporating 3D variations in their electrical resistivities/conductivities.

Assuming transverse isotropy (VTI), the variation in percent AEC (% σ_h/σ_v) in the Horn River Group from the Imperial Komie well are shown in **Figure 5.9B**. In the Evie, they range from 140% to 390%, while in the Muskwa and Otter Park they are between 157% and 1557%.

The Horn River Group formations are however not transversely isotropic. They show resistivity/conductivity variations in the bedding plane of 0.1% to 17%. Taking this horizontal anisotropy and variability in the off diagonal directions into account, the percent AEC determined is shown in **Figure 5.9A**. AEC values are between 65% and 107% in the Evie formation and between 73% and 180% in the Muskwa and Otter Park formations. Using the traditional two resistivity (transversely isotropic) approach, anisotropy is overestimated by a factor of 1.4 to 12.9.

AEC ellipsoid principal axes orientations

Table 5.2 lists the principal axes orientations for Imperial Komie samples and **Figure 5.10** is a stereographic projection showing their orientations. In all three formations, maximum and intermediate electrical conductivity are parallel to the bedding plane and minimum electrical conductivity is perpendicular to it.

Table 5.1: Directional electrical resistivities (in Ωm) for Muskwa, Otter Park and Evie members.

Formation	Depth (m)	**x**	xy	y	-xy	yz	-yz	-zx	zx	z
Muskwa	2240.5	381.1	444.1	328.8	423.2	877.1	818.8	729.1	672	1546.9
	2247.82	20.9	18	22.3	23.5	104.4	126.6	222.8	218.9	304.2
	2255.5	365.4	543	321.6	295.6	313.2	540.5	614.3	562.9	573.9
	2264.48	65.3	45.2	54.3	69.8	165.7	145.6	172.6	192.6	439.6
	2266.46	30.9	39.5	52.9	34.2	173.1	144.7	174.2	173.5	481.5
	2266.5	72.7	61.4	78	66.7	171.1	179	150.7	248.8	328.8
	2270.05	48.1	29.4	34	42.6	100.3	160.1	200.9	228.3	403
	2275.75	43.5	34.2	38.8	47.9	142.2	141	285.3	266.2	625.3
	2278.14	66.8	46.8	46.5	61.4	97.9	106.4	142.1	223.6	375.2
Otter Park	2278.2	159.9	110	101.6	120.7	219.7	210.5	215	264.9	407
	2281	650.2	519.4	559.5	573.2	1277.5	1351.4	1525.2	1069.9	1300.3
	2296.23	95.2	59.3	72.5	75.4	179.1	230.7	250.3	310.9	722.2
	2302.07	160.3	127.3	322.6	180.3	575.3	566	511.9	477.1	807.9
	2305.25	46.7	27.2	24.1	31.1	151.1	158.6	233.6	232.6	307.4
	2314.75	97.4	97.9	86.3	72.9	291.5	267.7	517.3	400.8	553.7
	2315.8	84.6	89.3	111	100.4	366.6	347.4	634.5	467.8	623.9
	2317.95	59.3	35.2	41.4	41.3	216.3	184.2	237.3	232.8	526.2
	2323.3	72.5	60.5	78.8	79.3	295.9	316.8	321.2	357.4	701.5
	2325	31.4	23.6	38.1	33.9	159.3	211.7	206.1	165.6	470.8
	2328.5	65.5	46.3	52.8	67.8	283	287.1	328.7	246.7	760.3
	2331.1	41.1	37.4	32.3	34.3	152	243.9	228.4	216.7	631.5
	2335.13	234.4	200	209.7	219.8	381	408.5	588.9	498.1	906.2
	2347.05	152.8	144.2	195.3	172.9	415.9	375	382.6	324.8	619.7
	2349.2	43.7	50.7	60	50.3	242.4	274.8	296.9	214.8	564.3
	2352.5	34.5	50.3	40.7	48.8	85.6	112.3	127.6	169.9	134.2
	2360.3	26.9	29	21.5	27.7	71.3	90.4	98.9	116.5	211.1
Evie	2367.7	123.3	185.4	125.9	224.6	231.2	417.4	325.8	308.2	319.8
	2376.55	663.6	386.8	379.9	470.8	388.2	510.7	592.4	697.3	1058.4
	2377.3	862.3	638.7	474.1	691.4	1191.1	1457.7	1607.4	1525.3	3367.1
	2380.53	279.1	232.7	240.7	186.3	334.8	429.3	509.4	429	556.2
	2383.1	208.9	142.6	173.3	159.3	252.1	250.5	279.6	309.2	371.2
	2386.55	288.9	212.6	230.7	269	453.6	456.1	655.9	555.9	845.1
	2397.25	2366.9	1674.2	1565.2	1592.9	1992.2	2243.2	3205.6	2833.1	3369.1

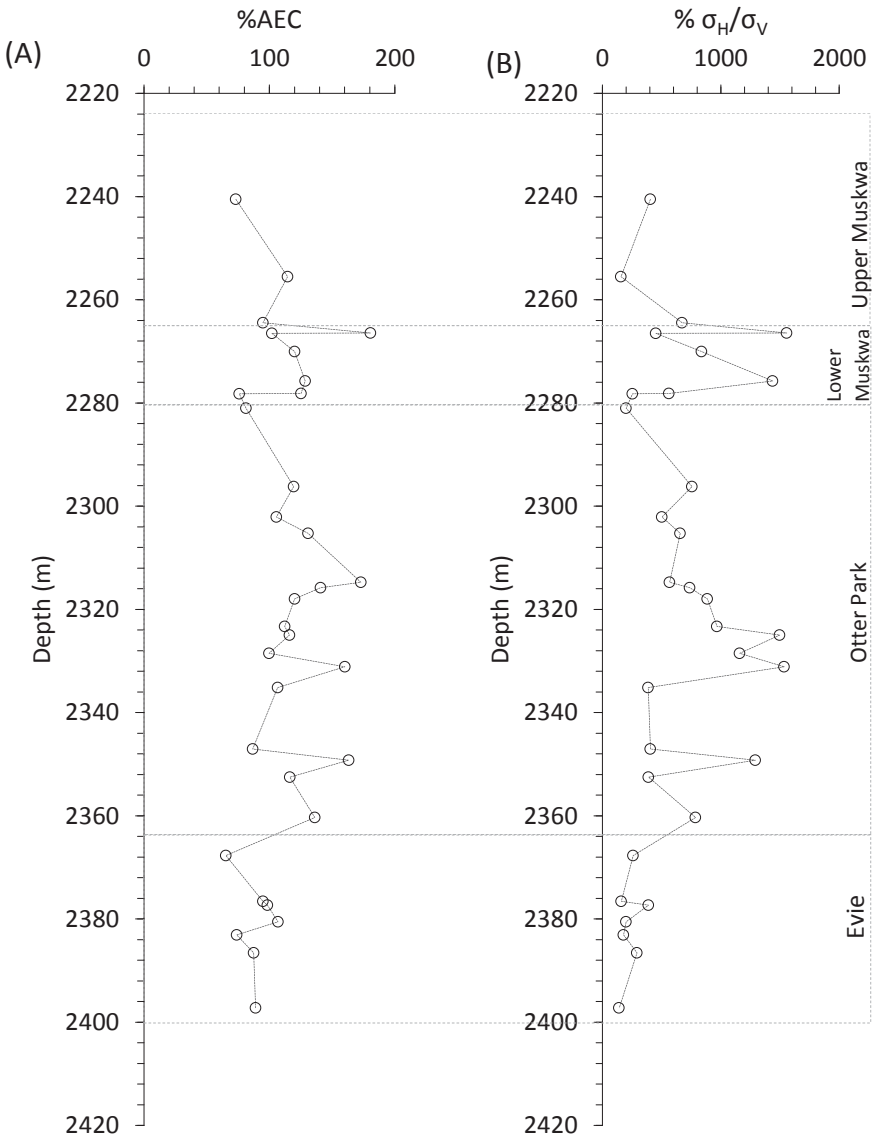

Figure 5.9: (A) % AEC incorporating 3D variations in electrical conductivity. (B) % AEC assuming the Horn River Group members are transversely isotropic.

Table 5.2: Anisotropy of Electrical Conductivity principal axes orientations for Horn River Group samples from the Imperial Komie well.

Formation	Depth (m)	σ_{max}		σ_{int}		σ_{min}	
		Declination (°)	Inclination (°)	Declination (°)	Inclination (°)	Declination (°)	Inclination (°)
Muskwa	2240.5	291	1.5	20.9	1.1	289.9	47
	2255.5	118.1	14.6	19.3	30.2	230.6	55.7
	2264.48	234.5	1.3	144.5	0	53.7	88.7
	2266.46	347.7	0.2	257.7	1.3	87.5	88.7
	2266.5	215.2	4	125	3.8	264.7	85.1
	2270.05	63.8	2.4	153.9	2.7	291.8	86.4
	2275.75	58.2	0.1	328.2	0.3	161.6	89.7
	2278.14	252	0	162	5.7	352.5	84.2
	2278.2	261.5	1.2	171.4	4.6	5.9	85.3
Otter Park	2281	61.8	3.4	331.3	5.4	183.7	83.6
	2296.23	65.5	1.4	155.6	2.9	310.2	86.8
	2302.07	22.7	0.5	292.7	0.6	151.6	89.2
	2305.25	81.4	0.2	171.4	0	268.7	89.8
	2314.75	301.5	1.1	31.5	0.9	160.2	88.5
	2315.8	28.5	1	298.5	1.1	161.2	88.5
	2317.95	250.8	0.7	340.8	0.4	102.5	89.2
	2323.3	221.2	0.1	131.2	0.8	321.7	89.2
	2325	37.1	1.2	127.1	0.5	238.8	88.7
	2328.5	54.7	0.7	324.7	1.4	173.4	88.4
	2331.1	103	1.9	12.9	0.8	261.3	88
	2335.13	75	1.6	344.9	2	204.5	87.5
	2347.05	22.4	1.6	292.3	2.7	195.1	68.8
	2349.2	1.1	1.5	91.7	0.6	204.8	88.4
	2352.5	164.2	2.3	74.2	3.5	287.4	85.9
	2360.3	95.5	2	185.5	1	301.8	87.8
	2366	337.4	0.7	67.4	0.9	206	88.9
Evie	2367.7	50.8	9.2	142	7.5	270.6	78.1

	2376.55	80.7	9.3	174.1	19.5	326.5	68.2
	2377.3	85.2	2.4	355.2	0.7	256.1	85.4
	2380.53	116.9	3.4	26.5	7.5	230.9	81.8
	2383.1	252.3	0.8	162.2	3.1	357.5	86.8
	2386.55	66.7	0.8	336.7	2.6	174.2	87.2
	2397.25	93.2	3.3	2.8	6.9	208.3	82.4

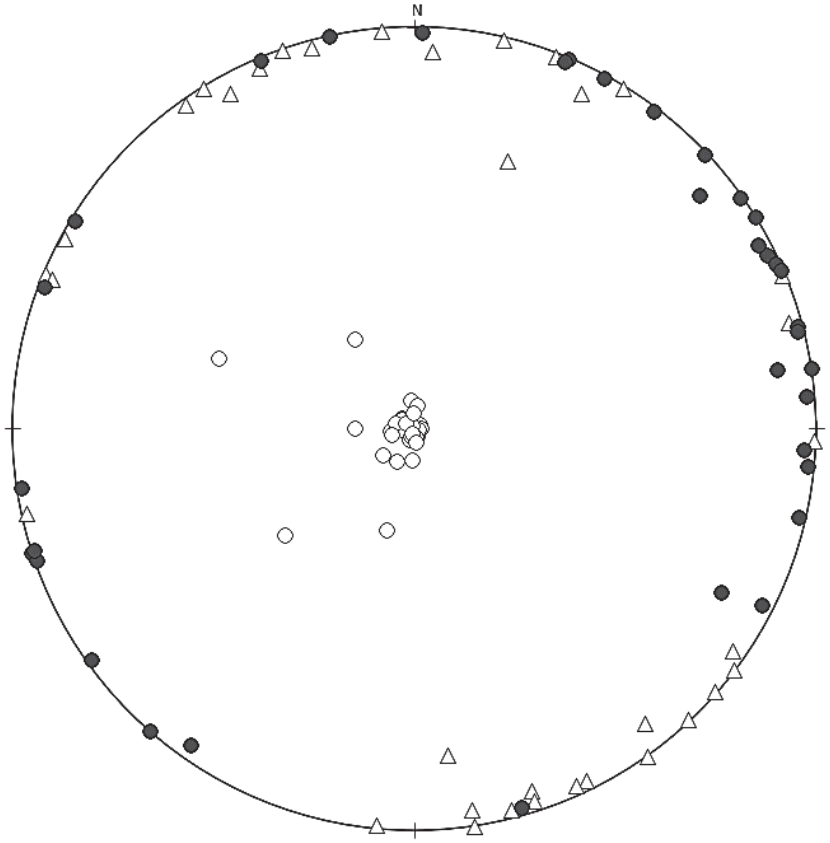

Figure 5.10: Stereographic projection showing σ_{max}, σ_{int} and σ_{min} orientations. Open circles are minimum conductivity axes (σ_{min}), closed circles are maximum conductivity axes (σ_{max}) and open triangles are intermediate conductivity axes (σ_{int}).

5.5 Discussion

5.5.1 Electrical Resistivity controls

Current flow in the Horn River Group mudrocks is mainly by surface conductance through the electrical double layer of clay minerals. **Figure 5.11** shows that directional resistivities are primarily dependent on illite clay content. There is a moderate to strong correlation between the concentration of illite and electrical resistivity in all nine measurement directions. Resistivity decreases sharply with increasing illite concentration, reaches a low of between 48Ωm and 302 Ωm (48Ωm to 55Ωm in the horizontal plane, 160Ωm to 240Ωm in the off diagonal directions and 302Ωm perpendicular to the bedding plane), and becomes more or less constant when illite concentration exceeds 60% -65%. In all nine directions shown in **Figure 5.11**, the relationship between illite content and resistivity is linear when the first two high resistivity points are excluded from the regression analysis.

In all samples, resistivity values also increase as the inclination of the applied current increases from bedding parallel (Inclination ~0°) to bedding perpendicular (Inclination ~90°). This speaks to the morphology and orientation of clay minerals. Resistivity is highest perpendicular to the preferred alignment direction because clay surface area, and hence surface conductance, is lowest in this direction. As the inclination of applied current decreases, and current flow is increasingly parallel to the direction of preferred orientation of clay minerals, surface area and surface conductance increase so resistivity decreases. Overall, resistivity is highest in the Evie and sections of the Upper Muskwa because they have the lowest clay content.

5.5.2 Anisotropy of electrical conductivity controls and fabric implications

The major textural elements generally reflected on the anisotropy of electrical conductivity (1/resistivity) of mudrocks are the orientations of minerals (especially clays) and or pore or fracture networks, one of which may dominate. Although clay content is the primary control on resistivity/conductivity of Horn River Group mudrocks, its correlation with the anisotropy of electrical conductivity is poor (**Figure 5.12**). A correlation is instead observed between anisotropy of electrical conductivity and porosity. Porosities were determined as follows using

density logs. The following equation also corrects values for organic matter effects (Razaee, 2015):

$$\phi = \frac{(\rho_{ma} - \rho_b) + \rho_b \left(W_{TOC} - \rho_{ma} \frac{W_{TOC}}{\rho_{TOC}} \right)}{\rho_{ma} - \rho_f} \quad (5.23)$$

where ϕ is the total density porosity, ρ_{ma} is the matrix density, ρ_b is the bulk density, W_{TOC} is total organic matter weight fraction, ρ_{TOC} is organic matter or kerogen density and ρ_f is density of the saturating fluid. A matrix density of 2.65g/cm^3 (assuming a quartz matrix) was used. The density of kerogen is between 1.0g/cm^3 and 1.3g/cm^3 (Okiongbo et al., 2005) so a density of 1.2g/cm^3 was used. The density of 20wt. % potassium chloride at 20°C is 1135kg/m^3. Calculated porosities are shown in **Table 5.3**. The clay rich Lower Muskwa and Otter Park have the lowest porosities (between 0.88% and 2.3%), and the siliceous and calcareous, clay poor Upper Muskwa and Evie have the highest porosities (between 3.8% and 9.2%).

In **Figure 5.13**, porosities are compared with % anisotropy of electrical conductivity (AEC) values obtained from 18 directional resistivities and with % values obtained from just 2 directional resistivities (assuming the samples are transversely isotropic). A clear correlation is observed in the 18 resistivity case but not in the 2 resistivity transversely isotropic case. The correlation is positive and stronger in the clay rich Lower Muskwa and Otter Park, and negative in the siliceous, clay poor Upper Muskwa and in the calcareous, clay poor Evie. Increasing AEC with increasing porosity indicates that although the clay rich members have the lowest porosities (0.88% to 2.5%), their pores are better connected (they have higher permeabilities). Since these members are clay rich, it is most likely that pores are between bedding parallel clay platelets. The pores in the higher porosity quartz and calcite rich members are however more isolated from one another. SEM images shown in **Figure 5.14** and **Figure 5.15** show pores between bedding parallel clays in the clay rich Otter Park and **Figures 5.16** and **5.17** show the more isolated, intraparticle pores common in the siliceous Upper Muskwa and calcareous Evie.

AEC principal orientations suggest that pores are mainly oblate, with long axes parallel to the bedding plane and short axes perpendicular to the bedding plane. SEM images, particularly of the Lower Muskwa and Otter Park (**Figure 5.14** and **5.15**), confirm that pore spaces are typically oblate and bedding parallel.

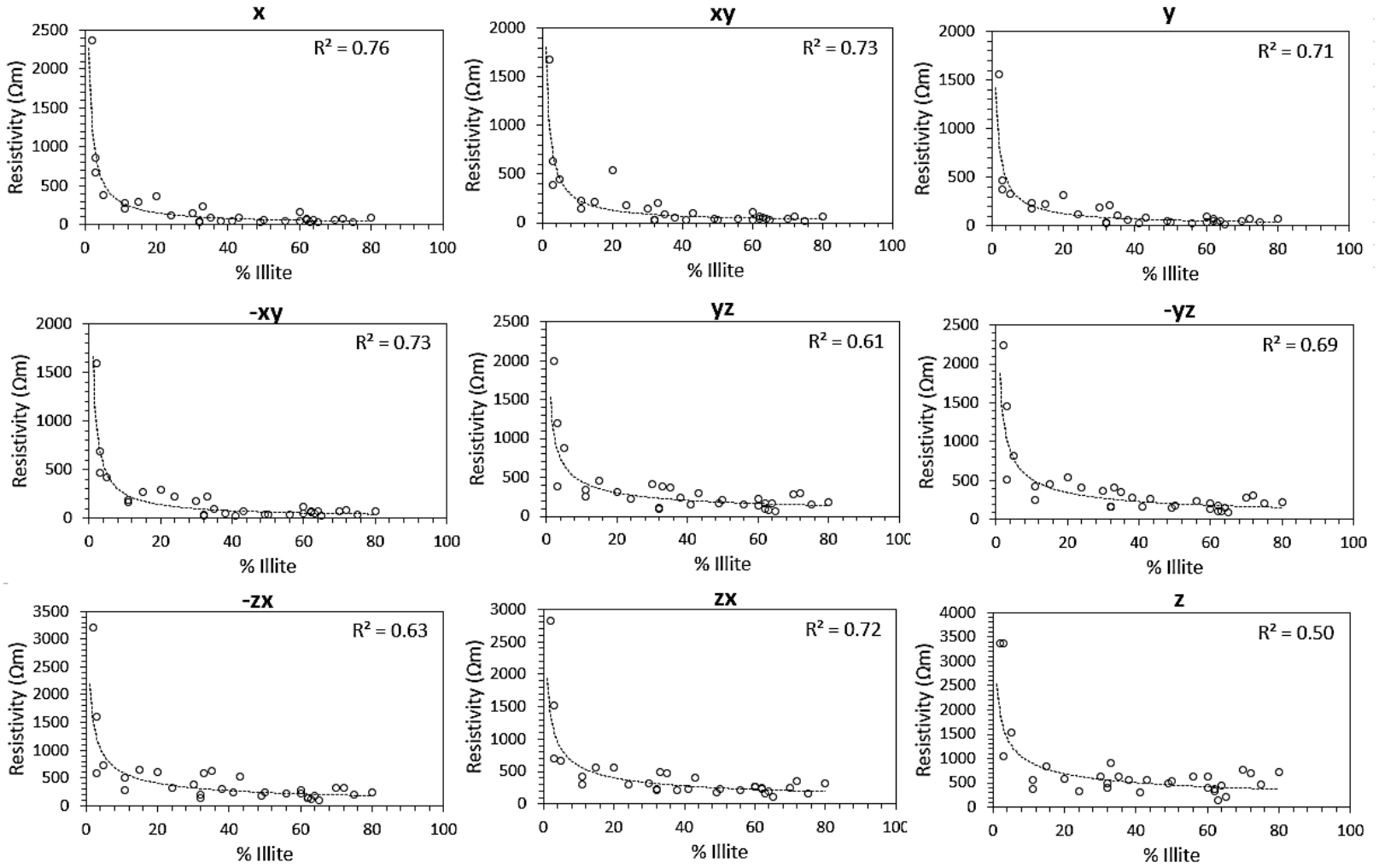

Figure 5.11: Relationship between illite clay content (derived from low temperature magnetic susceptibility measurements in **Chapter 4**) and directional resistivities for 31 Horn River Group samples. Resistivity increases with increasing inclination of the applied current. Directions parallel to the bedding plane (x, xy, y and -xy) have the lowest resistivities, those at an angle to the bedding plane (yz, -yz, -zx, zx) have intermediate resistivities, and the z direction (current direction normal to the bedding plane) has the highest resistivity.

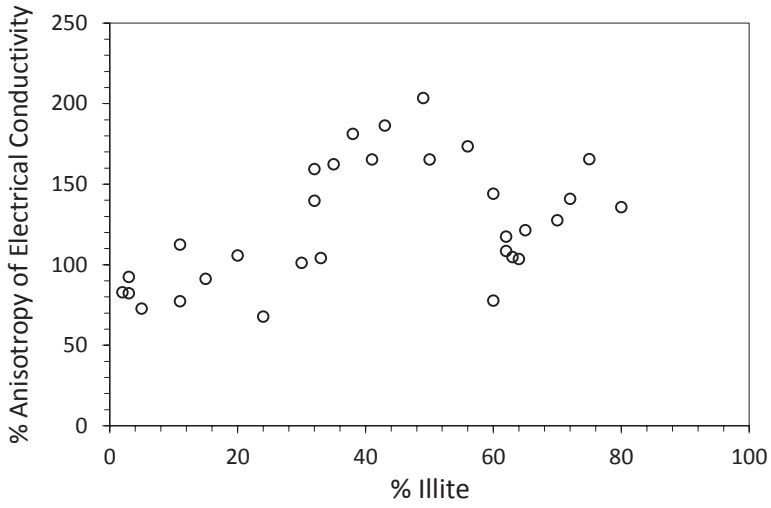

Figure 5.12: Relationship between clay content (derived from low temperature magnetic susceptibility measurements detailed in **Chapter 4**) and percent Anisotropy of Electrical Conductivity (AEC) in the Horn River Group.

Table 5.3: Porosities calculated from the density log of representative Muskwa, Otter Park and Evie samples. Porosities were corrected for TOC effects so only samples for which TOC data were available are shown in this table.

Formation	Depth (m)	Porosity (%)
Muskwa	2240.5	8.21
	2255.5	4.18
	2266.46	3.80
	2266.5	3.79
	2270.05	5.15
	2278.14	1.15
Otter Park	2281	1.20
	2296.23	0.92
	2302.07	1.07
	2305.25	1.59
	2314.75	2.54
	2315.8	1.63
	2317.95	1.64
	2325	1.47
	2331.1	2.21
	2347.05	4.85
	2352.5	1.69
	2360.3	1.65
Evie	2367.7	0.89
	2376.55	9.19
	2377.3	7.43
	2380.53	0.08
	2383.1	6.83
	2386.55	5.90
	2397.25	5.01

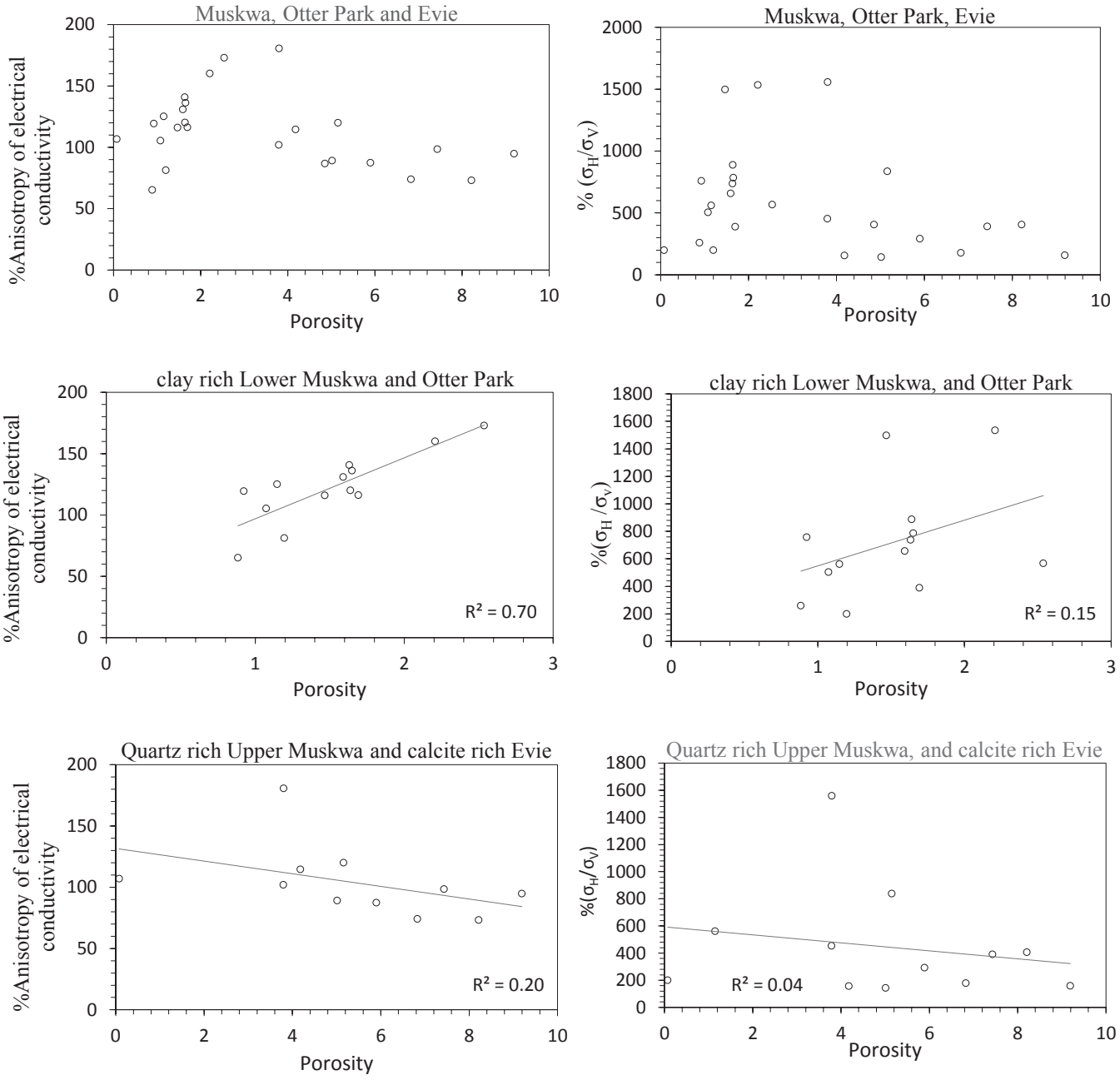

Figure 5.13: A comparison of electrical anisotropy-porosity relationships for a fully 3D anisotropy of electrical conductivity (left hand figures) and assuming a transverse isotropic model (right hand figures) for the Horn River Group samples. The correlation between porosity and 3D anisotropy of electrical conductivity is much better than that between porosity and the transverse isotropic model.

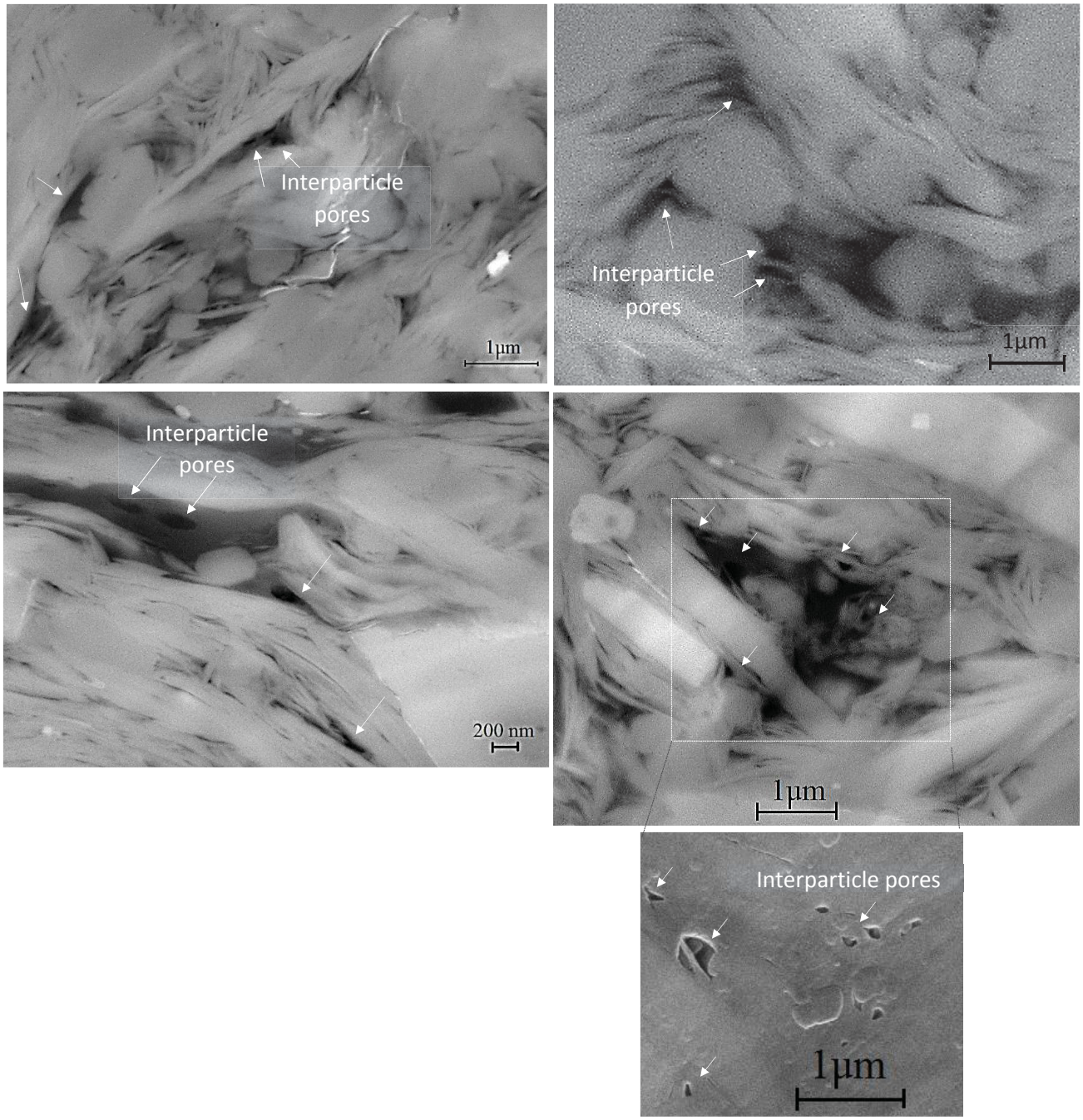

Figure 5.14: SEM images showing interparticle pores in clay rich sections of the Horn River Group. Pores are bedding-parallel, with long axes parallel to the bedding plane.

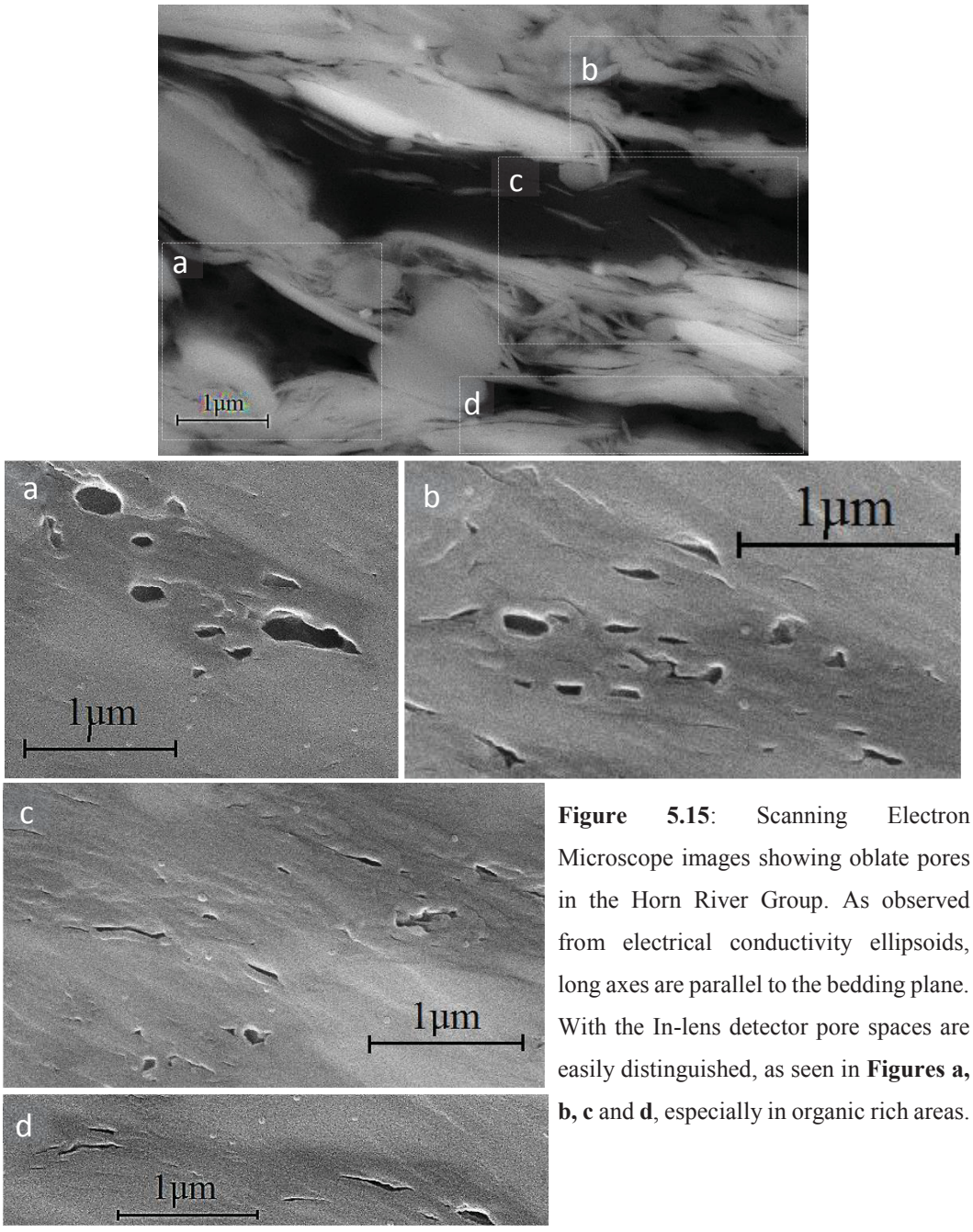

Figure 5.15: Scanning Electron Microscope images showing oblate pores in the Horn River Group. As observed from electrical conductivity ellipsoids, long axes are parallel to the bedding plane. With the In-lens detector pore spaces are easily distinguished, as seen in **Figures a, b, c** and **d**, especially in organic rich areas.

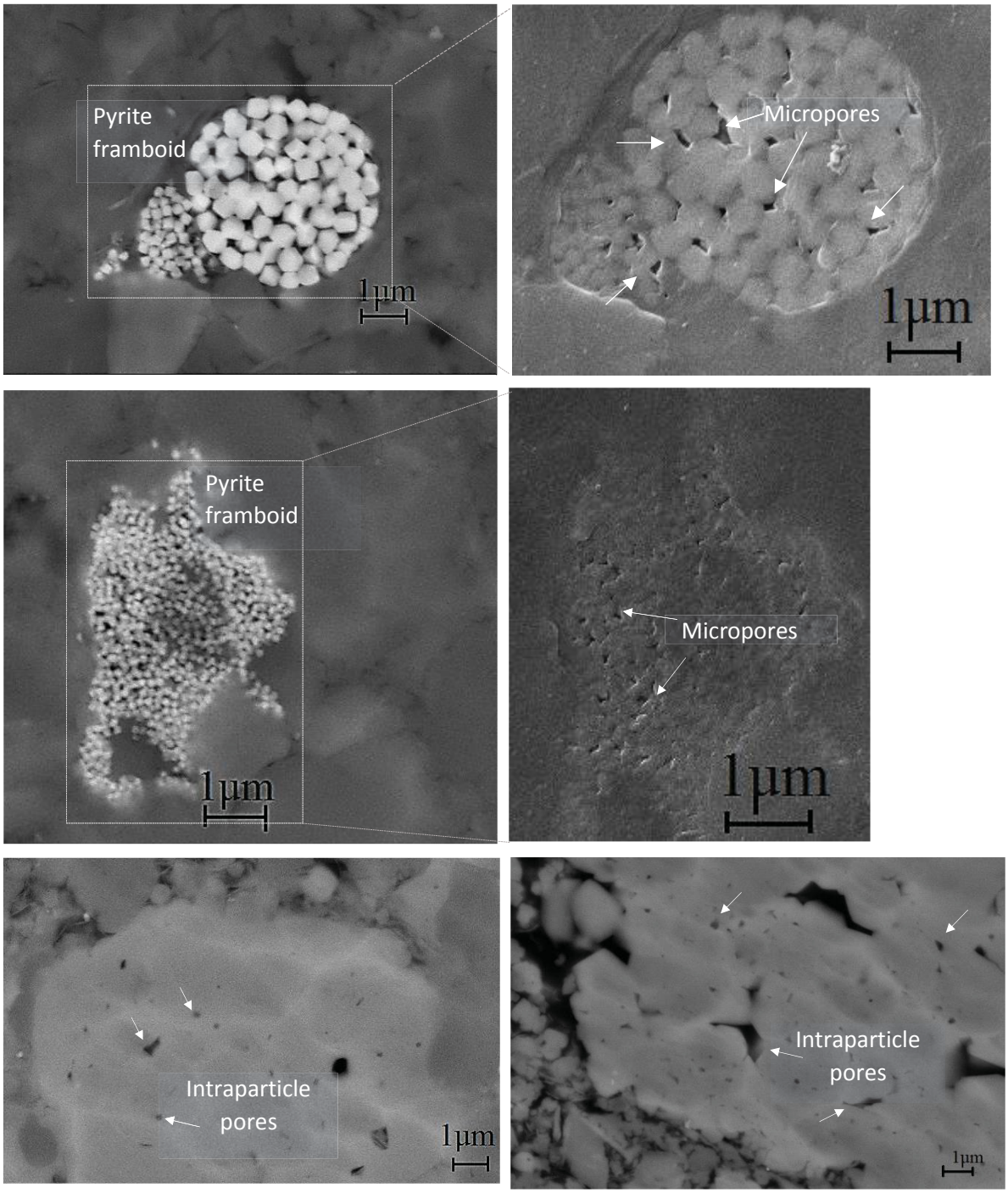

Figure 5.16: SEM images showing isolated intraparticle pores typical in the siliceous Upper Muskwa and calcareous Evie members in the Imperial Komie well.

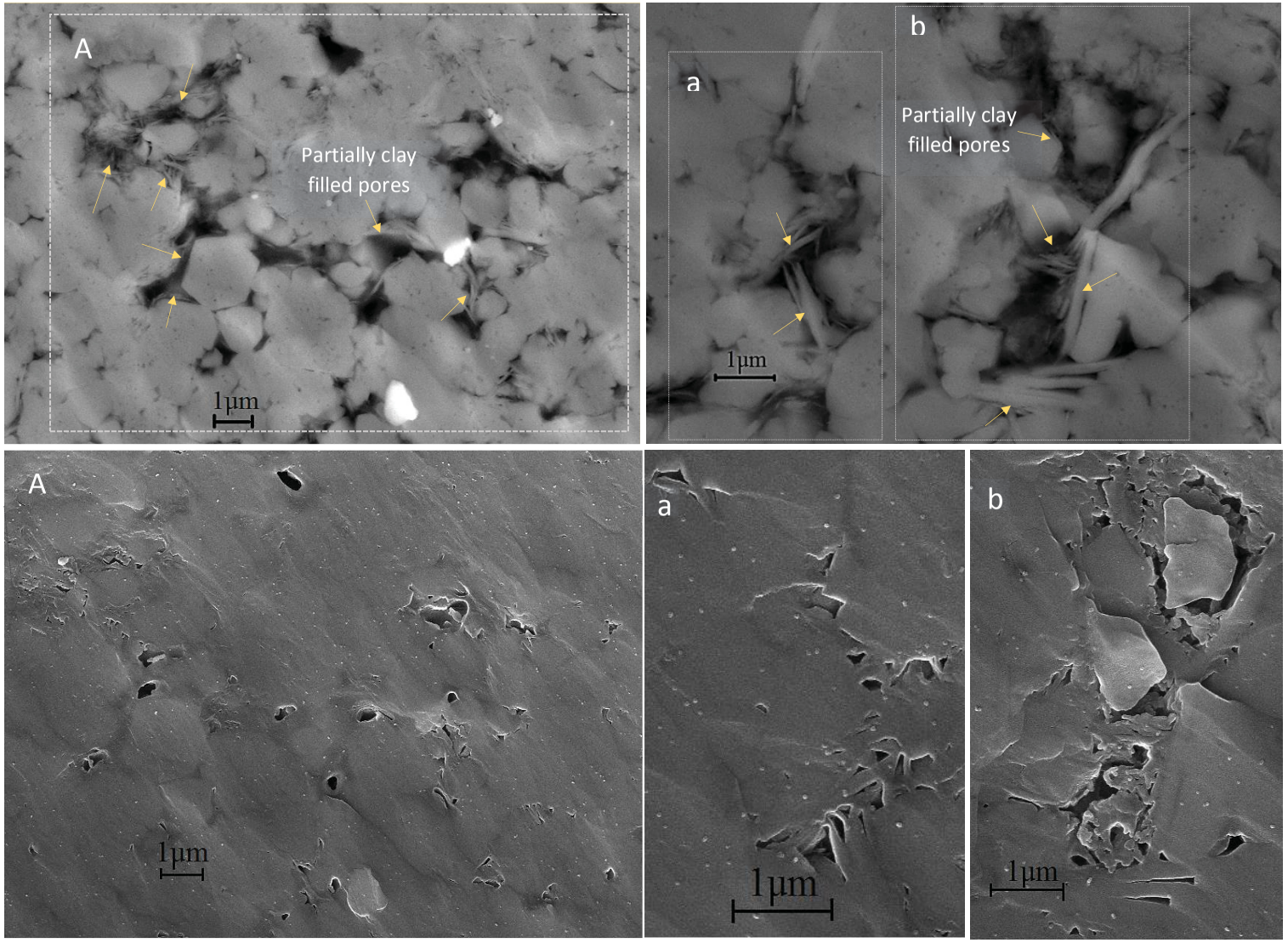

Figure 5.17: SEM images showing partially clay filled, isolated pores in the siliceous Upper Muskwa.

5.6 Conclusions

Current flow in the Horn River Group is primarily by surface conductance through the electrical double layer of clays and electrolytic conduction through connected pores. The following conclusions are made on the basis of results obtained:

1. The Horn River Group mudrocks from the Imperial Komie well are not transversely isotropic with respect to electrical conductivity. When transverse isotropy is assumed, the relationship between porosity and percent anisotropy of electrical conductivity is not obvious. Including 3D variation of electrical conductivity/resistivity in anisotropy determination yields a much clearer and obvious correlation.
2. Clays are the primary control on electrical conductivity while porosity is the primary control on the anisotropy of electrical conductivity.
3. Although the Upper Muskwa and Evie have higher porosity, their pores are mostly isolated. Clay rich, lower porosity shales of the Lower Muskwa and Otter Park are more permeable.
4. From the orientation of principal conductivity axes, pores are interpreted as showing preferred alignment parallel to the bedding plane.

5.7 References

Archie, G.E., 1942. The electrical resistivity log as an aid in determining some reservoir characteristics. Transactions of the American institute of Mining, Metallurgical and Petroleum Engineers, 146, 54-62.

Bachrach, R., 2011. Elastic and resistivity anisotropy of shale during compaction and diagenesis: Joint effective medium modeling and field observations. Geophysics, 76 (6), E175- 186.

Bourlange, S., Henry, P., Moore, J.C., Mikada, H., and Klaus, A., 2003. Fracture porosity in the décollement zone of Nankai accretionary wedge using Logging while Drilling resistivity data. Earth and Planetary Science Letters, 209, 103-112.

Chemali, R., Gianzero, S., and Su, S.M., 1987. The effect of shale anisotropy on focused resistivity devices. SPWLA 28th Annual Logging Symposium.

Clavaud, J.B., 2008. Electrical anisotropy of shale: the effect of compaction. Petrophysics, 49 (3), 243-260.

Clavier, C., Coates, G., and Dumanoir, J., 1984. The theoretical and experimental bases for the Dual-Water Model for the interpretation of shaly-sands. Society of Petroleum Engineers Journal, 24 (2), 153-168.

Duan, H.L., Karihaloo, B.L., Wang, J., and Yi, X., 2006. Effective conductivities of heterogeneous media containing multiple inclusions with various spatial distributions. Phys. Rev. B, 73 (17), 174203.

Ellis, M., Ruiz, F., Nanduri, S., Keirstead, R., Azizov, I., Frenkel, M., and MacGregor, L., 2011. Importance of anisotropic rock physics modelling in integrated seismic CSEM interpretation. First break, 29, 87-95.

Ghorbani, A., Cosenza, P., Ruy, S., Doussan, C., and Florsch, N., 2008. Noninvasive monitoring of water infiltration in a clay loamy soil using Spectral Induced Polarization. Water Resour. Res., 44, W08402.

Hewanger, J. V. Herwanger, J.V., Pain, C.C., Binley, A., De Oliveira, C.R.E., and Worthington, M.H., 2004. Anisotropic resistivity tomography. Geophysical Journal International, 158 (2), 409-425.

Juhász, I., 1981. Normalised Qv – The key to shaly sand evaluation using the Waxman-Smits equation in the absence of Core data. Society of Petrophysicists and Well-Log Analysts conference, SPWLA-1981-Z.

Keller G.V. and Frischknecht F.C., 1966. Electrical methods in geophysical prospecting. Pergamon Press Inc., Oxford, pp. 519.

Klein, J. D., Martin, P. R. and Allen, D. F., 1997. The petrophysics of electrically anisotropic reservoirs. The Log Analyst, 38, 25-36.

Leroy, P. and Revil, A., 2004. A triple-layer model of the surface electrochemical properties of clay minerals. Journal of Colloid and Interface Science, 270 (2), 371-380.

Lowrie, W., 2007. Fundamentals of geophysics. Cambridge University Press, p. 255.

Lyons, W., Plisga, G.J., and Lorenz, M., 2015. Standard handbook of petroleum and natural gas engineering. Gulf professional publishing, p. 99.

Mares, S., 1984. Introduction to applied geophysics. Springer Science and Business Media, pp. 266.

McCarter, W.J., 1984. The electrical resistivity characteristics of compacted clays. Geotechnique, 34 (2), 263-267.

McCarter, W.J., Blewett, J., Chrisp, T.M. and Starrs, G., 2005. Electrical property measurements using a modified hydraulic oedemeter. Canadian Geotechnical Journal, 42, 655-662.

Mitchell, J.K., 1993. Fundamentals of soil behaviour. Wiley Inter-Science, New York, p.422.

Mousseau, R.J., and Trump, R.P., 1967. Measurement of electrical anisotropy of clay-like materials. Journal of Applied Physics, 38 (11), 4375 - 4379.

Negi, A.S., and Anand, S.C., 1985. A textbook of physical chemistry. New Age International (P) Limited, Publishers, pp. 489.

Okiongbo, K.S., Aplin, A.C., and Larter, S.R., 2005. Changes in Type II Kerogen Density as a Function of Maturity: Evidence from the Kimmeridge Clay Formation. Energy Fuels, 19 (6), 2495-2499.

Patnode, H.W., and Wyllie, M.R.J., 1950. The Presence of Conductive Solids in Reservoir Rocks as Factor in Electric Log Interpretation. Society of Petroleum Engineers, 2 (2), 47-52.

Rezaee, R., 2015. Geomechanics of gas shales In: Fundamentals of shale gas reservoirs. John Wiley and Sons, Inc., pp. 169-190.

Revil, A.P., and Glover, W.J., 1997. Theory of ionic surface electrical conduction in porous media. Phys. Rev. 55, 1757-1773.

Revil, A., Cathles, M.L., and Losh, S., 1998. Electrical conductivity in shaly sands with geophysical applications. Journal of Geophysical Research, 103 (B10) 23, 925-936.

Saeidi, O., Rasouli, V., Vaneghi, R.G., Gholami, R., and Torabi, S.R., 2014. A modified failure criterion for transversely isotropic rocks. Geoscience Frontiers, 5, 215-225.

Telford, W. M., Geldart, L. P., and Sheriff, R. A., 1990. Applied geophysics, 2nd edition: Cambridge Univ. Press, pp. 770.

Tsvankin, I., 1997. Anisotropy parameters and P-wave velocities for orthorhombic media. Geophysics, 62 (4), 1292-1309.

Vinegar, H.J. and Waxman M.H., 1984. Induced polarization of shaly sands. Geophysics, 49, 1267-1287.

Waxman, M.H. and Smits, L.J.M., 1968. Electrical conduction in oil-bearing sands. Society of Petroleum Engineers Journal, 8, 107-122.

Chapter 6

Anisotropy of Magnetic Remanence (AMR)

6.1 Introduction

In the presence of an external magnetic field, a magnetization is induced in all matrix components in a sample. The magnetic susceptibility tensor and AMS ellipsoid are a reflection of the concentrations, shape and orientations of all magnetic phases present in the sample. When the external magnetic field is removed, paramagnetic and diamagnetic phases lose their induced magnetization but ferromagnetic, ferrimagnetic and antiferromagnetic phases retain some of their induced magnetization. The induced magnetization retained is called permanent or remanent magnetization and anisotropy of magnetic remanence (AMR) measures the variation of this remanent magnetization with direction. Unlike magnetic susceptibility, which is a property of all minerals/phases in a sample, only the ferromagnetic, ferrimagnetic and antiferromagnetic minerals in a sample are capable of carrying a remanent magnetization. Therefore, AMR results are a reflection of ferromagnetic/ferrimagnetic/antiferromagnetic fabric. The remanence intensity is dependent on the type and concentration of remanence carrying minerals, and the orientations and relative magnitudes of the AMR ellipsoid principal axes depend on their degree and direction of alignment.

Anisotropy of magnetic remanence (AMR) and anisotropy of magnetic susceptibility (AMS) results also differ in the orientation of their ellipsoid principal axes with domain state. Multidomain (MD) grains have maximum magnetic susceptibility parallel to their long axes and minimum magnetic susceptibility normal to their long axes, while stable single domain (SD) grains have maximum susceptibility normal to their long axes and minimum susceptibility parallel to it

(**Figure 6.1**) (Stephenson et al., 1986; Potter and Stephenson, 1988). The orientation of the AMR ellipsoid axes do not however vary with domain state in individual stable single domain (SD) and multidomain (MD) grains. An MD grain and a stable SD grain both have maximum remanence intensity parallel to their long axes and minimum remanence perpendicular to their long axes (**Figure 6.1**). In a rock sample with inverse magnetic fabric (containing predominantly stable SD grains), the maximum magnetic susceptibility axis is thus parallel/subparallel to the minimum remanence direction, and the minimum susceptibility axis parallel/subparallel to the maximum remanence direction. Where a rock sample consists of a mixture of multidomain and stable single domain grains, the summation of all grain tensors may produce an AMS ellipsoid whose maximum susceptibility axis is not parallel to grain long axes or foliation plane. Since maximum magnetic remanence remains parallel to grain long axes or foliation plane, AMR ellipsoids likely provide more accurate estimates of actual mineral orientations and distribution (Tarling and Hrouda, 1993; Potter, 2004).

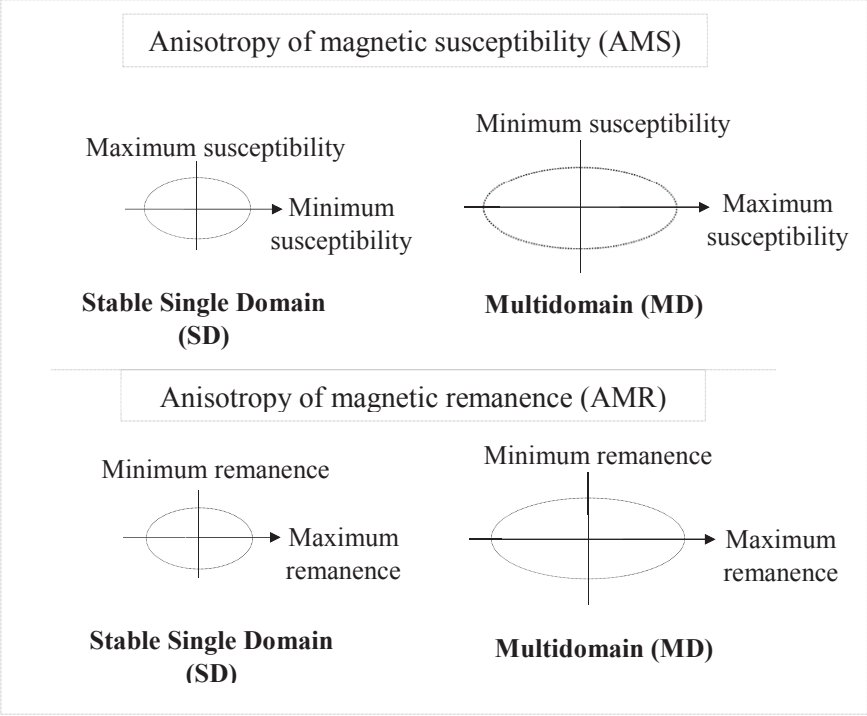

Figure 6.1: Minimum and maximum magnetic susceptibility and magnetic remanence directions for single and multidomain grains.

Anisotropy of magnetic remanence techniques have found several petrological and paleomagnetic applications including:

1. The determination of paleointensity and direction (Spassov et al., 2010).
2. Studies of weakly magnetic or weakly deformed rocks whose anisotropy of magnetic susceptibility cannot be accurately determined. This application takes advantage of the fact that ferrimagnetic and ferromagnetic minerals are more anisotropic than paramagnetic and diamagnetic minerals (AMR is greater than AMS) (Stephenson et al., 1986; Jackson, 1991).
3. The quantitative estimation of strain magnitudes and orientations (Jackson et al., 1989).
4. The identification of ferromagnetic and ferrimagnetic minerals in a sample. A comparison of AMS and AMR orientations is also used to test for stable single domain grains (Stephenson et al., 1986; Potter and Stephenson, 1988).

6.2 Theoretical background

Like AMS, AMR is described by an anisotropy ellipsoid with three orthogonal principal axes whose remanence intensities and orientations indicate how anisotropic a sample is and the 3D orientation of its remanence carrying minerals. For weak field magnetic remanences such as TRM (thermoremanent magnetization) and DRM (detrital remanent magnetization), the remanent magnetization, M_R, induced in a particular direction is linearly proportional to the strength, H, of the field that induced it. Both are related by the constant K_R, known as the volumetric remanence susceptibility.

$$M_R = K_R H \tag{6.1}$$

The dimensionless proportionality constant K_R is a measure of a material's capacity to retain a remanent magnetization. Where ferromagnetic and ferrimagnetic minerals in a sample are randomly oriented, M_R and K_R are independent of direction and the sample is isotropic. If a sample is anisotropic, the relationship between M_R and H is described by a symmetric second rank tensor, K_R, which like the magnetic susceptibility tensor, can be represented geometrically by an ellipsoid whose axes are the principal remanence directions (Stacey and Banerjee, 1974; Jackson, 1991).

$$K_R = \begin{bmatrix} K_{11} & K_{12} & K_{13} \\ K_{21} & K_{22} & K_{23} \\ K_{31} & K_{32} & K_{33} \end{bmatrix} \quad (6.2)$$

Although for strong field remanences like IRM (isothermal remanent magnetization) the relationship between M_R and H is nonlinear below magnetic saturation fields, the relationship can still be described by a second rank tensor

$$M_R = [K_R] f(H) \quad (6.3)$$

where $f(H)$ describes the non-linear field-dependence of M_R (Cox and Doell, 1967; Jackson, 1991; Hrouda, 2002).

6.3 Common anisotropy of magnetic remanence techniques

Remanent magnetization can be both natural and artificial. Natural remanences include thermoremanent magnetization (TRM) which is acquired during cooling from above the Curie temperature in a magnetic field, and detrital remanent magnetization (DRM) which is acquired during the deposition and lithification of sediments in a magnetic field (Butler, 1992). Artificial remanences are imparted in the laboratory. The most common laboratory induced remanences are isothermal remanent magnetization (IRM) and anhysteretic remanent magnetization (ARM) (Potter, 2004; Martín-Hernández and Ferré, 2007).

Laboratory methods that are used to determine the anisotropy of magnetic remanence tensor require that magnetization be induced along a set number of sample directions. Since, to a first approximation, the second rank AMR tensor is symmetric, at least six independent remanence measurements are needed to define the tensor. Cox and Doell (1967) described a method of determining the anisotropy of isothermal remanent magnetization (AIRM) tensor from 15 independent positions. Stephenson et al. (1986) determined the AIRM tensor from 9 directional remanence measurements made in 3 positions, while McCabe et al. (1985) determined the anisotropy of anhysteretic remanent magnetization (AARM) tensor using the 9 positions used by Girdler (1961) to determine the AMS tensor. Regardless of the type of remanence imparted and

the number of positions used, all AMR techniques follow the same basic procedure. The sample is demagnetized and its remanent magnetization is measured. This remanence value is the base level magnetization. A magnetic field is then applied along the first direction and the imparted remanent magnetization is measured. The remanence due to the applied field is found by subtracting the base level magnetization. Successive demagnetization and magnetization are repeated for all chosen positions and the measurements are used to define the 3×3 K_R matrix (Hirt, 2007).

The following is a brief description of the two most common AMR techniques, anisotropy of anhysteretic remanent magnetization (AARM) and anisotropy of isothermal remanent magnetization (AIRM).

6.3.1 Anisotropy of Anhysteretic Remanent Magnetization (AARM)

An anhysteretic remanence is acquired when a sample is exposed to an alternating field (AF) in the presence of a small bias direct magnetic field (DF). The strength of the alternating field is generally less than 300mT and the bias field is on the order of 0.05mT to 0.1mT (Hirt, 2007). All remanence carrying particles with coercivity less than the applied alternating field are magnetized. The acquired anhysteretic remanence intensity is linearly proportional to the strength of the direct field as described in equation (6.1) and a proportionality constant, known as the anhysteretic susceptibility, relates both variables (King et al., 1982; McCabe et al., 1985). To obtain the anisotropy of anhysteretic remanent magnetization (AARM) ellipsoid, the ARM acquired when the AF is applied in a set number of directions is measured and used to determine the best fit anisotropy tensor using a least squares method. Between each directional impartation of ARM, the sample is demagnetized in an alternating field to establish a base level natural magnetization (McCabe et al., 1985). ARM is thought to be a good analogue of TRM in the Earth's field; the alternating field simulates thermal agitation and the direct field is synonymous with the Earth's magnetic field (Potter, 2004).

6.3.2 Anisotropy of Isothermal Remanent Magnetization (AIRM)

Isothermal remanent magnetization is magnetization that is retained after a strong magnetic field (typically >10mT) is removed. Because strong direct fields are applied, higher coercivity phases in a sample are magnetized. To determine the AIRM tensor and ellipsoid, a direct field (DF) is applied along three orthogonal sample axes and nine components of remanence are measured. Prior to each direct field application, the sample is demagnetized in an alternating field (AF) to establish a base level magnetization (Potter, 2004).

6.4 Chapter Goals

In this chapter, the application of the anisotropy of isothermal remanent magnetization (AIRM) to fabric analysis in the Horn River Group is explored. IRM was chosen because it gives the largest signal compared to other remanence types and it is suitable, since compared to diamagnetic and paramagnetic mineral composition, these shales and mudstones have very low ferromagnetic and ferrimagnetic mineral concentrations. IRM and AIRM results are used to:

1. Test for the presence of stable single domain (SD) grains, especially in Horn River Group samples with inverse AMS fabric at room temperature.
2. Test if stable single domain grains are partly responsible for inverse AMS fabrics observed at room temperature in some Horn River Group samples that retain inverse AMS fabrics at progressively lower temperatures.
3. Better constrain mineral fabrics in the Horn River Group. Since ferrimagnetic/ ferromagnetic minerals are more anisotropic than diamagnetic and paramagnetic minerals, AIRM ellipsoids may be a more accurate means of quantifying mineral/grain shapes, orientations and distribution.

6.5 Methodology

The AIRM tensors and ellipsoids of 15 representative Horn River Group samples were determined; 3 from the Muskwa, 8 from the Otter Park and 4 from the Evie. Of the 15 samples selected, based

on room temperature AMS principal axes orientations, 7 have normal magnetic fabrics, 5 have inverse magnetic fabrics and 3 have intermediate fabrics.

Before inducing an IRM, each sample was first demagnetized by tumbling in an alternating field of 80mT. Following demagnetization, the intensity of any residual remanence was measured. An IRM was then induced by successively applying a direct field (DF) of 60 mT along the +x, +y, and +z sample axes using a pulse magnetizer. Following the application of the DF along the +x axis, the remanence acquired in the x, y and z directions are measured. The IRM acquired along these directions are obtained by subtracting the residual remanence (following demagnetization) for each direction from the remanence measured after DF application in the +x direction. This yields three components of the IRM matrix. After AF tumble demagnetization, the 60mT field was applied along the +y direction and the three components of IRM acquired were again determined by subtracting any residual remanence left after demagnetization. The procedure is repeated for the +z-axis to obtain the last three components of the IRM tensor.

To determine the primary remanence carrying mineral, IRM acquisition curves for three samples were constructed. Direct fields ranging from 10mT to 90mT were applied along the +x sample axes, and the IRM acquired along the x-axes, for incrementally higher direct fields, were measured. Between each DF application, samples were demagnetized by tumbling in an AF of 80mT (for DF less than 80mT) and 90mT (for DF of 90mT).

6.6 Results

Figure 6.2 shows the orientations of the three orthogonal AIRM principal axes. In all 15 Horn River Group samples, maximum and intermediate IRM are parallel to the bedding plane and minimum IRM axes are normal to the bedding plane. When AIRM principal orientations are compared to anisotropy of magnetic susceptibility (AMS) principal orientations, samples with normal AMS fabric, that is those with maximum magnetic susceptibility parallel/subparallel to the bedding plane and minimum susceptibility normal to it, have similar orientations. Minimum IRM, like minimum magnetic susceptibility is steeply inclined and maximum IRM, like maximum susceptibility, has a shallow inclination (**Figure 6.3A).** Samples with inverse AMS fabric have steeply inclined maximum magnetic susceptibility and minimum IRM axes and shallowly inclined

maximum IRM and minimum susceptibility axes (**Figure 6.3B**). These AIRM results confirm that inverse fabric in these samples is due to stable SD particles, and is the first time to our knowledge that inverse AMS fabrics due to stable SD particles have been reported in shales.

To determine which ferromagnetic or ferrimagnetic mineral(s) control IRM and AIRM, IRM acquisition curves for three Horn River Group samples were constructed. **Figure 6.4** shows the IRM acquisition curves. Samples begin to saturate at 70-90mT suggesting that magnetite is the primary remanence carrying mineral in these samples. If hematite, a canted antiferromagnetic mineral common in rocks, was the dominant ferrimagnetic mineral, magnetic fields as high as 1T would be necessary for saturation. The degree of alignment of magnetite, reflected by the %AIRM, varies as shown in **Figure 6.5**. Percent AIRM (%AIRM) values are shown alongside percent anisotropy of magnetic susceptibility (%AMS). Percent AIRM values in the Muskwa, Otter Park and Lower Evie exceed AMS values by 15% to 181%, but in the Lower Evie both AMS and AIRM values are approximately equal.

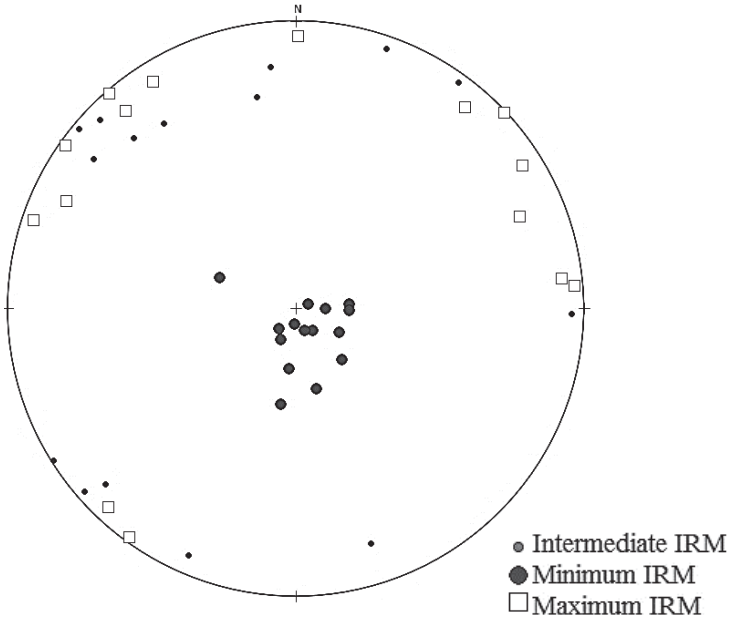

Figure 6.2: Equal area plot showing the orientation of the principal anisotropy of isothermal remanent magnetization (AIRM) axes for Horn River Group mudrocks.

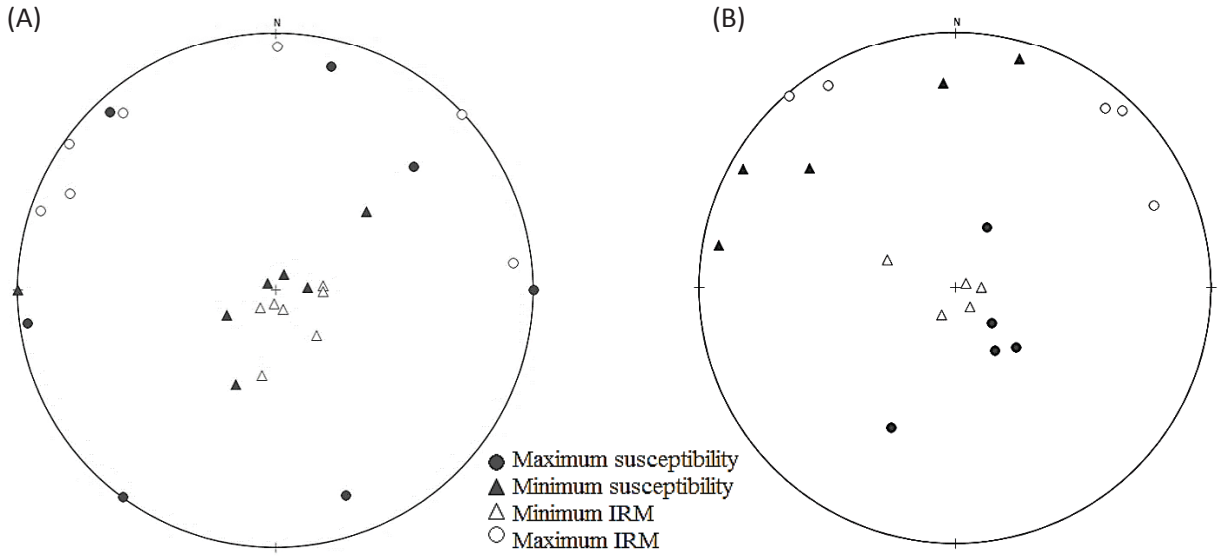

Figure 6.3: Equal area plot comparing the principal susceptibility and IRM orientations for 15 Horn River Group mudrocks. (A) Samples with normal AMS fabrics have K_{max} (maximum susceptibility) and R_{max} (maximum IRM) subparallel/parallel to the bedding plane and K_{min} (minimum susceptibility) and R_{min} (minimum IRM) normal to the bedding plane (B) Samples with inverse AMS fabrics have K_{max} (maximum susceptibility) and R_{min} (minimum IRM) normal to the bedding plane and K_{min} (minimum susceptibility) and R_{max} (maximum IRM) subparallel/parallel to the bedding plane.

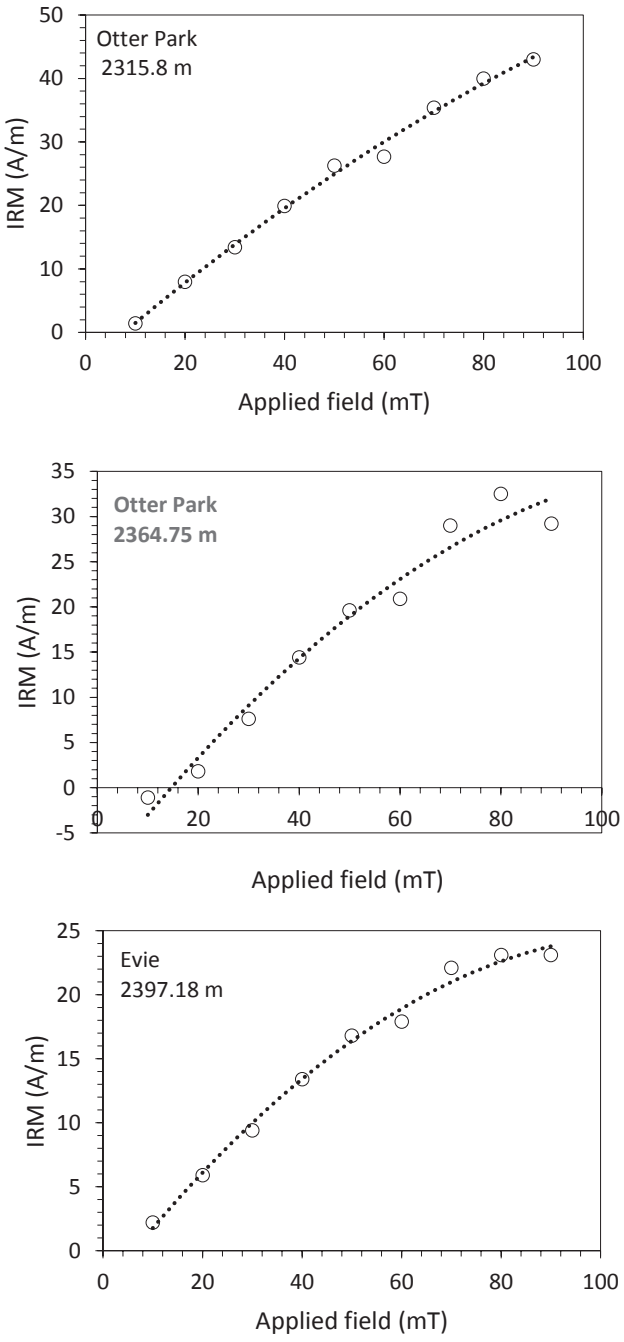

Figure 6.4: IRM acquisition curves for three Horn River Group samples exposed to fields between 10mT-90mT.

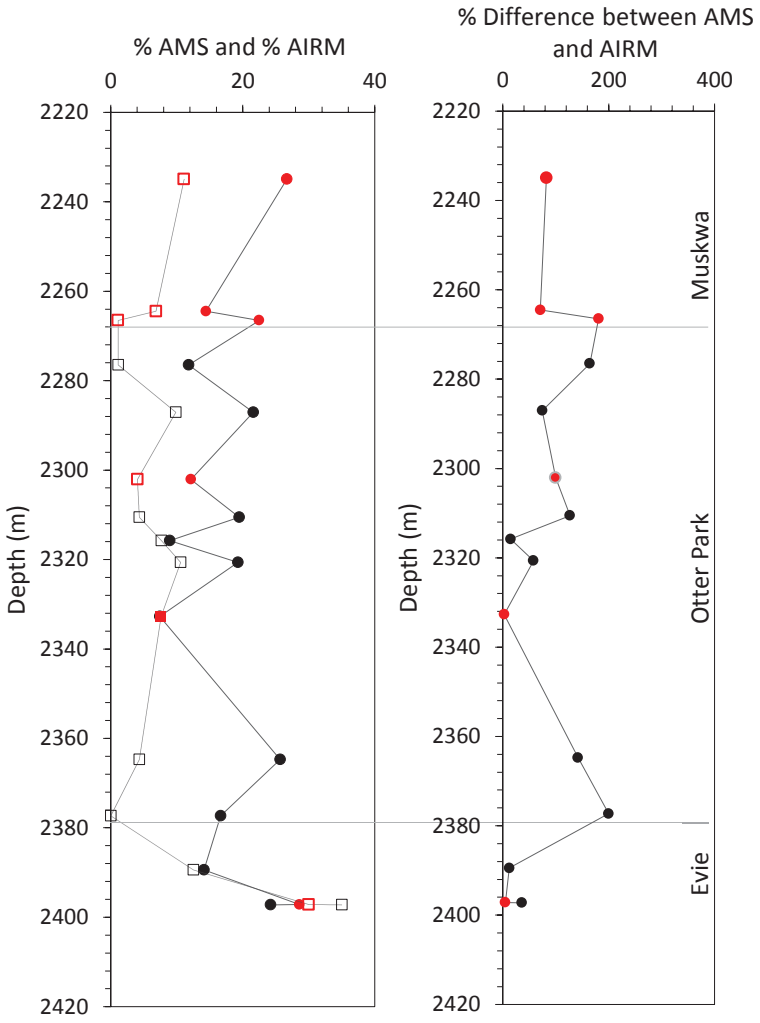

Figure 6.5: Comparison of room temperature %AMS (open squares) and %AIRM (closed circles). Samples with inverse magnetic fabric at room temperature are in red, and the percent difference between %AMS and %AIRM is shown on the plot to the right.

6.7 Discussion

The presence of ferrimagnetic minerals in the Muskwa, Otter Park and Evie is illustrated by their IRM acquisition curves, which indicate that magnetite is the dominate ferrimagnetic mineral. If ferrimagnetic minerals have undergone the same depositional and diagenetic processes as the diamagnetic and paramagnetic phases that control room temperature magnetic susceptibility and anisotropy of magnetic susceptibility in the Horn River Group, it is expected that they have similar grain orientations, and hence similar magnetic fabrics. If they were, however, formed after

diamagnetic and paramagnetic minerals, and have different depositional and diagenetic histories, their magnetic fabrics may differ. For Horn River Group samples from the Imperial Komie well, the principal axes of AIRM ellipsoids have similar orientations as the principal axes of AMS ellipsoids except where samples contain stable single domain (SD) grains. Ferrimagnetic minerals, paramagnetic minerals (like illite) and diamagnetic phases (like calcite and quartz) therefore have similar orientations (their long axes define the bedding/foliation plane). Even in samples that contain stable single domain (SD) grains (samples with inverse AMS fabric), ferrimagnetic minerals have long axes that have the same orientation as paramagnetic and diamagnetic minerals. The difference in their AIRM and AMS ellipsoids is because in stable single domain grains, the maximum susceptibility axis is normal to the grain long axis.

The difference between %AIRM and % AMS indicates a difference in the degree of ferrimagnetic alignment and bulk matrix alignment. Higher AIRM compared to AMS values in the Muskwa, Otter Park and Upper Evie indicates that ferrimagnetic minerals in these intervals are more preferentially oriented than the bulk matrix. Approximately equal AMS and AIRM values in the lower Evie indicates that ferrimagnetic minerals in the Lower Evie are aligned to the same degree as the bulk matrix (dominated by diamagnetic and paramagnetic minerals). For samples with a mixture of MD and stable SD particles in the same alignment direction the AMS will be partially cancelled out (k_{max} parallel to particle long axis for MD and perpendicular to particle long axis for SD), so that %AIRM will exceed %AMS.

AIRM results also indicate that the Type 2 and Type 3 samples defined in **Chapter 4** on the basis of low temperature AMS results contain some stable single domain (SD) grains. Type 2 mudrocks have inverse AMS fabrics irrespective of temperature and Type 3 mudrocks have normal AMS fabrics that progressively become inverse with decreasing temperature. Inverse magnetic fabric at low temperature in both classes indicate paramagnetic minerals, such as siderite or ferroan calcite, are present in these groups of mudrocks. Comparison of AMS and AIRM principal axes orientation indicates that they also contain some stable single domain grains. Inverse fabrics observed at room temperature in Type 2 mudrocks is therefore not due solely to the presence of siderite or ferroan calcite. Because Type 3 mudrocks have normal AMS fabric at room temperature, they may not contain enough stable SD grains to dominate room temperature AMS results.

6.8 Conclusions

The acquisition of isothermal remanent magnetization (IRM) indicates that Horn River Group mudrocks contain remanence carrying minerals, and IRM acquisition curves indicate the primary remanence carrying mineral is magnetite. The fabric of these remanence carriers is quantified in terms of the anisotropy of isothermal remanent magnetization (AIRM). AIRM can be described by an ellipsoid whose principal orientations are computed here from 9 directional IRM measurements made after the application of a magnetic field along three sample axes. The following are the main conclusions reached from the results obtained:

1. A comparison of AMS and AIRM principal orientations indicates samples with inverse AMS fabric at room temperature contain stable single domain (SD) grains. This is the first time to our knowledge that inverse fabrics due to uniaxial stable SD grains have been reported in shales.

2. Ferrimagnetic minerals, mainly magnetite, are more preferentially oriented than the bulk matrix in the Muskwa, Otter Park and Upper Evie. AIRM values in these formations exceed AMS values by 15% to 181%. Higher %AIRM may be due to a mixture of stable SD and MD particles in the same alignment direction. In the Lower Evie however, AMS and AIRM values are almost equal.

3. A comparison of AIRM and AMS principal orientations indicates that like the diamagnetic and paramagnetic minerals that make up the bulk of the matrix, the long axes of ferrimagnetic minerals define the bedding plane. The alignment of ferrimagnetic minerals is therefore primarily caused by burial/compaction.

6.9 References

Butler, R.F., 1992. Paleomagnetism: magnetic domains to geologic terranes. Blackwell Scientific Publications, pp. 319.

Cox, A., Doell, R.R., 1967. Measurements of high coercivity magnetic anisotropy. *In*: Collinson, D.V., Creer, K.M., Runcorn, S.K. (Eds.), Methods in Palaeomagnetism. Elsevier, Amsterdam, p. 477 - 42.

Girdler, R.W., 1961. The measurement and computation of anisotropy of magnetic susceptibility in rocks. Geophys. Jour. R. Astron. Soc. 5, 34 - 44.

Hirt, A.M., 2007. Magnetic remanence, anisotropy. Encyclopedia of geomagnetism and paleomagnetism, p. 535 - 540.

Hrouda, F., 2002. The use of the anisotropy of magnetic remanence in the resolution of the anisotropy of magnetic susceptibility into its ferromagnetic and paramagnetic components. Tectonophysics, 347, 269 - 281.

Jackson, M., Craddock, J.P., Ballard, M., Van der Voo, R., and McCabe, C., 1989. Anhysteretic remanent magnetic anisotropy and calcite strains in Devonian carbonates from the Appalachian Plateau, New York. Tectonophysics, 161, 43 - 53.

Jackson, M., 1991. Anisotropy of magnetic remanence: A brief review of mineralogical sources, physical origins, and geological applications, and comparison with susceptibility anisotropy. Pageoph.,136 (1), 1 - 28.

King, J., Banerjee, S.K., Marvin, J., and Ozdemir, O., 1982. A comparison of different methods for determining the relative grain size of magnetite in natural sediments: some results from lake sediments. Earth Planet. Sci. Lett., 59, 404-419.

Martín-Hernández, F., and Ferré, E.C., 2007. Separation of paramagnetic and ferrimagnetic anisotropies: a review. Journal of Geophysical Research, 112, B03105, doi:10.1029/2006JB004340.

McCabe, C., Jackson, M., and B. B. Ellwood, B.B., 1985. Magnetic anisotropy in the Trenton limestone: Results of a new technique, anisotropy of anhysteretic susceptibility. Geophysical Research Letters, 12, 333-336.

Potter, D. K., and Stephenson, A., 1988. Single-domain particles in rocks and magnetic fabric analysis. Geophysical Research Letters, 15, 1097-1100.

Potter, D. K., and Stephenson, A., 1990. Field-impressed anisotropies of magnetic susceptibility and remanence in minerals. J. Geophys. Res., 95 (15), 573-588.

Potter, D.K., 2004. A comparison of anisotropy of magnetic remanence methods- a user's guide for application to palaeomagnetism and magnetic fabric studies. *In*: Martin-Hernandez, F., Luneburg, C.M., Aubourg, C., and Jackson, M. (eds.), Magnetic Fabric: Methods and applications. Geological Society, London, Special publications, 238, 21-35.

Spassov, S., Valet, J.P., Kondopoulou, D., Zananiri, I., Casas, L., and Le Goff, M., 2010. Rock magnetic property and paleointensity determination on historical Santorini lava flows. Geochemistry, Geophysics, Geosystems, 11(7), 1 - 12.

Stacey, F. D., and Banerjee, S. K., 1974. Physical Principles of Rock Magnetism. Elsevier, pp. 195.

Stephenson, A., Sadikun, S. and Potter, D. K., 1986. A theoretical and experimental comparison of the anisotropies of magnetic susceptibility and remanence in rocks and minerals. Geophysical Journal of the Royal Astronomical Society, 84, 185-200.

Tarling, D. H. and Hrouda, F., 1993. The magnetic anisotropy of rocks. Chapman and Hall, pp. 217.

Chapter 7

Comparison of results from different anisotropy techniques

7.1 Introduction

Each anisotropy technique discussed in the preceding chapters provides different insights into the petrofabric of the Horn River Group. In this chapter, results from the various techniques are compared to develop a more robust quantitative understanding of the distribution and spatial arrangement of fabric elements.

7.2 Comparison of room temperature Anisotropy of Magnetic Susceptibility results and thin section observations

Thin section based characterization of anisotropy degree depends on the presence of visible bedding planes, laminations or elongate aligned grains. Where these are absent or not visible, samples are classified as poorly anisotropic in thin section. Anisotropy of magnetic susceptibility on the other hand reflects the average degree of alignment of all matrix components in a sample. Depending on the magnetic fabric type, the orientation of the maximum or minimum susceptibility ellipsoid axis is therefore coincident with the grain alignment direction or grain long axes. **Figure 7.1** compares room temperature percent anisotropy of magnetic susceptibility and anisotropy degree based on the presence of visible bedding planes, laminations or aligned grains in thin section. Strongly laminated intervals, intervals with bedding parallel mineral lenses and intervals

with elongate grains, characterized as highly anisotropic in thin section, also have the highest percent anisotropy of magnetic susceptibility. It was however not obvious from thin section classification that minerals/grains in the Evie are significantly more aligned than those in the Muskwa and Otter Park.

Thin section based anisotropy degrees also agree with AMS values for siliceous (quartz rich), poorly laminated, organic matter and clay poor sections such as is noted in the thin section at 2266.5m. Such intervals are poorly anisotropic in thin section and have low room temperature AMS since quartz is isotropic and shows little to no preferred orientation.

Thin section based anisotropy degrees underestimate the degree of matrix preferred orientation in some organic rich, clay poor, pyritic intervals of the upper Muskwa and lower Otter Park. Reflected light photomicrographs of two such intervals are shown **Figure 7.1** (depths of 2247.82m. and 2343.3m). In plane polarized light, the opaqueness of organic matter obscures textural features making it impossible to visually characterize matrix preferred orientation in these samples. In reflected light, however, for the sample taken at 2247.82m, pyrite replaced grains show some preferred orientation so it is characterized as poorly to moderately anisotropic. The sample taken at 2343.3m shows no preferred orientation of pyrite in reflected light, yet its AMS is higher than those of well laminated Otter Park sections.

Thin section observations also explain the low anisotropy of magnetic susceptibility of certain intervals in the Evie Formation. **Figures 7.2A, 7.2B, 7.2C, 7.2D** and **7.2E** are thin section photomicrographs of the isotropic sample (%AMS = 0) at 2377.3m. Unlike other Evie samples with percent AMS between 12.5% and 35%, this sample has little to no bedding parallel bioclasts. Over 60% of the thin section photomicrograph area consists of pyritic, organic matter rich mudstones with no aligned bioclasts (**Figure 7.2E)**. The few bioclasts that do occur in some areas are weakly aligned. Zero AMS also indicates that the opaqueness due to organic matter richness does not obscure any matrix or mineral preferred orientation.

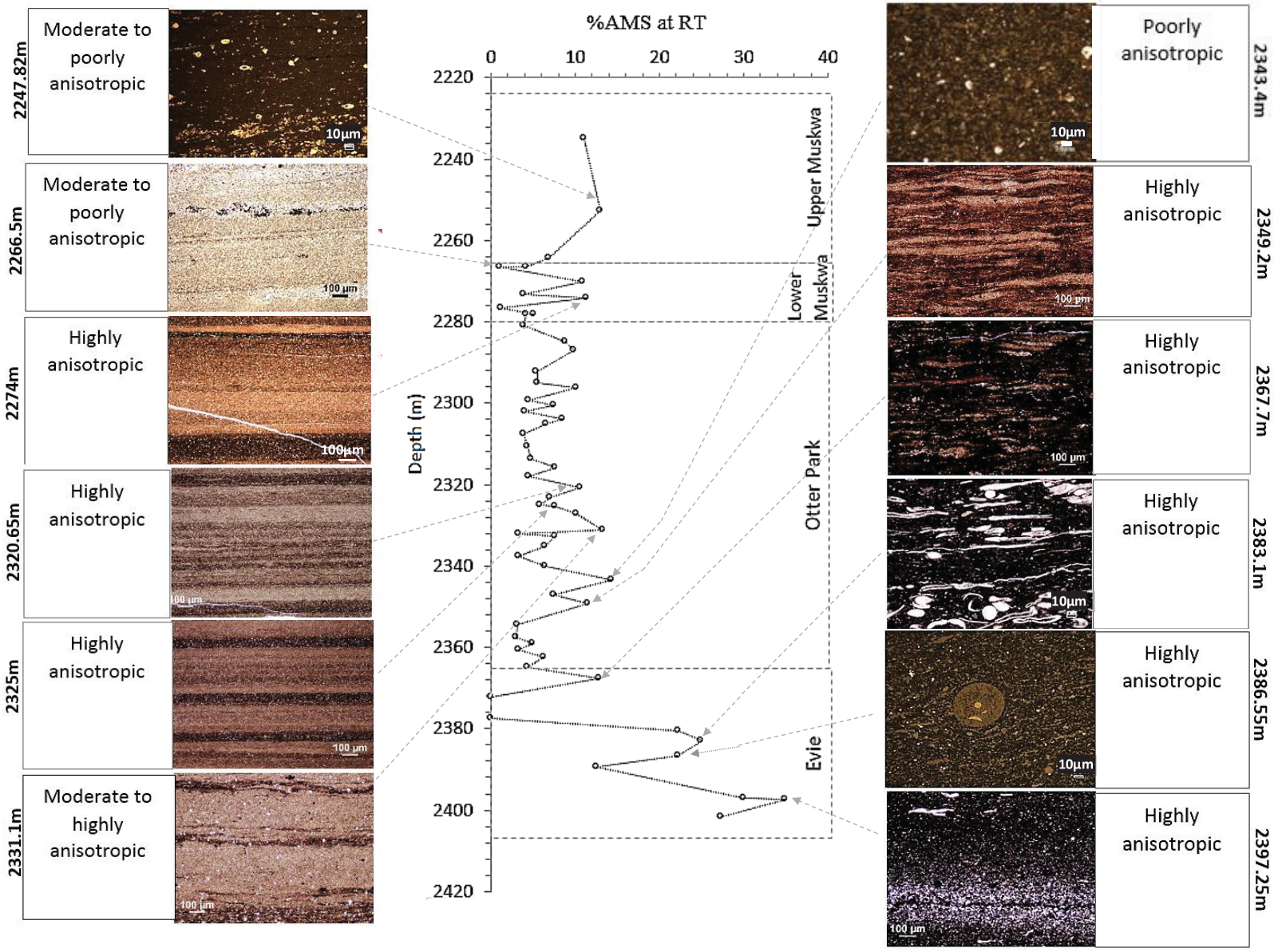

Figure 7.1: Comparison of room temperature anisotropy of magnetic susceptibility and thin section based anisotropy degree.

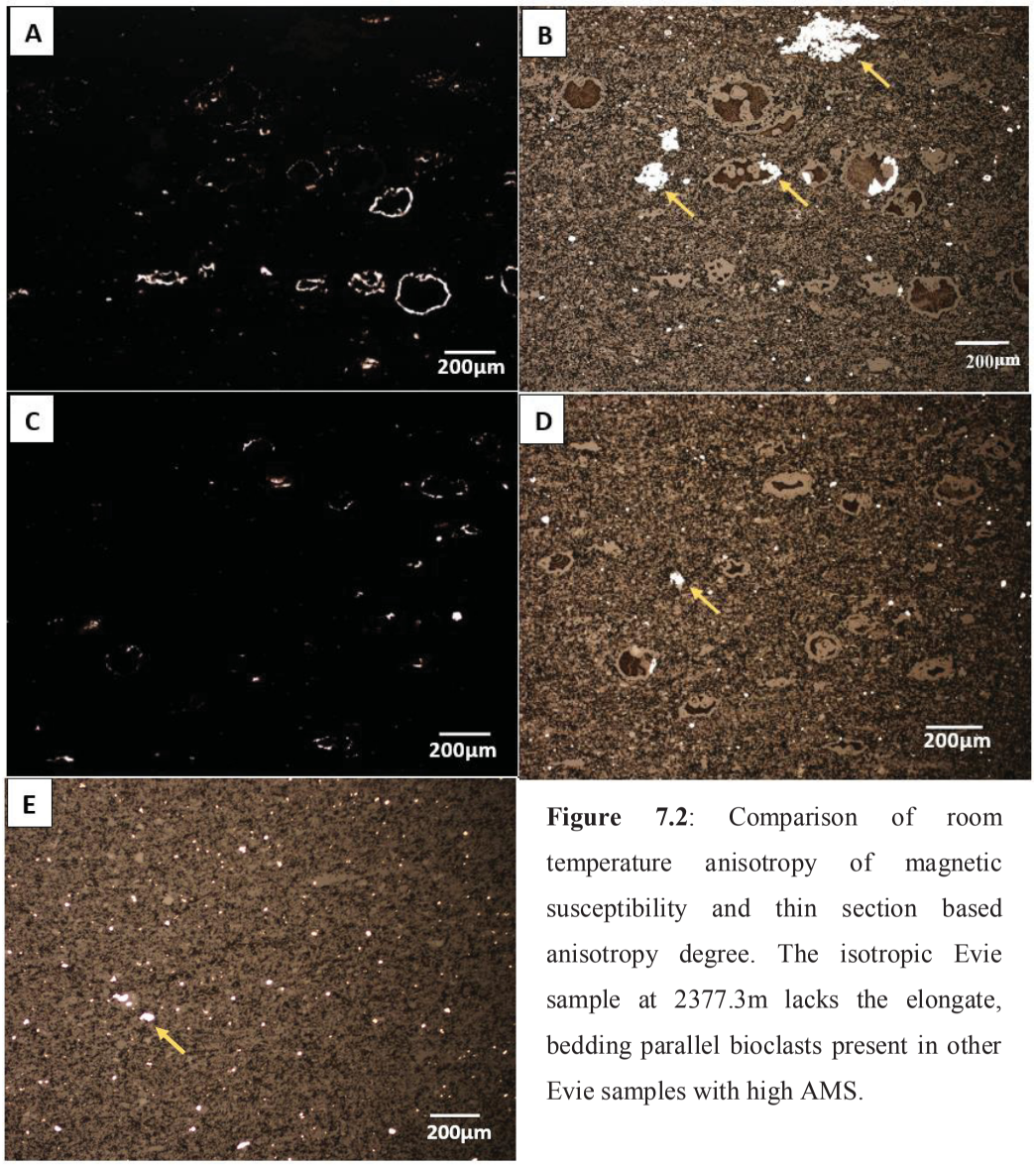

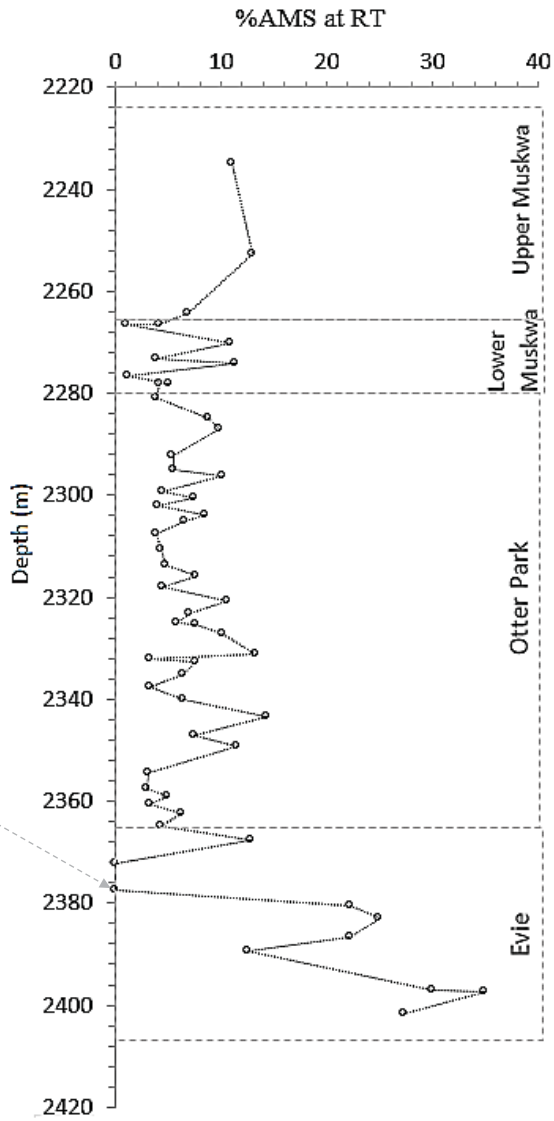

Figure 7.2: Comparison of room temperature anisotropy of magnetic susceptibility and thin section based anisotropy degree. The isotropic Evie sample at 2377.3m lacks the elongate, bedding parallel bioclasts present in other Evie samples with high AMS.

7.3 Comparison of Anisotropy of Electrical Conductivity (AEC) and room temperature Anisotropy of Magnetic Susceptibility (AMS) results

In **Chapter 3** anisotropy of magnetic susceptibility which is a reflection of the shape and preferred orientation of matrix components was determined to be principally controlled by the concentration of organic matter in the Horn River Group. In **Chapter 5** the shape, orientation and alignment of pores was determined to be the primary control on their anisotropy of electrical conductivity. Since both electrical conductivity and magnetic susceptibility are second rank tensors, and the same measurement directions were used to determine the AMS and AEC ellipsoids, results from both techniques can be directly compared. Because each anisotropy technique reflects a different fabric element, integration of both results yields a better understanding of the 3D distribution of fabric elements and their relationship with one another. From AMS principal orientations, the 3D orientations of minerals and other matrix components are obtained, and from the AEC principal orientations the average shape and orientation of micropores are determined.

The Horn River Group mudrocks are significantly more electrically anisotropic than they are magnetically anisotropic. Their AMS values range from 0% to 35% while their AEC values are between 65% and 180%. Minerals and other matrix components are therefore less preferentially aligned than pore spaces in these mudrocks. Although the most magnetically anisotropic member, the Evie, is in general the least electrically anisotropic, no direct correlation is observed between percent AMS and percent AEC. A relationship is however noted between the magnetic susceptibility and electrical conductivity principal axes orientations. Samples with normal magnetic fabric at room temperature (maximum susceptibility parallel to the bedding plane and minimum susceptibility normal to it) have minimum susceptibility axes orientations that with depth, vary in the same manner as their minimum electrical conductivity axes (**Figure 7.3 A**). Both AMS and AEC minimum axes are steeply inclined and normal to the bedding plane. This trend is observed in both their inclinations and declinations**.** Samples with inverse magnetic fabrics at room temperature have minimum conductivity axes that with depth, trend in the same manner as their maximum susceptibility axes. This trend is observed in both their inclinations and declinations as shown in **Figure 7.3B.**

Similar trends with depth in samples with the same magnetic fabric type suggest that preferred mineral or matrix orientation and pore space alignment are due primarily to the same diagenetic processes, probably burial compaction.

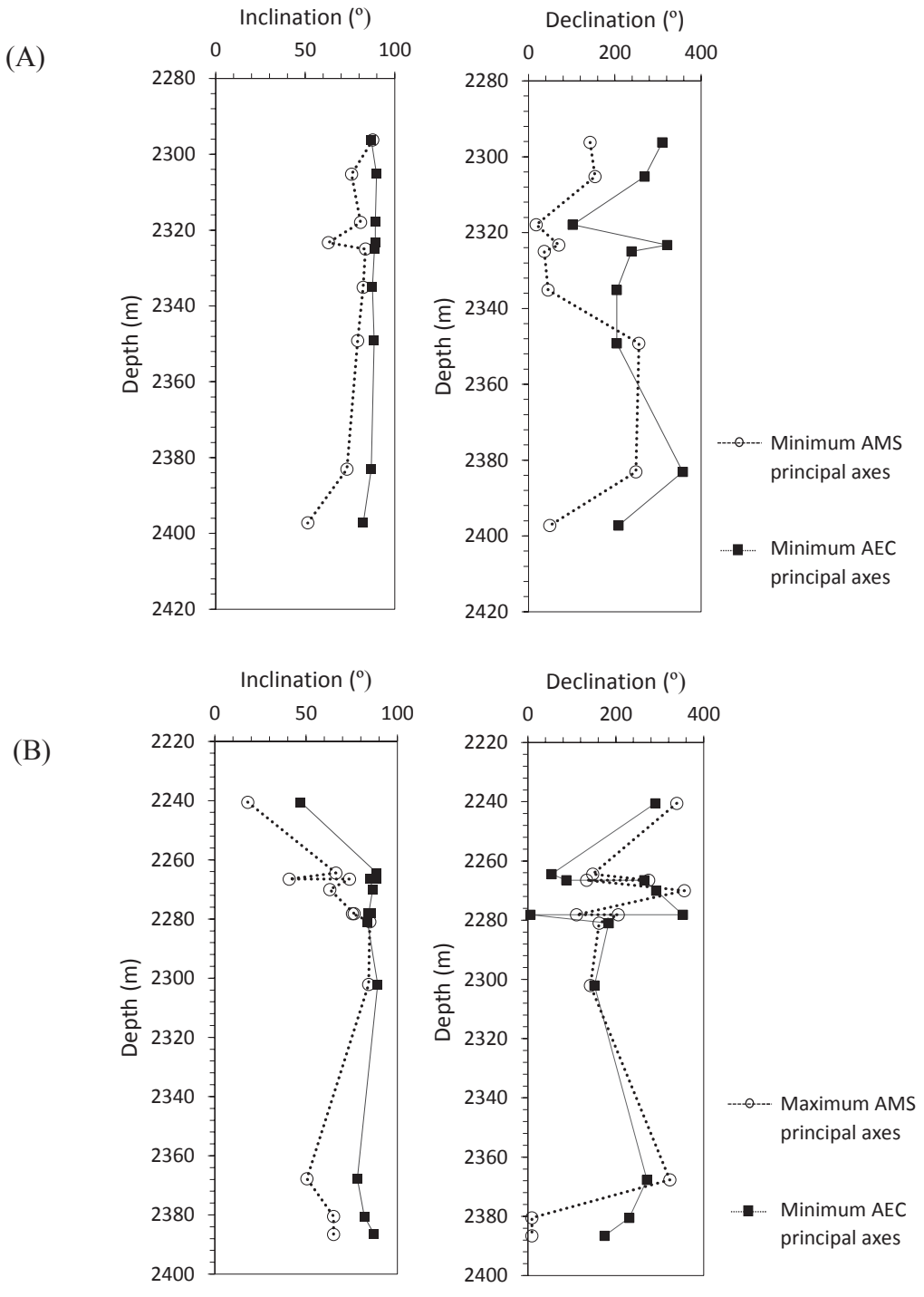

Figure 7.3: Variation with depth of (A) minimum magnetic susceptibility and minimum electrical conductivity axes for samples with normal magnetic fabrics. (B) minimum electrical conductivity axes and maximum magnetic susceptibility axes for samples with inverse magnetic fabrics.

Chapter 8

Conclusions and recommendations

8.1 Conclusions

The application of magnetic and electrical properties in the understanding of the fabric of shales and mudstones of the Horn River Group is presented in this thesis. A key contribution of this work is that it presents quantitative methods of describing clay and organic fabric. The properties investigated are: magnetic susceptibility and its anisotropy, magnetic remanence and its anisotropy and electrical resistivity/conductivity and its anisotropy. To test the reliability of these techniques as tools for quantitative fabric analysis, their results were compared to results from standard geochemical techniques and to visual rock fabric observations made from thin section and SEM images. The following are the main conclusions arising from my work:

(1) At room temperature, bulk magnetic susceptibility of the Horn River Group mudrocks was controlled by the concentration of paramagnetic and diamagnetic phases. Positive correlation between bulk volume magnetic susceptibility and iron oxide and aluminium oxide concentration indicated that higher susceptibilities in the Otter Park were due to increased concentration of clay minerals. Negative correlation between bulk volume magnetic susceptibility and silicon dioxide and total organic carbon (TOC) indicated that organic matter and quartz were primary diamagnetic phases responsible for the low susceptibilities in the Upper Muskwa and Evie. To our knowledge, this is the first time a relationship has been shown between organic matter concentration and bulk magnetic susceptibility.

(2) Room temperature anisotropy of magnetic susceptibility (AMS) showed little to no correlation with clay content, a correlation was instead observed with percent total organic carbon (TOC). The correlation is strongest in the Lower Muskwa and Otter Park formations (R^2=0.6 and 0.67 respectively). Organic matter is therefore either more preferentially oriented that other matrix components or dictates how preferentially oriented other matrix components are. Since TOC percentages for the Horn River Group mudrocks from the studied well are between 0.46wt% and 6.85wt%, the latter option is most probable. Correlation of room temperature AMS with organic richness also indicates that AMS results may also be useful for determining total organic carbon (TOC).

(3) The correlation between organic matter concentration and AMS is poorest in the Evie (R^2 = 0.2). Thin section observation of calcite twins whose twin planes coincide with the AMS axes suggested that extensional forces may be partly responsible for AMS in the Evie.

(4) Inverse AMS fabrics due to uniaxial stable single domain (SD) grains were identified in shales for the first time to our knowledge. This means that anyone using AMS alone may not uniquely be able to relate AMS to the structural petrofabric axes.

(5) Anisotropy of isothermal remanent magnetization (AIRM) measurements confirmed that some of the inverse AMS fabrics were due to uniaxial stable single domain grains. This demonstrates the importance of using AIRM to identify the correct structural petrofabric axes in samples that exhibit inverse AMS axes due to uniaxial stable single-domain grains. Other inverse AMS fabrics that remained inverse at low temperature, were due to iron bearing carbonates. AIRM measurements indicated that these latter samples also contained some uniaxial single-domain grains.

(6) There is good agreement between room temperature AMS results and thin section observations. Well laminated Horn River sections and sections with strongly aligned bedding parallel grains, characterized as highly anisotropic in thin section, also have the highest room temperature AMS values. In contrast, siliceous, poorly laminated intervals have the lowest AMS. Organic richness in sections of the Upper Muskwa and Otter Park limits applicability of thin section photomicrographs in characterizing anisotropy degree. Thin section and SEM images correlated with the AMS and AMR axes. Samples with normal AMS axes had maximum susceptibility axes parallel to the bedding plane/laminations/elongation orientation of grains, and minimum susceptibility

perpendicular to these features. On the other hand, samples with inverse AMS axes had minimum susceptibility parallel to the bedding plane/laminations/elongation orientation of the grains, and maximum susceptibility perpendicular to these features.

(7) %AIRM was significantly greater than %AMS. In samples with inverse AMS fabrics at room temperature this may be due to mixtures of multidomain (MD) and uniaxial stable single-domain grains with their long axes in the same orientation. The two sets of particles would cause the AMS to be reduced (due to the partial cancelling effect of the two sets of particles: MD particles have maximum susceptibility parallel to their long axes, whereas uniaxial stable SD particles have minimum susceptibility parallel to their long axes), whereas the AIRM would be enhanced.

(8) IRM acquisition curved indicated that magnetite is the primary remanence carrying mineral. In samples with predominately multidomain grains, the AIRM principal axes indicated that these grains have similar orientations as the diamagnetic and paramagnetic minerals that make up the bulk matrix.

(9) Low temperature bulk magnetic susceptibility and AMS measurements were demonstrated to be an extremely useful tool and resulted in the following key conclusions:

i) Comparison of theoretical template curves for simple illite + quartz mixtures with low temperature bulk magnetic susceptibility measurements on the Horn River Group shales enabled rapid estimated of the illite and quartz content to be obtained. Significantly, there was a strong correlation between the low temperature magnetically derived illite content and Al_2O_3 content (a key component in such clays) from inductively coupled plasma mass spectrometry. This provided independent support that the magnetic results were meaningful.

ii) The variation in the orientation of the principal anisotropy of magnetic susceptibility (AMS) axes between room temperature and low temperature gave important information regarding the mineral components in the samples and their orientations.

a) Samples with normal AMS fabric orientations that did not change significantly with temperature contain paramagnetic clays (mainly illite) that have similar orientations as other matrix minerals.

b) The paramagnetic signal from samples with inverse AMS fabrics that did not change with temperature are dominated by iron bearing carbonates.

c) Samples with a normal AMS fabric at room temperature and an inverse AMS fabric at low temperature contain a mixture of clay, small amounts of ferrimagnetic material, and iron bearing carbonate. Iron carbonates dominate the paramagnetic signal, hence the inverse AMS fabric at low temperature.

d) For samples with an inverse AMS fabric at room temperature and a normal AMS fabric at low temperature, the room temperature signal was dominated by the presence of uniaxial stable single domain ferrimagnetic particles, whereas at low temperature the enhanced paramagnetic signal of the illite clay dominated.

iii) The enhanced paramagnetic signal at low temperature allowed clearly defined AMS axes in samples that were weakly anisotropic from conventional room temperature AMS measurements. Thus low temperature AMS measurements are potentially extremely useful for identifying subtle features (like lineations related to flow or stress axes) not only in shales but also in other geological samples containing paramagnetic minerals.

10) A novel method of determining the electrical conductivity/resistivity tensor from directional resistivity measurements taken on multifaceted samples was described in **Chapter 5**. Since current flow in electrolyte saturated rocks is through pore spaces and grain surface conductance, anisotropy of electrical conductivity (AEC) results provide information regarding mineral and/or pore geometries, depending on which control dominates. Results indicated in the Horn River mudrocks that the anisotropy of electrical is controlled primarily by the shape and alignment of pore spaces. Anisotropy of electrical conductivity principal axes orientations indicated that most pore spaces have long axes parallel to the bedding plane and short axes perpendicular to it. Results also indicated that although clay rich shales of the Lower Muskwa and Otter Park have very low porosities, their pores are more connected that those in the higher porosity, quartz rich Upper Muskwa and calcareous Evie. When AEC principal axes orientations and AMS principal axes orientations are compared, they trend in a similar manner, indicating that their alignment is likely the result of the same diagenetic processes.

8.2 Recommendations for future studies

The following is a list of recommendations for future studies:

1. This thesis has focused on understanding anisotropy controls and fabric implications in centimeter scale samples. Additional work on how microscopic observations influence anisotropy and mechanical properties at reservoir scale is necessary.

2. Shales and mudstones are highly heterogeneous. Even within the same formation, composition and fabric differs greatly. A key question that arises following results obtained for the Horn River Group is whether anisotropy controls determined are unique to the Horn River Group. Does organic richness always control or dictate matrix preferred alignment in other shale and mudstone formations? Can low temperature methods be used for mineral quantification and clay fabric characterization in all mudstones and shales?

3. Given the observed correlation between total organic carbon (TOC), bulk magnetic susceptibility and anisotropy of magnetic susceptibility, the possible application of bulk magnetic susceptibility and anisotropy of magnetic susceptibility results in determining total organic carbon (TOC) in shales and mudstones can also be investigated.

4. Further studies on the relationship between the orientations of deformed calcite bioclasts and anisotropy of magnetic susceptibility principal axes orientations is necessary. Stereographic projections comparing calcite twin plane orientations, determined from multiple thin sections, and AMS principal orientations will confirm whether or not the preferred orientations of bioclasts is in part due to stresses other than compaction.

5. A comparison of AMS results before and after the application of stresses of different magnitudes and directions would shed light on how the spatial arrangement and distribution of organic matter, clays and other matrix minerals affect fracture propagation. Thin section and SEM images taken before and after stress application will serve as a visual confirmation of AMS results.

6. It would also be interesting to develop a method to study the application of anisotropy of electrical conductivity in monitoring changes in the orientation and geometry of fractures created by stresses of different intensities applied in different sample orientations. If for a single application of stress, the electrical resistivity is measured in different directions, the anisotropy of electrical conductivity may be a useful measure of fracture anisotropy (the directional variability of fracture intensity for stress application in a particular direction).

7. Low temperature AMS could be determined on a wider range of geological samples containing paramagnetic minerals in order to enhance the anisotropy of weakly anisotropic samples, and this could identify subtle features (such as lineations) that might be missed from conventional room temperature AMS measurements.

8. For samples with inverse AMS fabrics at room temperature, magnetic hysteresis parameters can be determined to confirm the presence of uniaxial stable single domain particles. Isothermal remanence decay curves will also confirm if samples contain significant superparamagnetic (SP) particles.

Bibliography

Archie, G.E., 1942. The electrical resistivity log as an aid in determining some reservoir characteristics. Transactions of the American institute of Mining, Metallurgical and Petroleum Engineers, 146, 54-62.

Aruldhas, G., 2010. Engineering physics. PHI Learning Pvt. Ltd., p. 295-296.

Aubourg, C., Rochette, P., and Vialon, P., 1991. Subtle stretching lineation revealed by magnetic fabric of Callovian-Oxfordian black shales (French Alps). Tectonophysics, 185(3), 211-223.

Bachrach, R., 2011. Elastic and resistivity anisotropy of shale during compaction and diagenesis: Joint effective medium modeling and field observations. Geophysics, 76 (6), E175- 186.

Ballet, O., Coey, J.M.D., and Burke, K.J., 1985. Magnetic properties of sheet Silicates; 2:1:1 layer minerals. Phys. Chem. Minerals, 12, 370-378.

Basavaiah, N., 2012. Geomagnetism: solid earth and upper atmosphere perspectives. Springer Science and Business Media, pp. 468.

Bhathal, R.S., 1971. Magnetic anisotropy in rocks. Earth Science Reviews, 7(4), 227-253.

Biedermann, A.R., Koch, C.B., Lorentz, W.E.A., and Hirt, A.M., 2014. Low-temperature magnetic anisotropy in micas and chlorite. Tectonophysics, 629, 63-74.

Bjorlykke, K., 2010. Petroleum Geoscience: From sedimentary environments to rock physics. Springer Science and Business Media, pp. 662.

Bødker, F., Hansen, M.F., Koch, C.B., Lefmann, K., and Møru P, S., 2000. Magnetic properties of hematite nanoparticles. Phys. Rev., B 61, 6826.

Boggs, S., 2009. Petrology of sedimentary rocks. Cambridge University Press, p.194.

Borradaile, G.J., and McArthur, J., 1990. Experimental calcite fabrics in a synthetic weaker aggregate by coaxial and non-coaxial deformation. Journal of Structural Geology, 12(3), 351-363.

Borradaile, G.J., and Jackson, M., 2004. Anisotropy of magnetic susceptibility (AMS): magnetic petrofabrics of deformed rocks. In: Martin-Hernández, F.,Lüneburg, C.M., Aubourg, C., Jackson, M. (Eds.), magnetic fabric methods and applications. The Geological Society of London, Special Publications, 238, 299 - 360.

Borradaile, G. J., and Henry, B., 1997. Tectonic applications of magnetic susceptibility and its anisotropy. Earth Sci. Rev., 42, 49-93.

Bourlange, S., Henry, P., Moore, J.C., Mikada, H., and Klaus, A., 2003. Fracture porosity in the décollement zone of Nankai accretionary wedge using Logging while Drilling resistivity data. Earth and Planetary Science Letters, 209, 103-112.

Brace, W. F., 1965. Some new measurements of linear compressibility of rocks, J. Geophysics Res., 70, 391-398.

British Columbia Ministry of Energy and Mines., 2011. Ultimate Potential for unconventional natural gas in northeastern British Columbia's Horn River Basin, pp. 39.

British Columbia Oil and Gas Commission., 2012. Investigation of observed seismicity in the Horn River Basin, pp. 29.

Broichhausen, H., Littke, R., and Hantschel, T., 2005. Mudstone compaction and its influence on overpressure generation, elucidated by a 3D case study in the North Sea: International Journal of Earth Sciences, 94, 956-978.

Butler, R.F., 1992. Paleomagnetism: magnetic domains to geologic terranes. Blackwell Scientific Publications, pp. 319.

Butler, R.F., 1992. Paleomagnetism: magnetic domains to geologic terranes. Blackwell Scientific Publications, pp. 319.

Carmichael, R. S., 1989. Practical handbook of physical properties of rocks and minerals. CRC Press, Boca Raton, pp. 345.

Carter, N.L., and Raleigh, C.B., 1969. Principal stress directions from plastic flow in crystals. Geological Society of America Bulletin, 80, 1231-1264.

Chadima, M., Pruner, P., Šlechta, S., Grygar, T., and Hirt, A.M., 2006. Magnetic fabric variations in Mesozoic black shales, Northern Siberia, Russia: Possible paleomagnetic implications. Tectonophysics, 418, 145-162.

Chalmers, G.R.L., Ross, D.J.K., and Bustin, R. M., 2012. Geological controls on matrix permeability of Devonian Gas shales in the Horn River and Liard basins, northern British Columbia, Canada. International Journal of Coal Geology. 103, 120-131.

Chemali, R., Gianzero, S., and Su, S.M., 1987. The effect of shale anisotropy on focused resistivity devices. SPWLA 28th Annual Logging Symposium.

Chen, Z., and Hannigan, P., 2015. A shale gas resource potential assessment of Devonian Horn River Strata using a well-performance method. Canadian Journal of Earth Science, 53, 156-167.

Clavaud, J.B., 2008. Electrical anisotropy of shale: the effect of compaction. Petrophysics, 49 (3), 243-260.

Clavier, C., Coates, G., and Dumanoir, J., 1984. The theoretical and experimental bases for the Dual-Water Model for the interpretation of shaly-sands. Society of Petroleum Engineers Journal, 24 (2), 153-168.

Cornell, R. M., and Schwertmann, U., 2006. The Iron oxides: Structure, properties, reactions, occurrences and uses. John Wiley and Sons, p. 32-33.

Cox, A., Doell, R.R., 1967. Measurements of high coercivity magnetic anisotropy. *In*: Collinson, D.V., Creer, K.M., Runcorn, S.K. (Eds.), Methods in Palaeomagnetism. Elsevier, Amsterdam, p. 477 - 42.

De Bresser J.H.P., and Spiers C.J., 1997. Strength characteristics of the r, f and c slip systems in calcite. Tectonophysics, 272, 1-23.

Deer, W.A., Howie, and R.A., Zussman, J., 1992. An introduction to the rock forming minerals. Longman Group UK Limited, pp. 498.

de Wall, H., Bestmann,. M., and Ullemeyer, K., 2000. Anisotropy of diamagnetic susceptibility in Thassos marble: a comparison between measured and modeled data. J. Struct. Geol., 22, 1761-1771.

Duan, H.L., Karihaloo, B.L., Wang, J., and Yi, X., 2006. Effective conductivities of heterogeneous media containing multiple inclusions with various spatial distributions. Phys. Rev. B, 73 (17), 174203.

Dunlop, D. J., Ozdemir, O., 1997. Rock magnetism: Fundamentals and frontiers. Cambridge University Press, Cambridge, p. 573.

Ellis, M., Ruiz, F., Nanduri, S., Keirstead, R., Azizov, I., Frenkel, M., and MacGregor, L., 2011. Importance of anisotropic rock physics modelling in integrated seismic CSEM interpretation. First break, 29, 87-95.

Ellwood, B.B., 1980. Application of the anisotropy of magnetic susceptibility method as an indicator of bottom-water flow direction. Marine Geology, 34, 783-790.

Ferré, E.C., 2002. Theoretical models of intermediate and inverse AMS fabrics. Geophysical Research Letters. 29(7).

Ferré E.C., Martin-Hernández, F., Teyssier, C., and Jackson, M., 2004. Paramagnetic and ferromagnetic magnetic susceptibility in migmatites: measurements in high and low fields and kinematic implications. Geophys. J. Int., 157, 1119-1129.

Ferri, F., Hickin, A.S., and Reyes, J., 2012. Horn River basin–equivalent strata in Besa River Formation shale, northeastern British Columbia (NTS 094K/15). In: Geoscience Reports 2012, British Columbia Ministry of Energy and Mines, 1-15.

Folk, R.L., 1974. Petrology of sedimentary rocks. 3rd Edition Hemphill Publishing Company, pp. 182.

Galehouse, J. S., 1968. A test of the method using the anisotropy of magnetic susceptibility as a paleocurrent indicator. Geol. Soc. Amer. Bull., 79, 887-890.

Ghorbani, A., Cosenza, P., Ruy, S., Doussan, C., and Florsch, N., 2008. Noninvasive monitoring of water infiltration in a clay loamy soil using Spectral Induced Polarization. Water Resour. Res., 44, W08402.

Girdler, R. W., 1961. The measurement and computation of anisotropy of magnetic susceptibility in rocks. Geophys. J. R. Astron. Soc., 5, 34–44.

Graham, J. W., 1966. Significance of magnetic Anisotropy in Appalachian Sedimentary rocks, In: Steinhart, S., and Smith, T.J., The earth beneath the continents, Geophysical Monograph Series 10, eds ,Washington, DC: American Geophysical Union, 627-648.

Graham, J. W., 1954. Magnetic susceptibility anisotropy, an unexploited petrofabric element. Bulletin of the Geological Society of America, 65, 1257-1258.

Gornitz, V., 2008. Encyclopedia of paleoclimatology and ancient environments, Springer Science and Business Media, p. 580.

Grim, R. E., Bray, R. H., and Bradley, W. F., 1937. The mica in argillaceous sediments. Amer. Mineral, 22, 813- 829.

Hall, S., and Sager, W.W., 1990. Paleomagnetic and rock magnetic properties of sediment samples from ocean drilling program leg 116, central Indian Ocean. Proceedings of the Ocean Drilling Program, Scientific Results, 116.

Hamilton N., 1963. Susceptibility anisotropy measurements on some Silurian siltstones. Nature, 197, 170-171.

Hamilton, N., Rees, A.I., 1970. Magnetic fabric of sediments from the shelf at La Jolla (California). Marine Geology, 9, M6-M11.

Hamilton, T.D., Borradaile, G.J., and Lagroix, F., 2004. Sub-fabric identification by standardization of AMS: an example of inferred neotectonic structures from Cyprus. In: Geological Society, London, Special Publications, 238, 527-540.

Henry, B. D., Jordanova , N., Souque, C., and Robion, P., 2003. Anisotropy of magnetic susceptibility of heated rocks. Tectonophysics, 366, 241-258.

Hewanger, J. V. Herwanger, J.V., Pain, C.C., Binley, A., De Oliveira, C.R.E., and Worthington, M.H., 2004. Anisotropic resistivity tomography. Geophysical Journal International, 158 (2), 409-425.

Hill, R.J., Craig, J.R., and Gibbs, G.V., 1979. Systematics of the spinel structure type. Physics and Chemistry of Mineral, 4(4), 317-339.

Hirt, A. M., and Gehring, A. U., 1991. Thermal alteration of the magnetic mineralogy in ferruginous rocks. J. Geophys. Res., 96, 9947-9953.

Hirt, A.M., Evans, K.F., and Engelder, T., 1995. Correlation between magnetic anisotropy and fabric for Devonian shales on the Appalachian Plateau. Tectonophysics, 247, 121-132.

Hirt, A.M., 2007. Magnetic remanence, anisotropy. Encyclopedia of geomagnetism and paleomagnetism, p. 535 - 540.

Hounslow, M. W., 1985. Magnetic fabric arising from paramagnetic phyllosilicate minerals in mud rocks. J. Geol. Soc. London, 142**,** 995-1006.

Hounslow, M. W., 2001. The crystallographic fabric and texture of siderite in concretions: implications for siderite nucleation and growth processes. Sedimentology, 48, 533-557.

Hrouda, F., and Ježek, J., 1999. Magnetic anisotropy indications of deformations associated with diagenesis. In: Tarling, U. H., and Turner, P. (eds), Palaeornagnetisrn and Diagenesis in Sediments, Geological Society, London, Special Publications, 151, 127-137.

Hrouda, F., 2002. The use of the anisotropy of magnetic remanence in the resolution of the anisotropy of magnetic susceptibility into its ferromagnetic and paramagnetic components. Tectonophysics, 347, 269 - 281.

Hrouda, F. and Jelinek,V., 1990. Resolution of ferrimagnetic and paramagnetic anisotropies in rocks, using combined low-field and high-field measurements. Geophys. J. Int., 103, 75-84.

Hrouda, F., Jelinek, V., and Zapletal K., 1997. Refined technique for susceptibility resolution into ferromagnetic and paramagnetic components based on susceptibility temperature variation measurement. Geophys. J. Int., 129, 715– 719.

Hrouda, F., Henry, B., and Borradaile, G., 2000. Limitations of tensor subtraction in isolating diamagnetic fabrics by magnetic anisotropy. Tectonophysics, 322, 303-310.

Hrouda, F., 2004. Problems in interpreting AMS parameters in diamagnetic rocks. In: Geol. Soc., London, Special Publications, 238, 49-59.

Ihmle, P.F., Hirt, A.M., Lowrie, W., and Dietrich, D., 1989. Inverse magnetic fabric in deformed limestones of the Morcles Nappe, Switzerland. Geophys. Res. Lett., 16, 1383–1386.

Ingram, G.M., and Urai, J. L., 1999. Top-seal leakage through faults and fractures: the role of mudrock properties. In Aplin, A.C., Fleet, A.J., and Macquaker, J.H.S., 1999. Mudstones: Physical and fluid flow properties. The Geological Society of London, 125-135.

Jackson, M., Craddock, J.P., Ballard, M., Van der Voo, R., and McCabe, C., 1989. Anhysteretic remanent magnetic anisotropy and calcite strains in Devonian carbonates from the Appalachian Plateau, New York. Tectonophysics, 161, 43 - 53.

Jackson, M., 1991. Anisotropy of magnetic remanence: A brief review of mineralogical sources, physical origins, and geological applications, and comparison with susceptibility anisotropy. Pageoph.,136 (1), 1 - 28.

Jackson, M., Sprowl, D., and Ellwood, B., 1989. Anisotropies of partial anhysteretic remanence and susceptibility in compacted black shales: Grainsize and composition dependent magnetic fabric. Geophysics Research Letters, 16, 1063-1066.

Jackson, M., 1991. Anisotropy of magnetic remanence: a brief review of mineralogical sources, physical origins, and geological applications, and comparison with susceptibility anisotropy. Pure Appl. Geophys*,* 136, 1-28.

Jacobs, I. S., 1963. Metamagnetism of siderite. J. Appl. Phys., 34, 1106-1107.

Jain, M., Gupta, R., Gupta, A., and Kumar, M., 2007. Diamagnetic susceptibility and anisotropy of organic and organometallic compounds. Springer Science and Business Media, 27(A), 3-4.

Jamison, W. R., and Spang, J. H., 1976. Use of calcite twin lamellae to infer differential stress. Bull. Geol. Soc. Am., 87, 868-872.

Juhász, I., 1981. Normalised Qv – The key to shaly sand evaluation using the Waxman-Smits equation in the absence of Core data. Society of Petrophysicists and Well-Log Analysts conference, SPWLA-1981-Z.

Keller G.V. and Frischknecht F.C., 1966. Electrical methods in geophysical prospecting. Pergamon Press Inc., Oxford, pp. 519.

Khan, M. A., 1962. Anisotropy of magnetic susceptibility of some igneous and metamorphic rocks. J. Geophys. Res., 67, 2873-2885.

Khan, M. A., and Rees, A. I., 1968. Magnetic analysis of rock fabric. In: Runcorn, S. K. ed., International Dictionary of Geophysics, Pergamon.

King, R. F., 1966. The magnetic fabric of some Irish granites. Geol. J., 5, 43-46.

King, J., Banerjee, S.K., Marvin, J., and Ozdemir, O., 1982. A comparison of different methods for determining the relative grain size of magnetite in natural sediments: some results from lake sediments. Earth Planet. Sci. Lett., 59, 404-419.

Klein, J. D., Martin, P. R. and Allen, D. F., 1997. The petrophysics of electrically anisotropic reservoirs. The Log Analyst, 38, 25-36.

Lander, R.H., and Walderhaug, O., 1999. Predicting porosity through simulating sandstone compaction and quartz cementation. AAPG Bulletin, 83(3), 433-449.

Larrasoaña, J.C., Gómez-Paccard, M., Giralt, S., and Roberts, A.P., 2011. Rapid locking of tectonic magnetic fabrics in weakly deformed mudrocks. Tectonophysics, 507, 16-25.

Lee, T.Q., and Angelier, J., 2000. Tectonic significance of magnetic susceptibility fabrics in Plio-Quaternary mudstones of southwestern foothills, Taiwan. Earth, Planets, Space, 52, 527-538.

Lehman, B., Sagnotti, L., Winkler, A., Lo Cascio, C., 1996. Magnetic mineralogy changes in the Pleistocene marine sequence of Montalto di Castro (central Italy) and influence on the magnetic anisotropy. Geophys. J. Int. 127, 529-541.

Leroy, P. and Revil, A., 2004. A triple-layer model of the surface electrochemical properties of clay minerals. Journal of Colloid and Interface Science, 270 (2), 371-380.

Levi, T., and Weinberger, R., 2011. Magnetic fabrics of diamagnetic rocks and the strain field associated with the Dead Sea Fault, northern Israel. J. Struct. Geol., 33, 566-578.

Lowrie, W., 2007. Fundamentals of geophysics. Cambridge University Press, p. 255.

Lundegard, P.D., and Samuels, N.D., 1980. Field classification of fine-grained sedimentary rocks. J. Sed. Petrol. 50, 781-786.

Lyons, W., Plisga, G.J., and Lorenz, M., 2015. Standard handbook of petroleum and natural gas engineering. Gulf professional publishing, p. 99.

Makhanov, K.K., 2013. An experimental study of spontaneous imbibition in Horn River shales. Master's thesis, University of Alberta, Edmonton, Canada. Retrieved from http://hdl.handle.net/10402/era.32660.

Manning, D.A.C., 1995. Introduction to industrial minerals. Chapmann and Hall publishing, p. 192.

Mares, S., 1984. Introduction to applied geophysics. Springer Science and Business Media, pp. 266.

Martín-Hernández, F., and Ferré, E.C., 2007. Separation of paramagnetic and ferrimagnetic anisotropies: a review. Journal of Geophysical Research, 112, B03105, doi:10.1029/2006JB004340.

McCabe, C., Jackson, M., and B. B. Ellwood, B.B., 1985. Magnetic anisotropy in the Trenton limestone: Results of a new technique, anisotropy of anhysteretic susceptibility. Geophysical Research Letters, 12, 333-336.

McCarter, W.J., 1984. The electrical resistivity characteristics of compacted clays. Geotechnique, 34 (2), 263-267.

McCarter, W.J., Blewett, J., Chrisp, T.M. and Starrs, G., 2005. Electrical property measurements using a modified hydraulic oedemeter. Canadian Geotechnical Journal, 42, 655-662.

McLean, A., and Gribble, C., 2003. Geology for civil engineers. CRC Press, pp.336.

Merrill, R.T., 2010. Our magnetic earth. University of Chicago Press, p. 12.

Mitchell, J.K., 1993. Fundamentals of soil behaviour. Wiley Inter-Science, New York, p.422.

Morrow, D.W., Zhao, M., and Stasiuk, L.D., 2002. The gas-bearing Devonian Presqu'ile dolomite of the Cordova embayment region of British Columbia, Canada: dolomitization and the stratigraphic template. AAPG Bulletin, 86 (9), 1609-1638.

Mousseau, R.J., and Trump, R.P., 1967. Measurement of electrical anisotropy of clay-like materials. Journal of Applied Physics, 38 (11), 4375 - 4379.

Negi, A.S., and Anand, S.C., 1985. A textbook of physical chemistry. New Age International (P) Limited, Publishers, pp. 489.

Okiongbo, K.S., Aplin, A.C., and Larter, S.R., 2005. Changes in Type II Kerogen Density as a Function of Maturity: Evidence from the Kimmeridge Clay Formation. Energy Fuels, 19 (6), 2495-2499.

Owens, W. H., 1974. Mathematical model studies on factors affecting the magnetic anisotropy of deformed rocks. Tectonophysics, 24, 115-131.

Owens W. H., and Bamford, D., 1976. Magnetic, seismic, and other anisotropic properties of rock fabric. Philosophical Transactions of the Royal Society of London, Series A, 283, 55-68.

Özdemir, Ö., Dunlop, D.J., and Jackson, M., 2009. Frequency and field dependent susceptibility of magnetite at low temperature. Earth Planets Space, 61, 125-131.

Parés, J.M., 2004. How deformed are weakly deformed mudrocks? Insights from magnetic anisotropy. Geological Society, London, Special Publication, 238, 191-203.

Parés, J.M., and van der Pluijm, B.A., 2014. Low temperature AMS and the quantification of subfabrics in deformed rocks. Tectonophysics, 629, 55-62.

Parés, J.M., 2015. Sixty years of anisotropy of magnetic susceptibility in deformed sedimentary rocks. Frontiers in Earth Science: Geomagnetism and Paleomagnetism, 3(4).

Patnode, H.W., and Wyllie, M.R.J., 1950. The Presence of Conductive Solids in Reservoir Rocks as Factor in Electric Log Interpretation. Society of Petroleum Engineers, 2 (2), 47-52.

Perez, M., Goodway, B., and Purdue, G., 2012. Integrated workflows for shale gas and case study results for the Horn River Basin, British Columbia, Canada. The Leading Edge, Special section: Seismic inversion for reservoir properties.

Potter, D.K., and Stephenson, A., 1988. Single-domain particles in rocks and magnetic fabric analysis. Geophysical Research Letters, 15(10), 1097-1100.

Potter, D. K., and Stephenson, A., 1990. Field-impressed anisotropies of magnetic susceptibility and remanence in minerals. J. Geophys. Res., 95 (15), 573-588.

Potter, D.K., Corbett, P.W.M., Barclay, S.A., and Haszeldine, R.S., 2004. Quantification of illite content in sedimentary rocks using magnetic susceptibility - a rapid complement or alternative to x-ray diffraction. J. Sed. Res., 74(5), 730-735.

Potter, D.K., 2004. A comparison of anisotropy of magnetic remanence methods- a user's guide for application to palaeomagnetism and magnetic fabric studies. *In*: Martin-Hernandez, F., Luneburg, C.M., Aubourg, C., and Jackson, M. (eds.), Magnetic Fabric: Methods and applications. Geological Society, London, Special publications, 238, 21-35.

Rees, A. I., 1961. The effect of water currents on the magnetic remanence and anisotropy of susceptibility of some sediments. Geophys. J. R. Astron. Soc., 5, 235-251.

Rees, A. I., 1965a. The use of anisotropy of magnetic susceptibility in the estimation of sedimentary fabric. Sedimentology, 4, 257-271.

Rees, A. I., 1965b. Preliminary measurements of the anisotropy of magnetic susceptibility of the Franciscan formation of central California. Geol. Soc. Amer. Bull., 76, 975-980.

Rees, A. I., 1968. The production of preferred orientation in a concentrated dispersion of elongated and flattened grains. Jour. Geology, 76, 457 - 465.

Revil, A.P., and Glover, W.J., 1997. Theory of ionic surface electrical conduction in porous media. Phys. Rev. 55, 1757-1773.

Revil, A., Cathles, M.L., and Losh, S., 1998. Electrical conductivity in shaly sands with geophysical applications. Journal of Geophysical Research, 103 (B10) 23, 925-936.

Reynolds, M.M., and Munn, D.L., Development update for an emerging shale gas giant field-Horn River Basin, British Columbia, Canada. SPE 130103.

Rezaee, R., 2015. Geomechanics of gas shales In: Fundamentals of shale gas reservoirs. John Wiley and Sons, Inc., pp. 169-190.

Richter, C., Frisch, W., Ratschbacher, L., and Schwarz, H.U., 1991. The magnetic fabrics of experimentally deformed artificial clays-water dispersions. Tectonophysics, 200, 143-155.

Richter, C., and van der Pluijm, B. A., 1994. Separation of paramagnetic and ferrimagnetic susceptibilities using low temperature magnetic susceptibilities and comparison with high field methods. Phys. Earth and Planet. Inter., 82, 113-123.

Robion, P., Delamotte, D.F., Kissel, C., and Aubourg, C., 1995. Tectonic versus mineralogical contribution to the magnetic fabric of epimetamorphic slaty rocks–an example from the Ardennes Massif (France–Belgium). J. Struct. Geol., 17, 1111-1124.

Rochette, P., and Fillion, G., 1988. Identification of multicomponent anisotropies in rocks using various field and temperature values in a cryogenic magnetometer. Phys. Earth Planet. Inter., 51, 379-386.

Rochette, P., Jackson, M., and Aubourg, C., 1992. Rock magnetism and the interpretation of anisotropy of magnetic susceptibility. Rev. Geophys., 30, 209-226.

Rochette, P., Scaillet, B., Guillot, S., Le Fort, P., Pecher, A., 1994. Magnetic properties of the High Himalayan leucogranites: structural implications. Earth Planet. Sci. Lett., 126, 217-234.

Ross, D.J.K., and Bustin, R.M., 2008. Characterizing the shale gas resource potential of Devonian Mississippian strata in the Western Canada sedimentary basin: Application of an integrated formation evaluation. American Association of Petroleum Geologists Bulletin, 92(1), 87-125. doi:10.1306/09040707048.

Spassov, S., Valet, J.P., Kondopoulou, D., Zananiri, I., Casas, L., and Le Goff, M., 2010. Rock magnetic property and paleointensity determination on historical Santorini lava flows. Geochemistry, Geophysics, Geosystems, 11(7), 1 - 12.

Saeidi, O., Rasouli, V., Vaneghi, R.G., Gholami, R., and Torabi, S.R., 2014. A modified failure criterion for transversely isotropic rocks. Geoscience Frontiers, 5, 215-225.

Schieber, J., and Ellwood, B., 1993. Determination of basinwide paleocurrent patterns in a shale succession from anisotropy of magnetic susceptibility (AMS): a case study of the Mid Proterozoic Newland Formation, Montana. Journal of Sedimentary Petrology, 63, 874-880.

Schmidt, V., Günther, D., Hirt, A.M., 2006. Magnetic anisotropy of calcite at room temperature. Tectonophysics, 418, 63-73.

Schmidt, V., Hirt, A.M., Hametner, K., Günther, D., 2007 Magnetic anisotropy of carbonate minerals at room temperature and 77 K. American Mineralogist, 92, 1673–1684.

Schmidt, V., Günther, D., Hirt, A.M., 2006. Magnetic anisotropy of calcite at room temperature. Tectonophysics, 418, 63-73.

Schumacher, B.A., 2002. Methods for the determination of total organic carbon (TOC) in soils and sediments. US. Environmental Protection Agency, NCEA-C- 1282 EMASC-00.

Smith, D.O., 1956. Magnetization of a magnetite single crystal near the Curie point. Phys. Rev., 102, 959.

Spears, D.A., 1980. Towards a classification of shales. J. Geol Soc. London, 137, 125-129.

Spencer, C.W., 1989. Review of characteristics of low-permeability gas reservoirs in Western United States. AAPG Bulletin, 73, 613-629.

Spencer, A.M., 1993. Generation, accumulation and production of Europe's hydrocarbons III. Special Publication of the European Association of Petroleum Geoscientists, No. 3, p. 101.

Stacey, F. D., and Banerjee, S. K., 1974. Physical Principles of Rock Magnetism. Elsevier, pp. 195.

Stephenson, A., Sadikun, N. and Potter, D.K., 1986. A theoretical and experimental comparison of the magnetic susceptibility and remanence in rocks and minerals. Geophys. J. R. Astron. Soc., 84, 185-200.

Stephenson, A., Sadikun, S. and Potter, D. K., 1986. A theoretical and experimental comparison of the anisotropies of magnetic susceptibility and remanence in rocks and minerals. Geophysical Journal of the Royal Astronomical Society, 84, 185-200.

Stow, D.A.V., and Piper, D.J.W., 1984. Deep-water fine-grained sediments; history, methodology and terminology. Geol. Soc. London, Special Publications 15, 3-14.

Tarling, D. H. and Hrouda, F., 1993. The magnetic anisotropy of rocks. Chapman and Hall, pp. 217.

Telford, W. M., Geldart, L. P., and Sheriff, R. A., 1990. Applied geophysics, 2nd edition: Cambridge Univ. Press, pp. 770.

Thompson, R. and Oldfield, F., 1986. Environmental Magnetism. Allen and Unwin, London, pp. 243.

Tourneret, C., and Laurent, P., 1990. Paleo-stress orientations from calcite twins in the North Pyrenean foreland, determined by the Etchecopar inverse method. Tectonophysics, 180, 287-302.

Tsvankin, I., 1997. Anisotropy parameters and P-wave velocities for orthorhombic media. Geophysics, 62 (4), 1292-1309.

Tucker, M.E., 2009. Sedimentary petrology: An introduction to the origin of sedimentary rocks. John Wiley and Sons, p.92.

Tullis, T. E., 1980. The use of mechanical twinning in minerals as a measure of shear stress magnitude. J. Geophys. Res., 85, 6263-6268.

Turner, F.J., Griggs, D.T., and Heard, H., 1954. Experimental deformation of calcite crystals. Geol. Soc. Am. Bull., 65, 883-934.

Verwey, E. J., 1939. Electronic conduction of magnetite (Fe3O4) and its transition point at low temperature. Nature, 144, 327–328.

Vinegar, H.J. and Waxman M.H., 1984. Induced polarization of shaly sands. Geophysics, 49, 1267-1287.

Waxman, M.H. and Smits, L.J.M., 1968. Electrical conduction in oil-bearing sands. Society of Petroleum Engineers Journal, 8, 107-122.

Williams, G. K., 1983. What does the term Horn River Formation mean? Bulletin of Canadian Petroleum Geology, 31, 117-122.

Wilson, M. D., and Stanton, P.T., 1994, Diagenetic mechanisms of porosity and permeability reduction and enhancement, in M. D. Wilson, ed., Reservoir quality assessment and prediction in clastic rocks: SEPM Short Course 30, p. 59–119.

Witkowsky, J.M., Galford, J.E., Quirein, J.A., and Truax, J.A., 2012. Predicting pyrite and total organic carbon from well logs for enhancing shale reservoir interpretation. Conference paper: SPE Eastern Regional Meeting, 3-5 October.

Yaalon, D.H., 1962. Mineral composition of the average shale. Clay Minerals, 5(27), 31-36.

Zee Ma, Y., and Holditch, S., 2015. Unconventional oil and gas resources handbook: evaluation and development. Gulf professional publishing, p.73.